Biogeochemical Proxies for Environmental and Biotic Conditions at the Permian-Triassic Boundary

by

Lindsay Elizabeth Hays

B.S. Earth, Atmospheric and Planetary Sciences
Massachusetts Institute of Technology, 2005

SUBMITTED TO THE DEPARTMENT OF EARTH, ATMOSPHERIC AND PLAENTARY SCIENCES IN PARTIAL FULFILLMENT OF THE REQUIREMENTS FOR THE DEGREE OF

DOCTOR OF PHILOSOPHY IN GEOBIOLOGY
AT THE
MASSACHUSETTS INSTITUTE OF TECHNOLOGY

JUNE 2010

© 2010 Massachusetts Institute of Technology
All rights reserved

ARCHIVES

MASSACHUSETTS INSTITUTE OF TECHNOLOGY
JUN 28 2010
LIBRARIES

Signature of Author.....
Department of Earth, Atmospheric and Planetary Sciences
April 26, 2010

Certified By.....
Roger E. Summons
Professor of Geobiology
Thesis Supervisor

Accepted By.....
Maria T. Zuber
E.A. Griswold Professor of Geophysics
Head of Department

Biogeochemical Proxies for Environmental and Biotic Conditions at the Permian-Triassic Boundary

by

Lindsay Elizabeth Hays

Submitted to the Department of Earth, Atmospheric and Planetary Sciences on April 30, 2010 in Partial Fulfillment of the Requirements for the Degree of Doctor of Philosophy in Geobiology

ABSTRACT

The extinction at the Permian-Triassic boundary marked one of the most profound events of the Phanerozoic Eon. Although numerous hypotheses have been proposed, the trigger mechanism continues to be debated. This thesis intends to examine the impact of oceanic conditions on the extinction event by analyzing hydrocarbon biomarkers. Hydrocarbon biomarkers are chemical fossils in sedimentary rocks that serve as proxies to measure the conditions that prevailed during deposition. In this thesis, biomarkers for redox conditions, depositional environment, microbial community and potential age-related biomarkers have been measured and are reported from four sections that span the Permian-Triassic boundary.

The first section, from the Peace River Basin in modern-day western Canada, was deposited on the eastern margin of the Panthalassic Ocean and samples conditions in this global water body. The second section is from Kap Stosch, Greenland, and was deposited on the southern margin of an epicontinental sea situated in the northwest of the supercontinent Pangaea. The Great Bank of Guizhou, China is the third section studied, and it is a carbonate platform deposited on the southern edge of one of the smaller continental blocks that formed the eastern margin of the Paleo-Tethys Ocean. The fourth section, for the Permian-Triassic boundary is from Meishan, China, the type section for this boundary, and was deposited on the western margin of another one of the continental blocks at the edge of the Paleo-Tethys Ocean. The biomarker evidence from these sections was measured in ratios, absolute abundances and for $\delta^{13}C$ isotopic values. This evidence points to global marine conditions dominated by bacterial inputs in which photic zone euxinia was prevalent for extended time periods. Additional findings from compound-specific isotope data suggest that at isolated intervals, the chemocline may have extended even closer to the surface. The timing of these intervals implies that ocean conditions may have affected the extinction itself.

Acknowledgements

First and foremost, my thanks go to my advisor, Roger Summons. During the five years that I have been a graduate student (and the two years that I worked as an undergraduate researcher) in his lab I have learned what it means to be an acclaimed scientist and a distinguished writer. I will continue to be inspired by his example throughout my career.

I would also like to thank my thesis committee. Andy Knoll and Lindy Elkins-Tanton both provided significant feedback during the editing of this manuscript, and their perspectives were invaluable. Sam Bowring has been a mentor since my second year at MIT (8 years ago!) and I will always be grateful for all the support he has provided. I said it before and will say it again – his gruff exterior hides a heart of gold.

Changqun Cao, John Payne, Charles Henderson, and Clinton Foster provided samples, and along wtih Kliti Grice and Gordon Love, contributed insight and discussions that have helped to bring this research to where it is now. I would also like to thank Christian Hallmann and Julio Sepulveda for being excellent and helpful when I needed instant feedback. Stefanie Templar was there to discuss anything science-related or non-science related, whichever the situation required at the moment, which was also important throughout the process. I would also like to thank Maggie Nelson for helping me make things pretty.

Throughout my whole graduate experience a number of people have been immensely helpful both in lab and navigating the administrative hoops (and sometimes both). These people deserve special thanks – Carolyn Colonero, Laura Sherman, Anthony Carrasquillo, Emily Wooton, Alla Skorokhod, Mary Eliff, Roberta Allard Carol Sprague and Vicki McKenna. Thank you all.

I want to thank my dear friends Kim Wickham and Tori Parisi, two amazing women toiling on their theses as well in the past few months and who provided moral support like only someone else in middle of all of this could.

My dear family – the others enrolled at Hays University – deserve thanks for never letting me get away with anything even a little bit less than my best. My mom, Lynn Hays, my dad, Bob Hays, my sister, Brooks Hays, and my grandmother, GHays are all such outstanding people, I am always proud to be part of our family. Extra thanks go to my Mom for helping me with the oxford comma and many other editing questions.

Finally I want to thank Brent for everything.

Table of Contents

Table of Contents

List of Tables and Figures

List of Tables and Figures

Chapter 1

Hydrocarbon Biomarkers

Abstract

Hydrocarbon biomarkers, or molecular fossils, are derived from the lipids of organisms that have undergone diagenetic breakdown within the sediments. The biomarkers described here can be used to infer redox conditions, microbial communities, depositional environments, and relative ages for sedimentary rocks from a variety of paleolocations. To measure redox conditions, the pristane/phytane ratio, homohopane index, 28,30 bisnorhopane/C_{30} hopane ratio, gammacerane index and a large number of Chlorobi-derived biomarkers are discussed. Biomarker proxies for microbial community include total hopane/total sterane ratio, C_{27}/C_{29} sterane ratio, the 2-methylhopane index, $\delta^{15}N$ values of the biomass, and the parameter, $\Delta\delta$, a measure of the difference between the $\delta^{13}C$ values for *n*-alkanes and isoprenoids. The depositional environment can be indicated by the C_{30} sterane index and a comparison of the ratios of C_{26}/C_{25} tricyclic terpane plotted against the $C_{31}22R/C_{30}$hopane. Finally, two age biomarkers are presented, the relative abundance of C_{33} *n*-alkylcyclohexane/*n*-C_{34} and the C_{28}/C_{29} sterane ratio.

Biomarker Significance

Although the term "biomarker" has various meanings, in this thesis it is used to signify molecular fossils, which are lipids derived from biomolecules deposited in sedimentary rocks. A biomarker

may refer to a single complex compound with a diagnostic origin or a less specific compound with an isotopic ratio that indicates a particular physiology. Select biomarker ratios can be used to reconstruct redox conditions during deposition, microbial communities (specific taxa or biosynthetic pathways) or depositional environments; they also may be used to place broad constraints on the geological age of their host sedimentary rocks (Peters et al. 2005). When lipid biomarkers are derived from compounds central to the functioning of an organism, such as carotenoids or chlorophylls (both important parts of the light-harvesting complex), it is likely that the compounds found in modern organisms will be the same as, or very similar to, the compounds that were once present in ancient organisms of the same taxa.

Biomarkers for Redox Conditions

Two biomarker proxies that can indicate anoxia in sediments during deposition depend solely on redox conditions and not on the biological environment: these are the pristane/phytane ratio and the homohopane index. When used together and with other proxies for anoxia, they can be good indicators of general redox chemistry during diagenesis of the sedimentary rocks. However, neither should be used as a sole indicator of the redox state of the water column.

The ratio of pristane to phytane and that of C_{35} homohopane to total $C_{31\text{-}34}$ homohopanes are similar in that the compounds measured and compared have the same precursor. In those cases where different redox conditions determine which diagenetic product is produced in greater abundance, these ratios are determined purely by chemical processes. Therefore, fluctuations between individual measured samples are not as significant as general trends in the redox state within a section.

The primary precursor for both pristane and phytane is phytol, the side chain of most chlorophyll molecules. In oxic sediments, the alcohol group of phytol is cleaved off together with the terminal carbon atom through a series of oxidation and decarboxylation reactions, which yields a predominance of pristane. (See Figure 1.1.) This contrasts to anoxic sediments, in which the alcohol group is cleaved through reductive processes alone and produces a greater proportion of phytane (Didyk et al. 1978; Peters et al. 2005). The utility of this biomarker ratio may be complicated by alternative sources for both pristane and phytane in sedimentary rocks. Indeed, some studies have indicated that this biomarker proxy is only applicable in hypersaline depositional environments (ten Haven et al. 1987), although this proxy seems to be applicable to a broader range of environments. The values of this ratio that are interpreted as indicative of different redox states are calculated empirically using other proxies as a guide, giving some leeway to include qualifying factors in the understanding of the ratio. However, a pristane/phytane ratio <0.8 is generally considered indicative of deposition under anoxic conditions in the sediments, while a pristane/phytane ratio >2 may be indicative of oxygenated environments.

Homohopanes are hopanes with an extended side chain above C_{30}. These compounds are derived from a number of hopane polyols produced by bacteria. The homohopane index is a measure of the abundance of C_{35} homohopane relative to the C_{31}-C_{34} homohopanes. During diagenesis under oxic conditions, the alcohol groups allow for cleavage of the side chain, producing a predominance of the lower-carbon homohopanes. In anoxic sediments, the alcohol groups serve as a location to bind the homohopanes to the hydrocarbon matrix and stabilize the side chain. This ultimately leads to a higher relative proportion of the C_{35} homohopane than is seen in oxic sediments (Peters et al. 2005), such that a homohopane index of <10% C_{35}/total hopanes (or >0.6 for the ratio of C_{35}/C_{34} homohopanes) may be considered indicative of deposition in anoxic sediments. Unlike the pristane

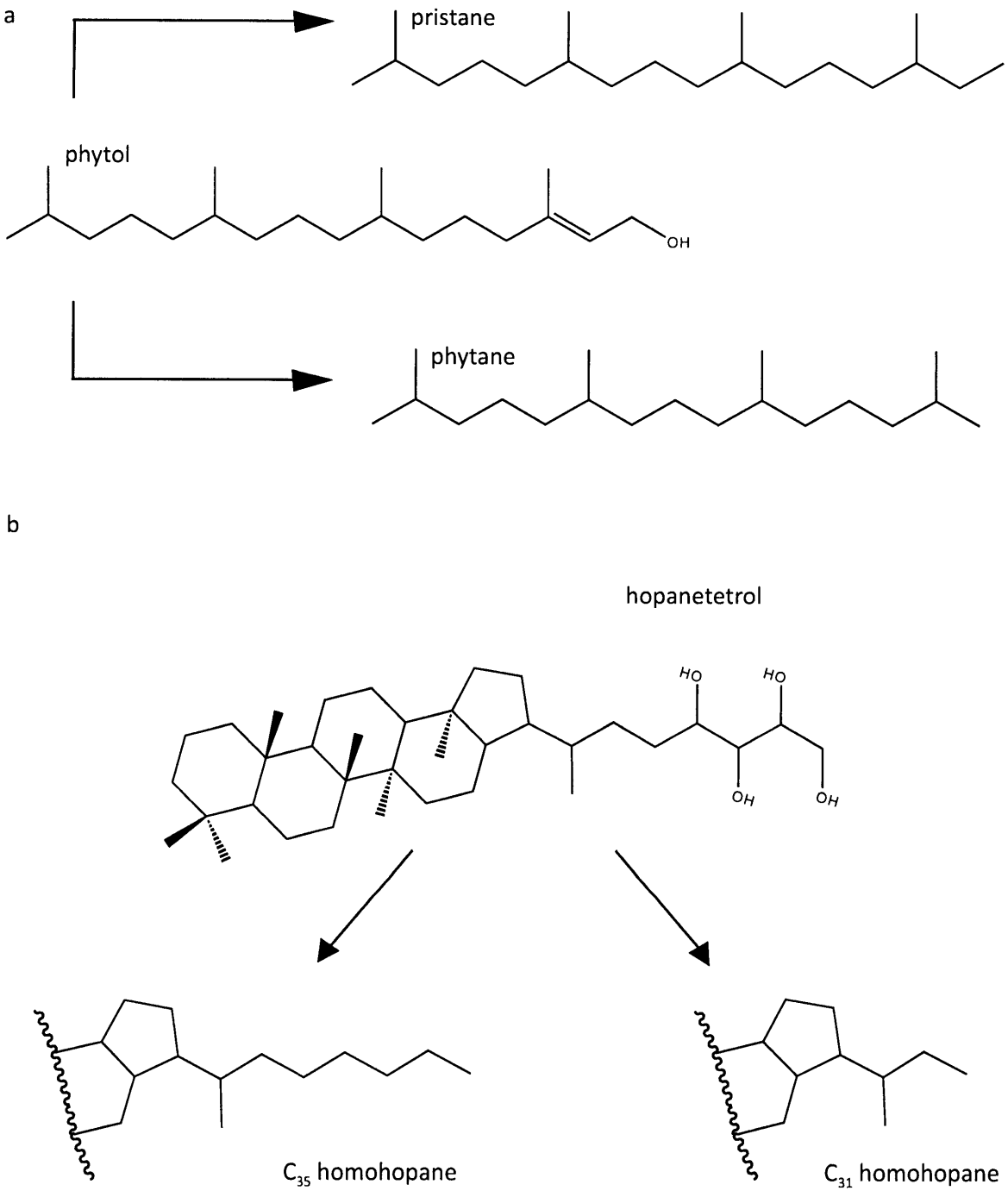

Figure 1.1 Sedimentary diagenetic production of (a) pristane and phytane from phytol and (b) homohopanes from hopanetetrol.

to phytane ratio, there are limited sources of the extended hopanes. However, like the pristane to phytane ratio, values interpreted as indicative of oxic versus anoxic deposition are determined empirically. For these reasons, the homohopane index, like the pristane/phytane ratio should be used in conjunction with other redox proxies in order to lead to a more robust understanding of the redox state of the paleoenvironment.

In addition to the biomarkers listed above, there are a number of other compounds that are considered indicative of anoxia in the water column. These compounds are derived from known biological precursors in specific modern organisms that only live in a euxinic enironments.

One group of microorganisms that is often used is the Chlorobi, or Green Sulfur Bacteria. The Chlorobi are obligate phototrophs that utilize hydrogen sulfide as the electron donor in photosynthesis and therefore live entirely in conditions of photic zone euxinia. Chlorobi are commonly found in planktonic habitats with thermal or salinity stratified water columns and are only rarely detected in marine sedimentary rocks (Overmann 2001) where the sulfide is commonly below the photic zone. Some uncommon compounds produced as part of the photosystem of the Chlorobi can be traced through their diagenetic products in sedimentary rocks to the presence of these organisms and, by proxy, conditions of photic zone euxina, in the paleoenvironment (Summons and Powell 1986; Brocks and Summons 2003). The compounds that are most often studied can be roughly divided into two groups: derivatives of carotenoids and derivatives of chlorophyll.

Chlorobi produce the carotenoids, chlorobactene and isorenieratene, both C_{40} compounds. The green-pigmented Chlorobi produce the former, and the brown-pigmented Chlorobi produce the

later, although the specific carotenoid content is higher in the brown-pigmented variety (Overmann 2001). Although these carotenoids are not strictly required for photosynthesis, a significant growth rate defect was observed in mutant organisms where key genes for the carotenoid biosynthesis were knocked out, and these compounds were not produced (Frigaard et al. 2004).

Isorenieratene has two aromatic rings with a 2,3,6-trimethyl-substitution pattern linked by an isoprenoid chain. Chlorobactene has only one aromatic ring and an extended isoprenoid chain. The isoprenoid chains in both molecules have conjugated double bonds. The primary diagenetic products of these carotenoids are the partially reduced compounds, chlorobactane and isorenieratane. These compounds have the aromatic rings but not the conjugated double bond system. (See Figure 1.2.) During diagenesis, the primary product of chlorobactene and isorenieratene, in addition to the partially reduced parent compounds, is a series of aryl isoprenoids with the aromatic group attached to an isoprenoid chain of varying lengths. The aryl isoprenoids derived from either carotenoid are mutually indistinguishable (Summons and Powell 1986). A study by Koopmans et al (1996) presented a series of reactions involving both hydrogenation and oxidation within the sediments that can produce 2,3,6 aryl isoprenoids from precursors other than isorenieratene or chlorobactene, such as β-carotene. The conditions required for this reaction series to take place may be unlikely in sediments, but the presence of this pathway shows the importance of the identification of the C_{40} carotenoid derivatives along with aryl isoprenoids in arguing for their origin from Chlorobi.

Another compound that may derive from the diagenesis of these carotenoids is crocetane, a C_{20} isoprenoid with a tail-to-tail linkage in the center. (See Figure 1.2.) It has been suggested that the cleavage of the terminal aryl groups of isorenieratane or chlorobactane may be a source of crocetane

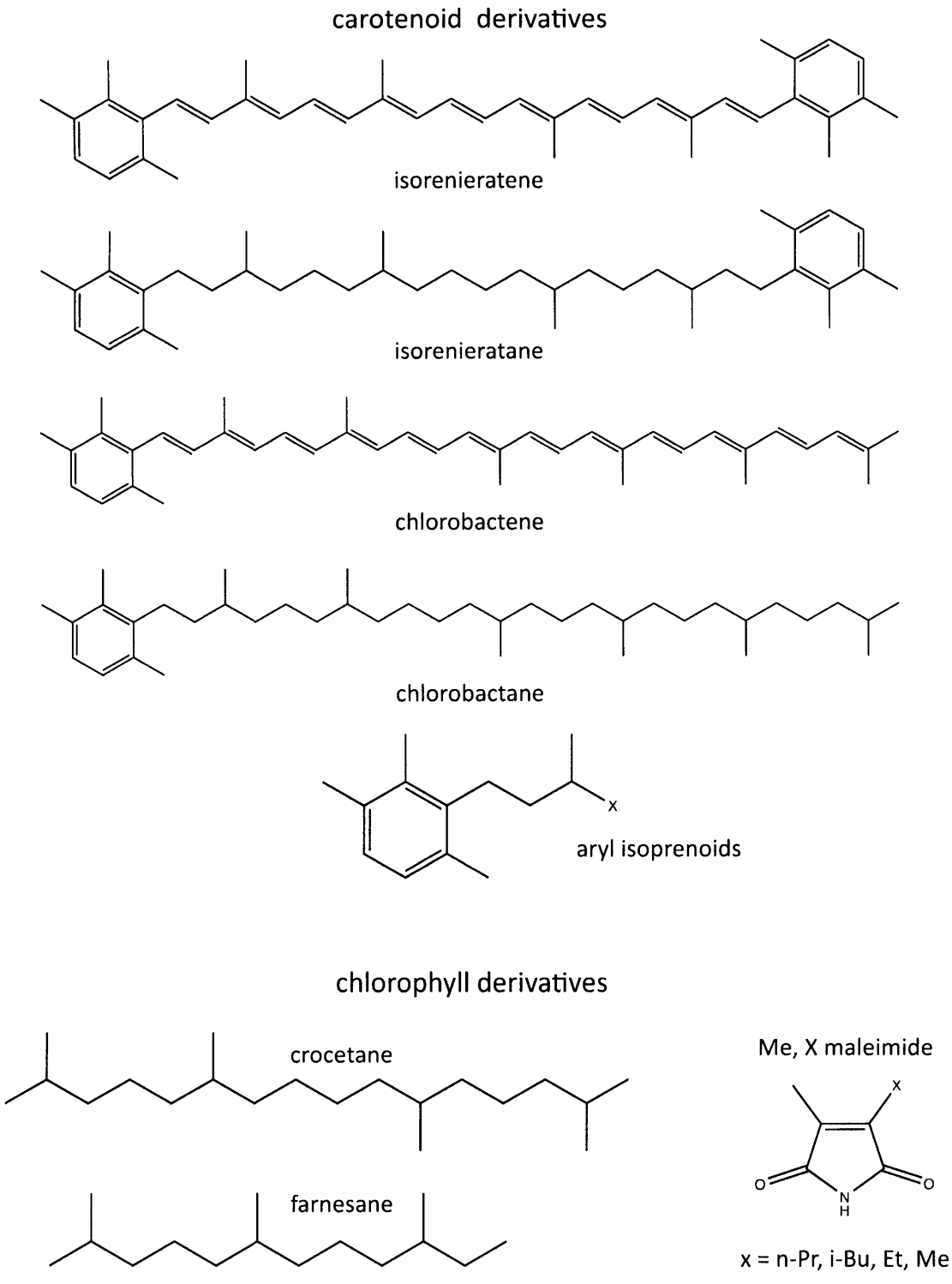

Figure 1.2 Structures of compounds derived from the photosynthetic complex of Chlorobi.

in the sedimentary rocks (Maslen et al. 2009). However, this compound may also be formed from the diagenetic breakdown of archaeal lipids and must be measured in conjunction with other compounds to be considered a biomarker for euxinia. Crocetane can be a difficult compound to measure because it nearly co-elutes with phytane under standard gas chromatographic conditions typical for the measurement of saturated hydrocarbons. Therefore, this compound is most accurately measured by using either multiple reaction-monitoring (MRM) or GC-MS-MS instruments.

In addition to the distinct carotenoids produced by Chlorobi, the brown-pigmented variety also produces a unique form of chlorophyll, bacteriochlorophyll e, in addition to the more common bacteriochlorophylls c and d produced by the green-pigmented variety (Overmann 2001). Different side chains and substitution patterns on the tetrapyrrole ring distinguish the many forms of chlorophyll. Diagenetic products that preserve these features are useful in biomarker analysis.

Farnesane, a C_{15} isoprenoid, is derived from farnesol, the side chain for chlorophyll e. (See Figure 1.2.) However, farnesane should not be considered a proxy for Chlorobi by itself, since like many isoprenoids, it may be produced through the diagenetic breakdown of longer isoprenoid chains sourced from other organisms, such as Archaea.

Maleimides, oxidation products of the tetrapyrrole chlorophyll ring itself, are five-membered N-containing rings with two attached oxygen atoms (1H-pyrrole-2,5-dione) that maintain the substitution patterns present on the original molecule during diagenesis. (See Figure 1.2.) Because of the relatively large number of heteroatoms in these molecules, they are found in the polar fraction of the lipid extract and can be difficult to identify. Maleimides are named according to the small

carbon chain substitutions on C-3 and C-4 carbons in the ring. Of the wide range of maleimides present, the generally rare Me *n*-Pr and Me *i*-Bu are thought to be derived from the bacteriochlorophylls c, d and e. The more abundant Me Et and Me Me maleimides are thought to be derived from chlorophyll a, the major chlorophyll in higher plants and photoplankton (Grice et al. 1996). Since the Chlorobi are the dominant source of chlorophyll e to the sedimentary record in anoxic environments, the Me *n*-Pr and Me *i*-Bu maleimides are generally considered fairly specific for the presence of these organisms.

The $\delta^{13}C$ value of biomarkers biosynthesized by Chlorobi is the most significant feature that differentiates them from similar or identical compounds produced by other organisms. Chlorobi use the reverse TCA cycle to fix carbon (Evans et al. 1966; Sirevåg and Ormerod 1970), leading to biomass that is enriched in ^{13}C relative to biomass produced from the same carbon source through other carbon-fixing pathways (Quandt et al. 1977; Sirevåg et al. 1977). This enrichment is conferred upon all of the molecules in the organism. Compounds discussed above that may be derived from multiple sources should show an enrichment relative to the bulk organic carbon when derived from Chlorobi. Indeed, this enrichment has been measured in carotenoid derivatives and chlorophyll derivatives in a number of locations in the rock record (Grice et al. 1997; Grice et al. 1998). In practice, it can be difficult to measure the isotopic values of Chlorobi-derived organic matter for two reasons: first, they represent a relatively small contribution to the overall hydrocarbon pool, and second, aromatic and polar compounds can be difficult to isolate. Even farnesane, which is a saturated hydrocarbon, can have somewhat ambiguous carbon isotopic values. Because farnesane may be derived from a number of organisms, including Chlorobi, its enrichment may not be as significant as if it were derived from a single source. However, the combination of the specific

biomarker compounds with a distinct $\delta^{13}C$ value, when these measurements are possible, provides evidence for inputs from the lipids of Chlorobi.

Carotenoid and chlorophyll derived biomarkers from Chlorobi with high $\delta^{13}C$ values relative to biomass are a powerful indicator of significant input from Chlorobi to sedimentary rocks, and therefore the presence of photic zone euxinic conditions during deposition.

Although the origins of the compounds gammacerane and 28,30 bisnorhopane are considered less certain than those derived from the carotenoids or chlorophyll of Chlorobi, the presence of these biomarkers is considered indicative of anoxia. Both compounds are produced by organisms that live at an oxic-anoxic interface in the water column; empirically, these compounds increase in conjunction with other biomarkers for water column anoxia. These compounds are not as widely used as other biomarker proxies of water-column anoxia because of their less-specific nature and dependence on specific, yet unknown, members of the microbial community. Instead, gammacerane and 28,30 bisnorhopane are more often used in conjunction with the other biomarker proxies to strengthen the argument for the presence of a well-defined and stable water-column chemocline.

Gammacerane is a hydrocarbon with five cyclohexane rings, and (See Figure 1.3) it is thought to derive from tetrahymanol (ten Haven et al. 1987; Kleemann et al. 1990). This compound is predominantly produced by ciliates that live at the anoxic interface in water columns and feed on microorganisms that take advantage of the redox boundary (Harvey and McManus 1991; Sinninghe Damsté et al. 1995), though it is also produced by purple non-sulfur bacteria (Kleemann et al. 1990). Although this compound may be present in a wide range of sedimentary rocks, high abundances in

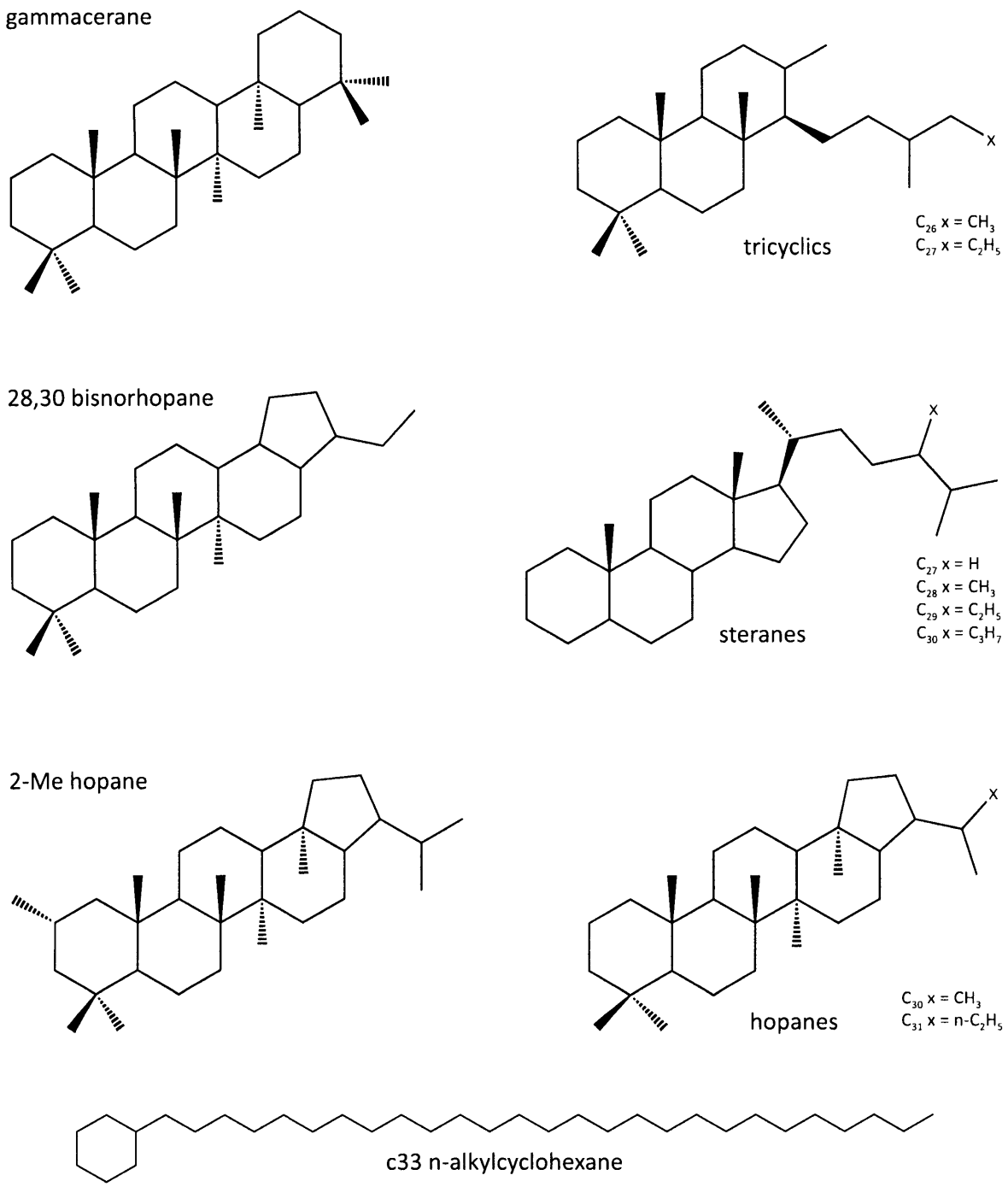

Figure 1.3 Structures of biomarkers referred to in text.

the rock record (values >10 measured 10*gammacerane/(gammacerane+C_{30} hopane)) indicate a stratified marine water column during deposition and correlate well with low pristane/phytane ratios (Peters et al. 2005).

High concentrations of 28,30 bisnorhopane, a desmethylhopane, (see Figure 1.3) have also been shown to correlate well with other markers of anoxic conditions such as the pristane to phytane ratio and the homohopane index in sedimentary rocks of similar thermal maturity. Although it is unclear which organism produces the precursor biomolecule of 28,30 bisnorhopane or what this precursor compound may be, one suggestion is that it is produced by chemoautotrophic bacteria that inhabit the oxic-anoxic interface such as Beggiatoa (Peters et al. 2005).

Biomarkers for Microbial Community

Biomarkers that are indicative of the microbial community can be linked to specific precursor molecules. The associations made with these biomarkers are considered more robust than those that are calculated empirically, although they rely on the assumption that ancient organisms produced the same or very similar compounds to those produced by their modern counterparts.

The ratio of total hopanes to total steranes is biomarker proxy indicative of the general microbial community that contributed biomass to the sedimentary rocks. This measure reflects the relative input of bacteria to eukaryotes, although individual organisms can have wide variations in their hopanoid and steroid contents (Peters et al. 2005). In marine sedimentary rocks high values of this ratio are indicative of a significant bacterial input or significant bacterial reworking of microbial matter, and lower values are more indicative of organic matter with higher contributions from algae.

Since the compound classes of hopanes and steranes contain a large number of assorted compounds made by a range of bacteria and eukaryotes, respectively, this is one of the less specific biomarker ratios. Still, it can be used to give a broad understanding of large-scale changes in the microbial community.

More specifically, the C_{27} and C_{29} steranes are produced by the red and green algae, respectively (Kodner et al. 2008). (See Figure 1.3.) Although both of these organisms live in the oxic photic zone, their different nutrient requirements allow them to thrive in different conditions. Red algae, with a lower requirement for iron, can survive in oceans with sulfidic deep waters where free iron might be removed through reaction with the sulfur. Green algae, which have a higher iron requirement, may be more abundant in oceans with ferruginous deep waters (Kelly 2009). A radiation of plastids derived from red algae in the early Triassic period, leading to higher relative values of C_{27} steranes, may have been driven by the selective pressures encouraging heterotrophic organisms to acquire a plastid (Falkowski et al. 2004).

In cultured organisms, it has been shown that some cyanobacteria produce bacteriohopane polyols with a 2-methyl substitution (Summons et al. 1999). (See Figure 1.3.) What purpose these compounds have in the cyanobacteria is unknown; however, their structural similarities to the membrane sterols of eukaryotes lead to the presumption that they serve some function in membrane stabilization. When these compounds are altered through diagenesis, the alcohol groups are substituted with a methyl group in the C-2 position, but the hopane hydrocarbon structure is preserved, producing a compound known as a 2-methylhopane. Shales with a high percentage (above 10%) of 2-methylhopane to standard C_{30} hopane (a ratio known as the 2-methylhopane index, or 2-MHI) are thought to have been deposited at times when the cyanobacterial input to the

sediments was significant (Summons et al. 1999). In black shales from the Mesozoic oceanic anoxic events, the highest values of the 2-MHI, around 20%, were measured in the same intervals in which other indicators of anoxia, both lithological and isotopic, were the highest. It is suspected that this indicates a greater contribution from cyanobacteria, which, in a stratified water column, are conferred a competitive edge by their ability to fix nitrogen when nutrients are scarce (Kuypers et al. 2004). Other organisms have been shown to produce 2-methylhopane, specifically the purple non-sulfur bacterium *Rhodopseudomonas palustris* (Rashby et al. 2007). However, these organisms do not thrive in conditions of euxinia, and may not be a significant contributor to marine sediments.

Positive values of $\delta^{15}N$ have been interpreted as signifying normal trophic conditions. As bulk isotopic values decrease to zero and move to negative, it is thought to indicate disturbances to the nitrogen cycle that involve less of the oxidized nitrogen species and more nitrogen fixation and possibly NH_3 uptake. In an anoxic water column, there would be increased denitrification, the conversion of nitrate to N_2, by heterotrophic bacteria. This serves to reduce nutrient N/P ratios during oceanic anoxic events, allowing cyanobacteria an advantage over algae and other phototautotrophs that cannot fix nitrogen. During this process, the cyanobacteria also impart a lower $\delta^{15}N$ isotopic value on the biomass (Rejmankova et al. 2004). When these organisms contribute significantly to sediments, this nitrogen depletion is seen in bulk nitrogen isotopes in the rock record (Kuypers et al. 2004; Chikaraishi et al. 2008).

Another isotopic measurement that has been used to identify the presence of a stratified water column during deposition of sedimentary rocks is the difference in the $\delta^{13}C$ isotopic value of the isoprenoids pristane and phytane relative to the $\delta^{13}C$ isotopic value of the *n*-alkanes *n*-C_{17} and *n*-C_{18}. As discussed above, the isoprenoids pristane and phytane are derived primarily from the phytol side

chain of chlorophyll a, and therefore record the isotopic value of primary producers. In contrast, the *n*-alkanes are derived from both primary producers and heterotrophs. Heterotrophs record an enrichment $\delta^{13}C$ in their lipids of roughly 3‰, which increases with trophic level (Hayes 2001). (See Figure 1.4.)

In the hypothesis proposed by Logan et al. (1995), when autotrophs are the dominant source of organic matter to the sediments, the *n*-alkanes are depleted in $\delta^{13}C$ relative to the isoprenoids. However, enrichment in the $\delta^{13}C$ of *n*-alkanes relative to the isoprenoids was measured in numerous Proterozoic marine sections. (See Figure 1.5.) This reversal of isotopic ordering was interpreted as a signal of significant heterotrophic reworking in a stratified water column, leading to an increased proportion of isotopically enriched heterotrophic biomass being deposited in the sediments. The isotopic ordering considered "normal" occurs in Phanerozoic sediments in which an enrichment of the isoprenoids was measured. Intermittent enrichment of *n*-alkanes over isoprenoids corresponds to periods where other biomarkers for anoxia are highest. This biomarker proxy, like the hopane/sterane ratio, involves input from a very wide range of sources and should only be used for a broad understanding of changes in the microbial community and perturbations to the carbon cycle.

Biomarkers for Depositional Environments

The depositional environments of sedimentary rocks can be inferred from their lithologies and patterns of sedimentation. In hydrocarbon-producing basins, where sedimentary organic matter is abundant and of appropriate maturity, hydrocarbon biomarkers can provide an independent means of reconstructing paleoenvironmental conditions (Seifert and Moldowan 1981; Zumberge 1987;

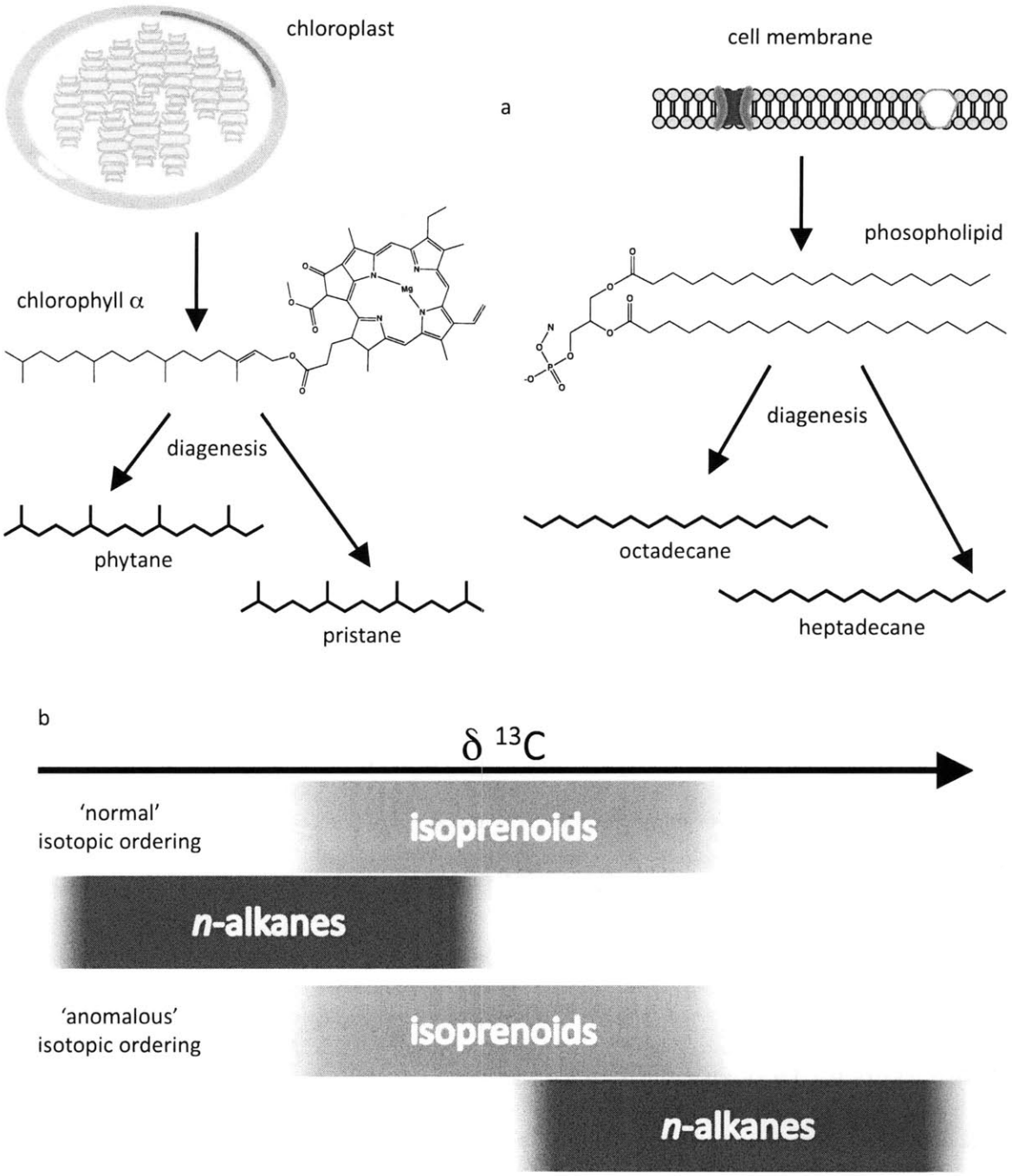

Figure 1.4 Isotopic ordering of isoprenoids vs. *n*-alkanes. (a) Chlorophyll α from chloroplasts has a phytol side chain, which degrades to pristane and phytane during diagenesis. Phospholipids from cell membranes degrade to n-alkanes such as octadecane and heptadecane. (b) In modern environments, with 'normal' isotopic ordering, autotrophs are the dominant source of organic matter and isoprenoids are enriched relative to *n*-alkanes. Reversal of this isotopic ordering gives a positive Δδ value, or 'anomalous' isotopic ordering.

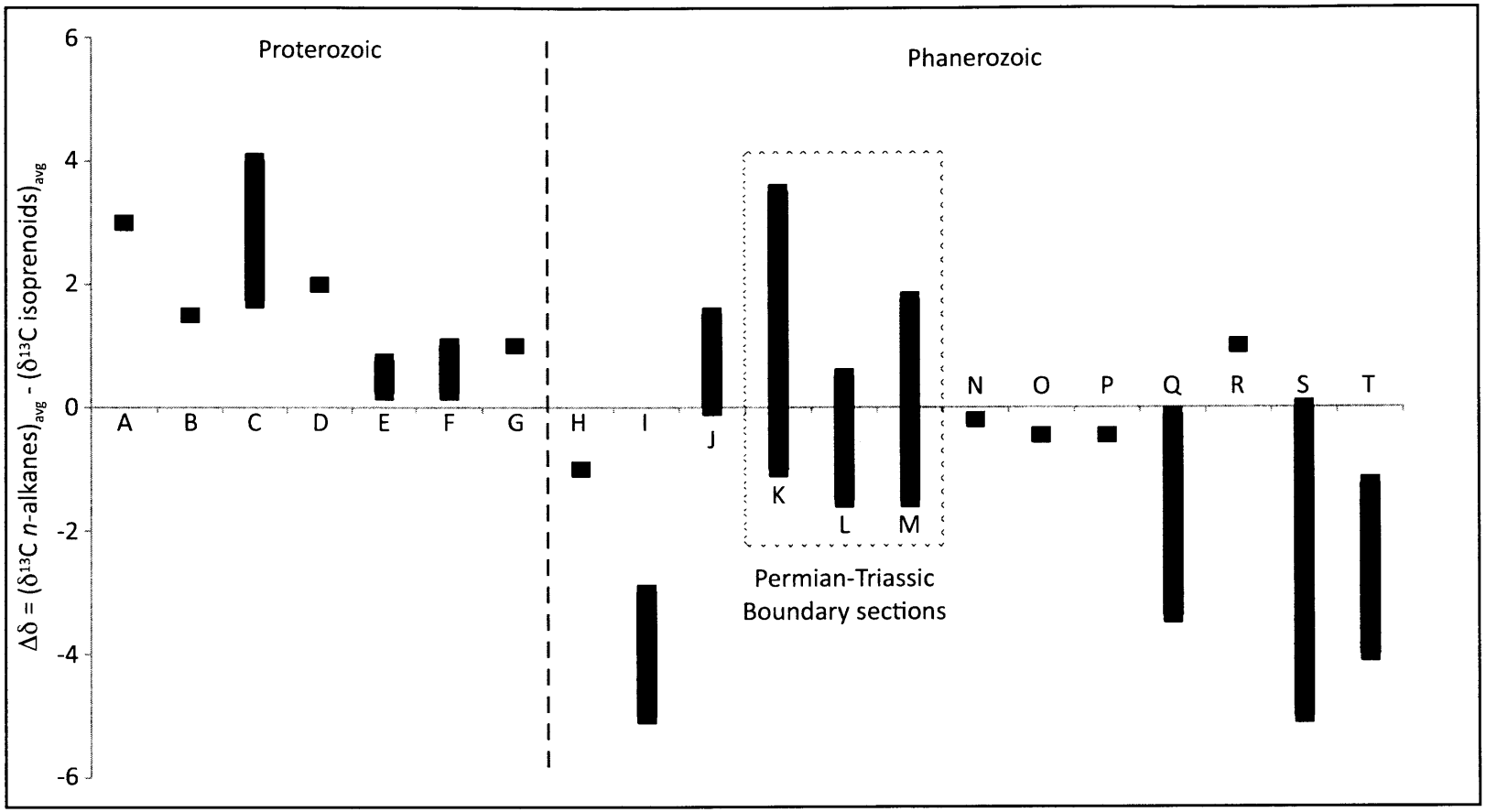

Figure 1.5 Enrichment of *n*-alkanes relative to isoprenoids from a range of environments. **K**, from Meishan, China and **L**, from Peace River Basin, Canada, were measurements made in this thesis from the Permian-Triassic boundary; **M**, from the Perth Basin, Australia (Grice et al. 2005) is also from this boundary. **J** and **R** are from Phanerozoic basins deposited beneath anoxic water columns. **A** Mount Bruce Supergroup, Pilbara Craton, Australia, 2.78-2.45Ga (Brocks et al. 2003). **B** Barney Creek Formation, McArthur Basin, Australia, 1690Ma; **C** Nonesuch Formation, USA, 1055Ma; **D** Walcott Member, Chuar Group, USA, 850Ma; **E** Bitter Springs Formation, Amadeus Basin, Australia, 800Ma; **F** Visingso Group, Sweeden, 775Ma (Logan et al. 1995). **G** South Oman Salt Basin, Buah Formation, Oman, 600Ma; **H** South Oman Salt Basin, Buah Formation, Oman, 547Ma (Kelly 2009). **I** Officer Basin, Australia, 510Ma; **J** Maquoketa Group, Illinois Basin, USA, 450Ma (Logan et al. 1995). **N** Paris Basin Shale, France, 180Ma; **O** West Hammersfest Basin, Barents Sea, 168Ma; **P** Guatamalan Carbonate, 100Ma (Bjoroy 1992). **Q** Eastern Llanos Baisn, Colombia, 65Ma (Cortez et al 2010). **R** Green River Shale, USA, 40Ma; **S** Baise Basin, Guanxi, China and Mulhouse Basin, Alsace, France, 28Ma (Logan et al. 1995). **T** Modern cultured algal lipids (Schouten et al. 1998).

Brocks and Summons 2003; Peters et al. 2005). Biomarker proxies can also be used to ensure that bitumen migration or later contamination has not affected the correlation between the bitumen and the source rock. Both of the biomarker proxies described below are measured relative to values that have been empirically determined by a large suite of oils and are most robust when evaluated in conjunction with each other.

The C_{30} sterane index is the ratio of C_{30} steranes (24-*n*-propylcholestanes) to total C_{27}-C_{30} steranes. (See Figure 1.3.) This index facilitates the identification of sedimentary rocks with high marine OM input due to the observation that marine pelagophyte algae biosynthesize 24-*n*-propylcholesterol (Giner et al. 2009), which is diagenetically altered to 24-*n*-propylcholestane isomers in sediments (Moldowan 1984). Empirical analysis of a large suite of oils has shown that C_{30} sterane abundances in excess of 4% of total C_{27}-C_{30} steranes indicate significant contribution from these organisms to OM deposition (Peters et al. 2005).

A combination of two different biomarker ratios, the C_{26}/C_{25} tricyclic terpane plotted against the $C_{31}22R/C_{30}$hopane, is a parameter that has been shown empirically to differentiate between marine and lacustrine source rocks as these compounds are produced in different ratios by microorganisms from these environments. (See Figure 1.3.) More than 500 crude oil samples from locations across the globe were used to show that marine source rocks generally have a low (<1.2) C_{26}/C_{25} tricyclic ratio and higher (>0.2) C_{31}/C_{30}hopane ratio, whereas lacustrine sedimentary rocks show the opposite result (Peters et al. 2005).

Potential Age-Sensitive Biomarkers

The final group of biomarkers described here includes those that can be used as a broad indicator of the age of the organic carbon preserved in sedimentary rocks. Like the depositional environments, the age of the source rock can be determined by independent means that do not require biomarkers, such as index fossils and radioactive isotopes. As the preservation of biomarkers is dependent on a number of factors, biomarkers alone cannot be used for dating sections. However, as different organisms evolve and microbial communities change, the compounds preserved in sedimentary rocks change with respect to time in uniform fashion. Also, as with biomarkers for depositional environments, age-related biomarkers provide an independent means to ensure good correlation between bitumen and source rock, assuring that younger petroleum has not migrated through the rocks and compromised the interpretation of the other biomarkers

Quantities of the biomarker C_{33} *n*-alkylcyclohexane (*n*-heptacosylcyclohexane) (see Figure 1.3) higher than background relative to the C_{34} *n*-alkane have been identified in sedimentary rocks from the Perth Basin in Australia and East Greenland (Grice et al. 2005; McIldowie and Alexander 2005). The first appearance of this compound in the East Greenland section corresponds with the start of the late Permian extinction event. Although the specific origin is unknown, Grice et al. (2005) showed a correlation between the C_{33} *n*-alkylcyclohexane and the spinose acritarch genera *Michrystridium* and *Veryhachium*, indicating that these compounds may be derived from these organisms. Thermal maturity seems to have no effect on the abundance of this compound. A study of 500 oils of various types and ages failed to show any evidence of elevated levels of this compound outside of the Permian-Triassic boundary (McIldowie and Alexander 2005), indicating that this compound is of use as a biomarker for the relatively small range of time around this boundary.

Increases in the proportion of C_{28} steranes can record the relative importance of the chlorophyll c-containing plankton (dinoflagellates, diatoms and coccolithophorids). (See Figure 1.3.) This is particularly evident in long timescale datasets when they rose to prominence during the Mesozoic and Cenozoic (Knoll et al. 2007). Studies of this parameter in rocks from all ages (Peters et al. 2005) have suggested that typical values for the ratio of C_{28} to C_{29} steranes are:

- <0.5 for the oldest Paleozoic rocks;
- between 0.4 and 0.7 for oils between the younger Paleozoic and the end of the Jurassic; and
- ~0.7 for rocks from the upper Jurassic to the Miocene.

However, since the values of this biomarker do not have a very wide range, they should not be used to distinguish the age of different rocks without comparison to other age-related biomarkers or without using other methods. It is also worth noting that distinct but short-lived increases have been observed in this ratio in correlation with extinction events in the early Phanerozoic (Schwark and Empt 2006), which may complicate the understanding of age relationships.

The biomarkers presented here are a broad group of compounds that can be useful for identifying the redox conditions, the microbial community and the depositional environment for sedimentary rocks from the late Paleozoic and early Mesozoic. (See Table 1.1 for summary.)

References

Brocks, J. J. and R. E. Summons (2003). Sedimentary Hydrocarbons, Biomarkers for Early Life. Treatise on Geochemistry. D. H. a. K. K. T. Heinrich. Oxford, Pergamon: 63-115.

Chikaraishi, Y., Y. Kashiyama, N. O. Ogawa, H. Kitazato, M. Satoh, S. Nomoto and N. Ohkouchi (2008). "A Compound-Specific Isotope Method for Measuring the Stable Nitrogen Isotopic Composition of Tetrapyrroles." Organic Geochemistry **39**(5): 510-520.

Didyk, B. M., B. R. T. Simoneit, S. C. Brassell and G. Eglinton (1978). "Organic Geochemical Indicators of Palaeoenvironmental Conditions of Sedimentation." Nature **272**(5650): 216-222.

Biomarkers	Origin	Precursor lipid(s)	Significant Values
pristane/phytane	phototrophs (archaea)	chlorophyll a, b	rough proxy; >1 indicates anoxic sediments; <1 indicates oxic sediments
homohopane index (C_{35}/total hopane or C_{34}/C_{35})	bacteria	bacterohopanepolyols	>10% C_{35}/total hopane (or >0.6 C_{35}/C_{34}) indicates anoxic sediments
2,3,6 aryl isoprenoids	Chlorobi	chlorobactene or isorenieratene	presence indicates photic zone euxinia (PZE)
chlorobactane	Chlorobi (green)	chlorobactene	photic zone euxinia
isorenieratane	Chlorobi (brown)	isorenieratene	photic zone euxinia
crocetane	Chlorobi (archaea)	C_{40} carotenoids	photic zone euxinia
farnesane	Chlorobi (phototrophs)	bacteriochlorophyll e	photic zone euxinia
maleimide (Me *n*-Pr and Me i-Bu)	Chlorobi	bacteriochlorophyll c,d,e	photic zone euxinia
gammacerane	ciliate or purple non-sulfur bacteria	tetrahymanol	presence indicates stratified water column
28,30 bisnorhopane	unknown (chemoautotrophs)	unknown	anoxic sedimentary environment
hopane/sterane	bacteria/eukarya	hopanols; sterols	rough proxy; >1 bacterial inputs predominate; <1 eukaryotic inputs predominate
C_{27}/C_{29} sterane	algae	C_{27} sterols; C_{29} sterols	>1 red algal inputs predominate; <1 green algal inputs predominate
2-methylhopane index	cyanobacteria	2-methylhopane polyols	>10% (in shales) indicate increased cyanobacterial input during OAE
$\delta^{15}N$ isotope	cyanobacteria	chlorophylls	negative values indicate disturbances in nitrogen cycle
$\Delta\delta$ ($[\delta^{13}C\ n\text{-alk}]_{avg}$ - $[\delta^{13}C\ iso]_{avg}$)	bacteria/eukarya	phospholipids; chlorophyll a, b	positive values indicate perturbations to Phanerozoic carbon cycle
C_{30} sterane index	pelagophyte algae	24-*n*-propylcholestanes	>4% indicates marine input
C_{26}/C_{25} tricyclic vs. C_{31}/C_{30} hopane	bacteria/eukarya	unknown (regular polyisoprenols); hopanols	<1.2 tricyclic and >0.2 hopane ratio correlate with high marine input
C_{33} *n*-ACH	unknown	unknown	>*n*-C34 observed exclusively in early Triassic sediments
C_{28}/C_{29} sterane	algae	C_{28} sterols; C_{29} sterols	<0.5 in oldest Paleozoic; between 0.4 and 0.7 young Paleozoic to Jurassic; ~0.7 for Jurassic to Miocene

Table 1.1 Summary of biomarkers discussed in the text. References are included in the text.

Evans, M. C. W., B. B. Buchanan and D. I. Arnon (1966). "A New Ferredoxin-Dependent Carbon Reduction Cycle in a Photosynthetic Bacterium." Proceedings of the National Academy of Sciences of the United States of America **55**(4): 928-934.

Falkowski, P. G., M. E. Katz, A. H. Knoll, A. Quigg, J. A. Raven, O. Schofield and F. J. R. Taylor (2004). "The Evolution of Modern Eukaryotic Phytoplankton." Science **305**(5682): 354-360.

Frigaard, N. U., J. A. Maresca, C. E. Yunker, A. D. Jones and D. A. Bryant (2004). "Genetic Manipulation of Carotenoid Biosynthesis in the Green Sulfur Bacterium Chlorobium Tepidum." Journal of Bacteriology **186**(16): 5210-5220.

Giner, J.-L., H. Zhao, G. L. Boyer, M. F. Satchwell and R. A. Andersen (2009). "Sterol Chemotaxonomy of Marine Pelagophyte Algae." Chemistry & Biodiversity **6**(7): 1111-1130.

Grice, K., R. Gibbison, J. E. Atkinson, L. Schwark, C. B. Eckardt and J. R. Maxwell (1996). "Maleimides (1h-Pyrrole-2,5-Diones) as Molecular Indicators of Anoxygenic Photosynthesis in Ancient Water Columns." Geochimica et Cosmochimica Acta **60**(20): 3913-3924.

Grice, K., P. Schaeffer, L. Schwark and J. R. Maxwell (1997). "Changes in Palaeoenvrionmental Conditions During Deposition of the Permian Kupferschiefer (Lower Rhine Basin, Northwest Germany) Inferred from Molecular and Isotopic Compositions of Biomarker Components." Organic Geochemistry **26**(11-12): 677-690.

Grice, K., S. Schouten, K. E. Peters and J. S. Sinninghe Damste (1998). "Molecular Isotopic Characterisation of Hydrocarbon Biomarkers in Palaeocene-Eocene Evaporitic, Lacustrine Source Rocks from the Jianghan Basin, China." Organic Geochemistry **29**(5-7): 1745-1764.

Grice, K., R. J. Twitchett, R. Alexander, C. B. Foster and C. Looy (2005). "A Potential Biomarker for the Permian-Triassic Ecological Crisis." Earth and Planetary Science Letters **236**(1-2): 315-321.

Harvey, H. R. and G. B. McManus (1991). "Marine Ciliates as a Widespread Source of Tetrahymanol and Hopan-3b-Ol in Sediments." Geochim. Cosmochim. Acta **55**: 3387-3390.

Hayes, J. M. (2001). Fractionation of the Isotopes of Carbon and Hydrogen in Biosynthetic Processes. Stable Isotope Geochemistry, Reviews in Mineralogy and Geochemistry. J. W. Valley and D. R. Cole. Washington, DC, Mineralogical Society of America**:** 225-278.

Kelly, A. E. (2009). Hydrocarbon Biomarkers for Biotic and Environmental Evolution through the Neoproterozoic-Cambrian Transition. Earth, Atmospheric and Planetary Sciences. Cambridge, MA, Massachusetts Institute of Technology. **PhD:** 154.

Kleemann, G., K. Poralla, G. Englert, H. Kjøsen, S. Liaaen-Jensen, S. Neunlist and M. Rohmer (1990). "Tetrahymanol from the Phototrophic Bacteriaum Rhodopseudomonas Palustris: First Report of a Gammacerane Triterpene from a Prokaryote." J. of General Microbiology **136**: 2551-2553.

Knoll, A. H., R. E. Summons, J. R. Waldbauer and J. Zumberge (2007). The Geological Succession of Primary Producers in the Oceans. The Evolution of Photosynthetic Organisms in the Oceans P. Falkwoski and A. H. Knoll. Boston, Elsevier**:** 133-163.

Kodner, R. B., A. Pearson, R. E. Summons and A. H. Knoll (2008). "Sterols in Red and Green Algae: Quantification, Phylogeny, and Relevance for the Interpretation of Geologic Steranes." Geobiology **6**(4): 411-420.

Koopmans, M. P., J. Köster, H. M. E. Van Kaam-Peters, F. Kenig, S. Schouten, W. A. Hartgers, J. W. de Leeuw and J. S. Sinninghe Damste (1996). "Diagenetic and Catagenetic Products of Isorenieratene: Molecular Indicators for Photic Zone Anoxia." Geochimica et Cosmochimica Acta **60**(22): 4467.

Kuypers, M. M. M., Y. van Breugel, S. Schouten, E. Erba and J. S. S. Damste (2004). "N2-Fixing Cyanobacteria Supplied Nutrient N for Cretaceous Oceanic Anoxic Events." Geology **32**(10): 853-856.

Logan, G. A., J. M. Hayes, G. B. Hieshima and R. E. Summons (1995). "Terminal Proterozoic Reorganization of Biogeochemical Cycles." Nature **376**(6535): 53-56.
Maslen, E., K. Grice, J. D. Gale, C. Hallmann and B. Horsfield (2009). "Crocetane: A Potential Marker of Photic Zone Euxinia in Thermally Mature Sediments and Crude Oils of Devonian Age." Organic Geochemistry **40**(1): 1-11.
McIldowie, M. and R. Alexander (2005). "Identification of a Novel C33 N-Alkylcyclohexane Biomarker in Permian-Triassic Sediments." Organic Geochemistry **36**(10): 1454-1458.
Moldowan, J. M. (1984). "C30-Steranes, Novel Markers for Marine Petroleums and Sedimentary Rocks." Geochimica et Cosmochimica Acta **48**(12): 2767-2768.
Overmann, J. (2001). Green Sulfur Bacteria. Encyclopedia of Life Sciences. J. Battista, John Wiley & Sons.
Peters, K. E., J. M. Moldowan and C. C. Walters (2005). The Biomarker Guide. Cambridge, UK; New York, Cambridge University Press.
Quandt, L., G. Gottschalk, H. Ziegler and W. Stichler (1977). "Isotope Discrimination by Photosynthetic Bacteria." FEMS Microbiology Letters **1**(3): 125-128.
Rashby, S. E., A. L. Sessions, R. E. Summons and D. K. Newman (2007). "Biosynthesis of 2-Methylbacteriohopanepolyols by an Anoxygenic Phototroph." Proceedings of the National Academy of Sciences of the United States of America **104** (38): 15099-15104.
Rejmankova, E., J. Komarkova and M. Reimanek (2004). "D15n as an Indicator of N2-Fixation by Cyanobacterial Mats in Tropical Marshes." Biogeochemistry **67**: 353-368.
Schwark, L. and P. Empt (2006). "Sterane Biomarkers as Indicators of Palaeozoic Algal Evolution and Extinction Events." Palaeogeography, Palaeoclimatology, Palaeoecology **240**(1-2): 225-236.
Seifert, W. K. and J. M. Moldowan (1981). "Paleoreconstruction by Biological Markers." Geochimica et Cosmochimica Acta **45**(6): 783-798.
Sinninghe Damsté, J. S., F. Kenig, M. P. Koopmans, J. r. K^ster, S. Schouten, J. M. Hayes and J. W. de Leeuw (1995). "Evidence for Gammacerane as an Indicator of Water Column Stratification." Geochimica et Cosmochimica Acta **59**(9): 1895-1900.
Sirevåg, R., B. B. Buchanan, J. A. Berry and J. H. Troughton (1977). "Mechanisms of Co2 Fixation in Bacterial Photosynthesis Studied by the Carbon Isotope Fractionation Technique." Archives of Microbiology **112**(1): 35-38.
Sirevåg, R. and J. G. Ormerod (1970). "Carbon Dioxide Fixation in Green Sulphur Bacteria." Biochem. J. **120**(2): 399-408.
Summons, R. E., L. L. Jahnke, J. M. Hope and G. A. Logan (1999). "2-Methylhopanoids as Biomarkers for Cyanobacterial Oxygenic Photosynthesis." Nature **400**: 554-557.
Summons, R. E. and T. Powell (1986). "Chlorobiaceae in Paleozoic Seas Revealed by Biological Markers, Isotopes and Geology." Nature **319**(6056): 763-765.
ten Haven, H. L., J. W. de Leeuw, J. Rullkotter and J. S. S. Damste (1987). "Restricted Utility of the Pristane/Phytane Ratio as a Palaeoenvironmental Indicator." Nature **330**(6149): 641-643.
Zumberge, J. E. (1987). "Prediction of Source Rock Characteristics Based on Terpane Biomarkers in Crude Oils: A Multivariate Statistical Approach." Geochimica et Cosmochimica Acta **51**: 1625-1637.

Chapter 2

Events at the Permian-Triassic Boundary

Abstract

When the continents were amassed as Pangaea, and two oceans, the global Panthalassic and smaller Paleo-Tethys, were the major water bodies during the end-Permian period, the Earth experienced the largest extinction of the last 550 million years. Evidence in both the marine and terrestrial realms shows that this massive extinction was preceded by a prolonged period of ecosystem disruption. Four main trigger mechanisms have been proposed: bolide impact, methane hydrate release, Siberian Traps volcanism and anoxic oceanic conditions. Of these, the volcanism and anoxic oceans most closely correspond with the measured data and may be the result of underlying tectonic processes.

Palaeogeography and environment of the Permian-Triassic Boundary

As occurred a number of times in Earth's history, at the verge of the Permian-Triassic boundary (PTB) 252.2 Ma (Bowring et al. 1998; Mundil et al. 2004; Crowley et al. 2006), a single large super-continent called Pangaea amalgamated, encompassing the major portion of land mass. Pangaea nearly encircled a small ocean called the Paleo-Tethys, which had begun to open about 100 million years before. Two much smaller land blocks, which in modern times would become North and

South China, sat on the eastern margin of this ocean. The global Panthalassic Ocean covered the remaining portion of Earth's surface.

Paleo-reconstructions of the Late Permian period are based on fossil evidence and paleomagnetic studies, as well as climatic and sedimentological data (Torsvik and Cocks 2004). A relatively long glacial event from 330-260Ma lasted through the middle Permian period (Crowley and Berner 2001; Cocks 2007), although there is no evidence of glacial deposits spanning the boundary itself. During the late Permian period, humid belts extended into the high paleolatitudes where coals were deposited, whereas the environment near the equator within Pangaea was arid, as confirmed by the presence of evaporites. However, the blocks in the eastern Paleo-Tethys that were separated from Pangaea showed evidence of a wet equator (Torsvik and Cocks 2004), as did areas near the modern Arabian Peninsula, which were located on the edge of the supercontinent at the western margin of the Paleo-Tethys (Muttoni et al. 2009).

Biological evidence for extinction

The extent of the PTB extinction is best explained as the sudden disappearance of a large number of marine vertebrate and invertebrate families (Raup and Sepkoski 1982; Sepkoski 1984). (See Figure 2.1.) From this perspective it is clear that the mass extinction event that occurred at the end of the Permian period was the most profound of the Phanerozoic Era (Erwin 2006). In the marine ecosystem the extinction resulted in the loss of between 90-95% of invertebrate and vertebrate species (Jin et al. 2000; Knoll et al. 2007) in a less than half a million years (Bowring et al. 1999; Rampino et al. 2000). This extinction event particularly affected animals with passive respiratory systems and heavy calcification (Knoll et al. 1996; Knoll et al. 2007), and led to a profound

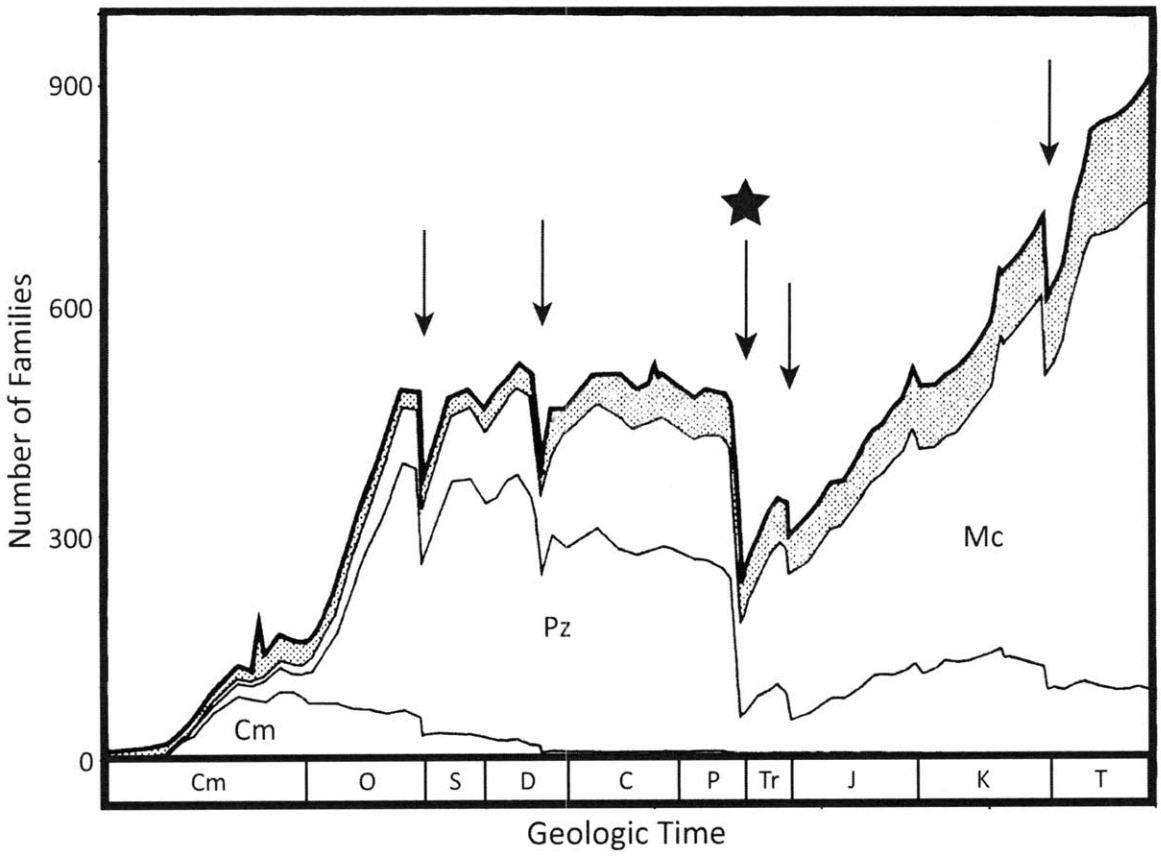

Figure 2.1 Taxonomic diversity throughout the Phanerozoic. The upper curve is the total number of families of marine vertebrates and invertebrates. The stippled region represents "poorly preserved" families, and the curves below show the diversity of highly-skeletonized fauna into three groups, Cambrian fauna (Cm), Paleozoic fauna (Pz) and Mesozoic-Cenozoic fauna (Mc) that dominated diversity during their representative eras. The five arrows indicate the five major mass extinctions during the Phanerozoic (in chronological order starting with the oldest, followed by their relative magnitudes in parentheses): Late Ordivician (12%), Late Devonian (14%), Late Permian (54%), Late Triassic (12%) and Late Cretaceous (11%). The Permian-Triassic bounary extinction, the subject of this thesis is denoted with a star. Modified from Raup and Sepkoski 1982 and Sepkoski 1984.

reorganization of marine ecosystems (Bambach et al. 2002; Wagner et al. 2006). Studies of the marine environment from the Global Stratotype Section and Point (GSSP) in Meishan, China, have pointed to two distinct episodes of microbial change related to the extinction at the PTB, outlined by $\delta^{13}C$ excursions in the carbonate record and anomalous hopane distributions (Xie et al. 2005; Wang 2007; Xie et al. 2007). A more comprehensive study of the Meishan section (Cao et al. 2009) reported evidence of multiple intervals of enhanced bacterial input to sedimentary rocks, indicating the extinction in the marine environment was part of a long-term perturbation to the ecosystem.

On land, although the extinction was not as severe as in the marine realm, considerable loss of animals and plants occurred during a significant terrestrial ecosystem collapse (Retallack 1995; Visscher et al. 1996; Looy et al. 2001; Retallack et al. 2003; Ward et al. 2005). Earlier studies (Retallack 1995) reported that, as in the oceans, late-Permian terrestrial ecosystems suffered an extensive loss of diversity at the boundary, followed by a period dominated by a limited number of cosmopolitan flora during the recovery until the Middle Triassic period when regionally differentiated flora returned. More recently, it has been proposed that the terrestrial ecosystem collapse occurred before the marine $\delta^{13}C$ excursion, but the actual extinction of many of the Permian flora came about only after a significant time lag of between 0.5-0.6 million years (Looy et al. 2001). Compared to the marine record, however the terrestrial record is significantly less well-documented, and there are concerns regarding the applicability of interpreting globally effects that may be only locally determined (Rees 2002).

Although it is often difficult to correlate events in the marine and terrestrial environments, a section from Eastern Greenland seems to incorporate both. A study of this section indicates that the collapse of marine and terrestrial ecosystems began at the same time, slightly preceding the

significant $\delta^{13}C$ excursion, although the terrestrial floral extinction continues longer than other groups (Twitchett et al. 2001). A double pulse of $\delta^{13}C$ towards more negative values in a terrestrial section from Xinjiang, China, was reported in Cao et al. (2008). The authors suggest that the first excursion correlates to the onset of marine anoxic and euxinic conditions and the initiation of terrestrial ecosystem disturbance, while the second excursion corresponds to the main extinction event in both terrestrial and marine fauna. Although not identical in both ecosystems, the overall pattern that has emerged from recent studies is that the Permian-Triassic extinction was a singular and brief catastrophic event that followed a more extended period of environmental disturbance.

Negative carbon isotope shifts in both organic carbon and carbonate have been observed concurrent with the boundary and are evidence of the magnitude of disruption of the marine productivity and its effects on the global carbon cycle (Holser et al. 1989; Faure et al. 1995; Foster et al. 1997; Cao et al. 2002; Sephton et al. 2002; Korte et al. 2004; Payne et al. 2004; Grice et al. 2005; Berner 2006; Grasby and Beauchamp 2008). In Meishan, a significant negative spike in carbon isotopes occurs in organic and inorganic carbon and directly coincides with the main pulse of marine faunal extinction (Cao et al. 2009). Sulfur isotopes, in both pyrite and sulfate, also show shifts toward more negative values (Korte et al. 2004; Newton et al. 2004; Berner 2006; Kaiho et al. 2006; Riccardi et al. 2006; Algeo et al. 2007; Fenton et al. 2007). After PTB, carbon isotopes in inorganic carbonates continued to fluctuate significantly and did not stabilize for nearly 10 Ma (Payne et al. 2004).

Other lines of evidence suggest that the extinction event at the PTB should be considered part of a larger two-stepped event, with the first stage of the extinction occurring at the Guadalupian-Lopingian boundary (Stanley and Yang 1994; Isozaki and Ota 2001). A detailed diversity curve

(Knoll et al. 2007) demonstrated that the standing high diversity seen throughout the Permian period began to decrease before the boundary, and that the first significant decrease was seen at the end-Guadalupian. However, the Signor-Lipps effect, which serves to spread out the record of extinctions may also be complicating this record (Signor and Lipps 1982).

Main Hypotheses for Extinction Trigger Mechanisms

Although the PTB extinction has been well-studied, the trigger mechanism (or mechanisms) for the extinction remains unknown (Benton 2003; Erwin 2006). The term, "trigger mechanism," as used in this thesis is defined as the critical disturbance that brings into play individually disruptive processes that ultimately cause death (Knoll et al. 2007). Although many trigger mechanisms have been proposed, recent consensus has narrowed the choices down to four: bolide impact, methane hydrate release, Siberian Traps volcanism and anoxic conditions in the oceans.

Bolide Impact

Bolide impact as a trigger mechanism for the PTB extinction was first proposed by Becker et al. (2001), based on the presence of ^{3}He, supposedly of extraterrestrial origin, in fullerenes. Fullerenes have been linked to massive wildfires triggered in the aftermath of an impact (Wolbach et al. 1985; Holser and Magaritz 1992) using the end-Cretaceous extinction as a model. The measurements of certain unusual noble gas ratios by Becker et al. suggest an extraterrestrial origin and a bolide that may have been as large as the K-Pg impactor. A potential impact crater has been identified for this bolide – the Bedout High on the Northwestern Australian continental margin (Becker et al. 2004). (See Figure 2.2.) However, both the presence of extraterrestrial noble gas ratios in fullerenes and the Bedout High as an impact crater have been highly contested (Farley et al. 2001; Koeberl et al. 2004;

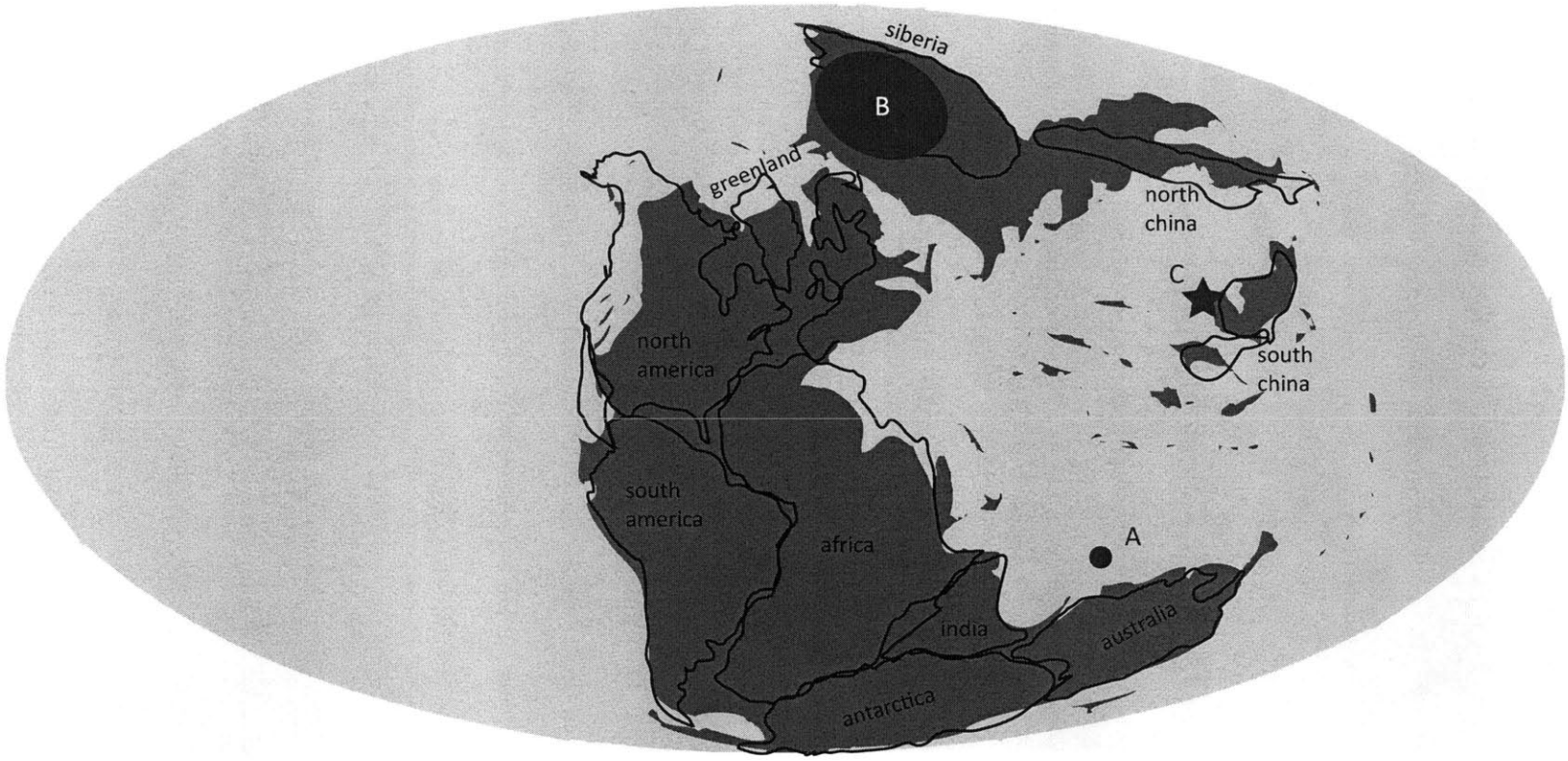

Figure 2.2 Global map from the Permian-Triassic boundary. The small black circle (A) is the paleolocation of the proposed Bedout impact crater. The large black oval labeled (B) is the general extent of Siberian Traps volcanism. Map modified from Scotese Paleomap Project website. The star (C) is the depositional location for the Meishan, China section, the Global Stratotype Section and Point of the Permian-Triassic boundary, and one location where biomarker proxies for euxinic conditions have been measured.

Renne et al. 2004; Lehrmann et al. 2005), suggesting that this mechanism of extinction is rather unlikely.

Methane Hydrate Release

The significant negative excursion in $\delta^{13}C$ at the PTB is key to the hypothesis of seafloor methane hydrate collapse as a trigger mechanism for the extinction event. The potential triggers of this massive methane release itself has been suggested as volcanic eruption and intrusion, bolide impact along with submarine landslide (Retallack and Krull 2006). Methane is significantly depleted in $\delta^{13}C$, and the release of this compound in great quantities from seafloor methane clathrates, causing the well-documented negative excursion, makes certain intuitive sense. Modeling of the carbon cycle at the PTB by Berner (2002) indicated that short term changes close to the boundary are best explained by methane release. Chemostratigraphic studies of $\delta^{13}C$ from boundary sections at two southern hemisphere localities (Krull and Retallack 2000; Krull et al. 2000), representing a terrestrial paleosol and a marine carbonate, also pointed to evidence of methane release at the boundary. However, later studies of $\delta^{13}C$ further into the Triassic period indicate that the carbon isotope fluctuations continued for nearly 5 Ma past the boundary (Payne and Kump 2007). These fluctuations occur during far too short a timescale for multiple regeneration and depletion events to be the source and are the strongest argument against methane release acting as a trigger mechanism for the Permian-Triassic extinction.

Siberian Traps Volcanism

The largest continental flood basalt eruption in Earth's history measured to date occurred roughly contemporaneously with the PTB in the northern region of Pangaea (Kamo et al. 1996; Kamo et al.

2003; Mundil et al. 2004). (See Figure 2.2.) The volatiles released from volcanism on such a large scale would have been significant. A favored hypothesis points to the effects these volatiles would have had on the atmospheric and marine environments as the trigger for the extinction event (Campbell et al. 1992; Renne et al. 1995; Bowring et al. 1998; Benton 2003; Kamo et al. 2003; Visscher et al. 2004). With estimated CO_2 emissions on the order of 10^{17} to 10^{19} mol (Wignall 2001) from this large igneous province, this eruption certainly had a significant effect on the global carbon cycle. The rate of eruption is an important factor in determining exactly how widespread of an effect this might have been, and this is currently under investigation. Other features of the eruption may have had additional consequences for the global environment. If the Siberian Traps erupted through coal beds, which underlie the basalts in many locations, the volatile release may have been significantly higher (Erwin 2006). An eruption that was higher in H_2SO_4 might have been especially damaging if it had led to increased production of organohalogens (Visscher et al. 2004). The wide-ranging effects of the volatiles released by this volcanism and their potential effects on global carbon isotope fluctuations in the early Triassic period (Payne and Kump 2007) suggest that this trigger mechanism may be significant to the end-Permian extinction event.

Anoxic Oceans

The presence of well-laminated black shales in relatively shallow marine sections from the PTB found in a variety of paleolocations suggest the occurance of shallow water anoxia (Wignall and Hallam 1992, 1993; Wignall and Twitchett 1996; Wignall and Twitchett 2002b; Grasby and Beauchamp 2009). This anoxia, potentially caused by ocean stagnation (Hotinski et al. 2001) as a result of some combination of global warming and continental arrangement, has been proposed as a trigger mechanism for the extinction event (Wignall and Twitchett 1996; Wignall and Twitchett 2002a). The chemistry of anoxic water bodies is favorable for the bacterial reduction of sulfate to

sulfide (Trull et al. 2001). The presence of biomarkers for Chlorobi in sections from the Paleo-Tethys and Panthalassic, including sedimentary rocks from the GSSP at Meishan, (Grice et al. 1996a; Grice et al. 1996b; Grice et al. 2005; Hays et al. 2006; Hays et al. 2007; Cao et al. 2009) provides supporting evidence that euxinia, or high concentrations of hydrogen sulfide, extended to within the photic zone. (See Figure 2.2.) Euxinic conditions were also long-standing in the deep waters of the Panthalassic Ocean (Kajiwara et al. 1994; Isozaki 1995; Isozaki 1997). The cause of this shoaling of the chemocline that brought euxinic waters into the photic zone has been linked to changes in sea-level (Hallam and Wignall 1999). However, both the development of anoxia and the shallowing of the chemocline may be related to large-scale tectonic activity (Faure et al. 1995). The release of carbon dioxide and hydrogen sulfide from such an anoxic and euxinic ocean may best explain the selective extinction of organisms in both the terrestrial and marine realms (Knoll et al. 1996; Wignall and Twitchett 1996; Huey and Ward 2005; Kump et al. 2005; Knoll et al. 2007). Global modeling of ocean and atmospheric chemistry suggests that hydrogen sulfide release could have served as a kill mechanism (Kump et al. 2005; Meyer et al. 2008), while the rapid saturation and slow regeneration of the atmospheric hydroxyl radical, a primary sink for hydrogen sulfide, may explain the protracted biotic recovery (Kump et al. 2005). However, others have criticized hydrogen sulfide as an individual kill mechanism (Lamarque et al. 2007), suggesting that it may be more effective in combination with methane or other products of an anoxic ocean, such as carbon dioxide and a resultant increase in temperature.

In modern environments, photic zone euxinia is stable for extended periods of time in water bodies with persistent salinity-stratification such as the Black Sea and deep fjords of the Arctic and Antarctic (Overmann et al. 1992; Smittenberg et al. 2004). Biogeochemical evidence, from Mesozoic samples from the Tethys and epicontinental seas that were the earliest opening of the Atlantic

Ocean, suggests that ocean anoxic events were prevalent in these narrow seaways as well (Kuypers et al. 2004; Wagner et al. 2004; van Breugel et al. 2006). However, no evidence exists for widespread euxinic conditions in modern open ocean waters.

Summary of the Permian-Triassic Boundary Conditions

The boundary between the Permian and Triassic Periods is also the boundary between the Paleozoic and Mesozoic Eons and marks a significant transition in Earth's history. Tectonic movements had produced a single major continent, on which large igneous provinces were erupting, and a major ocean with sluggish circulation and anoxic waters prevailed. This arrangement set the stage for a significant breakdown in both marine and terrestrial ecosystems that would be the largest mass extinction event in the Phanerozoic. It may not be appropriate to attribute this extinction event to any single trigger mechanism. Instead, it may be more likely that it was the result of a "tangled web of causality" (Erwin 1994; Erwin 2006) involving the effects of the Siberian Traps volcanism and euxinic ocean conditions.

References

Algeo, T. J., B. Ellwood, T. K. T. Nguyen, H. Rowe and J. B. Maynard (2007). "The Permian-Triassic Boundary at Nhi Tao, Vietnam: Evidence for Recurrent Influx of Sulfidic Watermasses to a Shallow-Marine Carbonate Platform." Palaeogeography, Palaeoclimatology, Palaeoecology **252**(1-2): 304-327.

Bambach, R. K., A. H. Knoll and J. J. J. Sepkoski (2002). "Anatomical and Ecological Constraints on Phanerozoic Animal Diversity in the Marine Realm." Proceedings of the National Academy of Sciences of the United States of America **99**(10): 6854-6859.

Becker, L., R. J. Poreda, A. R. Basu, K. O. Pope, T. M. Harrison, C. Nicholson and R. Iasky (2004). "Bedout: A Possible End-Permian Impact Crater Offshore of Northwestern Australia." Science **304**(5676): 1469-1476.

Becker, L., R. J. Poreda, A. G. Hunt, T. E. Bunch and M. Rampino (2001). "Impact Event at the Permian-Triassic Boundary: Evidence from Extraterrestrial Noble Gases in Fullerenes." Science **291**: 1530-1533.

Benton, M. J. (2003). When Life Nearly Died: The Greatest Mass Extinction of All Time. London, Thames and Hudson.

Berner, R. (2006). "Carbon, Sulfur and O_2 across the Permian-Triassic Boundary." Journal of Geochemical Exploration **88**(1-3): 416-418.

Berner, R. A. (2002). "Examination of Hypotheses for the Permo-Triassic Boundary Extinction by Carbon Cycle Modeling." PNAS **99**(7): 4172-4177.

Bowring, S. A., D. H. Erwin and Y. Isozaki (1999). "The Tempo of Mass Extinction and Recovery: The End-Permian Example." Proceedings of the National Academy of Sciences **96**(16): 8827-8828.

Bowring, S. A., D. H. Erwin, Y. G. Jin, M. W. Martin, K. Davidek and W. Wang (1998). "U/Pb Zircon Geochronology and Tempo of the End-Permian Mass Extinction." Science **280**(5366): 1039-1045.

Campbell, I. H., G. K. Czamanske, V. A. Fedorenko, R. I. Hill and V. Stepanov (1992). "Synchronism of the Siberian Traps and the Permian-Triassic Boundary." Science **258**(5089): 1760-1763.

Cao, C., G. D. Love, L. E. Hays, W. Wang, S. Shen and R. E. Summons (2009). "Biogeochemical Evidence for Euxinic Oceans and Ecological Disturbance Presaging the End-Permian Mass Extinction Event." Earth and Planetary Science Letters **281**(3-4): 188-201.

Cao, C., W. Wang, L. Liu, S. Shen and R. E. Summons (2008). "Two Episodes of 13c-Depletion in Organic Carbon in the Latest Permian: Evidence from the Terrestrial Sequences in Northern Xinjiang, China." Earth and Planetary Science Letters **270**(3-4): 251-257.

Cao, C. Q., W. Wang and Y. G. Jin (2002). "Carbon Isotope Excursions across the Permian-Triassic Boundary in the Meishan Section, Zhejiang Province, China." Chinese Science Bulletin **47**(13): 1125-1129.

Cocks, L. R. M. (2007). "Blowing Hot and Cold in the Palaeozoic." Proceedings of the Geologists Association **118**: 225-237.

Crowley, J. L., S. A. Bowring, S. Z. Shen, Y. Wang, C. Cao and Y. G. Jin (2006). "U-Pb Zircon Geochronology of the End-Permian Mass Extinction." Geochimica et Cosmochimica Acta **70**(18, Supplement 1): A119-A119.

Crowley, T. J. and R. A. Berner (2001). "Paleoclimate: Enhanced: Co2 and Climate Change." Science **292**(5518): 870-872.

Erwin, D. H. (1994). "The Permo-Triassic Extinction." Nature **367**: 231-236.

Erwin, D. H. (2006). Extinction: How Life on Earth Nearly Ended 250 Million Years Ago. Princeton, Princeton University Press.

Farley, K. A., S. Mukhopadhyay, Y. Isozaki, L. Becker and R. J. Poreda (2001). "An Extraterrestrial Impact at the Permian-Triassic Boundary?" Science **293**(5539): 2343a-.

Faure, K., M. J. de Wit and J. P. Willis (1995). "Late Permian Global Coal Hiatus Linked to 13c-Depleted Co2 Flux into the Atmosphere During the Final Consolidation of Pangea." Geology **23**(6): 507-510.

Fenton, S., K. Grice, R. J. Twitchett, M. E. Bottcher, C. V. Looy and B. Nabbefeld (2007). "Changes in Biomarker Abundances and Sulfur Isotopes of Pyrite across the Permian-Triassic (P/Tr) Schuchert Dal Section (East Greenland)." Earth and Planetary Science Letters **262**(1-2): 230-239.

Foster, C., G. Logan, R. E. Summons, J. Gorter and D. Edwards (1997). "Carbon Isotopes, Kerogen Types and the Permian-Triassic Boundary in Australia: Implications for Exploration." Australian Petroleum Production and Exploration Association Journal **37**: 442-459.

Grasby, S. E. and B. Beauchamp (2008). "Intrabasin Variability of the Carbon-Isotope Record across the Permian-Triassic Transition, Sverdrup Basin, Arctic Canada." Chemical Geology **253**(3-4): 141-150.

Grasby, S. E. and B. Beauchamp (2009). "Latest Permian to Early Triassic Basin-to-Shelf Anoxia in the Sverdrup Basin, Arctic Canada." Chemical Geology **264**(1-4): 232-246.

Grice, K., C. Cao, G. D. Love, M. E. Bottcher, R. J. Twitchett, E. Grosjean, R. E. Summons, S. C. Turgeon, W. Dunning and Y. Jin (2005). "Photic Zone Euxinia During the Permian-Triassic Superanoxic Event." Science **307**(5710): 706-709.

Grice, K., R. Gibbison, J. E. Atkinson, L. Schwark, C. B. Eckardt and J. R. Maxwell (1996a). "Maleimides (1h-Pyrrole-2,5-Diones) as Molecular Indicators of Anoxygenic Photosynthesis in Ancient Water Columns." Geochimica et Cosmochimica Acta **60**(20): 3913-3924.

Grice, K., P. Schaeffer, L. Schwark and J. R. Maxwell (1996b). "Molecular Indicators of Palaeoenvironmental Conditions in an Immature Permian Shale (Kupferschiefer, Lower Rhine Basin, North-West Germany) from Free and S-Bound Lipids." Organic Geochemistry **25**(3-4): 131-147.

Hallam, A. and P. B. Wignall (1999). "Mass Extinctions and Sea-Level Changes." Earth-Science Reviews **48**(4): 217.

Hays, L., T. Beatty, C. M. Henderson, G. D. Love and R. E. Summons (2007). "Evidence for Photic Zone Euxinia through the End-Permian Mass Extinction in the Panthalassic Ocean (Peace River Basin, Western Canada)." Palaeoworld **16**(1-3): 39-50

Hays, L. E., G. D. Love, C. B. Foster, K. Grice and R. E. Summons (2006). "Lipid Biomarker Records across the Permian-Triassic Boundary from Kap Stosch, Greenland." Eos Trans. AGU, 87(52), Fall Meet. Suppl., Abstract PP41B-1203.

Holser, W. T. and M. Magaritz (1992). "Cretaceous/Tertiary and Permian/Triassic Boundary Events Compared." Geochimica et Cosmochimica Acta **56**(8): 3297.

Holser, W. T., H.-P. Schonlaub, M. Attrep, K. Boeckelmann, P. Klein, M. Magaritz, C. J. Orth, A. Fenninger, C. Jenny, M. Kralik, H. Mauritsch, E. Pak, J.-M. Schramm, K. Stattegger and R. Schmoller (1989). "A Unique Geochemical Record at the Permian/Triassic Boundary." Nature **337**(6202): 39.

Hotinski, R. M., K. L. Bice, L. R. Kump, R. G. Najjar and M. A. Arthur (2001). "Ocean Stagnation and End-Permian Anoxia." Geology **21**(1): 7-10.

Huey, R. B. and P. D. Ward (2005). "Hypoxia, Global Warming, and Terrestrial Late Permian Extinctions." Science **308**(5720): 398-401.

Isozaki, Y. (1995). "Superanoxia across the Permo-Triassic Boundary: Record in Accreted Deep-Sea Pelagic Chert in Japan. ." Canadian Society of Petroleum Geologists, Memoir 17: 805-812.

Isozaki, Y. (1997). "Permo-Triassic Boundary Superanoxia and Stratified Superocean: Records from Lost Deep Sea." Science **276**(5310): 235-238.

Isozaki, Y. and A. Ota (2001). "Middle-Upper Permian (Maokouan-Wuchiapingian) Boundary in Mid-Oceanic Paleo-Atoll Limestone of Kamura and Akasaka, Japan." Proceedings of the Japan Academy **77 B**(6): 104-109.

Jin, Y., Y. Wang, W. Wang, Q. H. Shang, C. Cao and D. H. Erwin (2000). "Pattern of Marine Mass Extinction near the Permian-Triassic Boundary in South China." Science **289**: 432-436.

Kaiho, K., Y. Kajiwara, Z.-Q. Chen and P. Gorjan (2006). "A Sulfur Isotope Event at the End of the Permian." Chemical Geology **235**(1-2): 33-47.

Kajiwara, Y., S. Yamakita, K. Ishida, H. Ishiga and A. Imai (1994). "Development of a Largely Anoxic Stratified Ocean and Its Temporary Massive Mixing at the Permian/Triassic Boundary Supported by the Sulfur Isotopic Record." Palaeogeography, Palaeoclimatology, Palaeoecology **111**(3-4): 367-379.

Kamo, S. L., G. K. Czamanske, Y. Amelin, V. A. Fedorenko, D. W. Davis and V. R. Trofimov (2003). "Rapid Eruption of Siberian Flood-Volcanic Rocks and Evidence for Coincidence with the Permian-Triassic Boundary and Mass Extinction at 251 Ma." Earth and Planetary Science Letters **214**(1-2): 75-91.

Kamo, S. L., G. K. Czamanske and T. E. Krogh (1996). "A Minimum U---Pb Age for Siberian Flood-Basalt Volcanism." Geochimica et Cosmochimica Acta **60**(18): 3505.

Knoll, A. H., R. K. Bambach, D. E. Canfield and J. P. Grotzinger (1996). "Comparative Earth History and Late Permian Mass Extinction." Science **273**: 452-457.

Knoll, A. H., R. K. Bambach, J. L. Payne, S. Pruss and W. W. Fischer (2007). "Paleophysiology and End-Permian Mass Extinction." Earth and Planetary Science Letters **256**(3-4): 295-313.

Koeberl, C., K. A. Farley, B. Peucker-Ehrenbrink and M. A. Sephton (2004). "Geochemistry of the End-Permian Extinction Event in Austria and Italy: No Evidence for an Extraterrestrial Component." Geology **32**(12): 1053-1056.

Korte, C., H. W. Kozur, M. M. Joachimski, H. Strauss, J. Veizer and L. Schwark (2004). "Carbon, Sulfur, Oxygen and Strontium Isotope Records, Organic Geochemistry and Biostratigraphy across the Permian/Triassic Boundary in Abadeh, Iran." International Journal of Earth Sciences **93**(4): 565.

Krull, E. S. and G. J. Retallack (2000). "Δ13c Depth Profiles from Paleosols across the Permian-Triassic Boundary: Evidence for Methane Release." Geological Society of America Bulletin **112**(9): 1459-1472.

Krull, E. S., G. J. Retallack, I. H. Campbell and G. L. Lyon (2000). "Δ^{13}corg Chemostratigraphy of the Permian–Triassic Boundary in the Maitai Group, New Zealand: Evidence for High Latitudinal Methane Release." New Zealand Journal of Science **43**: 23–32.

Kump, L. R., A. Pavlov and M. A. Arthur (2005). "Massive Release of Hydrogen Sulfide to the Surface Ocean and Atmosphere During Intervals of Oceanic Anoxia." Geology **33**: 397–400.

Kuypers, M. M. M., Y. van Breugel, S. Schouten, E. Erba and J. S. S. Damste (2004). "N2-Fixing Cyanobacteria Supplied Nutrient N for Cretaceous Oceanic Anoxic Events." Geology **32**(10): 853-856.

Lamarque, J. F., J. T. Kiehl and J. J. Orlando (2007). "Role of Hydrogen Sulfide in a Permian-Triassic Boundary Ozone Collapse." Geophys. Res. Lett. **34**(2): L02801.

Lehrmann, D., P. Enos, J. Payne, P. Montgomery, J. Wei, Y. Yu, J. Xiao and M. J. Orchard (2005). "Permian and Triassic Depositional History of the Yangtze Platform and Great Bank of Guizhou in the Nanpanjiang Basin of Guizhou and Guangxi, South China." Albertiana **33**: 149-168.

Looy, C. V., R. J. Twitchett, D. L. Dilcher, J. H. A. Van Konijnenburg-Van Cittert and H. Visscher (2001). "Life in the End-Permian Dead Zone." Proceedings of the National Academy of Sciences of the United States of America **98**(14): 7879-7883.

Meyer, K. M., L. R. Kump and A. Ridgwell (2008). "Biogeochemical Controls on Photic-Zone Euxinia During the End-Permian Mass Extinction." Geology **36**(9): 747-750.

Mundil, R., K. R. Ludwig, I. Metcalfe and P. R. Renne (2004). "Age and Timing of the Permian Mass Extinctions: U/Pb Dating of Closed-System Zircons." Science **305**(5691): 1760-1763.

Muttoni, G., M. Gaetani, D. V. Kent, D. Sciunnach, L. Angiolini, F. Berra, E. Garzanti, M. Mattei and A. Zanchi (2009). "Opening of the Neo-Tethys Ocean and the Pangea B to Pangea a Transformation During the Permian." Geoarabia **14**(4): 17-48.

Newton, R. J., E. L. Pevitt, P. B. Wignall and S. H. Bottrell (2004). "Large Shifts in the Isotopic Composition of Seawater Sulphate across the Permo-Triassic Boundary in Northern Italy." Earth and Planetary Science Letters **218**(3-4): 331-345.

Overmann, J., H. Cypionka and N. Pfenning (1992). "An Extremely Low-Light-Adapted Phototrophic Sulfur Bacterium from the Black Sea." Limnology and Oceanography **37**(1): 150-155.

Payne, J. L. and L. R. Kump (2007). "Evidence for Recurrent Early Triassic Massive Volcanism from Quantitative Interpretation of Carbon Isotope Fluctuations." Earth and Planetary Science Letters **256**(1-2): 264-277.

Payne, J. L., D. J. Lehrmann, J. Wei, M. J. Orchard, D. P. Schrag and A. H. Knoll (2004). "Large Perturbations of the Carbon Cycle During Recovery from the End-Permian Extinction." Science **305**(5683): 506-509.

Rampino, M. R., A. Prokoph and A. Adler (2000). "Tempo of the End-Permian Event: High-Resolution Cyclostratigraphy at the Permian-Triassic Boundary." Geology **28**(7): 643-646.

Raup, D. M. and J. J. J. Sepkoski (1982). "Mass Extinctions in the Marine Fossil Record." Science **215**(4539): 1501-1503.

Rees, P. M. (2002). "Land-Plant Diversity and the End-Permian Mass Extinction." Geology **30**(9): 827-830.

Renne, P. R., M. T. Black, Z. Zichao, M. A. Richards and A. R. Basu (1995). "Synchrony and Causal Relations between Permian-Triassic Boundary Crises and Siberian Flood Volcanism." Science **269**(5229): 1413-1416.

Renne, P. R., H. J. Melosh, K. A. Farley, W. U. Reimold, C. Koeberl, M. R. Rampino, S. P. Kelly, Ivanov, B. A., L. Becker, R. J. Poreda, A. R. Basu, K. O. Pope, T. M. Harrison, C. Nicholson and R. Iasky (2004). "Is Bedout an Impact Crater? Take 2." Science **306**(5696): 610-612.

Retallack, G. J. (1995). "Permian-Triassic Life Crisis on Land." Science **267**(5194): 77-80.

Retallack, G. J. and E. S. Krull (2006). "Carbon Isotopic Evidence for Terminal-Permian Methane Outbursts and Their Role in Extinctions of Animals, Plants, Coral Reefs, and Peat Swamps." Geological Society of America Special Papers **399**: 249-268.

Retallack, G. J., R. M. H. Smith and P. D. Ward (2003). "Vertebrate Extinction across Permian-Triassic Boundary in Karoo Basin, South Africa." Geological Society of America Bulletin **115**(9): 1133-1152.

Riccardi, A. L., M. A. Arthur and L. R. Kump (2006). "Sulfur Isotopic Evidence for Chemocline Upward Excursions During the End-Permian Mass Extinction." Geochimica et Cosmochimica Acta(70): 5740-5752.

Sephton, M. A., C. V. Looy, R. J. Veefkind, H. Brinkhuis, J. W. De Leeuw and H. Visscher (2002). "Synchronous Record of $\Delta^{13}c$ Shifts in the Oceans and Atmosphere at the End of the Permian." Geological Society of America **Special Paper 356**: 455-462.

Sepkoski, J. J., Jr. (1984). "A Kinetic Model of Phanerozoic Taxonomic Diversity. Iii. Post-Paleozoic Families and Mass Extinctions." Paleobiology **10**(2): 246-267.

Signor, P. and J. Lipps (1982). "Sampling Bias, Gradual Extinction Patterns and Catastrophes in the Fossil Record." Geological Society of America Special Papers **190**: 291-296.

Smittenberg, R. H., Pancost R.D., E. C. Hopmans, M. Paetzel and J. S. Sinninghe Damsté (2004). "A 400-Year Record of Environmental Change in an Euxinic Fjord as Revealed by the Sedimentary Biomarker Record. ." Palaeogeography, Palaeoclimatology, Palaeoecology **202**: 331-351.

Stanley, S. and X. Yang (1994). "A Double Mass Extinction at the End of the Paleozoic Era." Science **266**(5189): 1340-1344.

Torsvik, T. H. and L. R. M. Cocks (2004). "Earth Geography from 400 to 250 Ma: A Palaeomagnetic, Faunal and Facies Review." Journal of the Geological Society **161**: 555-572.

Trull, T., J. Gibson, K. Beaumont, J. Bowman, H. Burton, A. Davidson, A. Guichard, J. Kirkwood, A. McMinn, P. Nichols, J. Skerratt, R. E. Summons, K. Swadling and J. K. Volkman (2001). "Site Holds Promise for Ecosystem and Biogeochemical Investigations." EOS, Transactions AGU **82**(28): 306.

Twitchett, R. J., C. V. Looy, R. Morante, H. Visscher and P. B. Wignall (2001). "Rapid and Synchronous Collapse of Marine and Terrestrial Ecosystems During the End-Permian Biotic Crisis." Geology **29**(4): 351-354.

van Breugel, Y., M. Baas, S. Schouten, E. Mattioli and J. S. Sinninghe Damsté (2006). "Isorenieratane Record in Black Shales from the Paris Basin, France: Constraints on Recycling of Respired Co_2 as a Mechanism for Negative Carbon Isotope Shifts During the Toarcian Oceanic Anoxic Event." Paleoceanography **21**: PA4220.

Visscher, H., H. Brinkhuis, D. L. Dilcher, W. C. Elsik, Y. Eshet, C. V. Looy, M. R. Rampino and A. Traverse (1996). "The Terminal Paleozoic Fungal Event: Evidence of Terrestrial Ecosystem Destabilization and Collapse." Proceedings of the National Academy of Sciences of the United States of America **93**(5): 2155-2158.

Visscher, H., C. V. Looy, M. E. Collinson, H. Brinkhuis, J. H. A. van Konijnenburg-van Cittert, W. M. Kurschner and M. A. Sephton (2004). "Environmental Mutagenesis During the End-Permian Ecological Crisis." Proceedings of the National Academy of Sciences of the United States of America **101**(35): 12952-12956.

Wagner, P., M. Kosnik and S. Lidgard (2006). "Abundance Distributions Imply Elevated Complexity of Post-Paleozoic Marine Ecosystems." Science **314**(5803): 1289-1292.

Wagner, T., P. Hofmann, B. Beckmann and J. Sinninghe Damsté (2004). "Euxinia and Primary Production in Upper Cretaceous Eastern Equatorial Atlantic Surface Waters Fostered Orbital-Driven Formation of Marine Black Shales in the Deep Ivory Basin, Odp Site 959." Paleoceanography **19**: PA3009.

Wang, C. (2007). "Anomalous Hopane Distributions at the Permian-Triassic Boundary, Meishan, China - Evidence for the End-Permian Marine Ecosystem Collapse." Organic Geochemistry **38**(1): 52-66.

Ward, P. D., J. Botha, R. Buick, M. De Kock, D. H. Erwin, G. Garrison, J. Kirschvink and R. Smith (2005). "Abrupt and Gradual Extinction among Late Permian Land Vertebrates in the Karoo Basin, South Africa." Science **307**: 709-714.

Wignall, P. and R. Twitchett (2002a). Extent, Duration and Nature of the Permian-Triassic Superanoxic Event. Catastrophic Events and Mass Extinctions: Impacts and Beyond:. C. Koeberl and K. C. MacLeod. Boulder, Colorado, Geological Society of America Special Paper 356**:** 395-413.

Wignall, P. and R. Twitchett (2002b). "Permian-Triassic Sedimentology of Jameson Land, East Greenland: Incised Submarine Channels in an Anoxic Basin." Journal of the Geological Society, London **159**: 691-703.

Wignall, P. B. (2001). "Large Igneous Provinces and Mass Extinctions." Earth-Science Reviews **53**(1-2): 1-33.

Wignall, P. B. and A. Hallam (1992). "Anoxia as a Cause of the Permian/Triassic Mass Extinction: Facies Evidence from Northern Italy and the Western United States." Palaeogeography, Palaeoclimatology, Palaeoecology **93**(1-2): 21-46.

Wignall, P. B. and A. Hallam (1993). "Griesbachian (Earliest Triassic) Palaeoenvironmental Changes in the Salt Range, Pakistan and Southeast China and Their Bearing on the Permo-Triassic Mass Extinction." Palaeogeography, Palaeoclimatology, Palaeoecology **102**(3-4): 215-237.

Wignall, P. B. and R. J. Twitchett (1996). "Ocean Anoxia and the End Permian Mass Extinction." Science **272**(5265): 1155-1158.

Wolbach, W. S., R. S. Lewis and E. Anders (1985). "Cretaceous Extinctions: Evidence for Wildfires and Search for Meteoritic Material." Science **230**(4722): 167-170.

Xie, S., R. D. Pancost, J. Huang, P. B. Wignall, J. Yu, X. Tang, L. Chen, X. Huang and X. Lai (2007). "Changes in the Global Carbon Cycle Occurred as Two Episodes During the Permian-Triassic Crisis." Geology **35**(12): 1083-1086.

Xie, S., R. D. Pancost, H. Yin, H. Wang and R. P. Evershed (2005). "Two Episodes of Microbial Change Coupled with Permo/Triassic Faunal Mass Extinction." Nature **434**: 494-497.

Chapter 3

Biomarker and Isotopic Trends from Peace River, Canada

Abstract

A composite Permian-Triassic transition section from Peace River, Canada, was constructed using samples from four petroleum exploration drill-cores. Previous research (Hays et al. 2007) reported on biomarker proxies from this section, but further study yielded additional information regarding the temporal and physical extent of the photic zone euxinia in these sedimentary rocks. Biomarkers for maturity, the isomerization of C_{27} steranes and C_{31} homohopanes, show that the lower three wells are within the "oil window" while the uppermost well has yet to reach this point. Aryl isoprenoids, isorenieratane and chlorobactane, were measured in the Peace River section and two peaks in their abundances were identified. The presence of the intact C_{40} carotenoid derivatives along with the enriched $\delta^{13}C$ values measured for the aryl isoprenoids provides strong evidence that the aryl isoprenoids were derived from the aromatic carotenoids of Chlorobi. Farnesane was enriched in $\delta^{13}C$ relative to pristane to phytane, indicating that this compound also originated in the lipids of Chlorobi. Crocetane was identified in a subset of Peace River sedimentary rocks, and the pattern of this compound's distribution closely matches those of the carotenoid derivatives, which suggests a common origin for these compounds. The difference between the $\delta^{13}C$ values for *n*-C_{17} and *n*-C_{18} and the isoprenoids, pristane and phytane, denoted $\Delta\delta$, was calculated. Values of $\Delta\delta$ for the Peace River sections were close to zero throughout, an isotopic ordering pattern considered to be 'anomalous.' Two intervals of negative $\Delta\delta$ values were identified and these had high concentrations of carotenoid derivatives. Together these proxies indicate the presence of a stratified

water column with high bacterial input. A rare hydrocarbon, C_{33} *n*-alkylcyclohexane, a potential age-specific marker for the boundary, also was measured in this section in sedimentary rocks at and immediately following the identified Permian-Triassic transition. Although the earlier study established the presence of photic zone euxinic conditions during the deposition of the Peace River section, this newer work identifies intermittent periods where chemocline upward excursions brought these anoxic waters even closer to the surface and significantly increased the portion of Chlorobi-derived organic material in the sedimentary rocks.

Locality and biostratigraphic information

Western and Arctic Canada

The Peace River Basin, located in modern-day western Canada, was situated at the eastern margin of the Panthalassic Ocean at the Permian-Triassic boundary. (See Figure 3.1.) Other sections from Western and Arctic Canada sample this same paleoregion. Initially late Permian sedimentary rocks were thought to be absent from these sections (Nassichuck et al. 1973) but more recent studies suggest that the supposed basin-wide unconformity that excluded the Permian-Triassic boundary does not exist. Basin-wide correlation of $\delta^{13}C_{org}$ values and conodont fossil data from the Sverdrup basin indicate that in some, if not all, sedimentary sections, the boundary is neither a major hiatus nor an erosional event (Grasby and Beauchamp 2008).

A study of sedimentary rocks from the Sverdrup basin in Arctic Canada (Grasby and Beauchamp 2009) found evidence of anoxia, including high concentrations of redox-sensitive elements, TOC values and TS/TOC ratios, that extended over the continental shelf just before the boundary. At

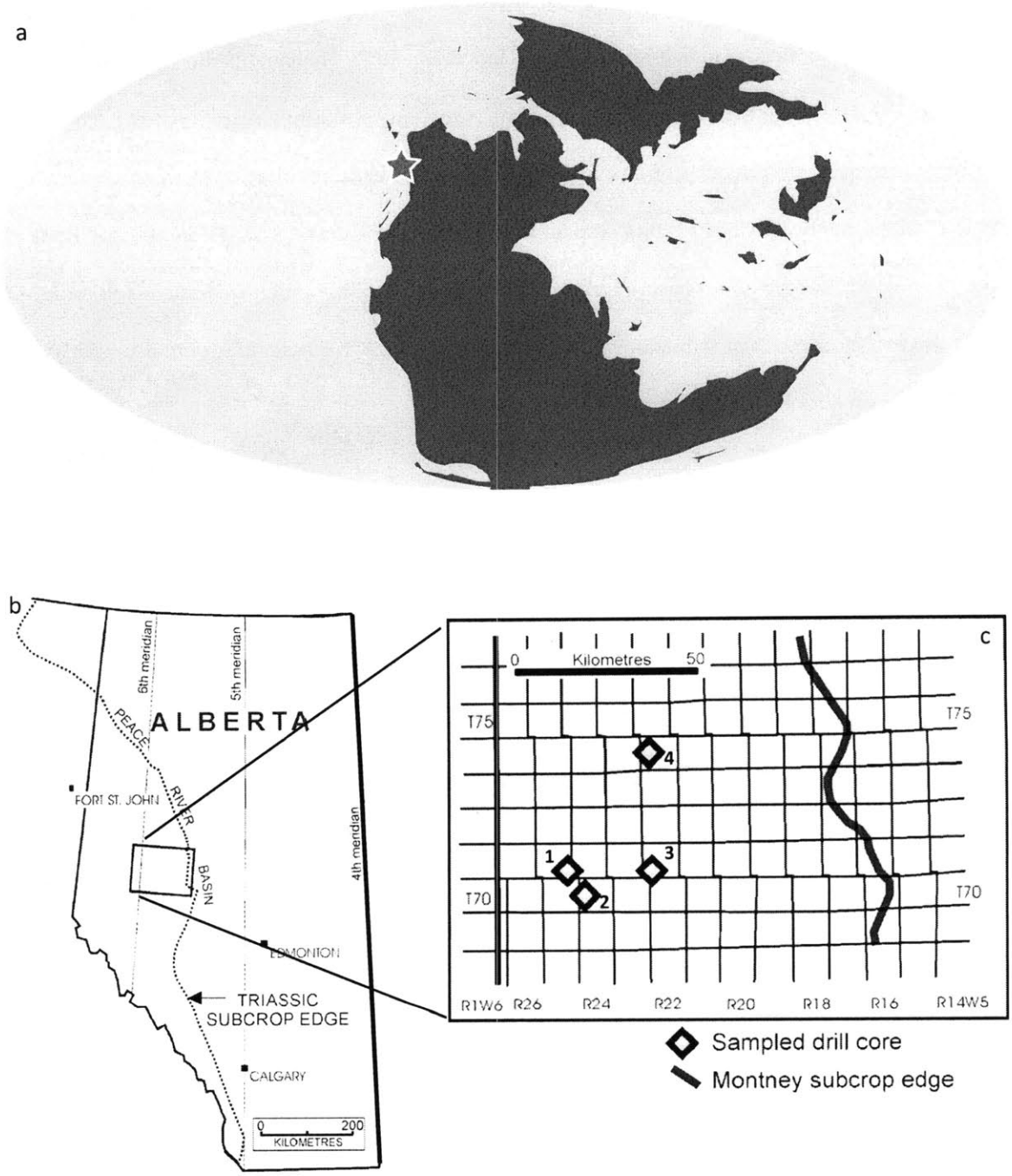

Figure 3.1 Locality of the Peace River, Canada section. (a) Global map from the Permian-Triassic boundary, with the depositional location of this section noted. Map modified from Scotese Paleomap Project website. (b) Map of modern Alberta with outlined margin of Peace River Basin. (c) Inset map showing detailed location of sampled drill cores for composite section and relation to edge of rock formation. (b) & (c) adapted from Hays et al. 2007.

this point euxinic conditions begin and extend through the transition. Two other studies of the Permian-Triassic boundary in Western Canada (Henderson 1997; Henderson and Baud 1997), focused on establishing the boundary, using sedimentary and conodont biostratigraphy from within sections previously described as exclusively Triassic in age. Focus has recently shifted from the Paleo-Tethys marine sections of the Permian-Triassic boundary (Grice et al. 2005a) to conditions in the greater Panthalassic ocean basin. For example, Hays et al. (2007), evaluated the distribution of hydrocarbon biomarkers in sedimentary rocks from the Peace River basin that were deposited beneath the Eastern Panthalassic.

Peace River, Canada

The Peace River basin in Western Canada, as described in detail in Hays et al. (2007), was deposited as part of the Montney Formation and encompasses the Permian-Triassic transition. (See Figure 3.1.) This composite section does not comprise a single core or outcrop. Instead, it was constructed from four petroleum exploration drill cores using a combination of gamma-ray wire-line logs and conodont biostratigraphy. Only one of the four cores captured the transition itself. This was confirmed by correlation of sedimentary packages in this core to those with late Permian conodonts identified elsewhere and the presence of *Hindeodus parvus*. Of the other three cores, one samples the early to mid-Griesbachian, and the other two sample the early Dienerian. For further information on the Peace River locality and its biostratigraphy, see the full text of Hays et al. 2007, Appendix 2.

Results and Discussion

Biomarkers for Maturity

As discussed in Hays et al. (2007), data from the bulk geochemical indices suggest that there has been significant thermally-driven transformation of kerogen to bitumen in the sediment column of the Peace River section. The C-20 and C-22 isomer ratios of C_{27} steranes and C_{31} homohopanes, respectively, indicates that the lowest three wells are within the oil window, though the uppermost well has not reached this point. In the lowest three wells, the average values for the 20S/(20S+20R) ratio of the C_{27} steranes are between 51.4% and 53.5%, and in the uppermost well, the average of this ratio is 42.4%. (See Figure 3.2.) For the C_{31} homohopanes, the average values for the 22S/(22S+22R) ratio are between 58.7% and 60% in the lower three wells and 45.8% in the highest well. Migration of this bitumen within the section in the lower wells may have served to attenuate some of the depth-dependence in organic geochemical variables and obscure important trends. Even with a minor amount of bitumen migration, however, the significant changes in the microbial community seen in the biomarkers throughout the range of this section will be preserved. (See Appendix 1 for uncertainties in biomarker measurements.)

Biomarkers for Sedimentary Redox Conditions

Preliminary hydrocarbon biomarker analyses of the Peace River section showed that that the Permian-Triassic transition sedimentary rocks were deposited in a marine environment with euxinia extending into the photic zone. Marine depositional conditions were indicated by high values of the C_{30} sterane index (Moldowan 1984; Peters et al. 2005), a low C_{26}/C_{25} tricyclic terpane ratio and a high $C_{31}22R/C_{30}$ hopane ratio (Zumberge 1987; Peters et al. 2005). In addition to biomarker proxies for marine deposition, the high homohopane index and low pristane to phytane ratios measured

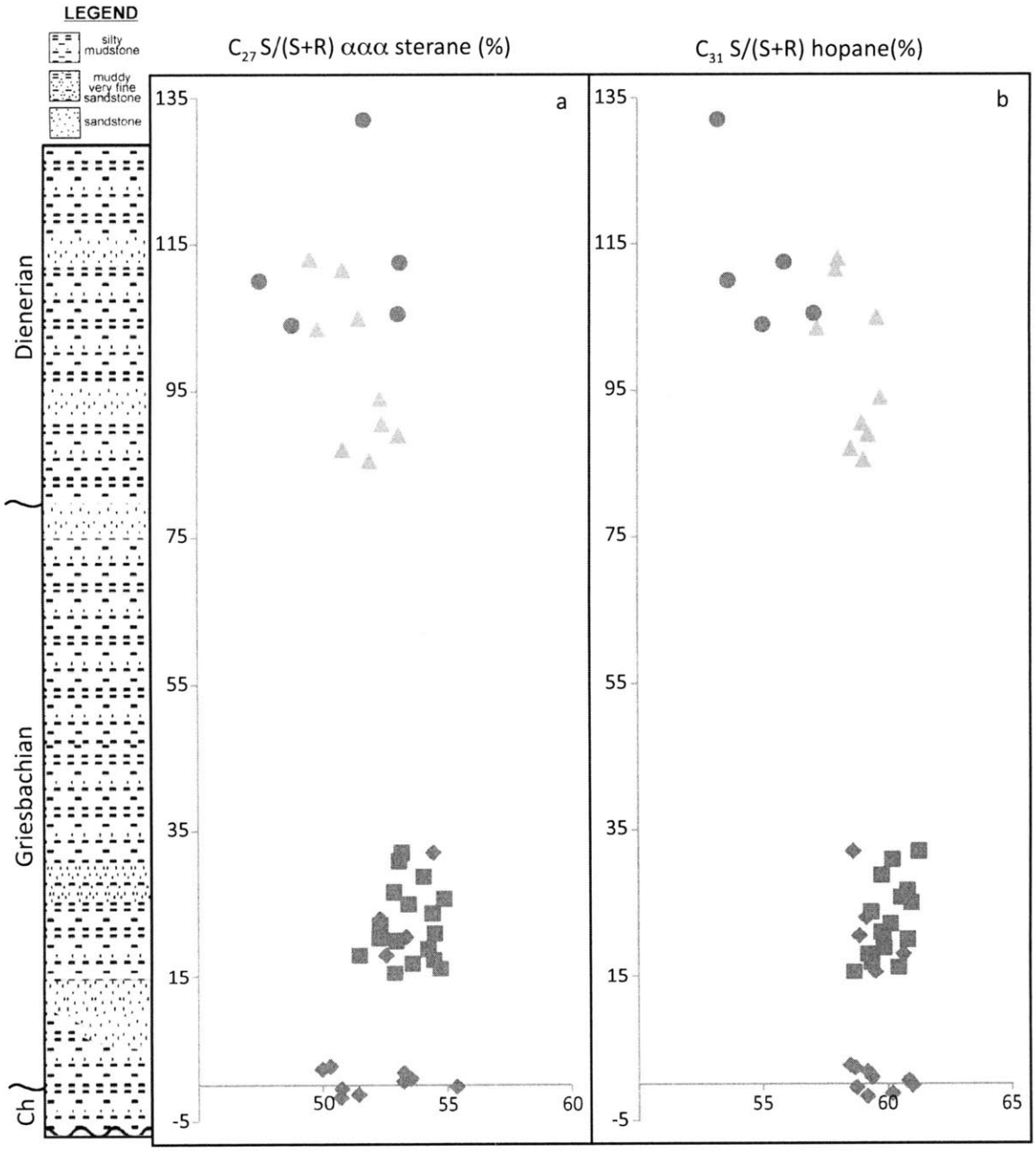

Figure 3.2 Biomarkers for maturity from the Peace River section. The four different symbols (diamonds, squares, triangles and circles) represent samples from the four different wells from this composite section. Compounds were measured by GC-MS in MRM mode. All parameters are plotted relative to depth. Composite litholog adapted from Hays et al. 2007.

throughout the section indicate that the Peace River was intensely anoxic during deposition. These biomarkers for anoxic marine settings are consistent with the fossil record of fish scales and conodonts in the primarily shale lithofacies (Hays et al. 2007).

A suite of C_{15}-C_{22} aryl isoprenoids were measured in all samples with the highest concentrations at the Permian-Triassic transition itself and in samples from the earliest Triassic period. In the interval in which the aryl isoprenoids had their highest values, they were accompanied by the intact C_{40} carotenoid skeletons of isorenieratane and chlorobactane. (See Figure 3.3.) Chlorobactane has not been previously reported from any Permian-Triassic boundary section. Isorenieratane and chlorobactane are produced by the brown-pigmented and green-pigmented strains of the Chlorobi, respectively, although the carotenoid content of the brown-pigmented Chlorobi is up to four times higher than the green-pigmented variety (Overmann 2001). In environments where the chemocline is deep and light has been attenuated through the water column, Chlorobi have a selective advantage over Chromatiaceae, or purple sulfur bacteria, because of the higher carotenoid and bacteriochlorophyll contents in Chlorobi, the arrangement of their chlorosomes on the periphery of their cytoplasm and lower maintenance energy requirements (Montesinos et al. 1983; Overmann 2001). Because of the larger quantities of isorenieratene, the brown-pigmented Chlorobi have a selective advantage over green-pigmented Chlorobi in these environments as well. When the chemocline is shallower, the Chromatiaceae dominate the anoxygenic phototrophic community, although they may co-exist with green-pigmented Chlorobi, and the brown-pigmented variety can thrive below this community.

Although the C_{40} isoprenoid hydrocarbons were not seen in all measured samples, both compounds showed abundance peaks at the transition and also in the early Triassic period. (See Figure 3.4.)

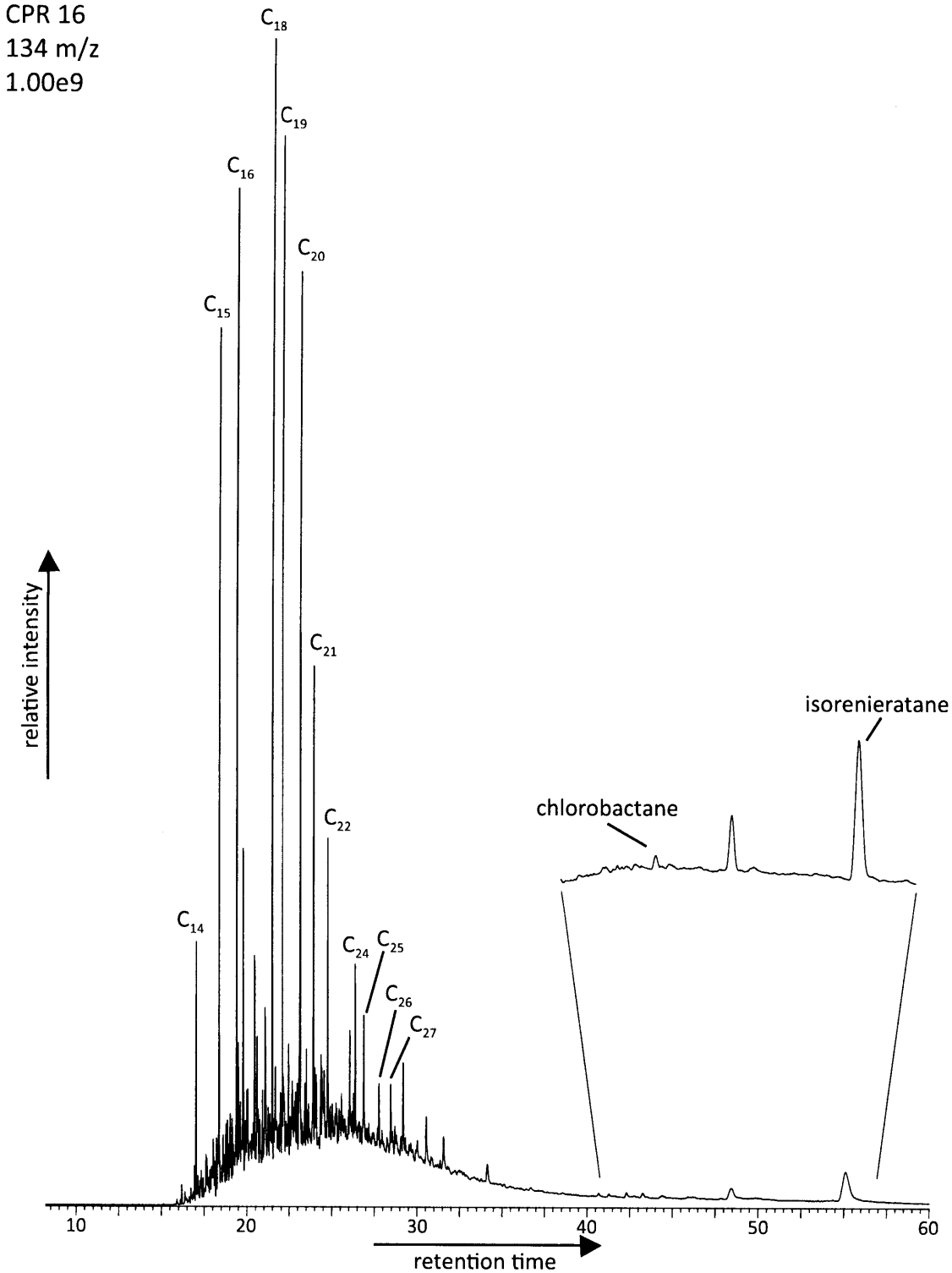

Figure 3.3 GC-MS select ion chromatogram of mass 134 from a sample aromatic hydrocarbon fraction from Peace River. Aryl isoprenoids from C_{14} to C_{27} have been identified, as well as the extended C_{40} carotenoid derivatives chlorobactane and isorenieratane

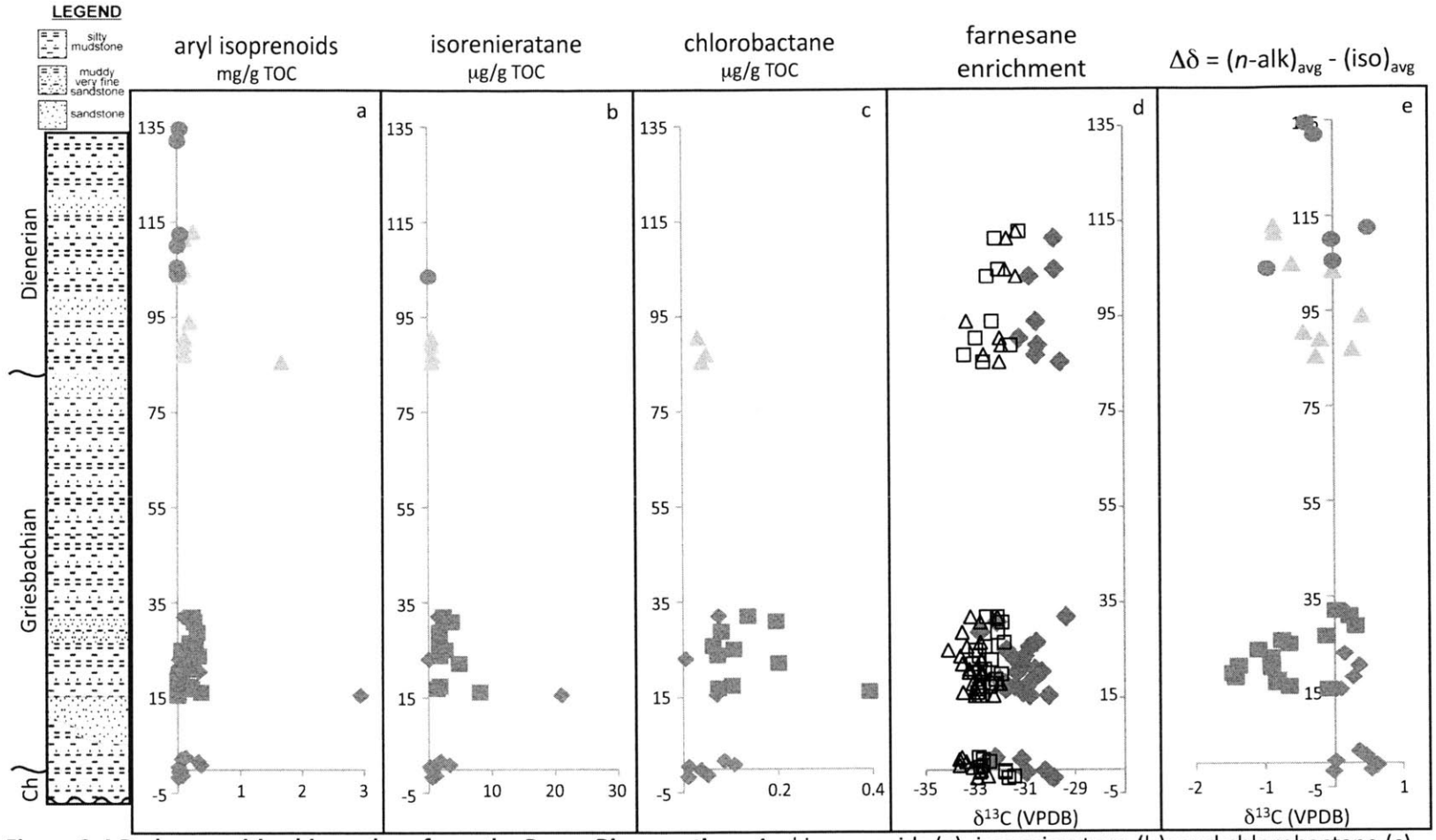

Figure 3.4 Redox-sensitive biomarkers from the Peace River section. Aryl isoprenoids (a); isorenieratane (b); and chlorobactane (c) quantities were normalized relative to total organic carbon contents and measured in GC-MS SIM mode. Isotopes for farnesane enrichment (d) and Δδ (e) are measured in permil relative to VPDB on GC-irMS. In (a), (b), (c), and (e) the four different symbols (diamonds, squares, triangles and circles) represent samples from the four different wells from this composite section. In (d) closed diamonds are farnesane; open triangles are phytane, and open squares are pristane. All parameters are plotted relative to depth. Composite litholog adapted from Hays et al. 2007.

These peaks in C_{40} isoprenoid abundance correspond well with the peaks in the abundances of lower molecular weight aryl isoprenoids and also with other biomarkers for anoxic conditions. The carotenoids were also measured in the uppermost Peace River section, although the quantity in these samples was much lower than in those nearer the transition. These observations support previous hypotheses that C_{40} isoprenoids and their aryl isoprenoid counterparts shared a common origin in the aromatic carotenoids of the Chlorobi and were not derived from non-aromatic carotenoids through sedimentary diagenetic processes as has been suggested (Koopmans et al. 1996).

The organic-rich nature of the Peace River sedimentary rocks also allowed isolation of aromatic hydrocarbon fractions sufficient for isotopic analysis to be attempted. Unfortunately however, the peaks in the m/z 134 chromatogram were superimposed on a high background of unresolved compounds and this compromised the accuracy of the isotopic measurements. (See Figure A1.1 in Appendix 1.) When the peaks were measured relative to the baseline for the sample, the average $\delta^{13}C$ value of the aryl isoprenoids was -26.9‰. When the background was removed entirely and only the peak was measured, the average $\delta^{13}C$ value of the aryl isoprenoids was -23.3‰. (See Table 3.1.) Since they could not be further purified, and it is impossible to know the proportions of the measured aryl isoprenoids relative to the other co-eluting compounds, the $\delta^{13}C$ value cannot be taken as a precise measurement for these compounds. Nevertheless, the $\delta^{13}C$ values that were measured were significantly enriched relative to other compounds with different origins, and this can be considered further evidence that the aryl isoprenoids were derived from isorenieratane and chlorobactane. (See Appendix 1 for uncertainties in isotope measurements.)

Some of the samples from the assembled Peace River section also contained the isoprenoid farnesane derived from the farnesol side chain of chlorophyll e. In the ~85% of samples that

sample	relative depth	farnesane	pristane	phytane	n-C_{17}	n-C_{18}	aryl isoprenoids
CPR 1	-1.7	-29.9	-31.7	-32.9	-31.8	-32.8	
CPR 2	-1.3	-30.0	-31.4	-32.5	-31.0	-31.8	
CPR 3	-0.5	-31.0	-31.8	-32.8	-31.3	-32.1	
CPR 4	-0.2	-30.2	-31.8	-32.8	-31.3	-32.0	
CPR 5	0.5		-32.8	-33.1	-32.4	-33.5	
CPR 6	0.9	-32.6	-32.7	-33.6	-32.4	-32.9	-26.9 (-21.5)
CPR 7	1.7	-32.6	-32.4	-33.4	-32.1	-32.8	-28.3 (-27.1)
CPR 8	2.2	-31.2	-32.7	-33.6	-32.6	-33.0	
CPR 9	2.6	-32.2	-32.9	-33.5	-32.5	-33.2	
CPR 10	15.5	-30.1	-32.7	-32.3	-32.6	-32.3	-25.2 (-22.0)
CPR 11	18.0	-30.8	-32.2	-32.0	-31.7	-32.0	
CPR 12	20.5	-30.3	-32.8	-32.7	-32.3	-32.5	
CPR 13	23.0	-31.4	-32.3	-32.8	-32.2	-32.7	
CPR 14	32.0	-29.4	-32.1	-32.1	-31.6	-32.3	
CPR 15	15.5	-30.8	-32.8	-33.0	-32.9	-33.1	
CPR 16	16.1	-31.1	-32.9	-33.5	-33.7	-34.0	-26.9 (-21.1)
CPR 17	16.9	-31.8	-32.8	-33.0	-33.8	-33.7	
CPR 18	17.4	-31.4	-32.4	-32.8	-33.2	-33.6	
CPR 19	18.0	-31.8	-32.4	-33.1	-33.9	-34.4	
CPR 20	18.9	-32.0	-32.2	-32.8	-33.7	-34.2	
CPR 21	20.0	-30.4	-32.0	-32.8	-33.1	-33.5	
CPR 22	20.4	-31.3	-33.0	-33.2	-34.4	-34.7	
CPR 23	21.0	-30.6	-32.6	-33.2	-33.6	-34.1	
CPR 24	22.1	-31.1	-33.1	-33.5	-34.1	-34.4	
CPR 25	23.8	-31.0	-32.8	-33.6	-34.1	-34.5	
CPR 26	25.0	-31.8	-33.0	-34.1	-34.0	-34.3	
CPR 27	25.8	-30.8	-32.6	-33.3	-33.4	-34.1	
CPR 28	26.6	-30.5	-31.8	-32.8	-32.0	-32.8	
CPR 29	28.8	-32.8	-32.1	-33.5	-32.3	-32.7	
CPR 30	30.9	-32.1	-31.9	-32.8	-31.8	-32.5	
CPR 31	32.0		-32.5	-33.2	-32.5	-33.2	
CPR 32	85.5	-29.6	-32.6	-32.0	-32.6	-32.5	-27.3 (-24.8)
CPR 33	87.0	-30.5	-33.4	-32.6	-33.1	-32.4	
CPR 34	89.0	-30.4	-31.5	-31.9	-31.9	-31.9	
CPR 35	90.5	-31.2	-32.9	-32.0	-32.9	-32.8	
CPR 36	94.0	-30.5	-32.3	-33.3	-32.5	-32.2	
CPR 37	103.5	-30.8	-32.5	-31.3	-32.1	-31.7	
CPR 38	105.0	-29.8	-32.0	-31.7	-32.5	-32.5	
CPR 39	111.5	-29.8	-32.1	-31.7	-32.7	-32.9	
CPR 40	113.0	-29.7	-31.2	-31.3	-32.1	-32.2	
CPR 41	104.0		-29.1	-29.0	-29.5	-30.4	
CPR 42	105.5		-30.9	-30.0	-30.4	-30.5	
CPR 43	110.0		-31.1	-30.1	-30.7	-30.5	
CPR 44	112.5		-31.1	-31.2	-30.6	-30.7	
CPR 45	132.0		-30.0	-30.0	-30.1	-30.4	
CPR 46	134.5		-30.0	-30.1	-30.0	-30.9	

Table 3.1 $\delta^{13}C$ Isotopic values for select compounds in the Peace River section. For aryl isoprenoid measurements, first value is relative to the baseline, and the value in parentheses is the peak alone. All values are measured permil relative to VPDB. Individual wells are demarcated by dashed lines.

contained farnesane, this compound was consistently enriched in $\delta^{13}C$ relative to the average of pristane and phytane by an average of 1.55‰. (See Table 3.1 and Figure 3.4.) As there are many potential sources for farnesane, of which farnesol from Chlorobi is only one, even a small enrichment in this compound can be considered consistent with input from Chlorobi.

The abundance and isotopic composition of crocetane was recently studied in Devonian sections of high thermal maturity and evaluated as a potential biomarker for photic zone euxinia (Maslen et al. 2009). Crocetane is an irregularly branched C_{20} isoprenoid hydrocarbon whose structure corresponds to the central, acyclic portion of a typical carotenoid molecule. It has been proposed that some crocetane could be derived, via catagenetic cleavage reactions, from aromatic carotenoid precursors including isorenieratane and chlorobactane. This same study also reported that crocetane was absent in previously studied sections from the Permian-Triassic boundary described by Grice et al. (Grice et al. 1996; Grice et al. 2005a; Grice et al. 2005b). Crocetane was not seen in the Late Permian rocks, but was measured in the Triassic rocks, with concentrations slightly higher in the Dienerian than the Griesbachian. Although no measurements were made of the $\delta^{13}C$ value of this crocetane, the presence of this compound in the Peace River section is significant. The intervals in Peace River where crocetane was measured corresponded to some of the highest values of carotenoid-derived compounds and TOC measured in the section. This may indicate that higher preservation of organic material and increased input of Chlorobi-derived biomarkers in this interval allowed for a relatively larger amount of this compound to be produced during diagenesis.

Biomarkers for the Microbial Community

In the earlier study of the Peace River composite section, the ratio of hopanes to steranes was found to be >1 throughout. While not abnormally high, this value suggests that a high proportion of the

organic matter in all except the youngest section was contributed by bacteria as opposed to algae. In addition, peaks for the 2-methylhopane index between 7% and 13% were measured in the section, which may indicate a greater input of cyanobacterial biomass to the sedimentary rocks.

Although the age of the Peace River section was well-documented using conodont biostratigraphy, it is important to verify, wherever possible, that biomarkers that represent microbial communities of a particular time period are appropriate for the known age of the rocks. This provides assurance that younger petroleum has not migrated through the rocks and compromised the interpretation of the other biomarkers.

Empirical evidence from a number of worldwide sections shows that the identification of an excess of C_{33} *n*-alkylcyclohexane (C_{33} *n*-ACH) above C_{34} *n*-alkane has been observed to correspond with the main extinction event at the Permian-Triassic boundary. Although the unusual distribution of this compound has been used for correlation within the Perth Basin for nearly two decades (Jefferies 1984), the origin of this compound remains unknown. In the Peace River location, many of the samples contain anomalously high C_{33} *n*-ACH relative to *n*-C_{34}. (See Figure 3.5.) The highest concentrations of this compound relative to the *n*-C_{34} are in the samples in the group that span the transition. (See Figure 3.6.) In the younger samples, from higher in the Triassic section, this compound is less abundant; however, it is still more abundant than *n*-C_{34}. In the youngest samples the peak for this compound retreats into the background. The presence of this compound in Peace River at the Permian-Triassic transition and immediately following it matches patterns seen in other worldwide sections of the same age.

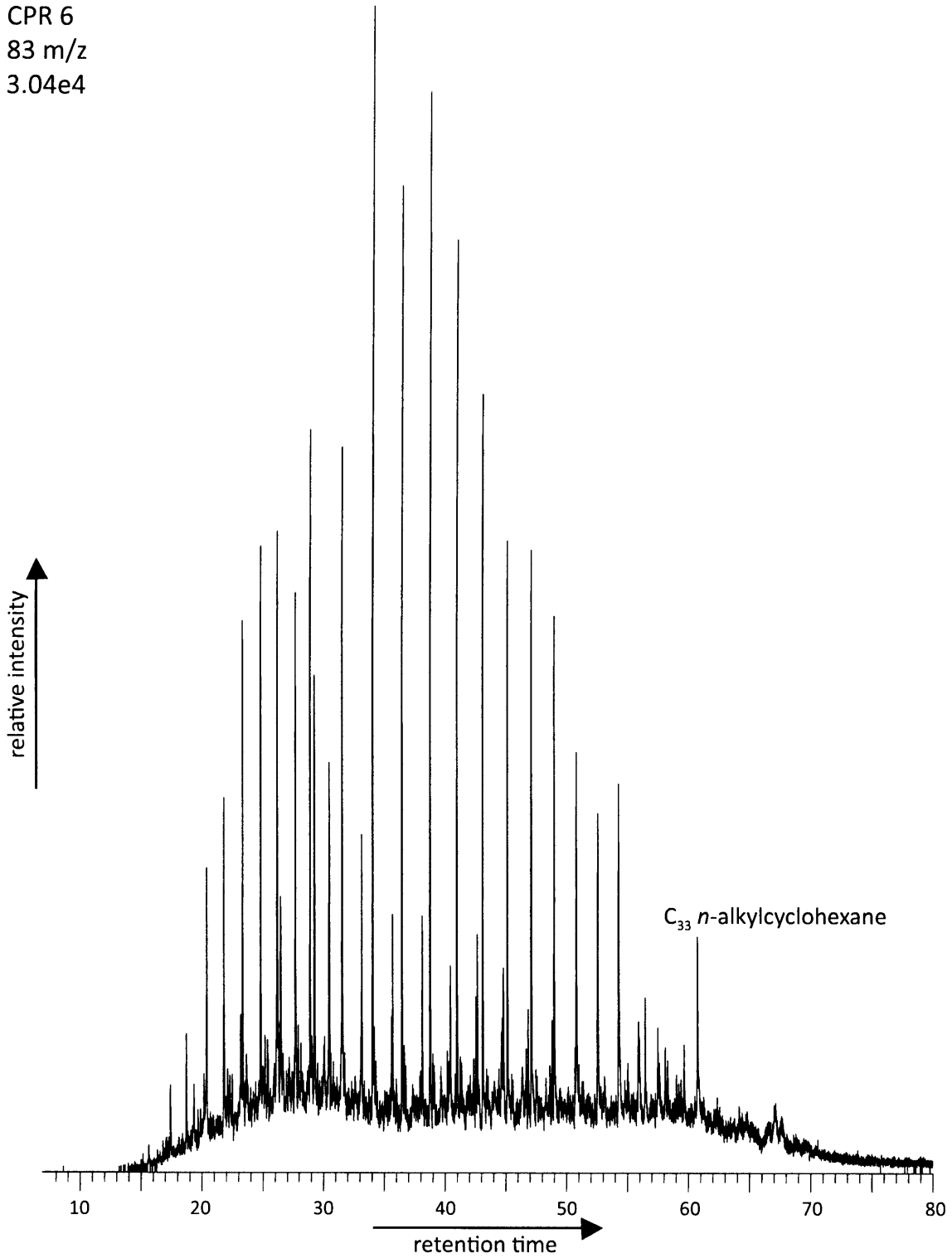

Figure 3.5 GC-MS select ion chromatogram of mass 83 from a sample saturated hydrocarbon fraction from Peace River. Elevated abundances of C_{33} *n*-alkylcyclohexane can be seen.

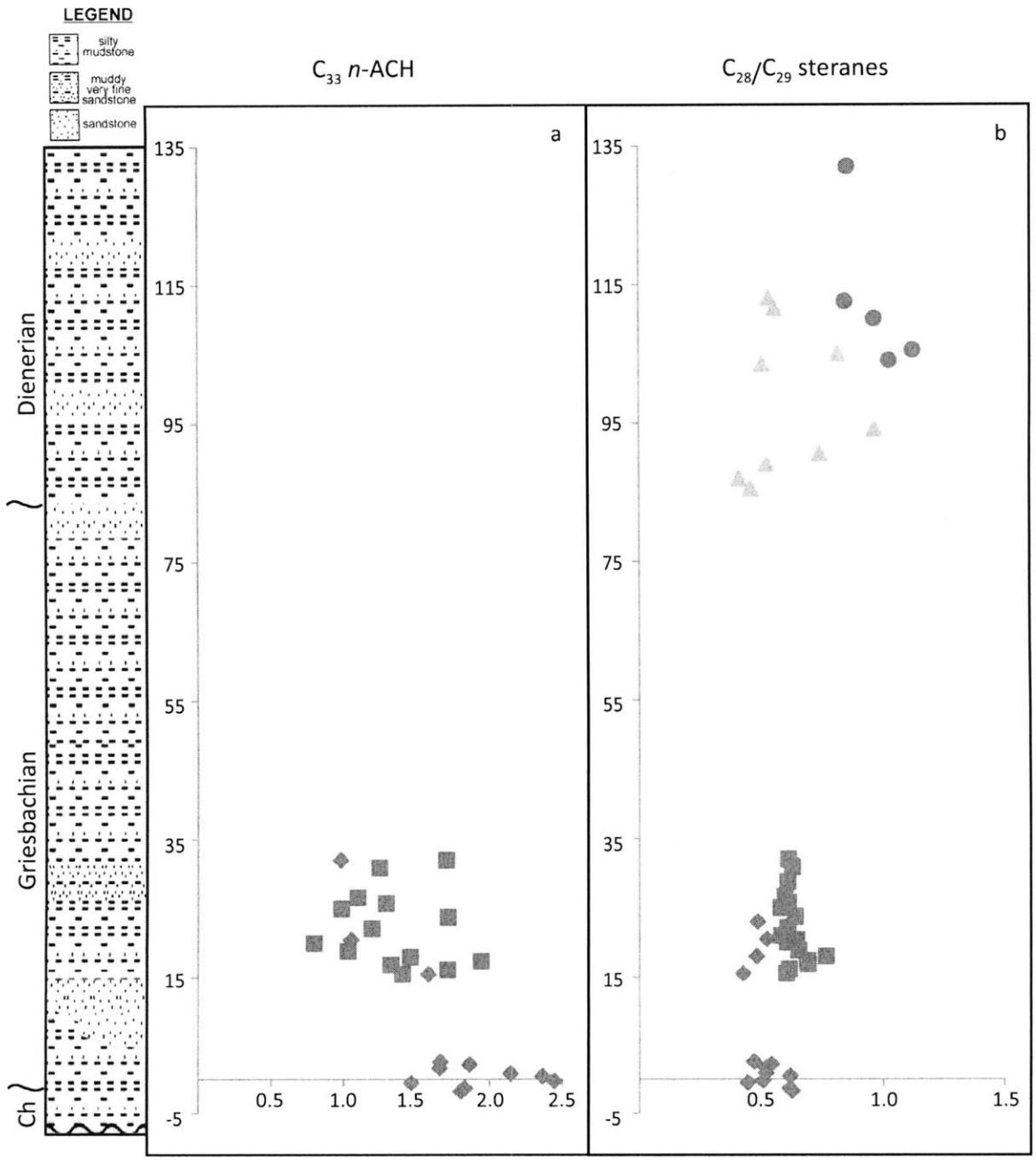

Figure 3.6 Age-sensitive biomarkers from the Peace River section. (a) The ratio of C_{33} *n*-alkylcyclohexane to C_{34} *n*-alkanes. (b) The ratio of total C_{28} to total C_{29} steranes. The four different symbols (diamonds, squares, triangles and circles) represent samples from the four different wells from this composite section. Compounds were measured by GC-MS in MRM mode. All parameters are plotted relative to depth. Composite litholog adapted from Hays et al. 2007.

Another biomarker proxy that is relevant for the general age of the section is the ratio of C_{28}/C_{29} steranes. Studies of this parameter in rocks and petroleum from all ages have suggested that a ratio between 0.4 and 0.7 is typical around the mid-Phanerozoic, and this value increases with time throughout the Phanerozoic. In Peace River, the oldest section that spans the transition has an average ratio of 0.61, whereas the younger section in the earliest Triassic period has slightly higher values with an average of 0.63. It is only in the youngest section that this ratio increases to an average of 0.8. (See Figure 3.6.) All of these values are consistent with these rocks being deposited at the Permian-Triassic transition.

Stable Carbon Isotopes in Hydrocarbons

In most Phanerozoic environments, it has been observed that the isoprenoids pristane and phytane, produced primarily by photoautotrophs, generally have higher $\delta^{13}C$ values than the *n*-alkanes, heptadecane and octadecane, which are derived from both the intact hydrocarbons and the fatty acids of a wide range of organisms. (See Figure 3.7.) The inverse phenomenon, termed anomalous isotopic ordering, which is the enrichment of *n*-alkanes relative to isoprenoids, is observed in sedimentary rocks from the Proterozoic as well as a few sections in the Phanerozoic associated with anoxic deposition (Logan et al. 1995). A study of a number of sections from the Neoproterozoic suggests the transition between these two states is related to ventilation of the marine realm (Kelly 2009). The measured difference between the $\delta^{13}C$ values of the *n*-alkanes *n*-C_{17} and *n*-C_{18} and the isoprenoids, pristane and phytane, has been termed $\Delta\delta$.

In the oldest portion of the Peace River section, the average $\delta^{13}C$ value of the *n*-alkanes is enriched relative to the average $\delta^{13}C$ value isoprenoids. (See Table 3.1 and Figure 3.8.) At the identified

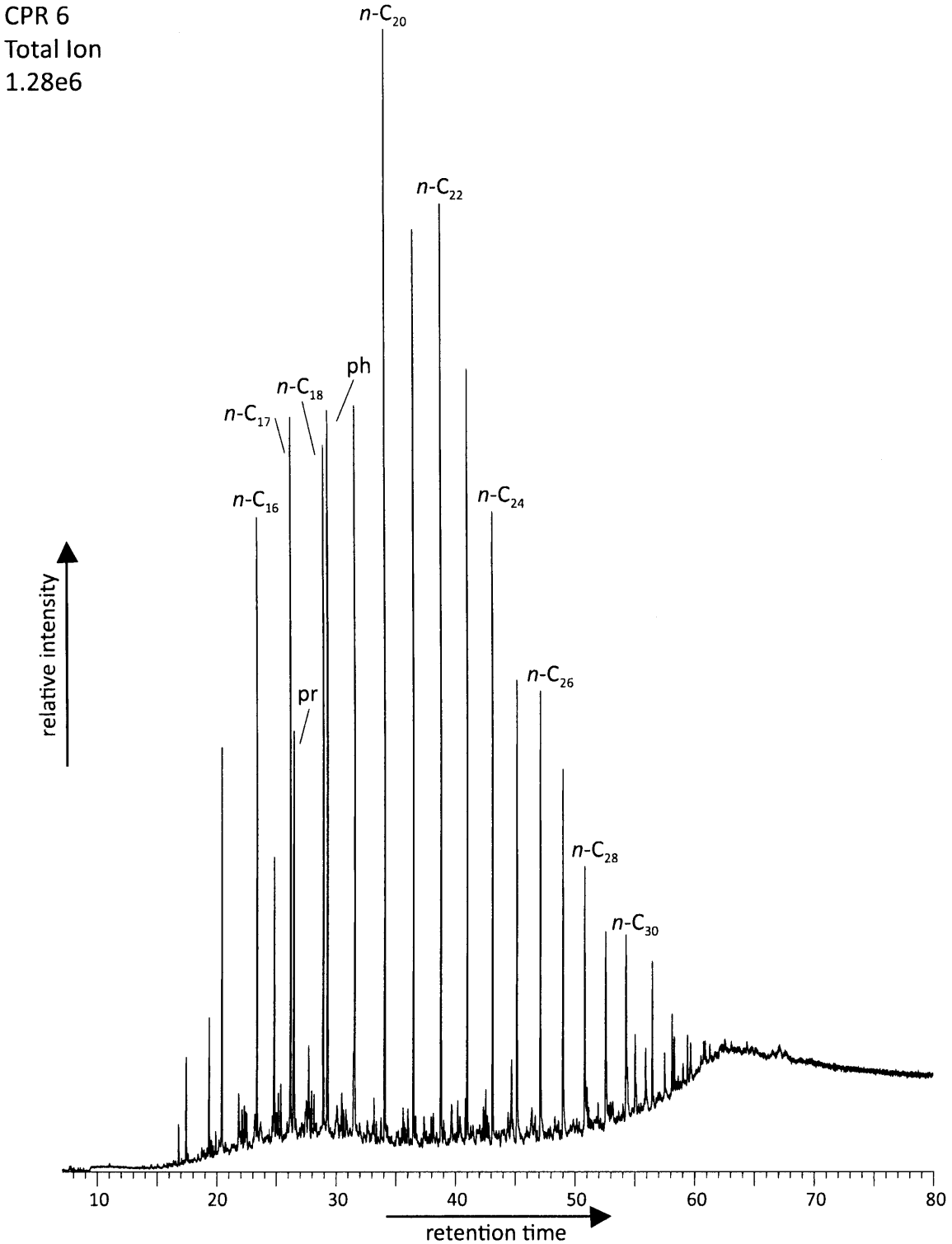

Figure 3.7 GC-MS full-scan chromatogram of total ion current from a sample saturated hydrocarbon fraction from Peace River. Isoprenoids pristane and phytane as well as *n*-alkanes are identified.

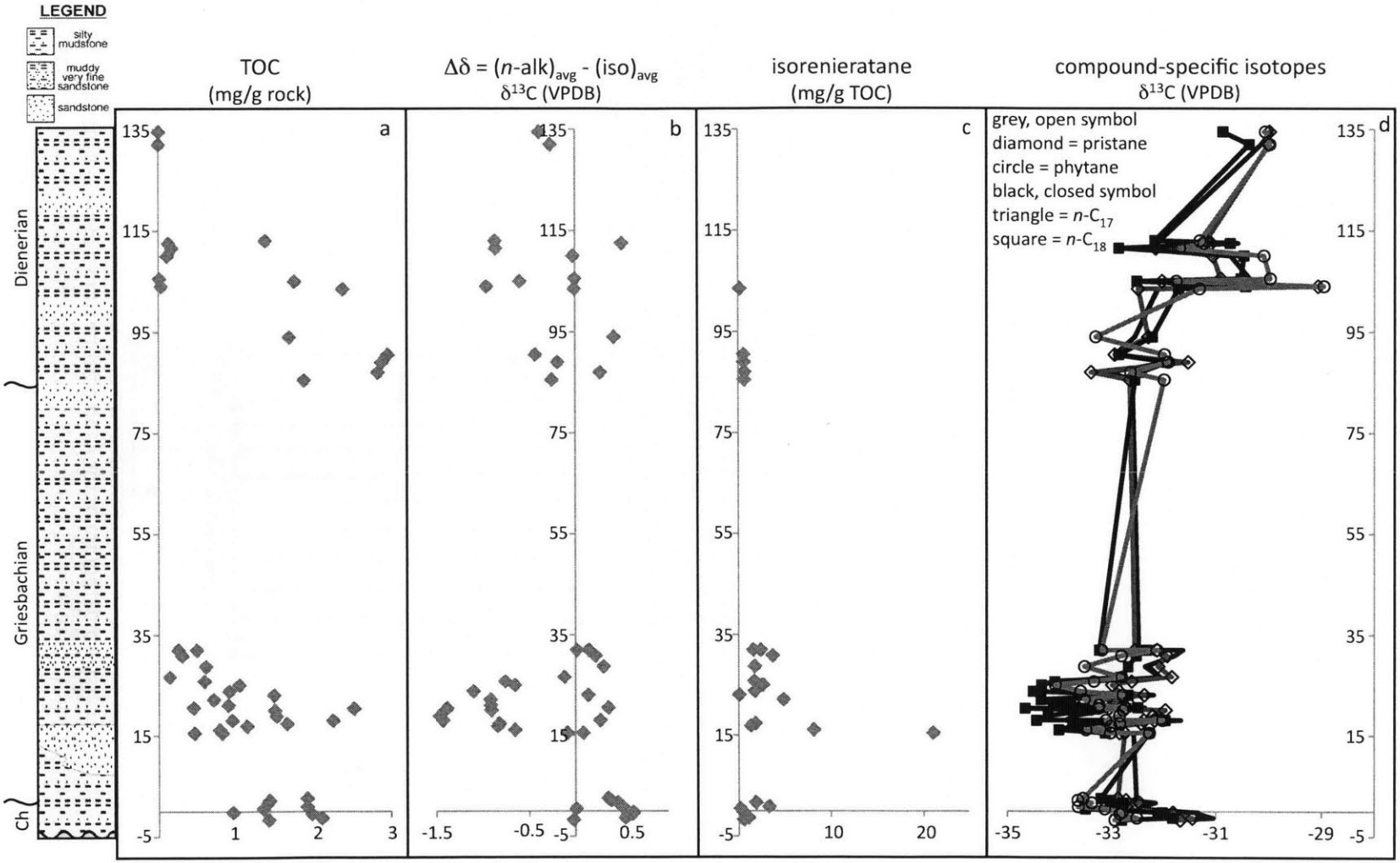

Figure 3.8 Δδ-related biomarkers from the Peace River section. Isotopes for Δδ (b) and compound-specific (d) were measured in permil relative to VPDB on GC-irMS. Isorenieratane (c) quantities were normalized relative to total organic carbon contents and measured on GC-MS SIM mode. All parameters are plotted relative to depth. Composite litholog adapted from Hays et al. 2007.

Permian-Triassic transition, the $\Delta\delta$ values are the highest in the section. Just after the transition, in the oldest Triassic rocks, many positive $\Delta\delta$ values were measured as well as some negative values. In the youngest section, a bit later in the Triassic period, there are both positive and negative values for $\Delta\delta$, but the average value in this section is close to zero. There is good agreement between the $\delta^{13}C$ values of the *n*-alkanes, but the $\delta^{13}C$ values of the isoprenoids are more varied. (See Figure A1.2 in Appendix 1.) However, no individual compound has a significantly different $\delta^{13}C$ value, which would indicate that it might have come from a separate, disparate, source. When $\delta^{13}C$ values of the four compounds are plotted individually relative to depth, no significant offset is observable between the *n*-alkanes and isoprenoids. Comparison of this plot to a plot of $\Delta\delta$ values shows no definitive pattern of the individual isotopes or groups of isotopes driving changes in the in $\Delta\delta$. (See Figure 3.6.) (See Appendix 1 for uncertainties in isotope measurements.)

Correlation coefficients were calculated between the $\Delta\delta$ pattern and all other parameters measured, and values > |0.3| indicate a relationship exists between the variables 95% of the time based on the Pearson Correlation Coefficient for these number of samples. (See Appendix 1 for methods.) The only significant correlations were measured to the pattern of the pristane/phytane ratio (0.34). Although this proxy is low throughout the section, this demonstrates that in the intervals in which the $\Delta\delta$ pattern was more negative, there was strong evidence for anoxia. Unfortunately no other significant correlations were observed, as the composite nature of this section makes it less than ideal for measuring patterns throughout the section.

These results, when examined in respect to the original work on this proxy (Logan et al. 1995), are consistent with proposals that the sedimentary input near the Permian-Triassic transition was dominated by heterotrophic organisms as would be expected in a stratified water column with

increased reworking of organic material in the upper oxic zone of the water column. In the Triassic interval, the $\Delta\delta$ isotopic signal shifts to a more negative value, but it is still an anomalous signal, less than typically encountered in the lipids of autotrophic organisms (Schouten et al. 1998; Hayes 2001). An alternative interpretation of these data, based on a more recent study of modern sediments (Close et al. 2008), is that anomalous isotopic ordering may be the result of an increased sedimentary input from organisms that dominate the small size fractions in particulate organic matter, such as bacteria.

Summary

The earlier published study (Hays et al. 2007), established the biomarker evidence for photic zone euxinia in the northeast region of the Panthalassic Ocean through the Permian-Triassic transition. Additional data presented here support and strengthen this conclusion. The presence of both isorenieratane and chlorobactane (and to a lesser extent crocetane) indicates that these carotenoids were likely the source of the aryl isoprenoids measured and reported earlier. The enriched values of $\delta^{13}C$ for the aryl isoprenoids and farnesane are consistent with a derivation from the photopigments of Chlorobi as well. The identification of chlorobactane in particular provides evidence that the chemocline was much more shallow, at least intermittently, than was previously assumed in this region of the Panthalassic ocean. This may be evidence of chemocline-upward-excursions that could have lead to the release of hydrogen sulfide into the atmosphere.

Although the age of the Peace River section is well established via biostratigraphy, the measurements of the C_{33} *n*-ACH and C_{28}/C_{29} steranes strengthens the assumption that the biomarkers measured here were deposited along with the sedimentary rocks from which they were extracted. Also, the

measurement of C_{33} *n*-ACH in this section is a significant result since it has been reported in only a few previous sections, all from the Permian-Triassic boundary (Grice et al. 2005c; McIldowie and Alexander 2005).

Perhaps most interesting of the new results is the measurement of positive $\Delta\delta$, a reversed isotopic ordering of hydrocarbons, which indicates an increase in heterotrophic reworking in the stratified water column and an increase in the prokaryotic input to the sedimentary rocks close to the Permian-Triassic transition. A microbial community dominated by bacterial biomass may be indicated when one considers the significant inputs from Chlorobi in this section and the corresponding values of 2-methylhopane index, which are high for the shales where they were measured, as well as the relatively high hopane/sterane ratio throughout this section. This is consistent with the conclusions reached in Cao et al. (2009), where the evidence for enhanced bacterial productivity was shown to extend into the Permian. Data from Peace River does not extend far into the Permian, but extends significantly into the Triassic period and indicates that the conditions that were conducive to the rise of this unusual planktonic community persisted and may have been a factor in the protracted recovery.

References

Cao, C., G. D. Love, L. E. Hays, W. Wang, S. Shen and R. E. Summons (2009). "Biogeochemical Evidence for Euxinic Oceans and Ecological Disturbance Presaging the End-Permian Mass Extinction Event." Earth and Planetary Science Letters **281**(3-4): 188-201.

Close, H., A. Diefendorf, K. H. Freeman and A. Pearson (2008). "A Modern Analogue for Proterozoic Inverse Carbon Isotope Signatures." Eos Trans. AGU **89**(53): Fall Meet. Suppl., Abstract PP14A-07.

Grasby, S. E. and B. Beauchamp (2008). "Intrabasin Variability of the Carbon-Isotope Record across the Permian-Triassic Transition, Sverdrup Basin, Arctic Canada." Chemical Geology **253**(3-4): 141-150.

Grasby, S. E. and B. Beauchamp (2009). "Latest Permian to Early Triassic Basin-to-Shelf Anoxia in the Sverdrup Basin, Arctic Canada." Chemical Geology **264**(1-4): 232-246.

Grice, K., C. Cao, G. D. Love, M. E. Bottcher, R. J. Twitchett, E. Grosjean, R. E. Summons, S. C. Turgeon, W. Dunning and Y. Jin (2005a). "Photic Zone Euxinia During the Permian-Triassic Superanoxic Event." Science **307**(5710): 706-709.

Grice, K., P. Schaeffer, L. Schwark and J. R. Maxwell (1996). "Molecular Indicators of Palaeoenvironmental Conditions in an Immature Permian Shale (Kupferschiefer, Lower Rhine Basin, North-West Germany) from Free and S-Bound Lipids." Organic Geochemistry **25**(3-4): 131-147.

Grice, K., R. E. Summons, E. Grosjean, R. J. Twichett, W. Dunning, S. X. Wang and M. E. Boettcher (2005b). "Novel Depositional Conditions of the Northern Onshore Perth Basin (Basal Triassic)." AAPEA Journal **45**: 263-273.

Grice, K., R. J. Twitchett, R. Alexander, C. B. Foster and C. Looy (2005c). "A Potential Biomarker for the Permian-Triassic Ecological Crisis." Earth and Planetary Science Letters **236**(1-2): 315-321.

Hayes, J. M. (2001). Fractionation of the Isotopes of Carbon and Hydrogen in Biosynthetic Processes. Stable Isotope Geochemistry, Reviews in Mineralogy and Geochemistry. J. W. Valley and D. R. Cole. Washington, DC, Mineralogical Society of America: 225-278.

Hays, L., T. Beatty, C. M. Henderson, G. D. Love and R. E. Summons (2007). "Evidence for Photic Zone Euxinia through the End-Permian Mass Extinction in the Panthalassic Ocean (Peace River Basin, Western Canada)." Palaeoworld **16**(1-3): 39-50

Henderson, C. M. (1997). "Uppermost Permian Conodonts and the Permian-Triassic Boundary in the Western Canada Sedimentary Basin." Bulletin of Canadian Petroleum Geology **45**(4): 693-707.

Henderson, C. M. and A. Baud (1997). Correlation of the Permian-Triassic Boundary in Arctic Canada and Comparison with Meishan, China. Proceedings of the 30th International Geological Congress.

Jefferies, P. (1984). Petroleum Geochemistry of the Northern Perth Baisn, Western Austrialian Institute of Technology.

Kelly, A. E. (2009). Hydrocarbon Biomarkers for Biotic and Environmental Evolution through the Neoproterozoic-Cambrian Transition. Earth, Atmospheric and Planetary Sciences. Cambridge, MA, Massachusetts Institute of Technology. **PhD:** 154.

Koopmans, M. P., J. Köster, H. M. E. Van Kaam-Peters, F. Kenig, S. Schouten, W. A. Hartgers, J. W. de Leeuw and J. S. Sinninghe Damste (1996). "Diagenetic and Catagenetic Products of Isorenieratene: Molecular Indicators for Photic Zone Anoxia." Geochimica et Cosmochimica Acta **60**(22): 4467.

Logan, G. A., J. M. Hayes, G. B. Hieshima and R. E. Summons (1995). "Terminal Proterozoic Reorganization of Biogeochemical Cycles." Nature **376**(6535): 53-56.

Maslen, E., K. Grice, J. D. Gale, C. Hallmann and B. Horsfield (2009). "Crocetane: A Potential Marker of Photic Zone Euxinia in Thermally Mature Sediments and Crude Oils of Devonian Age." Organic Geochemistry **40**(1): 1-11.

McIldowie, M. and R. Alexander (2005). "Identification of a Novel C33 N-Alkylcyclohexane Biomarker in Permian-Triassic Sediments." Organic Geochemistry **36**(10): 1454-1458.

Moldowan, J. M. (1984). "C30-Steranes, Novel Markers for Marine Petroleums and Sedimentary Rocks." Geochimica et Cosmochimica Acta **48**(12): 2767-2768.

Montesinos, E., R. Guerrero, C. Abella and I. Esteve (1983). "Ecology and Physiology of the Competition for Light between Chlorobium Limicola and Chlorobium Phaeobacteroides in Natural Habitats." Appl. Environ. Microbiol. **46**(5): 1007-1016.

Nassichuck, W., R. Thorsteinsson and E. Tozer (1973). "Permian-Triassic Boundary in the Canadian Arcitc Archipelago." Bulletin of Canadian Petroleum Geology **20**(4): 651-658.

Overmann, J. (2001). Green Sulfur Bacteria. Encyclopedia of Life Sciences. J. Battista, John Wiley & Sons.

Peters, K. E., J. M. Moldowan and C. C. Walters (2005). The Biomarker Guide. Cambridge, UK; New York, Cambridge University Press.

Schouten, S., W. C. M. Klein Breteler, P. Blokker, N. Schogt, W. I. C. Rijpstra, K. Grice, M. Baas and J. S. Sinninghe Damstè (1998). "Biosynthetic Effects on the Stable Carbon Isotopic Compositions of Algal Lipids: Implications for Deciphering the Carbon Isotopic Biomarker Record." Geochimica et Cosmochimica Acta **62**(8): 1397-1406.

Zumberge, J. E. (1987). "Prediction of Source Rock Characteristics Based on Terpane Biomarkers in Crude Oils: A Multivariate Statistical Approach." Geochimica et Cosmochimica Acta **51**: 1625-1637.

Table 3.S1: Total biomarker and isotopic data from Peace River, Canada

sample #	relative depth	extracted rock (g)	TLE (mg)	sats (mg)	aros (mg)	TOC (mg C/ g rock)	HI	OI	Pr/Ph
46	134.5	14.82	4.7	0.90	0.50	0.00	-	100	1.385
45	132.0	14.97	2.3	0.50	0.60	0.00	-	243	1.310
44	112.5	14.82	5.4	0.80	0.50	0.13	186	129	0.922
43	110.0	14.78	8.2	0.90	1.50	0.11	157	443	1.028
42	105.5	14.93	2.5	0.80	0.80	0.01	12	125	1.530
41	104.0	14.6	2.9	1.50	0.60	0.03	7	67	1.162
40	113.0	14.45	68.8	24.10	15.40	1.38	288	52	0.935
39	111.5	14.39	13.8	4.40	1.60	0.17	85	190	0.935
38	105.0	14.42	56.4	14.10	7.30	1.76	244	40	0.689
37	103.5	14.79	87	23.50	12.60	2.38	372	45	0.734
36	94.0	14.61	69.5	22.10	10.70	1.69	273	53	0.848
35	90.5	14.53	81.2	17.90	9.70	2.96	375	30	0.691
34	89.0	14.53	96.6	22.20	11.40	2.88	343	43	1.067
33	87.0	14.46	91.8	20.50	14.00	2.83	388	37	0.681
32	85.5	14.33	82	22.20	9.30	1.88	281	40	0.782
31	32.0	14.89	21	4.59	3.38	0.49	114	53	0.478
30	30.9	14.97	15.5	2.96	2.28	0.30	150	60	0.546
29	28.8	14.92	23	4.18	2.93	0.61	203	70	0.586
28	26.6	14.97	16.3	3.48	2.20	0.14	64	114	0.586
27	25.8	14.97	23.9	6.26	3.98	0.59	174	88	0.405
26	25.0	14.83	19.7	2.59	3.11	1.04	170	44	0.388
25	23.8	14.92	27.6	5.37	3.66	0.91	239	58	0.371
24	22.1	14.95	38.6	2.98	3.33	0.71	154	63	0.356
23	21.0	14.89	16.6	2.85	1.66	0.90	214	76	0.432
22	20.4	14.96	11.7	3.39	1.23	2.52	319	38	0.301
21	20.0	14.91	8.5	1.09	0.87	1.50	288	54	0.472
20	18.9	14.86	21.6	5.73	3.97	1.52	292	54	0.335
19	18.0	14.86	1.9	0.84	0.84	2.25	331	35	0.283
18	17.4	14.89	55.4	7.64	4.97	1.66	307	44	0.414
17	16.9	14.86	22.6	5.77	5.77	1.14	224	49	0.317
16	16.1	14.83	24.8	9.60	8.00	0.79	176	53	0.311
15	15.5	14.88	9.4	0.48	0.48	0.46	159	90	0.388
14	32.0	14.92	11.7	2.09	1.67	0.25	119	157	0.698
13	23.0	14.91	16.7	3.75	1.36	1.49	298	46	0.611
12	20.5	14.85	18.2	8.27	5.79	0.45	155	100	0.684
11	18.0	14.96	18.5	6.17	3.16	0.95	237	72	0.865
10	15.5	14.98	44.8	36.65	15.27	0.82	191	60	0.656
9	2.6	15.96	21.2	4.42	4.86	1.92	287	39	0.506
8	2.2	14.92	15.9	3.72	2.03	1.43	255	46	0.566
7	1.7	14.94	39.3	9.59	4.31	1.41	239	41	0.605
6	0.9	14.94	48.7	11.99	6.74	1.92	282	34	0.539
5	0.5	14.84	1.4	2.10	0.70	1.35	180	44	0.363
4	-0.2	14.84	27.7	7.40	3.38	0.96	213	67	0.786
3	-0.5	14.81	18.9	4.45	2.22	1.98	215	25	0.883
2	-1.3	14.1	39.8	8.13	5.42	2.11	254	35	0.777
1	-1.7	14.37	33.3	8.54	5.12	1.42	158	31	0.487

Table 3.S1: Total biomarker and isotopic data from Peace River, Canada

			Tricyclics				
sample #	relative depth	Hopane/ Sterane	C19/(Total Tricyclic)	C20/(Total Tricyclic)	C21/(Total Tricyclic)	C22/(Total Tricyclic)	C23/(Total Tricyclic)
46	134.5	ND	ND	ND	ND	ND	ND
45	132.0	0.621	0.053	0.129	0.156	0.045	0.308
44	112.5	0.950	0.064	0.141	0.177	0.047	0.305
43	110.0	0.710	0.045	0.103	0.138	0.046	0.343
42	105.5	0.744	0.113	0.239	0.183	0.045	0.204
41	104.0	0.713	0.094	0.242	0.223	0.051	0.225
40	113.0	1.785	0.018	0.075	0.119	0.061	0.341
39	111.5	1.530	0.024	0.082	0.124	0.057	0.341
38	105.0	2.571	0.012	0.049	0.116	0.055	0.341
37	103.5	2.803	0.011	0.046	0.097	0.042	0.307
36	94.0	1.599	0.022	0.070	0.129	0.045	0.270
35	90.5	2.212	0.018	0.068	0.129	0.037	0.274
34	89.0	2.310	0.020	0.072	0.135	0.038	0.275
33	87.0	2.084	0.015	0.066	0.126	0.039	0.303
32	85.5	1.660	0.017	0.077	0.132	0.035	0.284
31	32.0	2.985	0.005	0.046	0.132	0.034	0.310
30	30.9	2.315	0.007	0.053	0.138	0.035	0.312
29	28.8	2.318	0.009	0.060	0.161	0.036	0.308
28	26.6	2.086	0.008	0.060	0.172	0.036	0.303
27	25.8	1.896	0.003	0.044	0.139	0.033	0.284
26	25.0	2.102	0.003	0.051	0.159	0.035	0.318
25	23.8	2.123	0.003	0.053	0.173	0.035	0.302
24	22.1	2.015	0.003	0.052	0.166	0.035	0.298
23	21.0	1.907	0.003	0.053	0.160	0.037	0.331
22	20.4	1.752	0.002	0.035	0.118	0.034	0.298
21	20.0	2.524	0.004	0.050	0.145	0.037	0.335
20	18.9	2.554	0.003	0.047	0.136	0.036	0.323
19	18.0	3.483	0.004	0.054	0.151	0.043	0.333
18	17.4	2.944	0.004	0.051	0.136	0.038	0.319
17	16.9	2.494	0.003	0.049	0.143	0.039	0.306
16	16.1	2.731	0.005	0.058	0.177	0.035	0.282
15	15.5	2.703	0.008	0.064	0.203	0.041	0.286
14	32.0	2.752	0.012	0.063	0.195	0.035	0.264
13	23.0	2.452	0.010	0.068	0.209	0.037	0.289
12	20.5	2.175	0.013	0.075	0.179	0.035	0.281
11	18.0	1.773	0.016	0.078	0.153	0.030	0.265
10	15.5	1.674	0.013	0.083	0.161	0.034	0.273
9	2.6	3.975	0.010	0.064	0.191	0.044	0.284
8	2.2	3.385	0.010	0.057	0.185	0.040	0.312
7	1.7	2.152	0.012	0.058	0.182	0.041	0.314
6	0.9	2.185	0.008	0.054	0.183	0.039	0.309
5	0.5	1.777	0.004	0.043	0.169	0.036	0.314
4	-0.2	1.736	0.008	0.050	0.155	0.041	0.328
3	-0.5	1.778	0.009	0.049	0.145	0.039	0.362
2	-1.3	1.707	0.004	0.038	0.107	0.036	0.381
1	-1.7	1.731	0.004	0.038	0.112	0.039	0.383

Table 3.S1: Total biomarker and isotopic data from Peace River, Canada

		Tricyclics						
sample #	relative depth	C24/(Total Tricyclic)	C25/(Total Tricyclic)	C26/(Total Tricyclic)	C25 S/R	C26 S/R	C19/C23	C22/C21
46	134.5	ND	ND	ND	ND	ND	ND	ND
45	132.0	0.154	0.100	0.054	0.894	0.965	0.173	0.287
44	112.5	0.140	0.083	0.042	1.068	0.998	0.211	0.266
43	110.0	0.169	0.102	0.056	1.078	1.015	0.130	0.332
42	105.5	0.092	0.080	0.044	1.017	0.928	0.554	0.245
41	104.0	0.093	0.050	0.022	0.940	0.926	0.417	0.227
40	113.0	0.151	0.138	0.097	0.921	1.046	0.052	0.511
39	111.5	0.145	0.133	0.093	0.919	1.105	0.072	0.461
38	105.0	0.151	0.146	0.131	0.929	1.017	0.035	0.474
37	103.5	0.183	0.158	0.155	1.067	1.028	0.037	0.438
36	94.0	0.200	0.145	0.119	0.923	0.973	0.082	0.347
35	90.5	0.169	0.155	0.148	0.964	1.029	0.067	0.287
34	89.0	0.172	0.143	0.145	0.948	1.010	0.073	0.283
33	87.0	0.172	0.141	0.136	0.934	1.006	0.051	0.313
32	85.5	0.172	0.154	0.128	0.941	0.999	0.061	0.264
31	32.0	0.160	0.171	0.143	0.796	0.976	0.015	0.254
30	30.9	0.155	0.164	0.137	0.769	0.981	0.022	0.254
29	28.8	0.146	0.148	0.131	0.775	0.956	0.028	0.220
28	26.6	0.149	0.142	0.129	0.868	1.005	0.026	0.211
27	25.8	0.159	0.179	0.159	0.877	0.999	0.011	0.236
26	25.0	0.146	0.150	0.137	0.808	0.947	0.011	0.218
25	23.8	0.147	0.148	0.140	0.788	0.972	0.010	0.200
24	22.1	0.150	0.152	0.143	0.870	0.981	0.011	0.211
23	21.0	0.143	0.146	0.127	0.827	0.976	0.010	0.230
22	20.4	0.164	0.188	0.161	0.917	0.962	0.006	0.286
21	20.0	0.144	0.154	0.129	0.819	0.977	0.012	0.257
20	18.9	0.153	0.165	0.137	0.826	0.945	0.008	0.266
19	18.0	0.145	0.148	0.123	0.831	0.992	0.012	0.286
18	17.4	0.147	0.163	0.142	0.792	0.950	0.013	0.279
17	16.9	0.151	0.163	0.146	0.798	0.948	0.010	0.270
16	16.1	0.144	0.149	0.149	0.819	0.922	0.018	0.197
15	15.5	0.135	0.139	0.125	0.871	0.940	0.029	0.201
14	32.0	0.145	0.145	0.140	0.930	1.008	0.047	0.182
13	23.0	0.137	0.128	0.121	0.805	0.990	0.034	0.179
12	20.5	0.152	0.134	0.132	0.841	0.960	0.047	0.196
11	18.0	0.169	0.151	0.137	0.956	1.019	0.061	0.196
10	15.5	0.162	0.146	0.127	0.868	1.024	0.048	0.211
9	2.6	0.150	0.138	0.118	0.922	0.977	0.036	0.231
8	2.2	0.145	0.132	0.118	0.953	0.960	0.031	0.217
7	1.7	0.133	0.135	0.124	0.807	0.952	0.038	0.226
6	0.9	0.143	0.136	0.129	0.801	0.976	0.024	0.211
5	0.5	0.149	0.148	0.137	0.843	0.961	0.013	0.215
4	-0.2	0.145	0.148	0.124	0.818	0.942	0.025	0.263
3	-0.5	0.138	0.141	0.117	0.831	0.929	0.024	0.270
2	-1.3	0.146	0.161	0.127	0.936	0.982	0.011	0.332
1	-1.7	0.147	0.153	0.123	0.891	0.986	0.009	0.349

Table 3.S1: Total biomarker and isotopic data from Peace River, Canada

		Tricyclics			Steranes			
sample #	relative depth	C24/C25	C26/C25	Tet/C23	C27 Dia/Reg	C27 Dia S/(S+R)	C27 Reg abb/aaa	C27 Reg aaa S/(S+R)
46	134.5	ND	ND	ND	ND	ND	ND	ND
45	132.0	1.537	0.538	0.234	1.120	0.614	0.836	0.517
44	112.5	1.681	0.501	0.184	0.925	0.623	0.839	0.531
43	110.0	1.661	0.555	0.206	1.221	0.638	0.901	0.475
42	105.5	1.144	0.541	0.283	1.538	0.622	0.808	0.531
41	104.0	1.848	0.437	0.158	1.320	0.605	0.920	0.488
40	113.0	1.095	0.704	0.246	0.234	0.610	1.183	0.495
39	111.5	1.086	0.697	0.182	0.370	0.605	1.243	0.508
38	105.0	1.038	0.896	0.242	0.126	0.634	1.240	0.515
37	103.5	1.159	0.978	0.286	1.513	0.627	1.236	0.498
36	94.0	1.378	0.819	0.200	0.144	0.608	1.245	0.523
35	90.5	1.090	0.955	0.245	0.506	0.615	1.286	0.524
34	89.0	1.205	1.017	0.300	0.736	0.617	1.229	0.531
33	87.0	1.221	0.963	0.240	0.617	0.610	1.264	0.509
32	85.5	1.112	0.831	0.233	0.516	0.611	1.242	0.519
31	32.0	0.936	0.836	0.106	0.134	0.542	1.159	0.532
30	30.9	0.946	0.834	0.094	0.115	0.585	1.206	0.531
29	28.8	0.987	0.885	0.110	0.150	0.598	1.227	0.541
28	26.6	1.048	0.907	0.114	0.193	0.606	1.247	0.529
27	25.8	0.885	0.888	0.122	0.196	0.620	1.218	0.549
26	25.0	0.973	0.907	0.103	0.188	0.593	1.240	0.535
25	23.8	0.993	0.944	0.103	0.130	0.636	1.231	0.544
24	22.1	0.985	0.940	0.107	0.143	0.579	1.180	0.523
23	21.0	0.981	0.872	0.092	0.238	0.601	1.227	0.545
22	20.4	0.873	0.855	0.102	0.129	0.635	1.197	0.523
21	20.0	0.934	0.836	0.075	0.188	0.601	1.190	0.530
20	18.9	0.927	0.831	0.083	0.147	0.553	1.276	0.542
19	18.0	0.980	0.831	0.110	0.105	0.557	1.184	0.515
18	17.4	0.901	0.868	0.110	0.143	0.598	1.200	0.545
17	16.9	0.924	0.892	0.129	0.143	0.583	1.238	0.536
16	16.1	0.971	1.005	0.170	0.102	0.582	1.306	0.547
15	15.5	0.969	0.894	0.196	0.108	0.600	1.175	0.529
14	32.0	1.001	0.964	0.204	0.154	0.596	1.272	0.545
13	23.0	1.067	0.946	0.178	0.195	0.615	1.261	0.523
12	20.5	1.135	0.984	0.184	0.180	0.600	1.274	0.534
11	18.0	1.118	0.909	0.203	0.260	0.616	1.305	0.526
10	15.5	1.104	0.868	0.202	0.347	0.639	1.319	0.529
9	2.6	1.091	0.860	0.205	0.150	0.651	1.307	0.503
8	2.2	1.097	0.888	0.148	0.198	0.604	1.246	0.500
7	1.7	0.981	0.919	0.137	0.284	0.597	1.285	0.533
6	0.9	1.055	0.951	0.129	0.334	0.615	1.292	0.535
5	0.5	1.009	0.926	0.126	0.340	0.611	1.258	0.533
4	-0.2	0.978	0.836	0.102	0.418	0.621	1.386	0.554
3	-0.5	0.981	0.826	0.086	0.594	0.635	1.209	0.508
2	-1.3	0.905	0.788	0.050	0.352	0.608	1.245	0.514
1	-1.7	0.960	0.803	0.059	0.312	0.623	1.269	0.507

Table 3.S1: Total biomarker and isotopic data from Peace River, Canada

		Steranes						
sample #	relative depth	C27 Reg abb S/R	C28 Dia/Reg	C28 Dia S/(S+R)	C28 Reg abb/aaa	C28 Reg aaa S/(S+R)	C28 Reg abb S/R	C29 Dia/Reg
46	134.5	ND	ND	ND	ND	ND	ND	ND
45	132.0	0.826	1.578	0.614	1.132	0.446	0.797	0.670
44	112.5	0.882	1.403	0.596	1.001	0.493	0.639	0.617
43	110.0	0.941	1.399	0.621	1.197	0.455	0.745	0.728
42	105.5	1.425	1.019	0.630	1.436	0.513	0.895	0.581
41	104.0	0.874	1.443	0.629	1.629	0.329	0.769	0.726
40	113.0	0.933	0.332	0.585	1.545	0.491	0.938	0.245
39	111.5	0.920	0.377	0.601	1.479	0.432	0.861	0.353
38	105.0	0.906	0.149	0.630	1.503	0.442	0.852	0.160
37	103.5	0.986	1.008	0.606	1.789	0.499	1.121	1.409
36	94.0	0.954	0.143	0.554	1.583	0.485	0.848	0.215
35	90.5	0.963	0.278	0.603	1.554	0.464	0.855	0.540
34	89.0	0.963	0.470	0.570	1.553	0.473	0.960	0.629
33	87.0	0.901	0.547	0.598	1.687	0.460	0.924	0.607
32	85.5	0.918	0.518	0.608	1.655	0.435	0.891	0.469
31	32.0	0.889	0.122	0.475	1.483	0.461	0.841	0.095
30	30.9	0.870	0.133	0.589	1.614	0.472	0.820	0.096
29	28.8	0.889	0.135	0.590	1.581	0.480	0.826	0.128
28	26.6	0.924	0.189	0.586	1.560	0.486	0.823	0.153
27	25.8	0.927	0.181	0.598	1.480	0.507	0.847	0.159
26	25.0	0.919	0.180	0.564	1.522	0.487	0.831	0.151
25	23.8	0.915	0.134	0.586	1.563	0.477	0.843	0.113
24	22.1	0.871	0.140	0.627	1.492	0.470	0.864	0.114
23	21.0	0.889	0.255	0.625	1.490	0.466	0.820	0.193
22	20.4	0.902	0.154	0.574	1.608	0.473	0.851	0.112
21	20.0	0.887	0.203	0.584	1.559	0.475	0.826	0.156
20	18.9	0.887	0.152	0.584	1.602	0.455	0.855	0.119
19	18.0	0.838	0.185	0.534	1.521	0.471	0.845	0.095
18	17.4	0.908	0.137	0.580	1.470	0.487	0.859	0.102
17	16.9	0.870	0.171	0.576	1.559	0.494	0.827	0.110
16	16.1	0.862	0.117	0.580	1.610	0.491	0.860	0.091
15	15.5	0.916	0.146	0.556	1.446	0.463	0.863	0.103
14	32.0	0.954	0.216	0.569	1.610	0.447	0.892	0.137
13	23.0	0.934	0.218	0.570	1.664	0.459	0.858	0.164
12	20.5	0.887	0.201	0.594	1.593	0.432	0.901	0.194
11	18.0	0.949	0.258	0.580	1.616	0.478	0.884	0.235
10	15.5	0.880	0.324	0.611	1.573	0.503	0.886	0.308
9	2.6	0.950	0.182	0.606	1.639	0.466	0.998	0.138
8	2.2	0.935	0.218	0.596	1.602	0.504	0.842	0.155
7	1.7	0.876	0.303	0.627	1.517	0.477	0.822	0.245
6	0.9	0.900	0.314	0.591	1.625	0.508	0.865	0.250
5	0.5	0.873	0.305	0.608	1.601	0.480	0.836	0.264
4	-0.2	0.860	0.421	0.595	1.621	0.465	0.874	0.333
3	-0.5	0.897	0.551	0.633	1.568	0.491	0.853	0.449
2	-1.3	0.929	0.312	0.620	1.550	0.482	0.874	0.260
1	-1.7	0.933	0.309	0.596	1.651	0.500	0.922	0.241

Table 3.S1: Total biomarker and isotopic data from Peace River, Canada

		Steranes						
sample #	relative depth	C29 Dia S/(S+R)	C29 Reg abb/aaa	C29 Reg aaa S/(S+R)	C29 Reg abb S/R	C27/total sterane	C28/total sterane	C29/total sterane
46	134.5	ND	ND	ND	ND	ND	ND	ND
45	132.0	0.554	1.202	0.464	1.071	0.447	0.299	0.226
44	112.5	0.529	1.195	0.453	1.555	0.550	0.251	0.199
43	110.0	0.590	1.130	0.446	0.975	0.421	0.311	0.232
42	105.5	0.592	0.948	0.405	1.140	0.456	0.321	0.223
41	104.0	0.609	1.073	0.458	1.236	0.335	0.360	0.248
40	113.0	0.557	1.468	0.525	1.107	0.302	0.233	0.408
39	111.5	0.555	1.422	0.490	0.969	0.332	0.224	0.396
38	105.0	0.578	1.459	0.518	1.027	0.359	0.270	0.334
37	103.5	0.584	1.412	0.529	1.317	0.304	0.191	0.454
36	94.0	0.574	1.410	0.524	0.992	0.319	0.307	0.338
35	90.5	0.573	1.372	0.514	1.098	0.302	0.251	0.407
34	89.0	0.564	1.406	0.496	1.288	0.291	0.212	0.448
33	87.0	0.576	1.438	0.495	1.214	0.309	0.181	0.458
32	85.5	0.568	1.452	0.516	1.023	0.305	0.209	0.442
31	32.0	0.546	1.402	0.510	1.153	0.307	0.250	0.400
30	30.9	0.498	1.453	0.516	1.014	0.292	0.259	0.400
29	28.8	0.524	1.435	0.513	1.171	0.306	0.244	0.399
28	26.6	0.553	1.498	0.531	1.065	0.307	0.245	0.399
27	25.8	0.557	1.502	0.530	1.263	0.305	0.251	0.404
26	25.0	0.582	1.466	0.517	1.158	0.309	0.240	0.403
25	23.8	0.563	1.438	0.517	1.041	0.299	0.258	0.396
24	22.1	0.553	1.468	0.517	1.093	0.295	0.248	0.400
23	21.0	0.588	1.485	0.519	1.188	0.333	0.235	0.384
22	20.4	0.576	1.445	0.519	1.213	0.373	0.235	0.353
21	20.0	0.543	1.526	0.518	1.134	0.357	0.236	0.375
20	18.9	0.581	1.494	0.509	1.054	0.357	0.244	0.364
19	18.0	0.538	1.467	0.509	1.071	0.327	0.289	0.348
18	17.4	0.584	1.462	0.504	1.279	0.340	0.259	0.365
17	16.9	0.559	1.505	0.527	1.079	0.329	0.267	0.366
16	16.1	0.486	1.524	0.511	1.087	0.293	0.256	0.408
15	15.5	0.496	1.416	0.495	1.170	0.346	0.235	0.376
14	32.0	0.581	1.484	0.514	1.253	0.367	0.237	0.358
13	23.0	0.587	1.551	0.505	1.184	0.367	0.203	0.400
12	20.5	0.572	1.535	0.506	1.041	0.338	0.212	0.404
11	18.0	0.560	1.482	0.508	1.199	0.303	0.214	0.437
10	15.5	0.539	1.496	0.504	0.986	0.301	0.198	0.461
9	2.6	0.540	1.445	0.483	1.216	0.298	0.218	0.447
8	2.2	0.537	1.431	0.520	1.031	0.286	0.244	0.428
7	1.7	0.556	1.463	0.502	1.144	0.280	0.238	0.438
6	0.9	0.571	1.530	0.507	1.214	0.291	0.236	0.434
5	0.5	0.597	1.556	0.491	1.079	0.310	0.255	0.399
4	-0.2	0.595	1.578	0.506	1.079	0.310	0.229	0.423
3	-0.5	0.613	1.471	0.502	1.248	0.324	0.209	0.439
2	-1.3	0.596	1.474	0.497	1.188	0.328	0.248	0.387
1	-1.7	0.605	1.514	0.511	1.180	0.348	0.244	0.370

Table 3.S1: Total biomarker and isotopic data from Peace River, Canada

		Steranes					Hopanes	
sample #	relative depth	C30/total sterane	C27/C29 Sterane	C28/C29 Sterane	Dinosterane (ng in vial)	Ts/Tm	29,30-DNH/ 28,30-DNH	28,30-DNH/ C30 hopane
46	134.5	ND	ND	ND	ND	ND	ND	ND
45	132.0	0.027	1.974	0.856	0.000	1.160	0.778	4.28E-06
44	112.5	0.000	2.761	0.846	0.000	0.895	3.232	1.09E-06
43	110.0	0.036	1.816	0.966	0.000	1.136	1.267	1.94E-06
42	105.5	0.000	2.042	1.124	0.000	1.310	0.871	1.59E-06
41	104.0	0.057	1.351	1.027	0.000	1.636	0.557	1.76E-06
40	113.0	0.056	0.741	0.533	7.254	0.520	4.208	1.38E-05
39	111.5	0.048	0.840	0.556	0.625	0.503	2.270	6.77E-06
38	105.0	0.037	1.073	0.816	5.136	0.520	5.194	2.84E-05
37	103.5	0.051	0.670	0.505	4.666	0.928	1.002	6.57E-05
36	94.0	0.036	0.944	0.967	8.515	0.540	1.414	2.66E-05
35	90.5	0.041	0.741	0.741	0.698	0.829	1.006	6.89E-05
34	89.0	0.050	0.650	0.524	0.679	0.843	1.047	7.89E-05
33	87.0	0.052	0.674	0.410	0.702	0.941	1.059	7.42E-05
32	85.5	0.044	0.689	0.458	5.000	0.860	0.537	1.18E-04
31	32.0	0.043	0.767	0.610	1.047	0.523	1.456	9.37E-05
30	30.9	0.048	0.730	0.626	2.529	0.512	1.316	8.97E-05
29	28.8	0.051	0.765	0.607	1.369	0.548	1.199	1.16E-04
28	26.6	0.049	0.770	0.595	12.433	0.572	1.325	6.32E-05
27	25.8	0.040	0.755	0.610	14.950	0.655	1.114	7.74E-05
26	25.0	0.049	0.766	0.580	14.278	0.616	1.134	7.57E-05
25	23.8	0.047	0.755	0.638	1.246	0.628	1.286	7.33E-05
24	22.1	0.057	0.739	0.607	2.327	0.596	1.392	1.53E-04
23	21.0	0.048	0.866	0.582	23.556	0.643	1.271	7.90E-05
22	20.4	0.039	1.058	0.643	3.252	0.635	1.362	6.88E-05
21	20.0	0.033	0.951	0.605	11.139	0.575	1.298	5.87E-05
20	18.9	0.035	0.980	0.652	7.520	0.577	1.363	9.20E-05
19	18.0	0.036	0.939	0.765	0.894	0.511	1.389	1.31E-05
18	17.4	0.036	0.931	0.688	0.991	0.507	1.652	1.08E-04
17	16.9	0.038	0.899	0.691	2.320	0.541	1.117	1.14E-04
16	16.1	0.042	0.717	0.613	2.554	0.547	1.082	1.26E-04
15	15.5	0.043	0.920	0.602	0.508	0.564	1.184	2.51E-05
14	32.0	0.037	1.025	0.620	7.895	0.715	1.035	9.13E-05
13	23.0	0.031	0.917	0.484	7.091	0.702	0.927	6.00E-05
12	20.5	0.046	0.835	0.522	0.625	0.592	0.979	5.18E-05
11	18.0	0.047	0.693	0.480	1.094	0.657	0.632	4.42E-05
10	15.5	0.039	0.653	0.425	3.655	0.683	0.608	4.76E-05
9	2.6	0.037	0.666	0.469	1.351	0.533	8.716	2.61E-05
8	2.2	0.042	0.668	0.541	8.746	0.607	9.750	1.70E-05
7	1.7	0.044	0.639	0.518	1.429	0.683	4.126	3.53E-05
6	0.9	0.038	0.670	0.518	8.699	0.674	1.901	2.41E-05
5	0.5	0.036	0.778	0.618	5.896	0.787	1.174	3.36E-05
4	-0.2	0.038	0.732	0.507	1.054	0.596	1.606	1.64E-05
3	-0.5	0.028	0.739	0.444	0.559	0.569	1.647	2.78E-05
2	-1.3	0.037	0.847	0.617	4.260	0.509	3.440	4.30E-05
1	-1.7	0.038	0.940	0.626	4.004	0.491	4.263	7.85E-05

Table 3.S1: Total biomarker and isotopic data from Peace River, Canada

		Hopanes								
sample #	relative depth	29,30-DNH/ C30 hopane	C29 Ts/ab	C29 ba/ab	C30 30-nor/ab	C30 ba/ab	C30 2-MHI	C30 3-MHI	C31 S/(S+R)	C32 S/(S+R)
46	134.5	ND	ND	ND	ND	ND	ND	ND	ND	ND
45	132.0	0.000	0.261	0.119	0.059	0.071	0.047	0.025	0.532	0.591
44	112.5	0.000	0.272	0.131	0.073	0.052	0.040	0.037	0.559	0.621
43	110.0	0.000	0.338	0.115	0.100	0.057	0.056	0.053	0.536	0.575
42	105.5	0.000	0.203	0.110	0.151	0.086	0.051	0.072	0.571	0.584
41	104.0	0.000	0.410	0.115	0.038	0.089	0.049	0.033	0.550	0.594
40	113.0	0.001	0.183	0.048	0.118	0.037	0.024	0.020	0.580	0.614
39	111.5	0.000	0.201	0.080	0.075	0.047	0.040	0.036	0.579	0.588
38	105.0	0.002	0.157	0.066	0.081	0.061	0.131	0.053	0.596	0.604
37	103.5	0.001	0.289	0.057	0.047	0.037	0.034	0.036	0.572	0.589
36	94.0	0.000	0.181	0.062	0.066	0.040	0.046	0.060	0.597	0.603
35	90.5	0.001	0.236	0.077	0.041	0.033	0.060	0.039	0.590	0.597
34	89.0	0.001	0.269	0.064	0.058	0.033	0.045	0.037	0.592	0.607
33	87.0	0.001	0.263	0.048	0.067	0.037	0.040	0.038	0.586	0.595
32	85.5	0.001	0.245	0.051	0.071	0.037	0.067	0.028	0.591	0.611
31	32.0	0.001	0.239	0.065	0.037	0.042	0.026	0.029	0.612	0.596
30	30.9	0.001	0.211	0.070	0.055	0.041	0.029	0.036	0.602	0.617
29	28.8	0.001	0.258	0.081	0.037	0.044	0.031	0.032	0.597	0.600
28	26.6	0.001	0.275	0.083	0.049	0.040	0.030	0.034	0.608	0.608
27	25.8	0.001	0.317	0.083	0.043	0.039	0.025	0.046	0.605	0.614
26	25.0	0.001	0.283	0.056	0.049	0.046	0.029	0.034	0.609	0.595
25	23.8	0.001	0.232	0.080	0.037	0.050	0.024	0.032	0.593	0.600
24	22.1	0.002	0.247	0.063	0.040	0.045	0.030	0.032	0.601	0.608
23	21.0	0.001	0.282	0.071	0.038	0.040	0.020	0.034	0.597	0.600
22	20.4	0.001	0.275	0.064	0.049	0.039	0.023	0.050	0.598	0.596
21	20.0	0.001	0.269	0.066	0.039	0.040	0.021	0.037	0.608	0.596
20	18.9	0.001	0.220	0.065	0.047	0.039	0.015	0.039	0.599	0.608
19	18.0	0.000	0.229	0.065	0.035	0.040	0.052	0.032	0.592	0.606
18	17.4	0.002	0.262	0.069	0.047	0.038	0.050	0.037	0.593	0.601
17	16.9	0.001	0.229	0.067	0.040	0.039	0.050	0.038	0.594	0.603
16	16.1	0.001	0.209	0.072	0.038	0.039	0.017	0.029	0.604	0.610
15	15.5	0.000	0.251	0.066	0.059	0.040	0.018	0.049	0.586	0.610
14	32.0	0.001	0.282	0.072	0.047	0.040	0.016	0.059	0.586	0.602
13	23.0	0.001	0.287	0.064	0.052	0.041	0.014	0.055	0.591	0.595
12	20.5	0.001	0.209	0.067	0.055	0.041	0.025	0.046	0.589	0.599
11	18.0	0.000	0.222	0.060	0.045	0.045	0.030	0.052	0.606	0.595
10	15.5	0.000	0.202	0.052	0.065	0.042	0.035	0.036	0.595	0.607
9	2.6	0.002	0.283	0.055	0.120	0.040	0.028	0.027	0.585	0.598
8	2.2	0.002	0.265	0.053	0.096	0.042	0.019	0.030	0.587	0.592
7	1.7	0.002	0.299	0.056	0.076	0.041	0.027	0.040	0.592	0.604
6	0.9	0.000	0.311	0.055	0.068	0.040	0.020	0.024	0.594	0.597
5	0.5	0.000	0.381	0.067	0.060	0.035	0.015	0.038	0.608	0.587
4	-0.2	0.000	0.365	0.063	0.068	0.046	0.026	0.040	0.610	0.603
3	-0.5	0.000	0.358	0.058	0.056	0.037	0.014	0.040	0.587	0.605
2	-1.3	0.002	0.291	0.054	0.072	0.037	0.036	0.034	0.602	0.599
1	-1.7	0.004	0.280	0.055	0.080	0.038	0.034	0.037	0.592	0.595

Table 3.S1: Total biomarker and isotopic data from Peace River, Canada

		Hopanes						
sample #	relative depth	C33 S/(S+R)	C34 S/(S+R)	C35 S/(S+R)	C29 ab/ C30 ab	C29 ab/(Total ab Hopane)	C30 ab/(Total ab Hopane)	C31 ab/(Total ab Hopane)
46	134.5	ND	ND	ND	ND	ND	ND	ND
45	132.0	0.549	0.672	0.672	0.795	0.239	0.300	0.194
44	112.5	0.573	0.598	0.616	1.036	0.264	0.255	0.204
43	110.0	0.614	0.537	0.637	0.755	0.228	0.301	0.211
42	105.5	0.503	0.553	0.645	0.899	0.237	0.264	0.186
41	104.0	0.523	0.612	0.579	0.515	0.162	0.316	0.191
40	113.0	0.611	0.614	0.608	0.976	0.210	0.215	0.212
39	111.5	0.595	0.637	0.637	0.831	0.205	0.247	0.211
38	105.0	0.608	0.626	0.648	0.831	0.197	0.237	0.230
37	103.5	0.593	0.599	0.614	0.649	0.178	0.275	0.209
36	94.0	0.598	0.598	0.622	0.574	0.136	0.236	0.238
35	90.5	0.604	0.612	0.610	0.595	0.153	0.256	0.229
34	89.0	0.587	0.625	0.623	0.643	0.168	0.261	0.227
33	87.0	0.621	0.612	0.627	0.622	0.168	0.271	0.220
32	85.5	0.606	0.618	0.618	0.619	0.168	0.272	0.232
31	32.0	0.627	0.635	0.630	0.434	0.113	0.260	0.253
30	30.9	0.616	0.617	0.631	0.438	0.117	0.267	0.246
29	28.8	0.635	0.610	0.615	0.408	0.108	0.266	0.254
28	26.6	0.606	0.634	0.618	0.386	0.108	0.281	0.242
27	25.8	0.611	0.617	0.626	0.387	0.105	0.272	0.248
26	25.0	0.614	0.630	0.616	0.367	0.102	0.279	0.248
25	23.8	0.602	0.607	0.617	0.372	0.106	0.286	0.242
24	22.1	0.625	0.628	0.625	0.382	0.106	0.278	0.242
23	21.0	0.630	0.617	0.613	0.345	0.103	0.297	0.238
22	20.4	0.622	0.606	0.611	0.410	0.105	0.255	0.253
21	20.0	0.629	0.639	0.626	0.390	0.114	0.292	0.234
20	18.9	0.613	0.602	0.628	0.398	0.121	0.304	0.226
19	18.0	0.620	0.634	0.602	0.451	0.127	0.282	0.257
18	17.4	0.620	0.620	0.613	0.413	0.112	0.272	0.253
17	16.9	0.623	0.631	0.621	0.419	0.111	0.266	0.257
16	16.1	0.610	0.619	0.619	0.390	0.113	0.291	0.242
15	15.5	0.608	0.622	0.614	0.507	0.129	0.254	0.272
14	32.0	0.615	0.624	0.646	0.499	0.128	0.257	0.264
13	23.0	0.623	0.619	0.630	0.482	0.130	0.269	0.267
12	20.5	0.616	0.627	0.610	0.645	0.176	0.272	0.235
11	18.0	0.619	0.606	0.610	0.653	0.180	0.276	0.228
10	15.5	0.626	0.623	0.651	0.712	0.200	0.281	0.220
9	2.6	0.602	0.624	0.650	0.722	0.219	0.304	0.255
8	2.2	0.621	0.621	0.641	0.645	0.195	0.302	0.256
7	1.7	0.623	0.628	0.649	0.490	0.151	0.308	0.258
6	0.9	0.610	0.613	0.680	0.428	0.139	0.326	0.251
5	0.5	0.590	0.629	0.651	0.358	0.127	0.355	0.230
4	-0.2	0.624	0.604	0.637	0.430	0.132	0.307	0.243
3	-0.5	0.622	0.632	0.620	0.448	0.134	0.298	0.254
2	-1.3	0.615	0.616	0.626	0.474	0.144	0.304	0.235
1	-1.7	0.619	0.636	0.632	0.532	0.149	0.280	0.250

Table 3.S1: Total biomarker and isotopic data from Peace River, Canada

		Hopanes					
sample #	relative depth	C32 ab/(Total ab Hopane)	C33 ab/(Total ab Hopane)	C34 ab/(Total ab Hopane)	C35 ab/(Total ab Hopane)	C29/C30 hopane	C31/C30 hopane
46	134.5	ND	ND	ND	ND	ND	ND
45	132.0	0.129	0.058	0.042	0.037	0.971	0.267
44	112.5	0.137	0.063	0.053	0.023	1.291	0.314
43	110.0	0.124	0.056	0.048	0.033	0.950	0.281
42	105.5	0.154	0.072	0.034	0.053	0.954	0.245
41	104.0	0.155	0.091	0.055	0.029	0.696	0.242
40	113.0	0.130	0.093	0.063	0.077	1.040	0.359
39	111.5	0.138	0.087	0.055	0.057	0.949	0.319
38	105.0	0.173	0.076	0.042	0.046	0.890	0.343
37	103.5	0.139	0.086	0.056	0.057	0.805	0.300
36	94.0	0.175	0.082	0.056	0.076	0.646	0.367
35	90.5	0.161	0.086	0.052	0.064	0.727	0.341
34	89.0	0.149	0.084	0.052	0.058	0.786	0.325
33	87.0	0.144	0.086	0.053	0.057	0.738	0.306
32	85.5	0.148	0.082	0.049	0.049	0.724	0.316
31	32.0	0.191	0.082	0.044	0.056	0.526	0.351
30	30.9	0.181	0.085	0.046	0.058	0.512	0.335
29	28.8	0.190	0.081	0.045	0.056	0.506	0.356
28	26.6	0.192	0.081	0.044	0.053	0.480	0.309
27	25.8	0.194	0.080	0.046	0.054	0.501	0.334
26	25.0	0.190	0.084	0.044	0.052	0.449	0.317
25	23.8	0.188	0.079	0.043	0.054	0.448	0.316
24	22.1	0.195	0.083	0.045	0.051	0.461	0.320
23	21.0	0.189	0.081	0.043	0.050	0.433	0.300
22	20.4	0.207	0.077	0.048	0.055	0.504	0.366
21	20.0	0.191	0.077	0.043	0.049	0.482	0.292
20	18.9	0.187	0.073	0.040	0.048	0.471	0.275
19	18.0	0.174	0.072	0.041	0.046	0.542	0.346
18	17.4	0.185	0.082	0.043	0.053	0.507	0.349
17	16.9	0.194	0.076	0.042	0.053	0.503	0.365
16	16.1	0.189	0.073	0.040	0.052	0.464	0.306
15	15.5	0.187	0.069	0.040	0.049	0.607	0.403
14	32.0	0.184	0.069	0.046	0.051	0.622	0.392
13	23.0	0.181	0.069	0.043	0.042	0.596	0.371
12	20.5	0.157	0.073	0.045	0.043	0.751	0.324
11	18.0	0.149	0.074	0.045	0.049	0.768	0.298
10	15.5	0.133	0.075	0.045	0.046	0.807	0.287
9	2.6	0.113	0.053	0.030	0.026	0.833	0.301
8	2.2	0.126	0.059	0.033	0.028	0.747	0.308
7	1.7	0.140	0.067	0.042	0.033	0.594	0.306
6	0.9	0.146	0.068	0.038	0.032	0.527	0.283
5	0.5	0.156	0.063	0.036	0.034	0.474	0.232
4	-0.2	0.166	0.073	0.042	0.037	0.551	0.277
3	-0.5	0.161	0.073	0.041	0.039	0.581	0.321
2	-1.3	0.156	0.078	0.043	0.040	0.574	0.277
1	-1.7	0.172	0.071	0.040	0.037	0.635	0.326

Table 3.S1: Total biomarker and isotopic data from Peace River, Canada

		aromatics			isotopes		
sample #	relative depth	totalAI (mg/g TOC)	isorenieratane (ug/g TOC)	chlorobactane (ug/g TOC)	farnesane	pristane	phytane
46	134.5	0.040	ND	ND	ND	-29.99	-30.07
45	132.0	0.002	ND	ND	ND	-30.01	-29.98
44	112.5	0.043	ND	ND	ND	-31.09	-31.23
43	110.0	0.002	ND	ND	ND	-31.06	-30.09
42	105.5	0.001	ND	ND	ND	-30.91	-29.97
41	104.0	0.004	ND	ND	ND	-29.07	-28.96
40	113.0	0.251	ND	ND	-29.71	-31.19	-31.30
39	111.5	0.106	ND	ND	-29.79	-32.14	-31.69
38	105.0	0.093	ND	ND	-29.77	-32.02	-31.75
37	103.5	0.047	0.165	0.000	-30.79	-32.47	-31.32
36	94.0	0.189	ND	ND	-30.51	-32.28	-33.30
35	90.5	0.112	0.569	0.033	-31.20	-32.93	-31.97
34	89.0	0.106	0.576	0.000	-30.45	-31.53	-31.90
33	87.0	0.109	0.676	0.051	-30.53	-33.39	-32.62
32	85.5	1.673	0.631	0.041	-29.56	-32.64	-31.98
31	32.0	0.235	2.368	0.137	ND	-32.54	-33.18
30	30.9	0.259	3.666	0.197	-32.13	-31.92	-32.80
29	28.8	0.305	1.721	0.081	-32.81	-32.09	-33.52
28	26.6	0.189	ND	ND	-30.54	-31.83	-32.79
27	25.8	0.274	1.691	0.063	-30.80	-32.60	-33.33
26	25.0	0.058	2.600	0.108	-31.75	-32.98	-34.08
25	23.8	0.333	1.736	0.073	-31.02	-32.84	-33.59
24	22.1	0.177	4.842	0.201	-31.15	-33.09	-33.52
23	21.0	0.154	ND	ND	-30.60	-32.62	-33.23
22	20.4	0.041	ND	ND	-31.32	-33.03	-33.25
21	20.0	0.019	ND	ND	-30.43	-31.95	-32.76
20	18.9	0.000	ND	ND	-32.04	-32.19	-32.84
19	18.0	0.000	ND	ND	-31.81	-32.36	-33.10
18	17.4	0.193	1.792	0.104	-31.41	-32.41	-32.83
17	16.9	0.216	1.333	0.074	-31.79	-32.83	-33.00
16	16.1	0.371	8.122	0.393	-31.10	-32.90	-33.49
15	15.5	0.002	ND	ND	-30.83	-32.83	-33.01
14	32.0	0.095	1.581	0.075	-29.35	-32.11	-32.11
13	23.0	0.021	0.049	0.005	-31.40	-32.35	-32.77
12	20.5	0.341	ND	ND	-30.34	-32.81	-32.72
11	18.0	0.133	ND	ND	-30.84	-32.16	-32.00
10	15.5	2.938	21.008	0.071	-30.06	-32.73	-32.26
9	2.6	0.118	ND	ND	-32.21	-32.86	-33.55
8	2.2	0.060	ND	ND	-31.16	-32.70	-33.65
7	1.7	0.319	1.840	0.086	-32.61	-32.44	-33.38
6	0.9	0.363	3.275	0.108	-32.64	-32.70	-33.64
5	0.5	0.011	0.164	0.011	ND	-32.80	-33.12
4	-0.2	0.049	0.468	0.038	-30.21	-31.81	-32.78
3	-0.5	0.021	ND	ND	-30.96	-31.81	-32.83
2	-1.3	0.068	1.040	0.051	-30.02	-31.44	-32.50
1	-1.7	0.011	0.543	0.010	-29.87	-31.67	-32.93

Table 3.S1: Total biomarker and isotopic data from Peace River, Canada

		isotopes			extra compounds	
sample #	relative depth	n-C17	n-C18	aryl isoprenoids	C33 n-ACH /C34 n-alk	cr/ph %
46	134.5	-29.96	-30.87	-	ND	1.612
45	132.0	-30.15	-30.38	-	ND	ND
44	112.5	-30.58	-30.73	-	ND	1.731
43	110.0	-30.72	-30.47	-	ND	1.714
42	105.5	-30.36	-30.53	-	ND	ND
41	104.0	-29.50	-30.43	-	ND	ND
40	113.0	-32.07	-32.15	-	ND	1.588
39	111.5	-32.68	-32.85	-	ND	1.522
38	105.0	-32.47	-32.50	-	ND	1.475
37	103.5	-32.09	-31.71	-	ND	1.644
36	94.0	-32.54	-32.20	-	ND	1.363
35	90.5	-32.92	-32.84	-	ND	1.395
34	89.0	-31.88	-31.92	-	ND	1.436
33	87.0	-33.05	-32.42	-	ND	1.580
32	85.5	-32.58	-32.54	-21.74	ND	1.325
31	32.0	-32.46	-33.23	-	ND	ND
30	30.9	-31.78	-32.51	-	ND	1.322
29	28.8	-32.34	-32.67	-	1.705	1.256
28	26.6	-32.05	-32.81	-	1.246	1.221
27	25.8	-33.36	-34.09	-	0.000	ND
26	25.0	-34.03	-34.34	-	1.096	ND
25	23.8	-34.13	-34.51	-	1.292	ND
24	22.1	-34.09	-34.36	-	0.985	ND
23	21.0	-33.57	-34.11	-	1.715	ND
22	20.4	-34.39	-34.66	-	1.194	ND
21	20.0	-33.08	-33.45	-	0.796	1.193
20	18.9	-33.73	-34.22	-	1.029	ND
19	18.0	-33.88	-34.44	-	1.456	1.110
18	17.4	-33.23	-33.65	-	1.944	ND
17	16.9	-33.76	-33.75	-	1.323	ND
16	16.1	-33.69	-34.01	-27.32	1.713	ND
15	15.5	-32.90	-33.11	-	1.403	1.170
14	32.0	-31.62	-32.31	-	0.982	1.280
13	23.0	-32.18	-32.66	-	0.000	ND
12	20.5	-32.34	-32.48	-	1.051	ND
11	18.0	-31.66	-31.96	-	1.460	1.436
10	15.5	-32.56	-32.26	-25.14	1.581	1.396
9	2.6	-32.50	-33.20	-	1.664	ND
8	2.2	-32.58	-33.01	-	1.864	ND
7	1.7	-32.14	-32.76	-28.00	1.659	ND
6	0.9	-32.41	-32.92	-26.38	2.146	ND
5	0.5	-32.41	-33.50	-	2.365	ND
4	-0.2	-31.33	-32.01	-	2.447	ND
3	-0.5	-31.32	-32.09	-	1.464	ND
2	-1.3	-31.05	-31.82	-	1.831	ND
1	-1.7	-31.85	-32.79	-	1.804	ND

Chapter 4

Biomarker Trends from Kap Stosch, Greenland

Abstract

The Permian *Productus* limestone and *Martinia* shale and the *Glyptophiceras* beds of the Triassic period from Kap Stosch, Greenland were deposited at the margin of the Boreal Sea and first described as a Permian-Triassic boundary section in 1967. The composite section studied here comprises samples from four outcrop localities. Analyses of hydrocarbon biomarker ratios indicate the presence of pervasive photic zone euxinic conditions throughout a transition in organic material from marine- to terrestrial-dominated inputs. Bulk geochemical measurements, including a low Rock-Eval Tmax and good correlation between S2 and TOC, indicate organic matter of low maturity throughout the section. Biomarker ratios that are sensitive to the depositional environment also show a transition, with higher marine input in the Permian rocks and more terrestrial biomass in the Triassic rocks. The pristane/phytane ratio is low, and the homohopane index is high, indicating anoxic conditions persisted throughout deposition of this section. In addition, isorenieratane, aryl isoprenoids and crocetane are present in all samples. All three show a maximum abundance in sedimentary rocks closest to the identified Permian-Triassic transition. The hopane/sterane and 2-methylhopane index were measured and found to be at the higher end of the normal range for the Phanerozoic, indicating enhanced bacterial input. A potential age marker for the Permian-Triassic boundary, C_{33} *n*-alkylcyclohexane, was identified in sedimentary rocks at, and immediately following, the identified transition. The C_{28}/C_{29} sterane ratio is typical of sedimentary rocks and oils from the mid-Phanerozoic. Despite the distinct change in lithology across the Permian-Triassic transition, the

redox biomarkers and Chlorobi-derived biomarkers indicate that photic zone euxinic conditions prevailed throughout the deposition of the Kap Stosch sedimentary sequence.

Locality and biostratigraphic information

Boreal Sea at the Permian-Triassic Boundary

The sedimentary section exposed at Kap Stosch was deposited at the margin of the nascent Boreal Sea, an epicontinental basin forming in the northwest of Pangea in the late Permian period. (See Figure 4.1.) Sedimentary rocks deposited beneath this sea can be found throughout eastern Greenland and a connecting basin further inland, the Zechstein Sea. Sedimentary rocks from the latter can be studied in a wide range of European sections (Grice et al. 1996b, 1997; Pancost et al. 2002).

A study of a sedimentary succession in Jameson Land in East Greenland (Wignall and Twitchett 2002) reported paleontological and sedimentological data on the Permian-Triassic boundary from this region. The authors report conformable shale contacts within this section that record the complete Permian-Triassic boundary, as well as framboidal pyrites just beneath the boundary. When interpreted together, these indicate anoxic deposition. Evidence for increasing but intermittent oxic conditions were seen beginning in the Triassic period, but the return to oxic conditions was much more gradual than the sudden onset of anoxia. The documentation of anoxia in this region during the Late Permian period has been supported by other studies using various methodologies. For example, one study of a section in East Greenland focused on the size and stable sulfur isotopic composition of framboidal pyrites in the Ravnefjeld Formation (Nielsen and Shen 2004). The presence of smaller pyrite framboids within a limited range was considered indicative of the

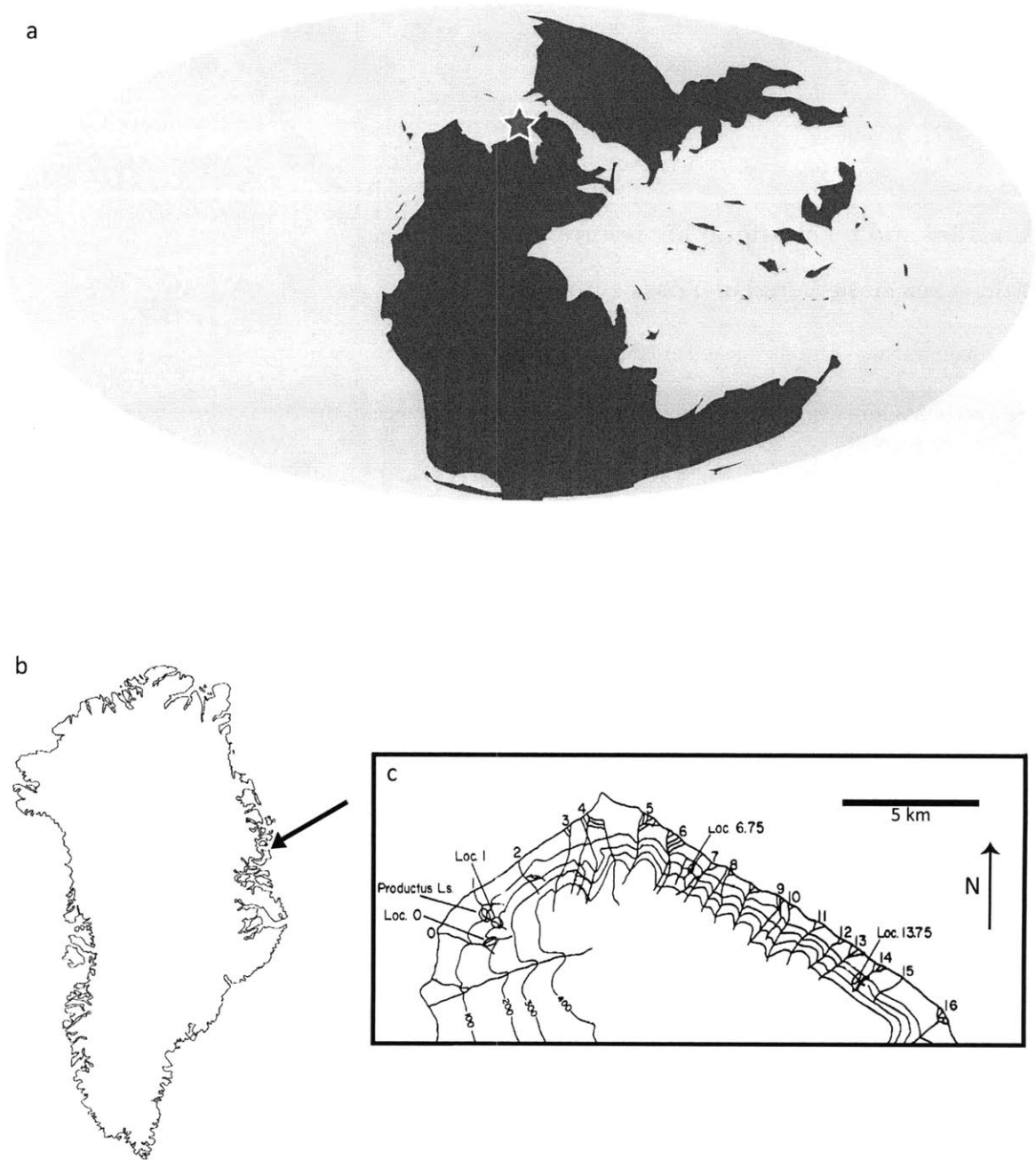

Figure 4.1 Locality of the Kap Stosch, Greenland section. (a) Global map from the Permian-Triassic boundary, with the depositional location of this section noted. Map modified from Scotese Paleomap Project website. (b) Map of modern Greenland with Kap Stosch locality noted. (c) Map of Kap Stosch showing localities sampled for this study. (b) and (c) modified from Teichert and Kummel 1972.

presence of sulfidic deep water during the late Permian period, and the large fractionation in $\delta^{34}S$ lead the authors to conclude that these values may represent different forms of sulfur cycling beneath the sulfidic water column.

A number of studies have examined the biogeochemistry of the late Permian Kupferschiefer succession of the Lower Rhine Basin, Germany. These sedimentary rocks, deposited at the southern margin of the Zechstein Sea, display molecular evidence for organisms that thrive in euxinic environments. Grice et al. (1996a; 1996b) found evidence of green sulfur bacteria (Chlorobi) in the form of diagnostic carotenoid pigment residues. One study (Grice et al. 1996b) identified both saturated and aromatic carotenoid-derived hydrocarbons. The authors were able to link these compounds to the Chlorobi by virtue of their relatively high $\delta^{13}C$ values. In a second study (Grice et al. 1996a), the structures of maleimides, in combination with their $\delta^{13}C$ values, revealed a similar association. The authors identified Me *i*-Bu maleimide, specific to the bacteriochlorophyll e of the Chlorobi. The less specific Me *n*-Pr was also documented. Both compounds were enriched in ^{13}C relative to other maleimides in the same samples, although the later was less so. A follow-up study of different samples from the Kupferschiefer deposit of the Lower Rhine Basin also documented the presence of Me *i*-Bu in maleimides in both the free bitumens and in oxidized porphyrin fractions (Pancost et al. 2002).

A study of the polycyclic aromatic hydrocarbons from just below the Permian-Triassic boundary in the Schuchert Dal section in Jameson Land found high abundances of dibenzofuran (DBF), dibenzothiophene (DBT) and biphenyl (Fenton et al. 2007). These authors attributed their observation to terrestrial organic matter inputs that decrease synchronously with the marine collapse and onset of euxinic conditions. This study also measured the $\delta^{34}S$ values for pyrite and found a

positive excursion concurrent with the increase of DBF and DBT. Together, these two observations were considered by these authors to be indicative of a trend in the redox conditions toward more anoxic conditions at the Permian-Triassic boundary in the studied interval.

Deep-water anoxia in the Boreal Sea during the late Permian period could be the result of the physically restricted nature in the basin. The evidence for photic zone euxinia in some samples indicates that the basin must have been stratified, at least intermittently, similar to the modern-day Black Sea. These findings suggest that Kap Stosch is an appropriate site to search for hydrocarbon biomarkers that would be informative about paleoenvironmental conditions during the Late Permian and Early Triassic periods and especially for compounds diagnostic for photic zone euxinia.

Kap Stosch, Greenland

The Kap Stosch region in east Greenland was first studied as an outcrop of a Permian-Triassic boundary section in the 1920s, but the section described here was collected in 1967 (Teichert and Kummel 1972, 1976). The sedimentary section is composed of homogeneous shale, silty shale, and siltstone facies that were deposited rapidly. The sampling was focused on four localities in two areas. The first area is southwest of Kap Stosch and encompasses outcrops between rivers designated as Zero and One. The second area is southeast of Kap Stosch between the rivers designated as 6 and 14. (See Figure 4.1.) These locations include units that had previously been referred to as "*Productus* limestone" and "*Martinia* shale," that have been grouped together as the late Permian Foldvik Creek Formation (Birkelund et al. 1974). The Triassic sedimentary rocks include *Glyptophiceras* beds, described by Perch-Nielsen et al. (1974) as part of the Wordie Creek Formation, although this has been questioned by Teichert and Kummel (1976). At the first location, the exact placement of the Permian-Triassic boundary is difficult to determine because the likely transition

interval is not exposed. The youngest Permian rocks are fossiliferous shale and siltstone facies, and, although many of the fossils have been broken and contain indeterminable fragments, those that can be identified are: bryozoans, crinoids, echinoid and brachiopods typical of the Upper Permian "*Productus* limestone" fauna. The Permian-Triassic transition in the second location is more clearly exposed and defined by a thin basal Triassic conglomerate that contains broken and likely re-worked fragments of Permian bryozoans and brachiopods and also the Triassic fossil, *Otoceras*.

Samples from the locations described above could be ordered stratigraphically using fossil data from ammonites and conodonts to form a composite section. (See Figure 4.2.) Although this section includes samples from a range less than 15km, slight differences in the depositional environment may occur between individual outcrop locations. In general, these Permian sedimentary rocks were deposited in deeper water facies. Across the boundary, the Triassic sedimentary rocks were likely deposited in a much more shallow water environment.

Although the Permian-Triassic transition is obscured in these sections by increased solifluction, the presence of fossil fragments of species that did not survive the extinction yet are present in a Triassic conglomerate suggest a depositional hiatus. The Permian-Triassic boundary likely occurs during this hiatus and therefore the transition at Kap Stosch represents a paraconformity. An unknown thickness of sedimentary rock was lost during this erosional event and the sections closest to the boundary may contain a mixture of sediments from the Triassic and re-worked late Permian sedimentary rocks. The boundary in this location cannot be precisely assigned other than placing at some level between the sections that are established as Permian and Triassic. Regardless, the section provides evidence of large-scale changes that spanned the Permian-Triassic transition (Teichert and Kummel 1972).

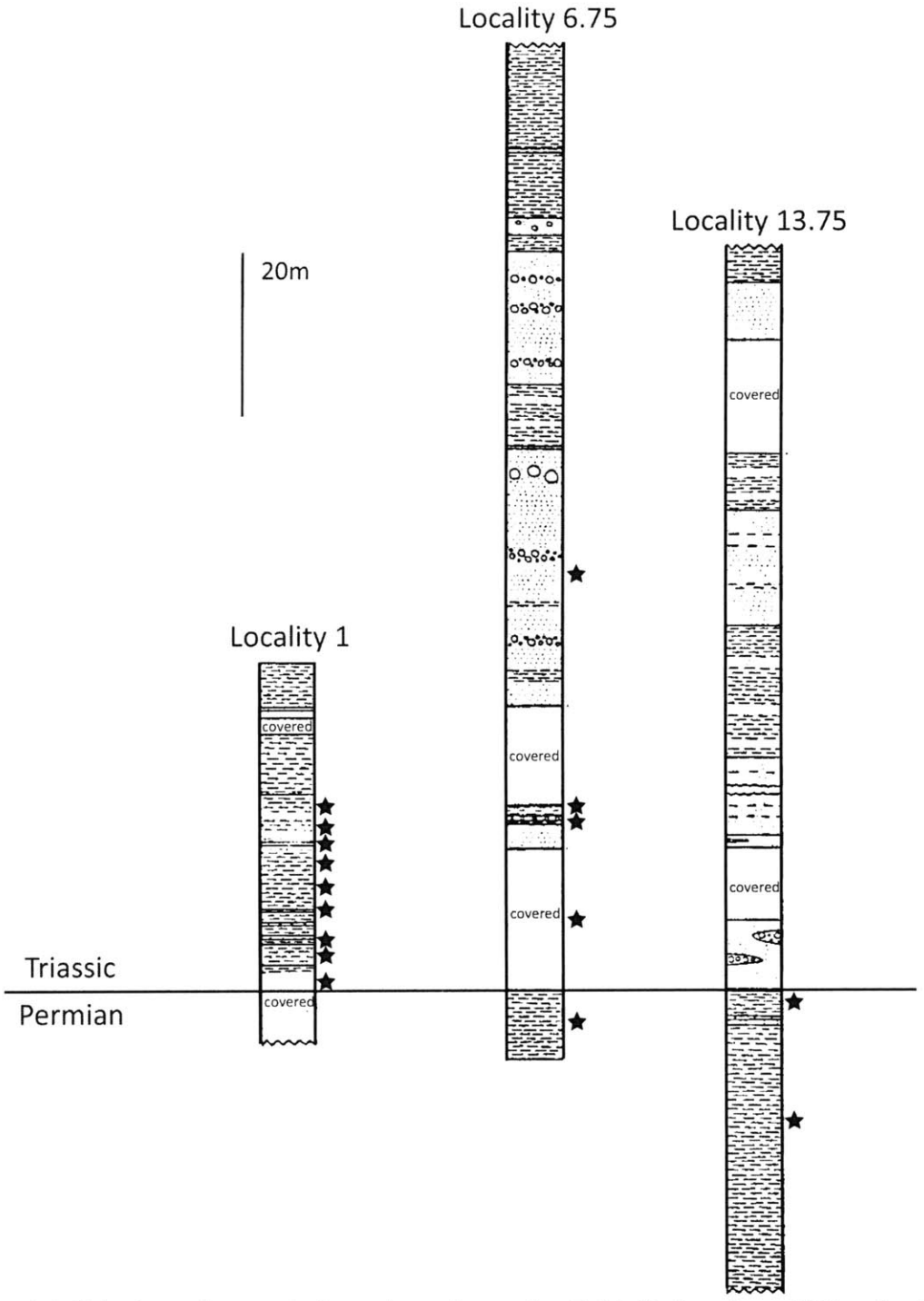

Figure 4.2 Litholog of sampled sections from the Foldvik Creek and Wordie Creek Formations in Kap Stosch. Shown are three of the four localities measured, with sampled sediment layers noted. The fourth locality (Locality 0) is not shown, but was sampled only in the Permian, where the rock was exclusively shale. Adapted from Teichert and Kummel 1976.

Preparation Methods

Outcrop samples from Kap Stosch were prepared at Geoscience Australia where Rock-Eval pyrolysis was performed to determine the bulk geochemical information and the $\delta^{13}C_{org}$. A fraction of the powdered sample was then analyzed for lipid biomarkers at the Massachusetts Institute of Technology.

Because of their limited size, samples were extracted manually from the powdered rock fraction using a 9:1 dichloromethane (DCM) to methanol (MeOH) solution and ultra-sonicated in a VWR Aquasonic 150HT. This process was repeated three times, and the extracts pooled, filtered and then treated with activated copper to remove elemental sulfur. This total lipid extract was separated chromatographically on a silica gel column into three fractions yielding the saturated hydrocarbons, aromatic hydrocarbons and polar compounds by eluting with solvents of increasing polarity. The saturated and aromatic fractions were weighed and re-suspended in hexane with either D_4 20R stigmastane or D_{14} p-terphenyl added, respectively, as internal standards.

Both the saturated and aromatic fractions were analyzed by gas chromatography coupled to mass spectrometry with a HP 6890 GC attached to an Agilent 5973 mass selective detector (MSD). The saturated fraction was also analyzed using gas chromatography coupled to tandem mass spectrometry using an AutoSpec Ultima operated in the multiple reaction monitoring (MRM) mode. The GC-MRM data allowed us to quantify biomarkers that are sensitive to change in plankton composition, sediment lithology and thermal. Lipids were identified by their mass spectra (on the GC-MSD) and predicted gas chromatography structure-retention time relationships, as well as

comparing their retention times to known standards. (See Appendix 1 for uncertainties in biomarker measurements.)

Results and Discussion

Bulk Geochemical Data

Rock-Eval data and subsequent biomarker analysis show no evidence for the samples being affected by post-depositional hydrocarbon migration. The total organic carbon (TOC) content of the samples vary from 0.2-8 wt% during the latest Permian period before trending to a more constant value of ~0.3 wt% in the Triassic period. (See Table 4.1.)

The S2 peak of the Rock-Eval data is a measure of the amount of hydrocarbons (mg/g) produced during kerogen pyrolysis over a range from 300° to 600° C. The S2 values are high compared to the contents of free bitumen (S1) and this, together with a sound correlation between S2 and TOC (see Figure 4.3), indicates that the organic matter from Kap Stosch is of low maturity and dominated by kerogen. This suggests that there is minimal oil migration in this locality, and that the biomarkers are primarily authigenic. However, shoulder peaks near the maximum pyrolysis temperature (Tmax) indicate that there was some degree of heterogeneity in the sources of the organic matter. (See Table 4.1.)

The average $\delta^{13}C$ of organic carbon ($\delta^{13}C_{org}$) in the Kap Stosch samples is -25‰ in the Permian rocks and -32‰ in the Triassic rocks. Between these two relatively stable environments, there is a set of fluctuations with magnitudes from ~5‰ to ~7‰ immediately before and continuing across the Permian-Triassic boundary. (See Table 4.1.) Foster et al. (1997) suggest that fluctuations in the

			RockEval 2 analysis of Rock Powder						RockEval 6 analysis of Kerogen Concentrate						
Sample Number	**relative depth**	**$d^{13}C_{PDB}$ (‰)**	**T_{MAX} (°C)**	**S1 (mg/g)**	**S2 (mg/g)**	**S3 (mg/g)**	**HI**	**OI**	**TOC (wt%)**	**T_{MAX} (°C)**	**S1 (mg/g)**	**S2 (mg/g)**	**S3 (mg/g)**	**HI**	**OI**	**TOC (wt%)**
19990454	88	-29.3	480±20	0.03	0.12	0.00	57	0	0.21	422	2.83	3.98	0.44	209	23	1.9
19990449	34	-30.6	430±20	0.00	0.16	0.15	46	43	0.35	421	1.80	3.79	1.10	152	44	2.5
19990448	29	-31.7	430±20	0.01	0.12	0.11	28	26	0.43	430	2.07	14.17	2.05	267	39	5.3
19990453	28	-30.8	480±20	0.02	0.14	0.00	61	0	0.23	417	2.05	2.68	1.03	168	64	1.6
19990447	26	-30.9	430±10	0.04	0.20	0.20	65	65	0.31	424	4.46	8.30	1.24	259	39	3.2
19990452	25	-32.5	>480	0.00	0.08	0.00	53	0	0.15	413	0.53	0.54	0.61	90	102	0.6
19990446	19	-32.9	430±10	0.00	0.15	0.17	33	38	0.45	419	1.33	5.29	2.74	171	88	3.1
19990445	18	-32.6	432	0.01	0.23	0.12	43	23	0.53	423	2.00	8.59	1.47	286	49	3.0
19990444	14	-32.3	431	0.02	0.49	0.23	58	27	0.85	426	1.95	15.72	2.52	349	56	4.5
19990443	9	-32.4	430±20	0.08	0.21	0.04	68	13	0.31	429	3.63	10.93	0.90	342	28	3.2
19990442	6	-32.8	430	0.05	0.62	0.20	71	23	0.87	430	3.34	29.31	2.79	425	40	6.9
19990441	3	-32.4	431	0.07	1.11	0.37	84	28	1.32	427	4.54	48.82	4.74	436	42	11.2
19990451	1	-33.0	430	0.03	0.33	0.42	53	68	0.62	426	2.46	16.49	1.94	383	45	4.3
19990450	0	-23.3	430±20	0.01	0.10	0.19	42	79	0.24	396*	1.01	1.83	1.03	54	30	3.4
19990457	-3	-28.9	431	0.56	14.64	2.10	296	43	4.94	429	7.55	109.65	12.55	367	42	29.9
19990439	-13	-24.8	430±20	0.02	0.19	0.32	46	78	0.41	419*	0.63	1.36	3.09	28	63	4.9
19990440	-17	-21.5	430±20	0.02	0.17	0.24	44	62	0.39	362	1.33	1.08	1.55	23	33	4.7
19990456	-21	-28.2	425	1.74	33.78	3.54	434	46	7.78	426	12.91	197.55	25.63	436	57	45.3
19990438	-24	-23.5	430±20	0.00	0.13	0.15	23	27	0.56	364	1.37	0.83	0.90	25	27	3.3
19990437	-25	-23.3	>415	0.02	0.13	0.32	72	178	0.18	415*	4.94	4.24	2.57	45	27	9.5
19990436	-29	-22.7	430±20	0.01	0.11	0.22	18	36	0.61	412*	2.96	3.63	3.56	30	29	12.1
19990435	-30	-24.5	430±20	0.04	0.22	0.38	32	56	0.68	414*	1.14	1.23	1.14	33	31	3.7

Table 4.1 Bulk geochemical parameters measured from the Kap Stosch section. Measurements were made at Geoscience Australia. The * in the T_{max} indicates a shoulder peak is present in the S2 measurement, though lower in intensity.

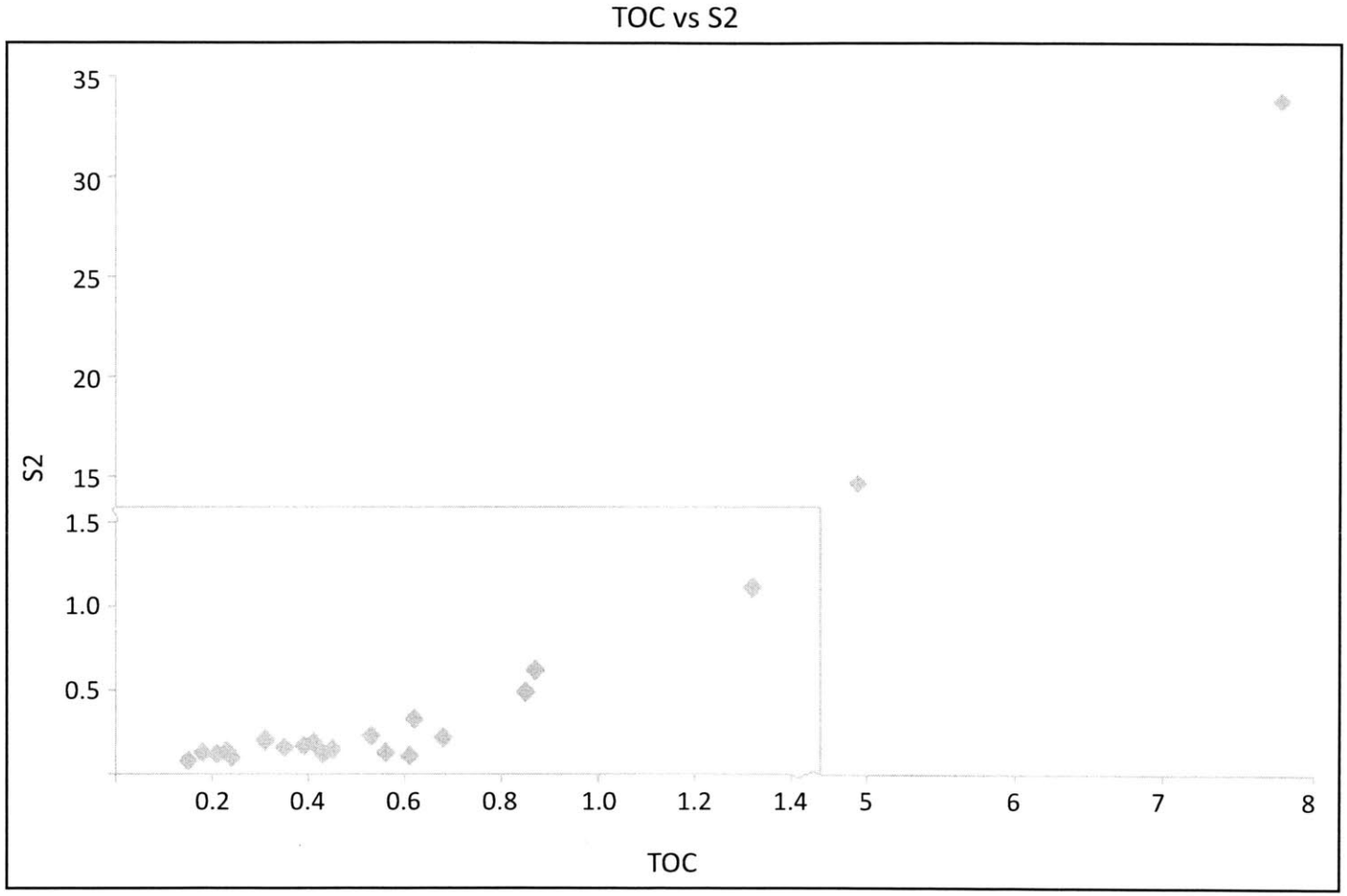

Figure 4.3 Bulk geochemical parameters indicative of organic matter maturity from the Kap Stosch section. Note different scale on inset portion.

isotopic values may be indicative of shifts in the nature of the organic material. By analogy to this study, a low value of $\delta^{13}C$ may indicate kerogen formed predominantly from marine organic matter input while trends to more positive values likely mark increased terrestrial input, a pattern that has been documented in a Permian-Triassic boundary sections from Perth and Bonaparte basins, Australia (Foster et al. 1997; Grice et al. 2007)

The $\delta^{13}C_{org}$ and the TOC of the Kap Stosch samples show distinctly different values on either side of the Permian-Triassic transition, similar to patterns seen in other sections worldwide (Grice et al. 2005a; Cao et al. 2009). Given the depositional environment of the Kap Stosch samples based on lithological evidence, there may have been an increase in terrestrial input to the sediments in the Triassic period; nevertheless, the Permian rocks are predominantly marine in character. According to the conclusions put forth in Grice et al. (2007), these differing sources of organic matter input are the opposite of what would be expected based on $\delta^{13}C_{org}$ measurements, which are significantly more positive in the Permian rocks than the Triassic rocks. Therefore the fluctuations in $\delta^{13}C_{org}$ and TOC across the Permian-Triassic transition at Kap Stosch may have underpinnings that are more complex than a simple facies shift including perturbations in the carbon cycle related to the extinction event.

Biomarkers

Depositional Environment

The C_{30} sterane index records the abundance of C_{30} steranes (24-*n*-propylcholestanes) relative to total C_{27-30} steranes, identifies marine input to sedimentary rocks. A C_{30} sterane index of greater than 4% is generally considered indicative of significant contributions from marine pelagophyte algae and

therefore a marine depositional environment (Peters et al. 2005; Giner et al. 2009). Although the fossils identified in Kap Stosch samples from the Triassic indicate that they were deposited in a marine environment, the values for this proxy are low, with the average value being ~2.5%, compared to samples from the latest Permian rocks where they reach a high of 7.5%. (See Figure 4.4.) The patterns in this biomarker proxy agree with the lithological evidence for changes in the content of organic matter deposited to the sediments: the Permian rocks retained significant marine character and there may have been increased terrestrial input in the Triassic rocks.

Another means of assessing depositional environment in the Kap Stosch section utilizes cross-plots of the ratio of C_{26}/C_{25} tricyclic terpane versus the $C_{31}22R/C_{30}$ hopane. Marine rocks generally have a low (<1.2) C_{26}/C_{25} tricyclic ratio and higher (>0.2) C_{31}/C_{30}hopane ratio (Peters et al. 2005). The Kap Stosch samples have somewhat ambiguous values for this proxy as well. However, like the C_{30} sterane index, the Permian samples appear to have more marine character than the Triassic samples. The tricyclic ratio for these samples is consistent with marine deposition with values that range from 0.30 to 1.03, with an average of 0.49 in the Permian samples and 0.70 in the Triassic samples. In contrast, the hopane ratio has values ranging from 0.14 to 0.33, with an average of 0.18 in the Permian rocks and 0.25 in the Triassic rocks. (See Figure 4.4.) This is slightly lower than the values usually considered indicative of a marine environment, but the general pattern still supports primarily marine deposition.

Redox conditions

Pristane and phytane in sedimentary rocks derive primarily from the diagenesis of the phytol side chain of chlorophylls (Brooks et al. 1969). (See Figure 4.7.) A pristane/phytane ratio (Pr/Ph) of <1 is widely considered to be indicative of deposition under anoxic conditions while a ratio >1 suggests

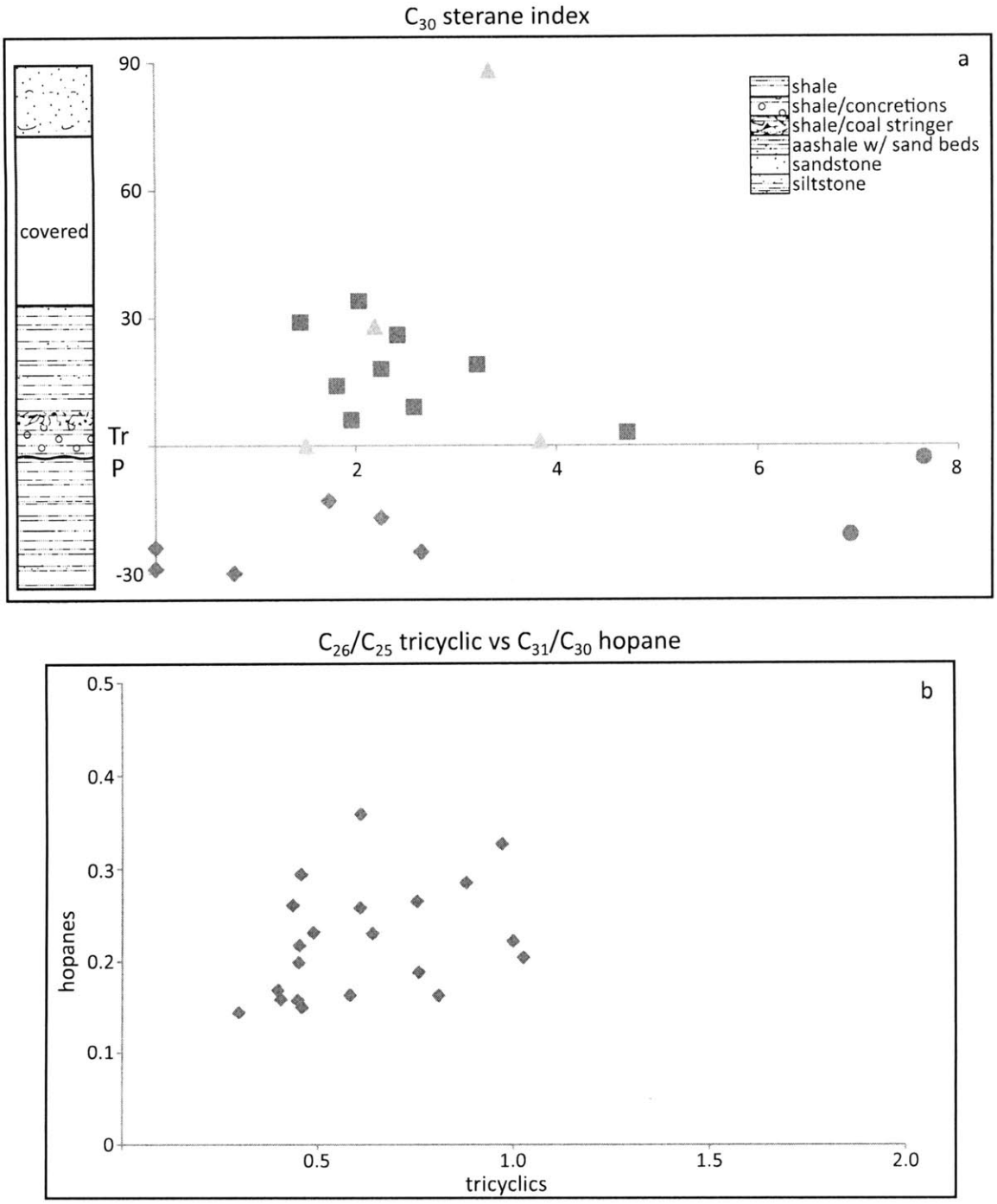

Figure 4.4 Biomarkers indicative of depositional environment from the Kap Stosch section. (a) The C_{30} sterane index (the ratio of 24 *n*-propylcholestane to total sterane) plotted relative to depth. The four different symbols (diamonds, squares, triangles and circles) represent samples from the four different localities from this composite section. (b) Cross-plot of ratio of C_{26} to C_{25} tricyclics to ratio of C_{31} to C_{30} hopane (from Peters et al. 2005). All ratios were measured by GC-MS in MRM mode.

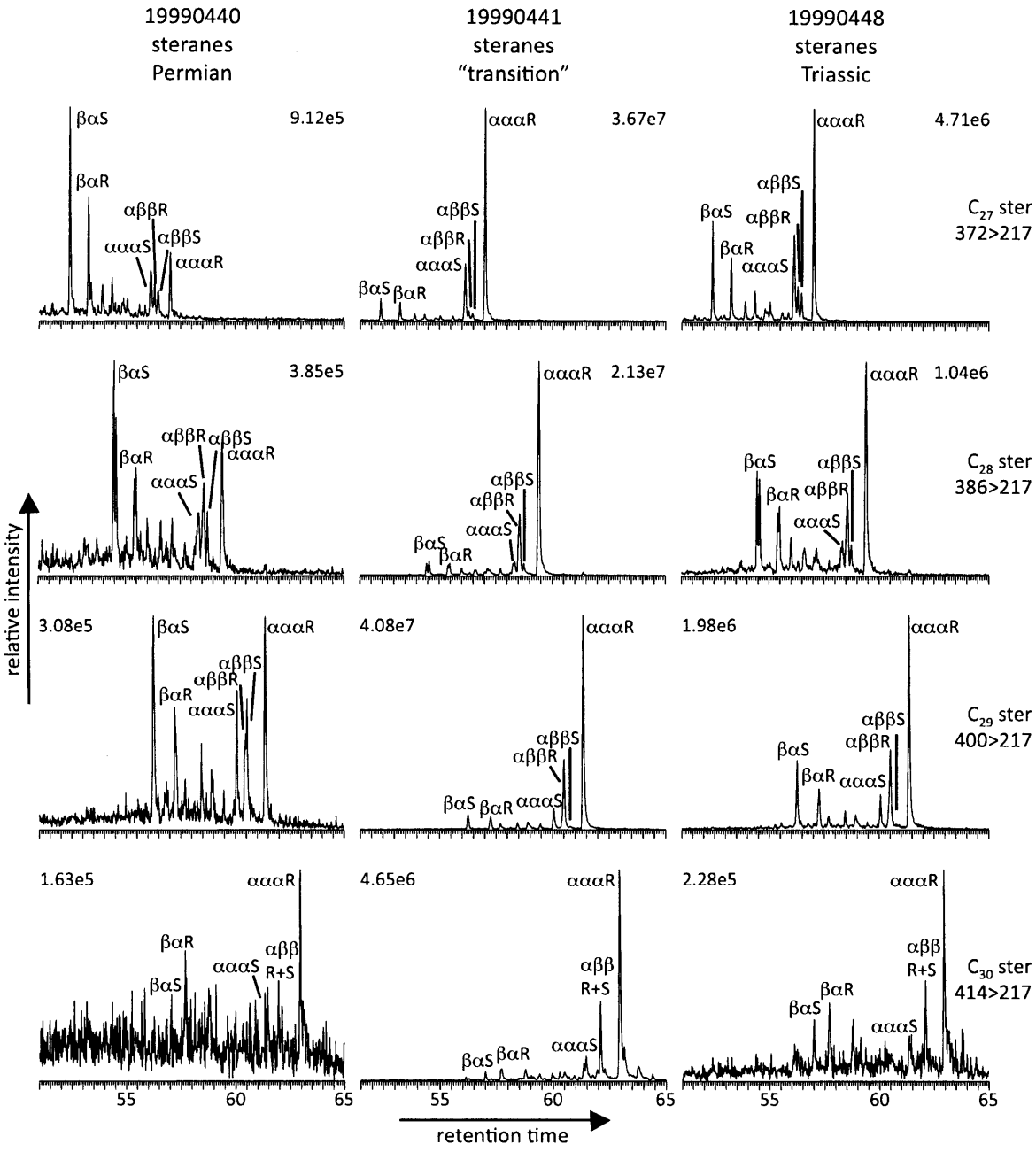

Figure 4.5 GC-MS MRM chromatograms from a select saturated hydrocarbon fraction from Kap Stosch showing relative abundances of steranes. For the steranes, the sample on the left is from the late Permian; the middle section is close to the assigned boundary; and the sample on the right is from the early Triassic.

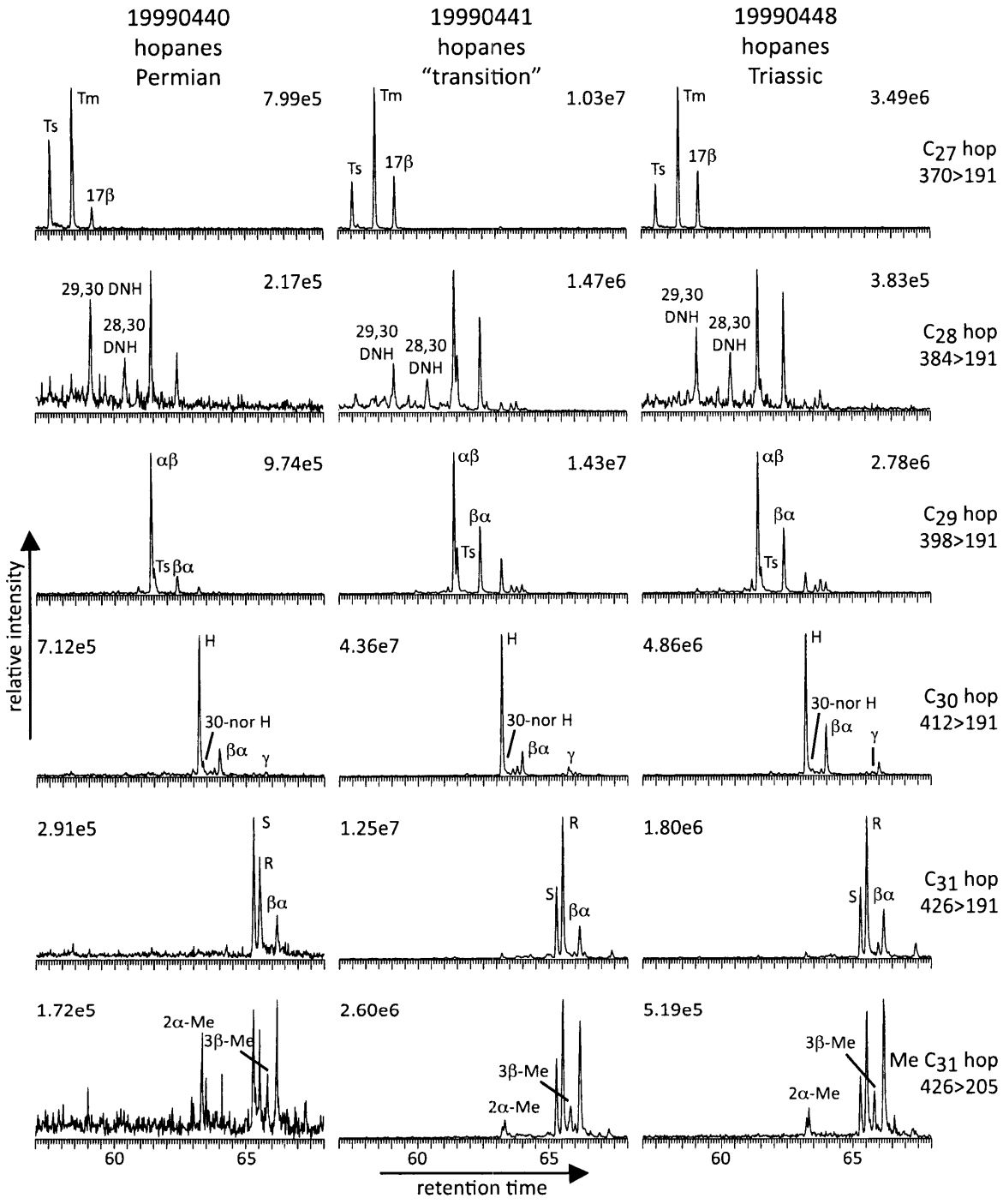

Figure 4.6 GC-MS MRM chromatograms from three saturated hydrocarbon fractions from Kap Stosch showing relative abundances of hopanes. The sample on the left is from the late Permian; the middle section is close to the assigned boundary; and the sample on the right is from the early Triassic.

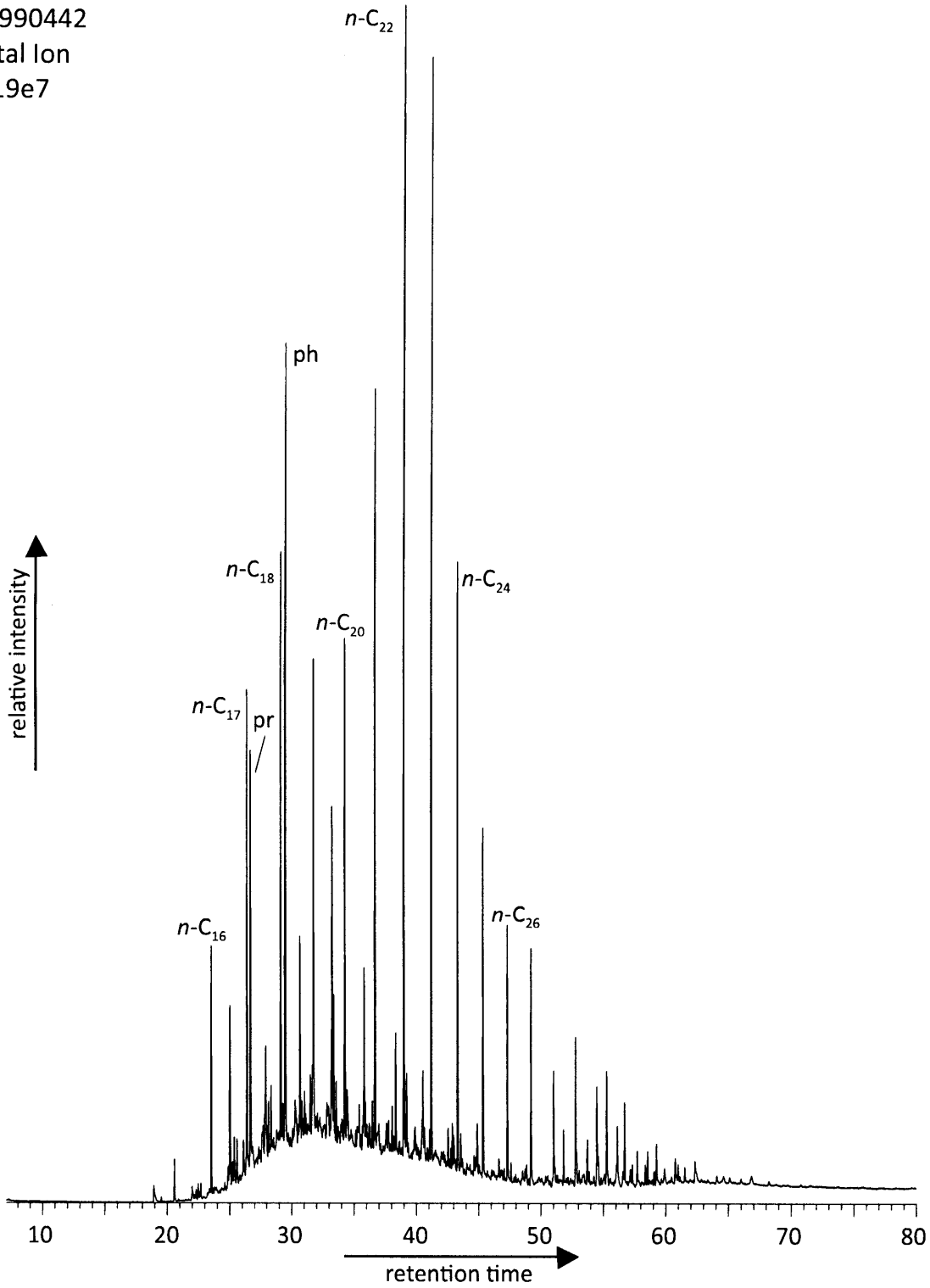

Figure 4.7 GC-MS full scan chromatogram of total ion current from a sample saturated hydrocarbon fraction from Kap Stosch. Isoprenoids pristane and phytane as well as *n*-alkanes are identified.

more oxic depositional conditions (Didyk et al. 1978). However, a value of <0.8 for anoxic and >2.0 for oxic has been suggested to be more reasonable (Peters et al. 2005). In Permian Kap Stosch rocks, the average Pr/Ph average value was 0.8, and the highest value measured in the section was 1.2. Lower values were measured in the Triassic rocks, where the Pr/Ph average is 0.6. (See Figure 4.8.) Although there were some Pr/Ph ratios >1, the generally low values indicate that anoxic conditions in the sediments largely prevailed during the deposition of the entire Kap Stosch section. Further understanding of redox conditions during deposition may be deduced from the homohopane index. Ratios of C_{35} relative to C_{34} hopanes greater than 0.6 have been interpreted as indicative of deposition under anoxic bottom water (Peters and Moldowan 1991). In the Kap Stosch samples, the homohopane index is relatively high with an average of 0.72 in the Permian rocks and an average of 0.69 in the Triassic rocks. (See Figure 4.8.) There are small peaks in the homohopane index with some values above 1, and these are also consistent with anoxic depositional conditions throughout.

Aryl isoprenoids with a 2,3,6-trimethyl substitution pattern are present in measurable quantities in nearly all of the samples studied. (See Figure 4.9.) In many samples close to the identified Permian-Triassic transition, the C_{40} isorenieratane precursor can also be identified. Aryl isoprenoids are measured relative to the total organic content in the samples. In the Kap Stosch section, the highest values are in the Permian rocks where the average is 0.16mg/g TOC and the highest value is 0.55mg/g TOC. In the Triassic rocks the values are lower with an average of 0.6mg/g TOC and a high value of 0.11mg/g TOC. (See Figure 4.8.) In significant concentrations, such as those measured Kap Stosch, the presence of these compounds in sedimentary rocks is indicative of photic zone euxinia in the source-rock depositional environment (Summons and Powell 1986; Sinninghe Damsté et al. 2001). This evidence supports previous biomarker and lithological evidence that

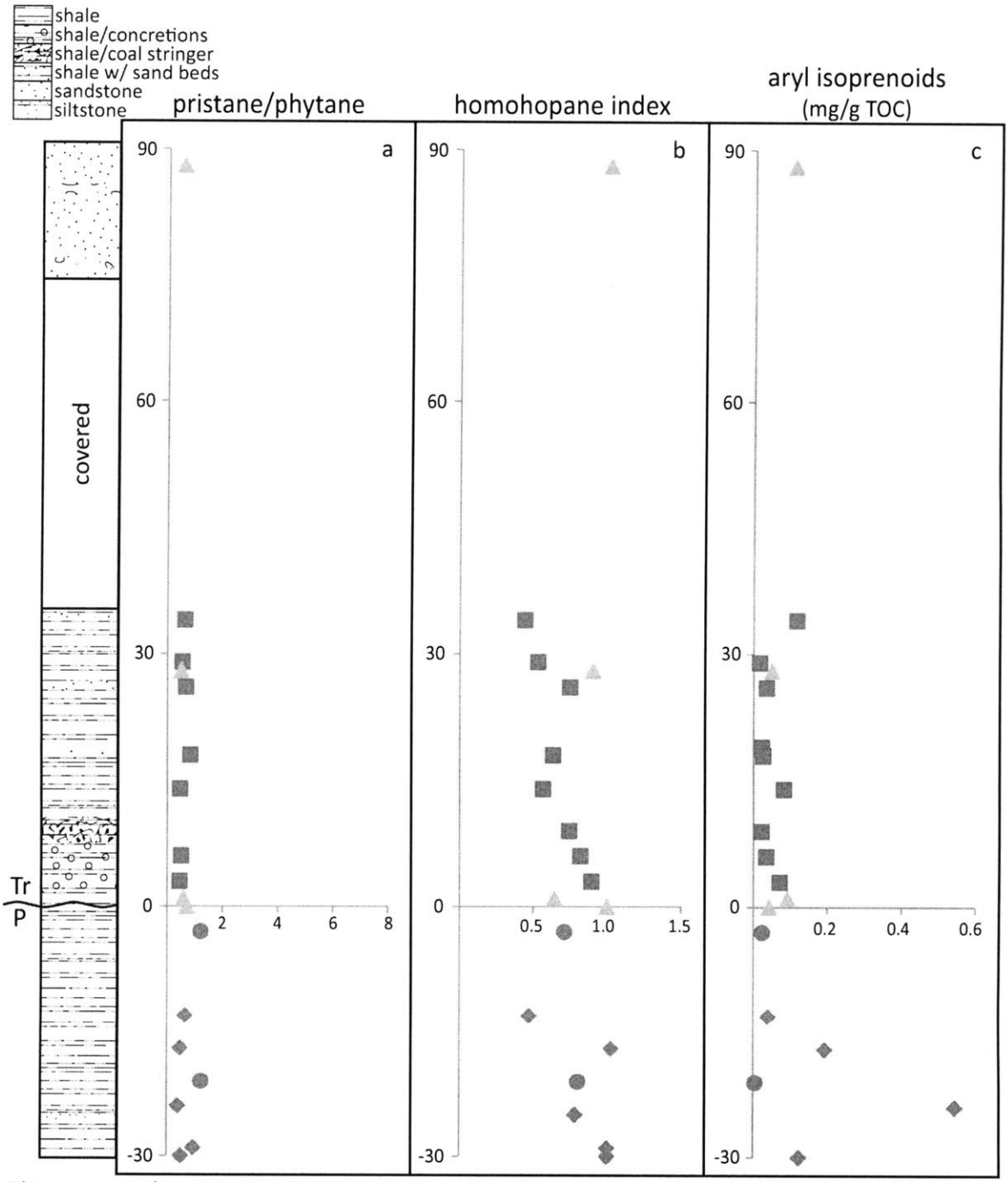

Figure 4.8 Redox sensitive biomarkers from the Kap Stosch section. (a) Pristane to phytane ratio measured from total ion current of full scan GC-MS data. (b) Homohopane index is the ratio of C_{35} hopane (22S + 22R isomers) measured relative to total C_{34} homohopanes, measured in GC-MS MRM mode. (c) Aryl isoprenoids were measured in GC-MS SIM mode and normalized relative to total organic carbon contents. The four different symbols (diamonds, squares, triangles and circles) represent samples from the four different localities from this composite section. All samples plotted relative to depth.

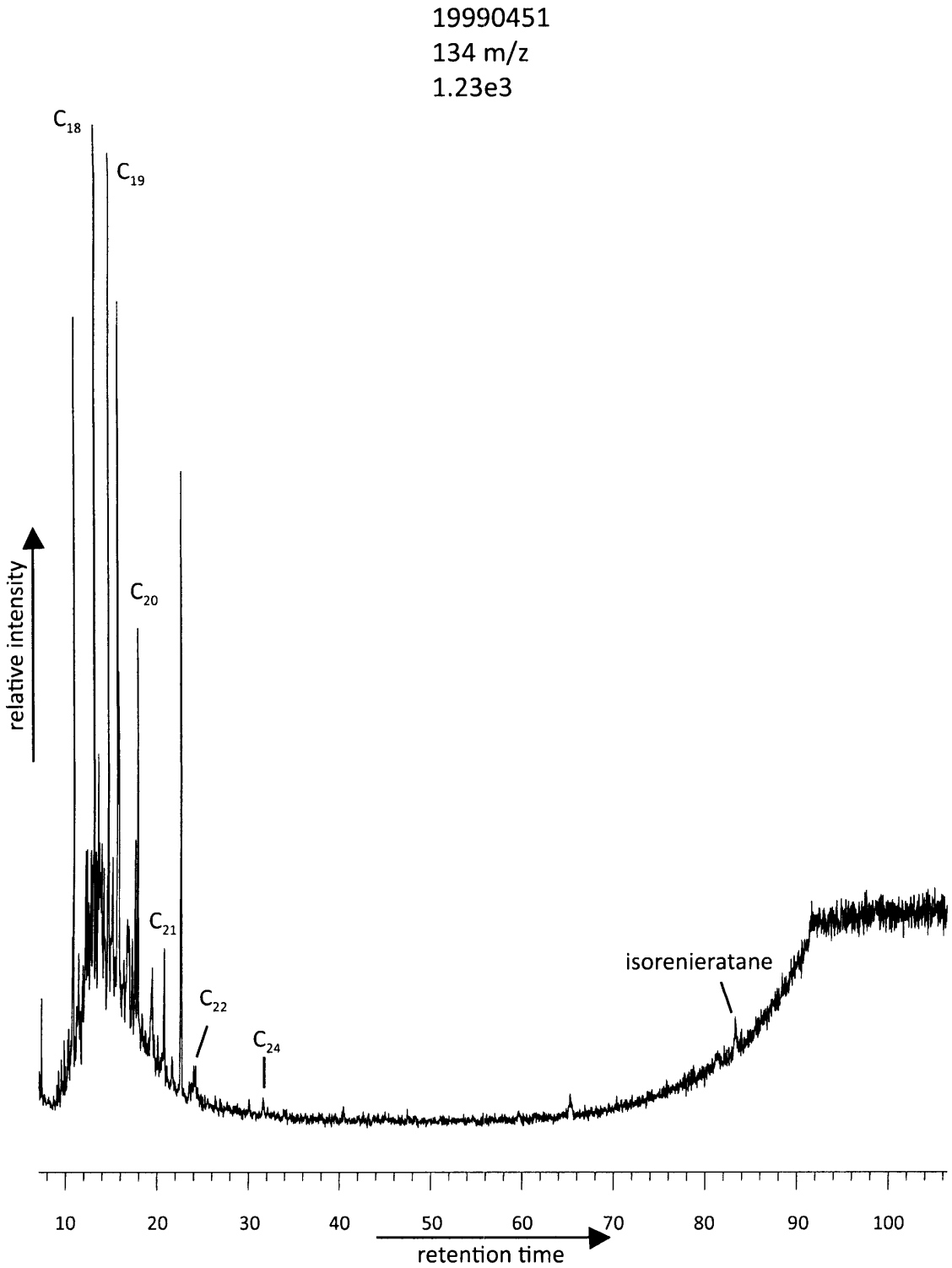

Figure 4.9 GC-MS select ion chromatogram of mass 134 from a sample aromatic hydrocarbon fraction from Kap Stosch. Aryl isoprenoids from C_{18} to C_{24} have been identified, as well as the extended C_{40} carotenoid derivative isorenieratane.

indicate the presence of PZE in this region at the end-Permian period (Grice et al. 1997; Pancost et al. 2002). The maximum in abundances of Chlorobi biomarkers in the upper Permian rocks is also consistent with biomarker records for Meishan and Perth Basin (Grice et al. 2005a).

Recently, crocetane was the subject of a study that examined its potential as a marker for photic zone euxinia in certain samples of high thermal maturity where it may have been derived from the central 20 carbon atoms of Chlorobi carotenoids (Maslen et al. 2009). However, this same study reported that no crocetane was identified in sections from the Permian-Triassic boundary described in the studies by Grice et al. (Grice et al. 1996b; 2005a). Although I could make no reliable measurement of the $\delta^{13}C$ value of this compound, I could unambiguously identify crocetane in the Kap Stosch samples using the diagnostic 168 → 126 reaction in GC-MRM (Greenwood and Summons 2003) in combination with analyses conducted on authentic standards. Also intriguing is the observation of the highest contents of crocetane, amounting to about 5% of the co-eluting phytane peak, occurred in many of the same sedimentary rocks with the highest quantities of aryl isoprenoids and isorenieratane.

The combination of factors described by the C_{30} sterane index, the ratio of C_{26}/C_{25} tricyclic terpane relative to $C_{31}22R/C_{30}$ hopane, the pristane/phytane ratio, and the homohopane index all indicate that the Kap Stosch samples were primarily deposited beneath an anoxic and euxinic marine water column. These rocks were deposited at the margin of a small inland sea, and it is not surprising that many of these proxies show that the region was subject to fluctuations in input sources. Even with an apparent increased terrestrial input in the Triassic part of the section, the presence of the aryl isoprenoids and isorenieratane, together with the crocetane, indicate that euxinic conditions extended into the photic zone.

Microbial Community Composition

The ratio of total hopanes to total steranes is a general proxy reflecting the relative proportions of biomass input to sediments from bacteria versus eukaryotes. Although the values are within normal ranges for Phaerozoic oils and sediments (0.5 to 2.0), the trends in hopane/sterane ratio do not show a particular pattern. There is a wide range of values for the hopane/sterane ratio in the youngest Permian rocks, between 0.3 and 6.3, with an average value of 1.9. The average value is slightly lower in the oldest Triassic rocks (1.4) but there is a smaller range of values with a low of 0.6 and a high of 3.5. (See Figure 4.10.) Although the values are higher in the Permian rocks, the hopane/sterane ratio throughout the section indicates a water column with relatively higher contents of bacterial biomass.

The ratio of 2-methylhopanes to C_{30} hopane, the 2-methylhopane index (2-MHI) has been proposed as a proxy for the proportion of organic matter derived from cyanobacteria (Summons et al. 1999; Knoll et al. 2007a). The values of the 2-MHI range from 1% to 11% in this section, with a slightly higher average in the youngest Permian rocks (~4%) than in the oldest Triassic rocks (~3%). (See Figure 4.10.) The pattern of 2-MHI shows fluctuations in tandem with the total aryl isoprenoids at the end of the Permian period, but in the Triassic period this index fluctuates inversely. These values are not particularly high compared other typical Phanerozic shales and sandstones, but the distribution may suggest that at the time of greatest carbon cycle perturbation and nutrient limitation (N and Fe), cyanobacteria had a competitive edge, an idea that has been previously proposed for Mesozoic anoxic events (Kuypers et al. 2004).

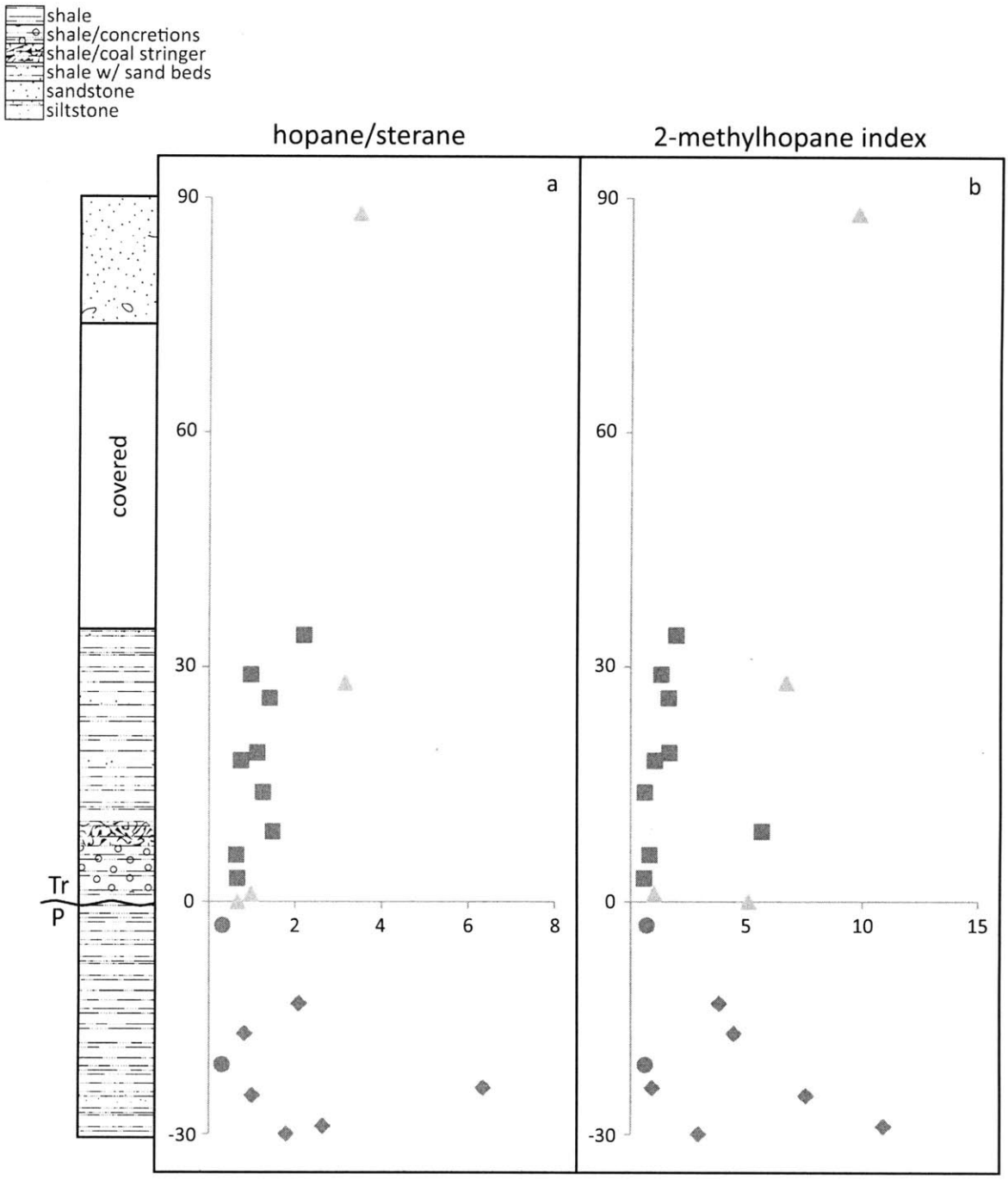

Figure 4.10 Biomarkers indicative of the microbial community from the Kap Stosch section. (a) Hopane/sterane ratio was measured including all identified hopane and steranes in the section. (b) 2-methylhopane index is the percentage of 2-methylhopane to the sum of this compound and C_{30} hopane. The four different symbols (diamonds, squares, triangles and circles) represent samples from the four different localities from this composite section. All ratios were measured by GC-MS in MRM mode and plotted relative to depth.

The presence of the moderately high hopane/sterane ratio, together with a 2-MHI that peaked in tandem with Chlorobi-derived biomarkers shows that at the Kap Stosch locality bacterial inputs were significant.

Although the source of the C_{33} *n*-alkylcyclohexanes (C_{33} *n*-ACH) is not yet known, empirical evidence suggests that its presence coincides with the main Permian-Triassic extinction (Thomas and Barber 2004; Grice et al. 2005b; McIldowie and Alexander 2005). This compound is present in elevated concentrations in the Schuchert Dal section of East Greenland (Grice et al. 2005b). It is not surprising that in the Kap Stosch section, the C_{33} *n*-ACH first appears in the youngest Permian sample and is seen in roughly one-third of the samples, ending in the earliest Triassic interval. The values of C_{33} *n*-ACH relative to *n*-C_{34} peak just above the transition and then decrease shortly thereafter. (See Figure 4.11 and 4.12.)

The ratio of C_{28} steranes to C_{29} steranes is observed to increase throughout the Phanerozoic as the organisms that produce the precursor steroids (the 'chlorophyl A+C' assemblages of diatoms coccolithophores and dinoflagellates) rise in relative importance as components of the phytoplankton community (Knoll et al. 2007b). Studies of this parameter in rocks and petroleum from all ages have suggested that a ratio between 0.4 and 0.7 is typical in samples from around the mid-Phanerozoic (Peters et al. 2005). The values seen in the Kap Stosch section (with an average of 0.60) are typical for the Late Paleozoic to Early Mesozoic. (See Figure 4.12.) The highest value of 1.2 was measured in a Permian sample and the average for the Permian samples is 0.7 compared to an average of 0.54 for Triassic samples.

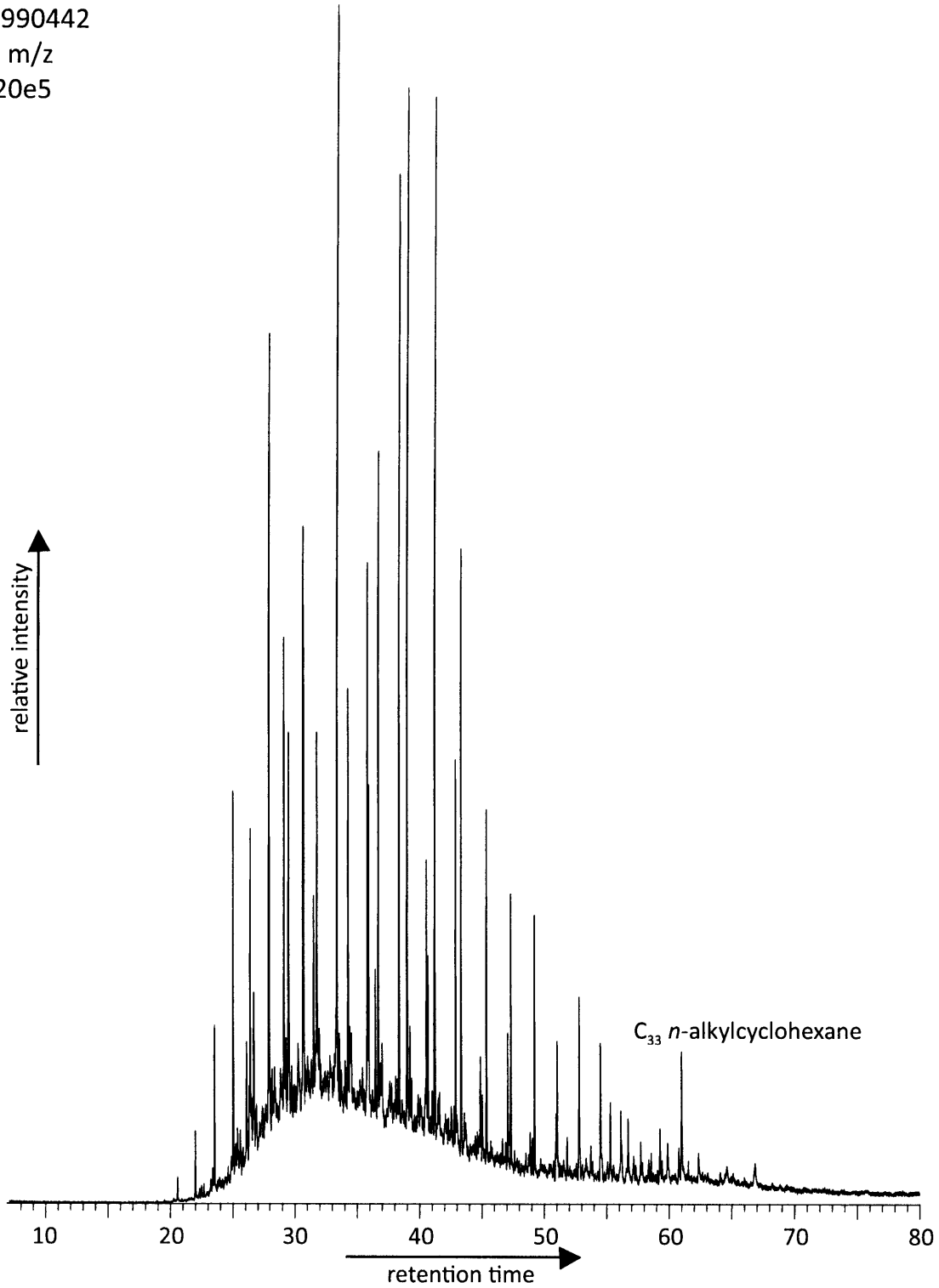

Figure 4.11 GC-MS select ion chromatogram of mass 83 from a sample saturated hydrocarbon fraction from Kap Stosch. Elevated abundances of C_{33} *n*-alkylcyclohexane can be seen.

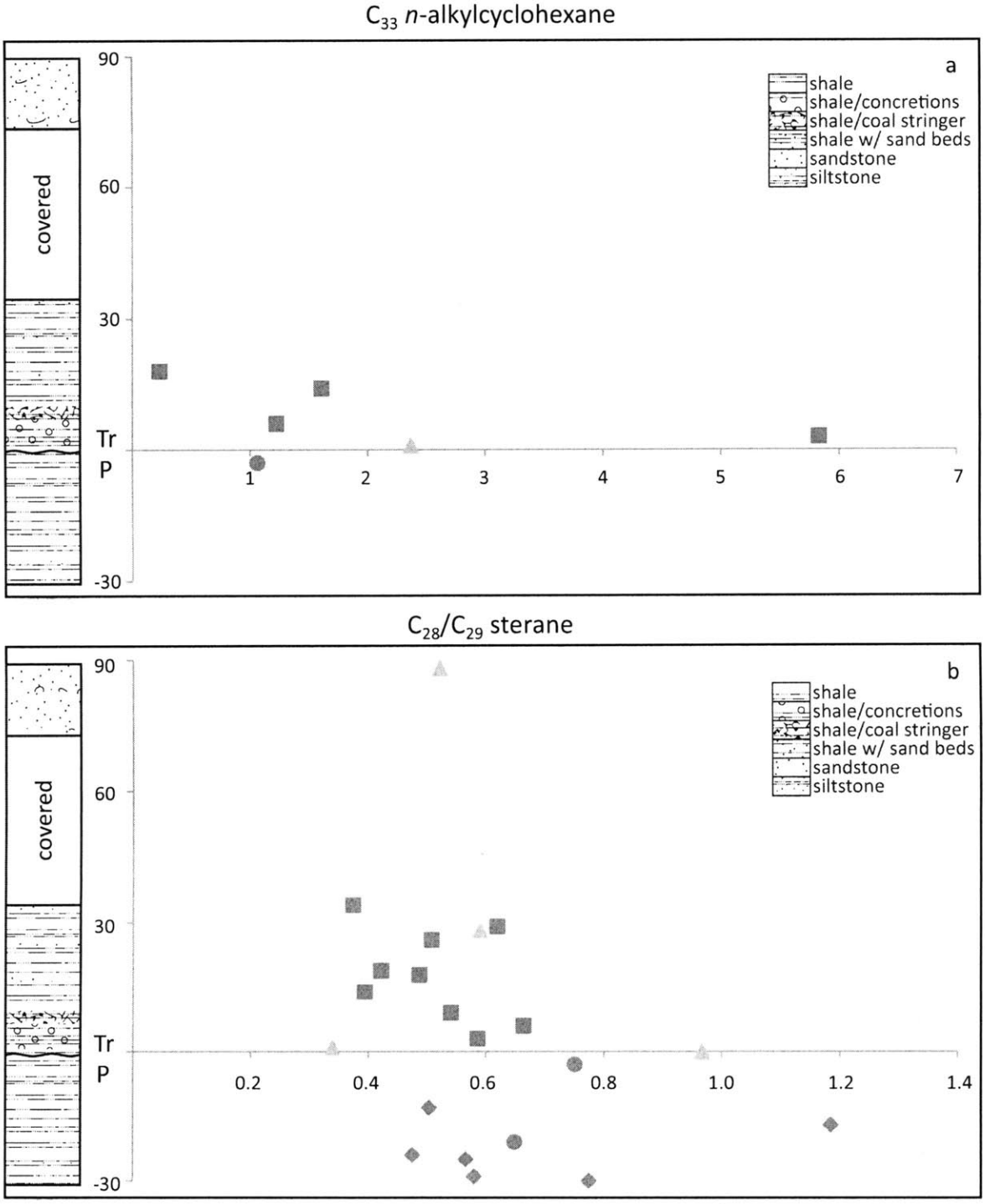

Figure 4.12 Age-sensitive biomarkers from the Kap Stosch section. (a) The ratio of C_{33} *n*-alkylcyclohexane to C_{34} *n*-alkanes. (b) The ratio of total C_{28} to total C_{29} steranes. The four different symbols (diamonds, squares, triangles and circles) represent samples from the four different localities from this composite section. Compounds were measured by GC-MS in MRM mode. All parameters are plotted relative to depth.

The C_{33} *n*-ACH and the C_{28}/total steranes are reflective of the microbial communities in the depositional environment and additionally suggest a relative age for these sedimentary rocks. Age-sensitive biomarkers indicate that the Kap Stosch section was deposited before the major radiation of dinoflagellates in the mid-Triassic period and concurrently with the major rise of the post-extinction source of the C_{33} *n*-ACH precursor.

Thermal Maturity and Lithology

The 20S/(20S+20R) ratio of the C_{29} steranes and the 22S/(22S+22R) ratio of the C_{31} homohopane are a reflection of the degree of isomerization at the sterogenic centers of the sterane and hopane, side-chains. When controlled by maturity, the hopane isomerization reaches its stable end-point (~60%) before peak petroleum generation, while the sterane isomerization reaches its stable end-point (~55%) somewhat later and closer to the end of peak generation. Below the assigned boundary the values for these maturation proxies suggest sedimentary rocks near to past peak hydrocarbon generation. (See Figure 4.13.) However, given the distinct lithological and facies changes throughout this section, it is difficult to rationalize how Triassic sedimentary rocks, which show evidence of organic matter input from mixed sources including older, reworked material, would show significantly lower maturity proxies than the Permian counterparts. Instead, the measured pattern suggests that at Kap Stosch, these biomarkers are predominantly controlled by these distinct changes in facies and lithology, a correlation that has been observed previously at Meishan (Cao et al. 2009) and in sections from other time periods (Moldowan et al. 1986; ten Haven et al. 1986).

The ratios of C_{30} βα hopane (moretane) to C_{30} αβ hopane (hopane) and C_{27} 17α-trisnorhopane (Tm) to C_{27} 18α-trisnorhopane (Ts) reflect more complex isomerizations and reactions during

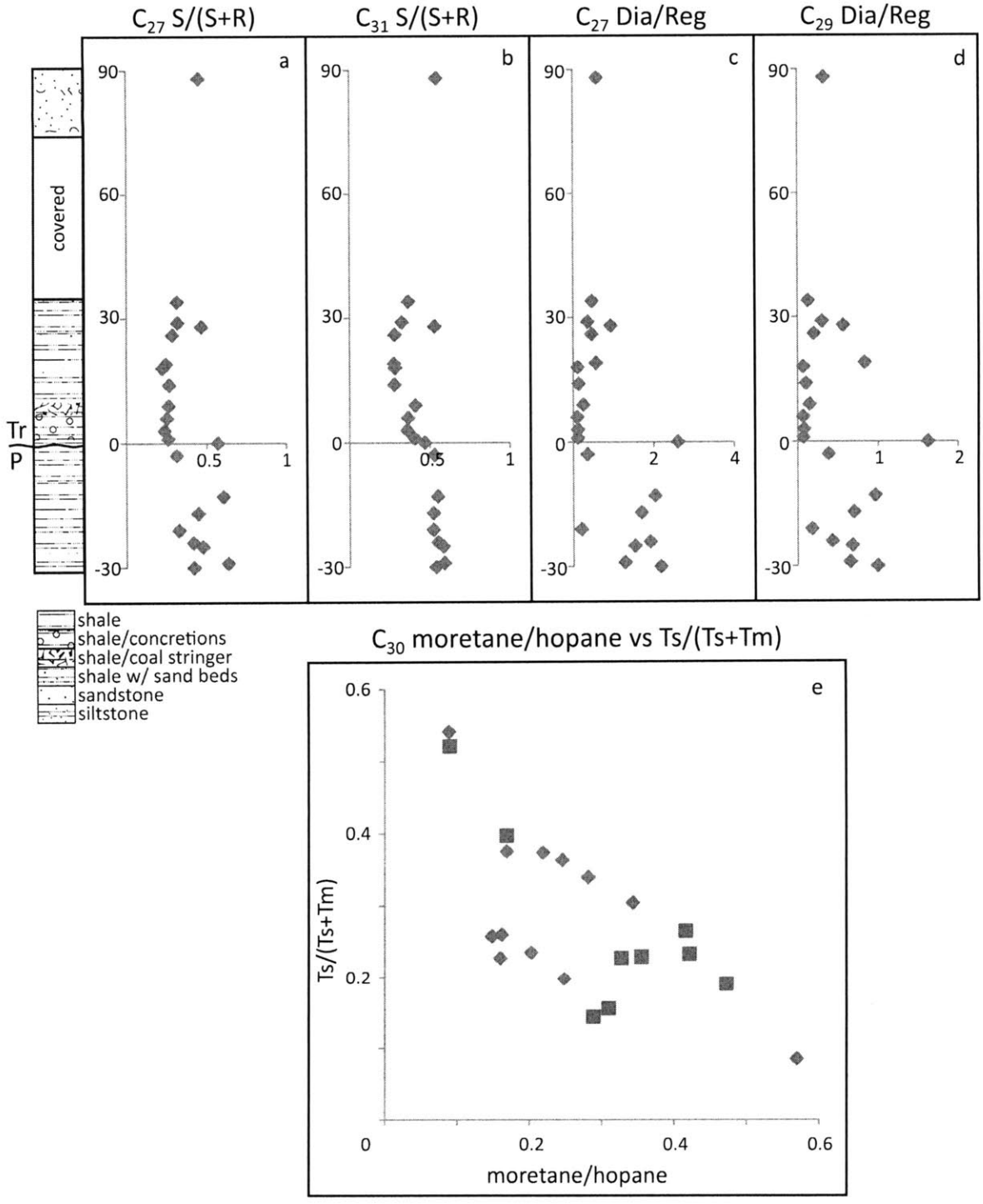

Figure 4.13 Biomarkers indicative of lithology from the Kap Stosch section. (a) through (d) are plotted relative to depth. In the cross-plot in (e) the diamonds represent samples from shale rocks and the squares represent samples from predominantly sandstone rocks. All ratios were measured by GC-MS in MRM mode.

catagenesis than those described above. Although these ratios are generally shown to increase with burial depth and thermal maturity, they can also be significantly affected by changes in facies and organic matter inputs (Moldowan et al. 1986). The two-stage changes in the Ts/(Ts+Tm) ratio and moretane/hopane ratio that were observed in the Kap Stosch section are similar, though not as significant as the pattern in C_{27} sterane and C_{31} homohopane isomerization.

When the moretane/hopane ratio and Ts/(Ts+Tm) ratio are examined relative to each other in a cross-plot and coded to include rock-type the correlation between these proxies and lithology in this section is apparent. (See Figure 4.13.) The correlation is not as clear in the S/(S+R) ratios, but the two-stage pattern that is observed in all of these proxies suggests that they are all controlled by lithology and organic material sources in this relatively low-maturity section.

An increase in the moretane/hopane ratio similar to the one measured here has also been observed in Meishan (Wang 2007; Xie et al. 2007; Cao et al. 2009). Initially this moretane anomaly was suggested to signify increased terrestrial input in the aftermath of the extinction event (Wang 2007; Xie et al. 2007). This hypothesis was discounted by Cao et al. (2009) where an increased $\beta\alpha$ to $\alpha\beta$ ratio was seen in all hopanes, including homohopanes, indicating that it was a result of diagenetic conditions that lead to the enhanced preservation of these isomers. The Kap Stosch section shows a similar phenomenon with increased $\beta\alpha$ to $\alpha\beta$ ratio evident in the homohopanes (see Figure 4.6). Although there is evidence of increased terrestrial input to the Triassic sediments it is clear that lithology and diagenetic processes exert a prime control on the relative abundances of these triterpane isomers.

Qualifying factors

Primarily, Kap Stosch is an outcrop section and it has been affected by erosion weathering to the extent that the boundary itself is physically obscured. Outcrop samples are not ideal for biomarker studies because of the potential for contamination, although this can be partially overcome by careful selection of the biomarkers for analysis as was done here. Also, the fact that the transition itself represents a paraconformity makes this section appropriate only for identification of the gross trends across the boundary, since source inputs and lithologies may have changed at rates that would be undetectable in our course sampling. Further, as the Greenland section was deposited beneath an epicontinental sea, there are some concerns that the biomarker evidence may record changes in a restricted basin that are not representative of global events. However, the correlation in biomarker proxies and isotopic measurements between this section and others may be sufficient reason to discount this argument.

Summary

Bulk carbon data from samples from Kap Stosch, Greenland, show evidence of inputs from both marine and terrestrial organic matter to these generally low-maturity sedimentary rocks. Biomarker evidence can also be used to provide a general understanding of the Kap Stosch depositional environment. Biomarker ratios indicate that the samples were deposited in an epicontinental marine setting with increasing terrestrial inputs in the Triassic period, but under a water column that was anoxic throughout. The identification of the aryl isoprenoids and isorenieratane indicates that photic zone euxinia was present (though perhaps only periodically) leading up to, and continuing through, the Permian-Triassic boundary. A correlation between biomarkers for the presence of PZE and the high TOC content and 2-MHI measured here is similar to Mesozoic oceanic anoxic events (Kuypers

et al. 2004). Although this relationship has been observed in the Hovea-3 core from Australia (Grice et al. 2005a), it has not been seen in all records of the Permian-Triassic boundary.

Throughout Kap Stosch, the bulk geochemical parameters and biomarker ratios are in general agreement with other studies that have been performed on samples from this region. The large fluctuations in these proxies reflect a dynamic carbon cycle and euxinic oceanic conditions before and through the Permian-Triassic boundary with significant perturbations during the extinction event.

References

Birkelund, T., D. Bridgwater and A. Higgins (1974). An Outline of the Geology of the Atlantic Coast of Greenland. The Ocean Basins and Margins. A. Nairn and F. Stehli. New York, Plenum Publishing Corporation. **2:** 125-159.

Brooks, J., K. Gould and J. Smith (1969). "Isoprenoid Hydrocarbons in Coal and Petroleum." Nature **222**(5190): 257-259.

Cao, C., G. D. Love, L. E. Hays, W. Wang, S. Shen and R. E. Summons (2009). "Biogeochemical Evidence for Euxinic Oceans and Ecological Disturbance Presaging the End-Permian Mass Extinction Event." Earth and Planetary Science Letters **281**(3-4): 188-201.

Didyk, B., B. Simoneit, S. Brassell and G. Eglinton (1978). "Organic Geochemical Indicators of Palaeoenvironmental Conditions of Sedimentation." Nature **272**(5650): 216-222.

Fenton, S., K. Grice, R. J. Twitchett, M. E. Bottcher, C. V. Looy and B. Nabbefeld (2007). "Changes in Biomarker Abundances and Sulfur Isotopes of Pyrite across the Permian-Triassic (P/Tr) Schuchert Dal Section (East Greenland)." Earth and Planetary Science Letters **262**(1-2): 230-239.

Foster, C., G. Logan, R. E. Summons, J. Gorter and D. Edwards (1997). "Carbon Isotopes, Kerogen Types and the Permian-Triassic Boundary in Australia: Implications for Exploration." Australian Petroleum Production and Exploration Association Journal **37**: 442-459.

Giner, J.-L., H. Zhao, G. L. Boyer, M. F. Satchwell and R. A. Andersen (2009). "Sterol Chemotaxonomy of Marine Pelagophyte Algae." Chemistry & Biodiversity **6**(7): 1111-1130.

Greenwood, P. F. and R. E. Summons (2003). "Gc-Ms Detection and Significance of Crocetane and Pentamethylicosane in Sediments and Crude Oils." Organic Geochemistry **34**(8): 1211-1222.

Grice, K., C. Cao, G. D. Love, M. E. Bottcher, R. J. Twitchett, E. Grosjean, R. E. Summons, S. C. Turgeon, W. Dunning and Y. Jin (2005a). "Photic Zone Euxinia During the Permian-Triassic Superanoxic Event." Science **307**(5710): 706-709.

Grice, K., R. Gibbison, J. E. Atkinson, L. Schwark, C. B. Eckardt and J. R. Maxwell (1996a). "Maleimides (1h-Pyrrole-2,5-Diones) as Molecular Indicators of Anoxygenic Photosynthesis in Ancient Water Columns." Geochimica et Cosmochimica Acta **60**(20): 3913-3924.

Grice, K., B. Nabbefeld and E. Maslen (2007). "Source and Significance of Selected Polycyclic Aromatic Hydrocarbons in Sediments (Hovea-3 Well, Perth Basin, Western Australia) Spanning the Permian-Triassic Boundary." Organic Geochemistry **38**(11): 1795-1803.

Grice, K., P. Schaeffer, L. Schwark and J. R. Maxwell (1996b). "Molecular Indicators of Palaeoenvironmental Conditions in an Immature Permian Shale (Kupferschiefer, Lower Rhine Basin, North-West Germany) from Free and S-Bound Lipids." Organic Geochemistry **25**(3-4): 131-147.

Grice, K., P. Schaeffer, L. Schwark and J. R. Maxwell (1997). "Changes in Palaeoenvrionmental Conditions During Deposition of the Permian Kupferschiefer (Lower Rhine Basin, Northwest Germany) Inferred from Molecular and Isotopic Compositions of Biomarker Components." Organic Geochemistry **26**(11-12): 677-690.

Grice, K., R. J. Twitchett, R. Alexander, C. B. Foster and C. Looy (2005b). "A Potential Biomarker for the Permian-Triassic Ecological Crisis." Earth and Planetary Science Letters **236**(1-2): 315-321.

Knoll, A. H., R. E. Summons, J. Waldbauer and J. Zumberge (2007a). The Geological Succession of Primary Producers in the Oceans. The Evolution of Photosynthetic Organisms in the Oceans. F. P. a. K. A.H.

Knoll, A. H., R. E. Summons, J. R. Waldbauer and J. Zumberge (2007b). The Geological Succession of Primary Producers in the Oceans. The Evolution of Photosynthetic Organisms in the Oceans P. Falkwoski and A. H. Knoll. Boston, Elsevier**:** 133-163.

Kuypers, M. M. M., Y. van Breugel, S. Schouten, E. Erba and J. S. S. Damste (2004). "N2-Fixing Cyanobacteria Supplied Nutrient N for Cretaceous Oceanic Anoxic Events." Geology **32**(10): 853-856.

Maslen, E., K. Grice, J. D. Gale, C. Hallmann and B. Horsfield (2009). "Crocetane: A Potential Marker of Photic Zone Euxinia in Thermally Mature Sediments and Crude Oils of Devonian Age." Organic Geochemistry **40**(1): 1-11.

McIldowie, M. and R. Alexander (2005). "Identification of a Novel C33 N-Alkylcyclohexane Biomarker in Permian-Triassic Sediments." Organic Geochemistry **36**(10): 1454-1458.

Moldowan, J. M., P. Sundararaman and M. Schoell (1986). Sensitivity of Biomarker Properties to Depositional Environment and/or Source Input in the Lower Toarcian of Sw-Germany. Advances in Organic Geochemistry 1985, Org. Geochem. D. Leythaeuser and J. Rullkötter. Pergamon. **10:** 915-926.

Nielsen, J. K. and Y. Shen (2004). "Evidence for Sulfidic Deep Water During the Late Permian in the East Greenland Basin." Geology **32**(12): 1037-1040.

Pancost, R. D., N. Crawford and J. R. Maxwell (2002). "Molecular Evidence for Basin-Scale Photic Zone Euxinia in the Permian Zechstein Sea." Chemical Geology **188**: 217-227.

Perch-Nielsen, K., K. Birkenmajer, T. Birkelund and M. Aellen (1974). "Revision of Triassic Stratigraphy of the Scoresby Land and Jameson Land Region, East Greenland." Meddelelser om Gronland **193**(6): 51-68.

Peters, K. and J. Moldowan (1991). "Effects of Source, Thermal Maturity, and Biodegredation on the Distribution and Isomerization of Homohopanes in Petroleum." Organic Geochemistry **17**(1): 47-61.

Peters, K. E., J. M. Moldowan and C. C. Walters (2005). The Biomarker Guide. Cambridge, UK; New York, Cambridge University Press.

Sinninghe Damsté, J. S., S. Schouten and A. C. T. van Duin (2001). " Isorenieratene Derivatives in Sediments: Possible Controls on Their Distribution." Geochimica et Cosmochimica Acta **65**: 1557-1571.

Summons, R. E., L. L. Jahnke, J. M. Hope and G. A. Logan (1999). "2-Methylhopanoids as Biomarkers for Cyanobacterial Oxygenic Photosynthesis." Nature **400**: 554-557.
Summons, R. E. and T. Powell (1986). "Chlorobiaceae in Paleozoic Seas Revealed by Biological Markers, Isotopes and Geology." Nature **319**(6056): 763-765.
Teichert, C. and B. Kummel (1972). "Permian-Triassic Boundary in the Kap Stosch Area, East Greenland." Bulletin of Canadian Petroleum Geology **20**(4): 659-675.
Teichert, C. and B. Kummel (1976). "Permian-Triassic Boundary in the Kap Stosch Area, East Greenland." Meddelelser om Gronland **197**(5): 2-49.
ten Haven, H. L., J. W. D. Leeuw, T. M. Peakman and J. R. Maxwell (1986). "Anomalies in Steroid and Hopanoid Maturity Indices." Geochimica et Cosmochimica Acta **50**(5): 853-855.
Thomas, B. M. and C. J. Barber (2004). "A Re-Evaluation of the Hydrocarbon Habitat of the Northern Perth Basin." Australian Petroleum Production and Exploration Association Journal **44**: 59-92.
Wang, C. (2007). "Anomalous Hopane Distributions at the Permian-Triassic Boundary, Meishan, China - Evidence for the End-Permian Marine Ecosystem Collapse." Organic Geochemistry **38**(1): 52-66.
Wignall, P. and R. Twitchett (2002). "Permian-Triassic Sedimentology of Jameson Land, East Greenland: Incised Submarine Channels in an Anoxic Basin." Journal of the Geological Society, London **159**: 691-703.
Xie, S., R. D. Pancost, J. Huang, P. B. Wignall, J. Yu, X. Tang, L. Chen, X. Huang and X. Lai (2007). "Changes in the Global Carbon Cycle Occurred as Two Episodes During the Permian-Triassic Crisis." Geology **35**(12): 1083-1086.

Table 4.S1: Total biomarker data from Kap Stosch, Greenland

							RockEval 2 analysis of Rock Powder		
Geochem #	**relative depth**	**Sample Name**	**Locality**	**Stratigraphic Name**	**rock type**	**$d^{13}C_{PDB}$ (‰)**	**TMAX (°C)**	**S1 (mg/g)**	**S2 (mg/g)**
19990454	88	750-8	6.75	basal Triassic, younger than 750-6	sandstone	-29.3	480±20	0.03	0.12
19990449	34	1-11B	1	basal Triassic of Locality 1, younger than 1-2	shale/ sandstone	-30.6	430±20	0.00	0.16
19990448	29	1-11A	1	basal Triassic of Locality 1, younger than 10	shale/ sandstone	-31.7	430±20	0.01	0.12
19990453	28	750-6	6.75	basal Triassic, younger that 750-4	shale/ sandstone	-30.8	480±20	0.02	0.14
19990447	26	1-10	1	basal Triassic of Locality 1, younger than 1-9A	sandstone	-30.9	430±10	0.04	0.20
19990452	25	750-4	6.75	basal Triassic, stratigraphic equivalent of Locality 1-10	shale	-32.5	>480	0.00	0.08
19990446	19	1-9C	1	basal Triassic of Locality 1, younger than 1-8B	shale/ sandstone	-32.9	430±10	0.00	0.15
19990444	18	1-8B	1	basal Triassic of Locality 1, younger than 1-3	laminar/ quartz	-32.3	431	0.02	0.49
19990445	14	1-9A	1	basal Triassic of Locality 1, younger than 1-8B	shale/ sandstone	-32.6	432	0.01	0.23
19990443	9	1-3	1	basal Triassic of Locality 1, younger than 1-2	shale	-32.4	430±20	0.08	0.21
19990442	6	1-2	1	basal Triassic of Locality 1, younger than 1-1	shale	-32.8	430	0.05	0.62
19990441	3	1-1	1	basal Triassic of Locality 1	shale	-32.4	431	0.07	1.11
19990451	1	750-2	6.75	basal Triassic, older than Locality 1-1	shale	-33.0	430	0.03	0.33
19990450	0	750-1	6.75	basal Triassic, older than Locality 1-1	shale	-23.3	430±20	0.01	0.10
19990457	-3	1375-1B	13.75	Posidonia Shale	shale	-28.9	431	0.56	14.64
19990440	-13	0-9B	0	Martinia Shale, younger than 0-7	shale	-24.8	430±20	0.02	0.19
19990439	-17	0-9A	0	Martinia Shale, younger than 0-7	shale	-21.5	430±20	0.02	0.17
19990456	-21	1375-1A	13.75		shale	-28.2	425	1.74	33.78
19990438	-24	0-7	0	Martinia Shale, younger than 0-6	shale	-23.5	430±20	0.00	0.13
19990437	-25	0-6	0	Martinia Shale, younger than 0-3	siltstone	-23.3	>415	0.02	0.13
19990436	-29	0-3	0	Martinia Shale, younger than 0-2	shale	-22.7	430±20	0.01	0.11
19990435	-30	0-2	0	Martinia Shale, oldest sample in study	shale	-24.5	430±20	0.04	0.22

Table 4.S1: Total biomarker data from Kap Stosch, Greenland

		RockEval 2 analysis of Rock Powder				RockEval 6 analysis of Kerogen Concentrate						
Geochem #	relative depth	S3 (mg/g)	HI	OI	TOC (wt%)	TMAX (°C)	S1 (mg/g)	S2 (mg/g)	S3 (mg/g)	HI	OI	TOC (wt%)
19990454	88	0.00	57	0	0.21	422	2.83	3.98	0.44	209	23	1.9
19990449	34	0.15	46	43	0.35	421	1.80	3.79	1.10	152	44	2.5
19990448	29	0.11	28	26	0.43	430	2.07	14.17	2.05	267	39	5.3
19990453	28	0.00	61	0	0.23	417	2.05	2.68	1.03	168	64	1.6
19990447	26	0.20	65	65	0.31	424	4.46	8.30	1.24	259	39	3.2
19990452	25	0.00	53	0	0.15	413	0.53	0.54	0.61	90	102	0.6
19990446	19	0.17	33	38	0.45	419	1.33	5.29	2.74	171	88	3.1
19990444	18	0.23	58	27	0.85	426	1.95	15.72	2.52	349	56	4.5
19990445	14	0.12	43	23	0.53	423	2.00	8.59	1.47	286	49	3.0
19990443	9	0.04	68	13	0.31	429	3.63	10.93	0.90	342	28	3.2
19990442	6	0.20	71	23	0.87	430	3.34	29.31	2.79	425	40	6.9
19990441	3	0.37	84	28	1.32	427	4.54	48.82	4.74	436	42	11.2
19990451	1	0.42	53	68	0.62	426	2.46	16.49	1.94	383	45	4.3
19990450	0	0.19	42	79	0.24	396*	1.01	1.83	1.03	54	30	3.4
19990457	-3	2.10	296	43	4.94	429	7.55	109.65	12.55	367	42	29.9
19990440	-13	0.32	46	78	0.41	419*	0.63	1.36	3.09	28	63	4.9
19990439	-17	0.24	44	62	0.39	362	1.33	1.08	1.55	23	33	4.7
19990456	-21	3.54	434	46	7.78	426	12.91	197.55	25.63	436	57	45.3
19990438	-24	0.15	23	27	0.56	364	1.37	0.83	0.90	25	27	3.3
19990437	-25	0.32	72	178	0.18	415*	4.94	4.24	2.57	45	27	9.5
19990436	-29	0.22	18	36	0.61	412*	2.96	3.63	3.56	30	29	12.1
19990435	-30	0.38	32	56	0.68	414*	1.14	1.23	1.14	33	31	3.7

Table 4.S1: Total biomarker data from Kap Stosch, Greenland

								Tricyclics				
Geochem #	**relative depth**	**extracted rock (g)**	**TLE (mg)**	**sats**	**aros**	**Pr/ Ph**	**Hopane/ Sterane**	**C19/(Total Tricyclic)**	**C20/(Total Tricyclic)**	**C21/(Total Tricyclic)**	**C22/(Total Tricyclic)**	**C23/(Total Tricyclic)**
19990454	88	3.0103	0.9	0.2	0.0	0.562	3.470	0.032	0.248	0.281	0.052	0.235
19990449	34	3.0466	0.5	0.1	0.0	0.636	2.203	0.051	0.188	0.203	0.066	0.307
19990448	29	3.4975	0.6	0.1	0.1	0.545	0.973	0.084	0.255	0.218	0.046	0.200
19990453	28	3.0493	0.8	0.3	0.1	0.512	3.161	0.072	0.255	0.229	0.065	0.231
19990447	26	3.0096	0.8	0.2	0.1	0.674	1.410	0.057	0.176	0.197	0.064	0.306
19990452	25	2.0487	0.2	0.0	0.0	ND	ND	ND	ND	ND	ND	ND
19990446	19	3.1165	0.5	0.3	0.0	ND	1.122	0.045	0.138	0.151	0.052	0.324
19990444	18	3.0522	1.0	0.2	0.2	0.470	1.251	0.055	0.203	0.213	0.053	0.255
19990445	14	2.0176	0.8	0.0	0.0	0.838	0.741	0.059	0.208	0.232	0.059	0.252
19990443	9	3.3281	1.5	0.5	0.3	ND	1.483	0.043	0.171	0.178	0.060	0.319
19990442	6	3.1382	1.6	0.1	0.0	0.509	0.634	0.047	0.175	0.204	0.044	0.243
19990441	3	3.3753	2.7	0.4	0.3	0.455	0.661	0.044	0.166	0.198	0.025	0.225
19990451	1	3.3289	1.0	0.1	0.2	0.598	0.976	0.089	0.266	0.237	0.042	0.178
19990450	0	3.3742	0.5	0.1	0.0	0.724	0.669	0.020	0.089	0.169	0.075	0.351
19990457	-3	3.0216	9.6	1.4	0.5	1.221	0.319	0.032	0.215	0.222	0.031	0.286
19990440	-13	3.013	0.4	0.0	0.0	0.662	2.092	0.054	0.255	0.245	0.056	0.235
19990439	-17	2.5133	0.1	0.0	0.1	0.482	0.826	0.015	0.152	0.220	0.051	0.314
19990456	-21	1.5303	6.6	1.1	1.0	1.239	0.308	0.010	0.110	0.150	0.024	0.369
19990438	-24	2.0545	0.1	0.0	0.0	0.395	6.347	0.052	0.317	0.291	0.055	0.199
19990437	-25	1.0235	0.0	0.1	0.0	ND	1.000	0.025	0.145	0.190	0.060	0.330
19990436	-29	1.5399	0.6	0.4	0.3	0.958	2.642	0.024	0.187	0.274	0.057	0.285
19990435	-30	2.9999	0.2	0.1	1.2	0.503	1.805	0.021	0.150	0.213	0.059	0.327

Table 4.S1: Total biomarker data from Kap Stosch, Greenland

		Tricyclics			Steranes						
Geochem #	**relative depth**	**C24/(Total Tricyclic)**	**C25/(Total Tricyclic)**	**C26/(Total Tricyclic)**	**C25 S/R**	**C26 S/R**	**C19/C23**	**C22/C21**	**C24/C25**	**C26/C25**	**Tet/C23**
19990454	88	0.090	0.043	0.019	0.981	0.994	0.136	0.186	2.071	0.437	0.234
19990449	34	0.115	0.048	0.022	1.164	1.064	0.166	0.326	2.396	0.460	0.188
19990448	29	0.092	0.060	0.045	0.867	0.939	0.422	0.211	1.533	0.754	0.461
19990453	28	0.083	0.044	0.021	0.958	0.900	0.313	0.282	1.886	0.489	0.276
19990447	26	0.117	0.057	0.026	0.928	0.957	0.185	0.324	2.057	0.458	0.185
19990452	25	ND	ND	ND	ND	ND	ND	ND	ND	ND	ND
19990446	19	0.142	0.093	0.057	0.895	1.079	0.138	0.343	1.524	0.610	0.208
19990444	18	0.104	0.059	0.057	1.039	0.967	0.216	0.251	1.764	0.972	0.209
19990445	14	0.095	0.050	0.044	0.932	0.950	0.232	0.255	1.896	0.880	0.190
19990443	9	0.121	0.067	0.041	0.958	1.032	0.136	0.336	1.812	0.608	0.203
19990442	6	0.106	0.091	0.091	0.855	0.950	0.193	0.214	1.168	1.000	0.186
19990441	3	0.108	0.115	0.118	0.914	0.964	0.194	0.127	0.938	1.026	0.233
19990451	1	0.076	0.064	0.048	0.812	0.960	0.500	0.178	1.198	0.758	0.220
19990450	0	0.152	0.091	0.053	1.069	1.097	0.058	0.447	1.664	0.583	0.198
19990457	-3	0.075	0.085	0.054	0.939	1.003	0.111	0.140	0.880	0.640	0.491
19990440	-13	0.094	0.043	0.017	0.821	0.953	0.230	0.228	2.185	0.397	0.229
19990439	-17	0.140	0.074	0.033	0.894	0.951	0.049	0.231	1.902	0.453	0.170
19990456	-21	0.099	0.132	0.106	0.839	0.956	0.028	0.159	0.751	0.809	0.269
19990438	-24	0.061	0.019	0.006	0.874	1.036	0.262	0.190	3.205	0.298	0.130
19990437	-25	0.140	0.076	0.034	0.868	0.983	0.077	0.318	1.830	0.449	0.185
19990436	-29	0.112	0.043	0.019	0.689	0.786	0.085	0.207	2.607	0.452	0.158
19990435	-30	0.140	0.064	0.026	0.805	0.901	0.063	0.275	2.175	0.405	0.196

Table 4.S1: Total biomarker data from Kap Stosch, Greenland

		Steranes								
Geochem #	relative depth	C27 Dia/Reg	C27 Dia S/(S+R)	C27 Reg abb/aaa	C27 Reg aaa S/(S+R)	C27 Reg abb S/R	C28 Dia/Reg	C28 Dia S/(S+R)	C28 Reg abb/aaa	C28 Reg aaa S/(S+R)
19990454	88	0.591	0.625	0.590	0.453	0.993	0.756	0.622	0.769	0.404
19990449	34	0.469	0.627	0.139	0.316	0.915	0.482	0.607	0.368	0.099
19990448	29	0.360	0.608	0.178	0.319	0.751	0.585	0.604	0.407	0.153
19990453	28	0.937	0.651	0.417	0.468	1.022	0.975	0.604	0.677	0.288
19990447	26	0.460	0.633	0.158	0.287	0.669	0.477	0.609	0.475	0.123
19990452	25	ND	ND	ND	ND	ND	ND	ND	ND	ND
19990446	19	0.569	0.589	0.113	0.247	0.756	1.429	0.568	0.429	0.126
19990444	18	0.136	0.566	0.060	0.267	0.705	0.112	0.552	0.392	0.082
19990445	14	0.113	0.550	ND	0.225	ND	0.099	0.542	0.317	0.072
19990443	9	0.250	0.595	0.131	0.264	0.688	0.257	0.570	0.494	0.109
19990442	6	0.098	0.532	0.055	0.253	0.686	0.082	0.531	0.328	0.060
19990441	3	0.119	0.519	0.063	0.237	0.725	0.102	0.538	0.326	0.069
19990451	1	0.114	0.546	0.048	0.261	0.646	0.110	0.560	0.340	0.111
19990450	0	2.603	0.664	0.911	0.570	0.591	2.622	0.677	1.391	0.409
19990457	-3	0.352	0.575	0.094	0.313	0.670	0.422	0.554	0.296	0.190
19990440	-13	2.036	0.691	0.686	0.605	0.561	2.477	0.654	0.745	0.460
19990439	-17	1.696	0.623	0.425	0.448	0.937	0.952	0.669	0.651	0.372
19990456	-21	0.201	0.578	0.104	0.328	0.652	0.263	0.548	0.293	0.182
19990438	-24	1.913	0.644	0.306	0.417	1.259	1.470	0.630	1.350	0.382
19990437	-25	1.531	0.643	0.818	0.476	0.954	1.701	0.578	0.933	0.340
19990436	-29	1.282	0.555	0.636	0.634	0.583	2.203	0.624	2.141	1.000
19990435	-30	2.174	0.650	0.467	0.420	0.686	2.021	0.652	1.006	0.387

Table 4.S1: Total biomarker data from Kap Stosch, Greenland

		Steranes									
Geochem #	relative depth	C28 Reg abb S/R	C29 Dia/Reg	C29 Dia S/(S+R)	C29 Reg abb/aaa	C29 Reg aaa S/(S+R)	C29 Reg abb S/R	C27/total sterane	C28/total sterane	C29/total sterane	C30/total sterane
19990454	88	0.822	0.326	0.608	0.799	0.399	1.242	0.384	0.238	0.344	0.033
19990449	34	0.131	0.130	0.579	0.392	0.075	ND	0.342	0.210	0.428	0.020
19990448	29	0.261	0.304	0.593	0.353	0.113	ND	0.571	0.178	0.236	0.015
19990453	28	0.559	0.567	0.542	0.531	0.210	1.056	0.417	0.240	0.322	0.022
19990447	26	0.228	0.202	0.564	0.395	0.084	ND	0.380	0.229	0.367	0.024
19990452	25	ND	ND	ND	ND	ND	ND	ND	ND	ND	ND
19990446	19	0.182	0.834	0.568	0.305	0.087	7.893	0.339	0.225	0.403	0.032
19990444	18	0.129	0.104	0.526	0.345	0.078	ND	0.266	0.203	0.513	0.018
19990445	14	0.101	0.070	0.524	0.330	0.080	ND	0.274	0.234	0.469	0.023
19990443	9	0.265	0.149	0.585	0.371	0.114	4.804	0.334	0.238	0.402	0.026
19990442	6	0.102	0.069	0.525	0.327	0.087	ND	0.252	0.293	0.435	0.020
19990441	3	0.117	0.082	0.537	0.318	0.086	6.708	0.300	0.244	0.409	0.047
19990451	1	0.129	0.070	0.543	0.289	0.090	ND	0.310	0.170	0.482	0.038
19990450	0	0.595	1.623	0.704	1.275	0.388	2.531	0.516	0.268	0.201	0.015
19990457	-3	0.194	0.385	0.569	0.239	0.159	4.665	0.383	0.235	0.305	0.077
19990440	-13	0.756	0.967	0.606	0.663	0.341	2.339	0.495	0.230	0.258	0.017
19990439	-17	0.366	0.701	0.627	0.552	0.337	1.149	0.448	0.305	0.224	0.022
19990456	-21	0.193	0.179	0.554	0.274	0.185	7.805	0.395	0.220	0.316	0.069
19990438	-24	0.772	0.432	0.620	0.592	0.175	2.277	0.466	0.241	0.294	ND
19990437	-25	0.534	0.683	0.604	0.964	0.300	1.958	0.429	0.259	0.286	0.026
19990436	-29	1.366	0.655	0.672	0.586	0.305	0.974	0.450	0.291	0.259	ND
19990435	-30	0.551	0.996	0.635	0.738	0.296	2.249	0.502	0.265	0.225	0.008

Table 4.S1: Total biomarker data from Kap Stosch, Greenland

		Steranes		Hopanes						
Geochem #	relative depth	C27/C29 Sterane	C28/C29 Sterane	Ts/(Ts+Tm)	29,30-DNH/28,30-DNH	28,30-DNH/C30 hopane	29,30-DNH/C30 hopane	C29 Ts/ab	C29 ba/ab	C30 30-nor/ab
19990454	88	0.928	0.522	0.397	4.455	0.000	0.003	0.202	0.150	0.139
19990449	34	0.614	0.375	0.190	1.666	0.000	0.002	0.107	0.539	0.041
19990448	29	2.314	0.620	0.227	1.250	0.000	0.001	0.164	0.457	0.040
19990453	28	1.046	0.591	0.265	2.579	0.000	0.001	0.109	0.431	0.045
19990447	26	0.852	0.508	0.233	1.291	0.000	0.001	0.180	0.564	0.055
19990452	25	ND	ND	ND	ND	ND	ND	ND	ND	ND
19990446	19	0.984	0.422	0.229	2.036	0.000	0.001	0.164	0.510	0.034
19990444	18	0.504	0.394	0.144	0.390	0.003	0.005	0.237	0.715	0.025
19990445	14	0.563	0.487	0.156	1.484	0.001	0.004	0.171	0.652	0.025
19990443	9	0.763	0.541	0.375	2.474	0.000	0.002	0.227	0.241	0.033
19990442	6	0.564	0.664	0.227	0.805	0.003	0.012	0.361	0.567	0.018
19990441	3	0.708	0.586	0.260	1.151	0.001	0.004	0.376	0.524	0.015
19990451	1	0.618	0.340	0.198	2.257	0.001	0.006	0.178	0.533	0.040
19990450	0	1.870	0.967	0.541	ND	0.000	ND	0.354	0.126	0.061
19990457	-3	1.287	0.751	0.235	0.996	0.001	0.003	0.400	0.325	0.052
19990440	-13	1.245	0.504	0.304	2.082	0.000	0.001	0.148	0.308	0.109
19990439	-17	1.259	1.185	0.373	1.931	0.000	0.001	0.177	0.148	0.096
19990456	-21	1.226	0.649	0.258	0.989	0.001	0.003	0.375	0.363	0.049
19990438	-24	0.779	0.475	0.085	3.782	0.000	0.001	0.040	0.484	0.091
19990437	-25	0.998	0.566	0.521	2.075	0.000	0.001	0.304	0.129	0.161
19990436	-29	1.261	0.581	0.363	0.838	0.000	0.000	0.186	0.295	0.352
19990435	-30	1.400	0.775	0.339	0.635	0.000	0.001	0.042	0.271	0.098

Table 4.S1: Total biomarker data from Kap Stosch, Greenland

		Hopanes								
Geochem #	**relative depth**	**C30 ba/ab**	**C30 2-MHI**	**C30 3-MHI**	**C31 S/(S+R)**	**C32 S/(S+R)**	**C33 S/(S+R)**	**C34 S/(S+R)**	**C35 S/(S+R)**	**C29 ab/ C30 ab**
19990454	88	0.169	0.098	0.024	0.542	0.594	0.580	0.587	0.587	1.099
19990449	34	0.472	0.019	0.022	0.366	0.271	0.325	0.321	0.475	0.663
19990448	29	0.328	0.013	0.022	0.325	0.288	0.349	0.286	0.573	0.500
19990453	28	0.416	0.067	0.031	0.530	0.538	0.539	0.496	0.682	1.068
19990447	26	0.422	0.016	0.025	0.280	0.271	0.292	0.371	0.536	0.555
19990452	25	ND	ND	ND	ND	ND	ND	ND	ND	ND
19990446	19	0.356	0.017	0.022	0.276	0.206	0.329	0.451	ND	0.568
19990444	18	0.289	0.006	0.014	0.279	0.210	0.268	0.326	0.391	0.340
19990445	14	0.310	0.010	0.023	0.283	0.245	0.306	0.383	0.435	0.353
19990443	9	0.169	0.057	0.026	0.410	0.432	0.486	0.580	0.589	0.640
19990442	6	0.160	0.008	0.019	0.364	0.307	0.344	0.356	0.404	0.298
19990441	3	0.162	0.006	0.012	0.358	0.294	0.350	0.360	0.392	0.279
19990451	1	0.249	0.010	0.015	0.405	0.336	0.349	0.353	0.405	0.414
19990450	0	0.089	0.051	0.024	0.468	0.660	ND	ND	ND	1.235
19990457	-3	0.203	0.007	0.017	0.528	0.452	0.488	0.460	0.502	0.527
19990440	-13	0.344	0.038	0.064	0.549	0.492	0.620	0.622	0.672	1.356
19990439	-17	0.219	0.044	0.037	0.521	0.557	0.606	0.382	0.553	1.318
19990456	-21	0.149	0.006	0.021	0.520	0.468	0.507	0.507	0.467	0.659
19990438	-24	0.570	0.009	0.047	0.549	0.541	0.453	0.514	ND	1.523
19990437	-25	0.090	0.076	0.036	0.583	0.569	0.517	0.646	0.704	1.257
19990436	-29	0.246	0.109	0.088	0.588	0.584	0.549	ND	ND	1.567
19990435	-30	0.282	0.029	0.048	0.536	0.501	0.586	ND	ND	1.450

Table 4.S1: Total biomarker data from Kap Stosch, Greenland

		Hopanes								
Geochem #	relative depth	C29 ab/(Total ab Hopane)	C30 ab/(Total ab Hopane)	C31 ab/(Total ab Hopane)	C32 ab/(Total ab Hopane)	C33 ab/(Total ab Hopane)	C34 ab/(Total ab Hopane)	C35 ab/(Total ab Hopane)	C29/C30 hopane	C31/C30 hopane
19990454	88	0.294	0.268	0.201	0.098	0.063	0.038	0.038	1.136	0.260
19990449	34	0.265	0.400	0.255	0.052	0.018	0.007	0.003	0.721	0.264
19990448	29	0.229	0.458	0.221	0.060	0.020	0.008	0.004	0.593	0.231
19990453	28	0.367	0.344	0.167	0.064	0.029	0.015	0.014	1.125	0.151
19990447	26	0.228	0.411	0.256	0.066	0.022	0.010	0.007	0.656	0.294
19990452	25	ND	ND	ND	ND	ND	ND	ND	ND	ND
19990446	19	0.228	0.401	0.283	0.058	0.019	0.011		0.685	0.359
19990444	18	0.156	0.458	0.281	0.064	0.025	0.011	0.006	0.505	0.326
19990445	14	0.166	0.469	0.257	0.066	0.026	0.011	0.007	0.482	0.285
19990443	9	0.243	0.379	0.209	0.084	0.041	0.026	0.019	0.782	0.258
19990442	6	0.153	0.514	0.218	0.059	0.032	0.013	0.010	0.488	0.221
19990441	3	0.146	0.523	0.204	0.059	0.040	0.014	0.013	0.450	0.204
19990451	1	0.202	0.489	0.204	0.057	0.029	0.011	0.007	0.549	0.188
19990450	0	0.456	0.369	0.141	0.035	ND	ND	ND	1.589	0.164
19990457	-3	0.192	0.366	0.228	0.079	0.072	0.036	0.026	0.724	0.230
19990440	-13	0.421	0.311	0.165	0.057	0.026	0.013	0.006	1.359	0.163
19990439	-17	0.417	0.317	0.151	0.059	0.027	0.014	0.014	1.328	0.169
19990456	-21	0.230	0.349	0.196	0.081	0.079	0.036	0.029	0.957	0.217
19990438	-24	0.467	0.307	0.165	0.045	0.010	0.006	ND	1.397	0.145
19990437	-25	0.397	0.315	0.164	0.058	0.031	0.019	0.015	1.441	0.158
19990436	-29	0.402	0.256	0.208	0.075	0.059	ND	ND	1.452	0.199
19990435	-30	0.470	0.324	0.160	0.035	0.010	ND	ND	1.379	0.159

Table 4.S1: Total biomarker data from Kap Stosch, Greenland

				aromatic	extra compounds	
Geochem #	**relative depth**	**Gammacerane index**	**Oleneane/ C30 hopane**	**AI (mg/g TOC)**	**C33ACH/ C34nalk**	**cr/ph %**
19990454	88	0.153	ND	0.108	ND	1.571
19990449	34	0.079	0.007	0.117	ND	ND
19990448	29	0.207	0.022	0.017	ND	ND
19990453	28	0.138	0.038	0.051	ND	ND
19990447	26	0.174	0.032	0.035	ND	ND
19990452	25	ND	ND	ND	ND	ND
19990446	19	0.340	ND	0.023	ND	ND
19990444	18	0.411	ND	0.082	1.611	1.223
19990445	14	0.435	ND	0.027	0.232	1.251
19990443	9	0.363	0.026	0.022	ND	1.426
19990442	6	0.398	ND	0.035	1.223	ND
19990441	3	0.540	ND	0.071	5.830	1.049
19990451	1	0.289	ND	0.093	2.369	1.380
19990450	0	0.131	0.076	0.043	ND	ND
19990457	-3	0.271	ND	0.024	1.062	1.265
19990440	-13	0.191	ND	0.194	ND	ND
19990439	-17	0.366	ND	0.040	ND	ND
19990456	-21	0.458	ND	0.005	ND	ND
19990438	-24	0.176	ND	0.546	ND	1.518
19990437	-25	0.469	0.073	ND	ND	ND
19990436	-29	0.812	ND	ND	ND	ND
19990435	-30	0.127	0.046	0.123	ND	ND

Chapter 5

Biomarker Trends from the Great Bank of Guizhou, China

Abstract

The Great Bank of Guizhou in China is a carbonate platform deposited on the eastern margin of the Paleo-Tethys Ocean. A small number of samples from three different outcrop sections were measured from this platform. Although these samples were too few to conclusively discern trends throughout the section, biomarker proxies can create a snapshot of this environment, which points to conditions of photic zone euxinia. Biomarkers for thermal maturity of the organic material indicate that the sedimentary rocks from Guizhou have reached "oil window" maturity. Biomarkers indicative of redox conditions such as the 28,30 dinorhopane and the homohopane index were relatively high throughout the section, and aryl isoprenoids were measured in all samples, indicating prevalent anoxia and euxinia during deposition. The total hopane/sterane ratio and 2-methylhopane index were within the range considered normal for the Phanerozoic. The C_{27}/C_{29} sterane ratio and C_{28}/C_{29} sterane ratio are both somewhat high in this section, indicating a predominance of red algae over green algae and increased input from prasinophyte algae, respectively. Although this is a limited data set, the biomarkers measured from the Guizhou sections support the theory that conditions of photic zone euxinia existed during the deposition of these sedimentary rocks.

Location and Biostratigraphic Information

The Great Bank of Guizhou is a carbonate platform deposited on the margin of the South China block in the Nanpanjiang Basin. (See Figure 5.1.) It has been the subject of numerous detailed stratigraphic studies (Lehrmann et al. 1998; Lehrmann et al. 2003; Lehrmann et al. 2005), and the sedimentary rock package encompasses the Permian-Triassic boundary. During the late Permian period, the platform was formed when the southern margin of the Yangtze Platform was submerged. At this time a few topographic highs served as points for the nucleation of small reef mounds and open-marine skeletal packstones. As the platform evolved, the simple low-relief bank of cyanobacterial boundstones in the Early Triassic period gave way during the early Middle Triassic period to a higher-relief, reef-rimmed platform with tidal-flat deposits in the center. By the late Middle Triassic period, the platform had further evolved to an atoll-like morphology before it was ultimately drowned in the early Upper Triassic period (Lehrmann et al. 1998; Lehrmann et al. 2005).

At Guizhou, a faulted block exposes a cross-section of the platform and allows for almost continuous sampling of shallow- to deep-water facies through the interval. This section has been correlated to the Permian-Triassic boundary Global Stratotype Section and Point (GSSP) at Meishan using conodont biostratigraphy and carbon isotopes. The expression of the mass extinction at the two locations has been shown to be nearly synchronous (Payne et al. 2004; Chen et al. 2009). Carbon isotope ratios measured in carbonates from Guizhou from the late Permian period show evidence of a slight negative excursion at the end of the Wuchiapingian (Shao et al. 2000), similar to what is seen near the base of the Meishan core (Cao et al. 2009). The section at Guizhou is significantly thicker and spans more time than the GSSP at Meishan, especially the Triassic sedimentary rocks (Lehrmann et al. 2003; Lehrmann et al. 2005).

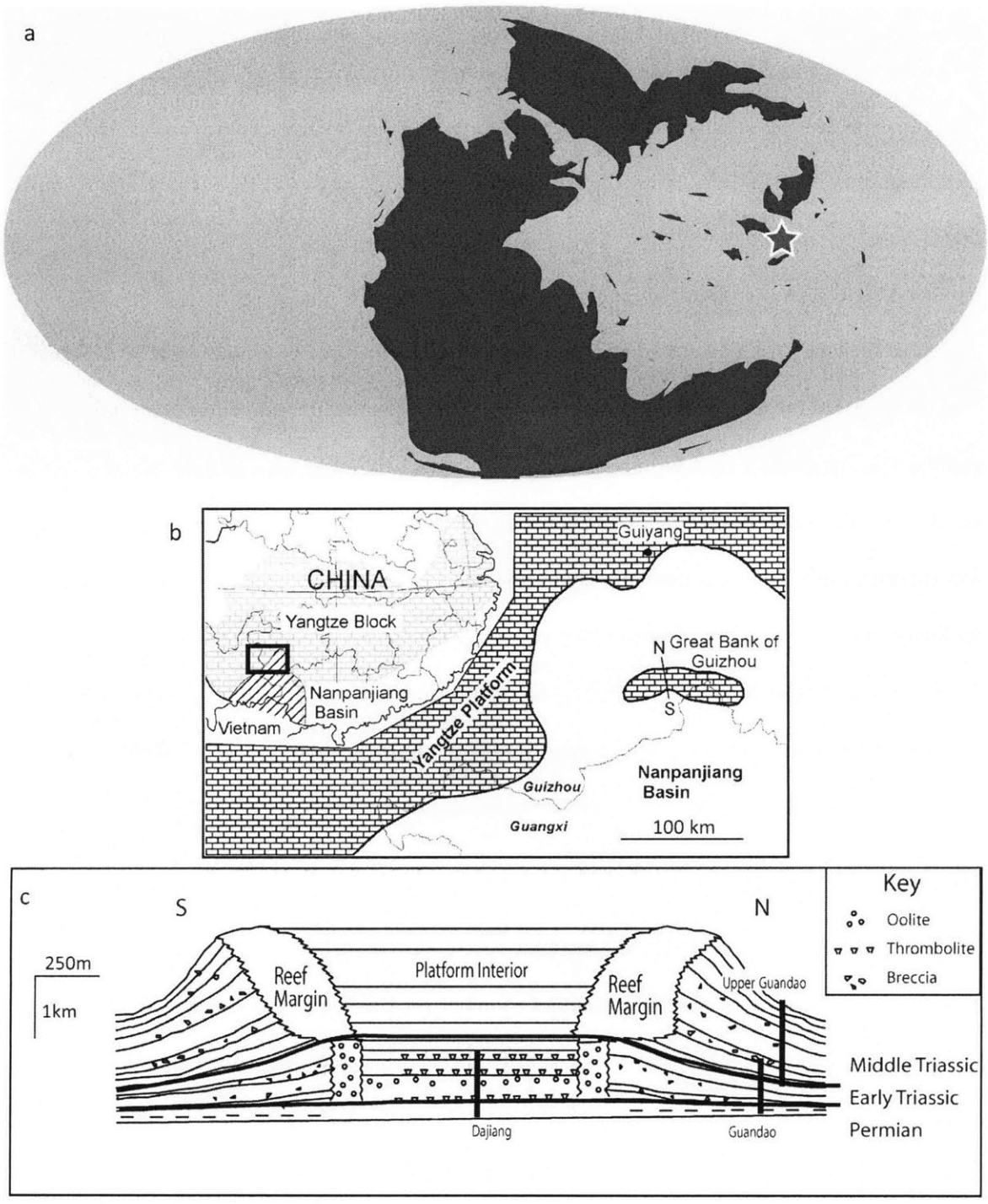

Figure 5.1 Locality of the Great Bank of Guizhou, China. (a) Global map from the Permian-Triassic boundary, with the depositional location of this section noted. Map modified from Scotese Paleomap Project website. (b) Map of early Triassic China block with location of Nanpanjiang basin outlined. (c) Cross-section of the Great Bank of Guizhou showing the locations of sections sampled for this study. (b) and (c) modified from Payne et al. 2004.

An erosion surface in the carbonate platform at, or immediately following, the Permian-Triassic boundary has been suggested to be an acid dissolution event (Chen et al. 2009; Collin et al. 2009). One theory is that this dissolution may be related to the buildup of atmospheric carbon dioxide stemming from ocean anoxia during the Late Permian period (Knoll et al. 1996; Payne and Kump 2007).

Although shallow water reef environments such as the Great Bank of Guizhou might be expected to have been spared the effects of deep-water anoxia during this time, the extinction event was particularly damaging for reef-forming metazoa and led to a complete restructuring of reef ecosystems (Pruss and Bottjer 2005). At Guizhou, the high-diversity Late Permian biota gave way to low-diversity Early Triassic skeletal packstone and reef mounds, which were primarily dominated by mollusks and showed little evidence of bioturbation (Lehrmann et al. 2001; Payne et al. 2006a). Even as the extinction affected the diversity of organisms, evidence of ostracod deposit feeders indicate well-oxygenated settings in Guizhou throughout its deposition (Forel et al. 2009).

Results and Discussion

A small selection of samples (~13) was available for biomarker analysis. Most of these originated from the Guandao section with the remainder coming from the Upper Guandao and Dajiang sections. (See Figure 5.1.) Samples were correlated between the sections using conodont occurrence, stratigraphic relationships and carbon isotopes (Payne et al. 2006b). The organic content of these samples was low, and not all had measurable quantities of every biomarker of interest. (See Table 5.1.) Therefore, it was difficult to use biomarkers to discern secular trends throughout the section. Instead, these samples provide a snapshot of general conditions during the

deposition of the Great Bank of Guizhou. (See Appendix 1 for uncertainties in biomarker measurements.)

Biomarkers proxies for thermal maturity

Many maturity-dependent biomarker ratios are affected by sediment lithology and can have different values in carbonates compared to shales with the same thermal history. Carbon skeleton rearrangement reactions, such as the conversion of trisnorhopane to trisnorneohopane (Tm to Ts), are catalyzed by Lewis acids and tend to be heavily influenced by contents of aluminosilicate clays. In the case of other parameters, the effects of isomerization can be obscured by the release of 'immature' bound compounds from kerogen as hydrocarbon generation takes place. With such a limited dataset, thermal maturity can only be estimated, and comparisons with biomarker proxies in other sections must take lithology into account. Nevertheless, the values for a range of parameters suggest that the Guizhou sedimentary rocks have just reached the threshold for petroleum generation.

The average 20S/(20S+20R) in the C_{27} steranes is 54%, and the average ratios of 22S/(22S+22R) in the C_{31} and C_{32} homohopanes are 52% and 54%, respectively, compared to values for oil-mature sedimentary rocks of ~60%. The Ts/(Ts+Tm) ratio, usually low in carbonates, is 0.524 in the Guizhou section, indicating mature organic matter. Finally, the C_{29} and C_{30} moretane/hopane ratios have averages of 8.8% and 8.7%, respectively. (See Table 5.1.) Although lithology and diagenetic processes can affect all of these biomarkers, the uniformity of the measurements throughout the section, which has a uniform lithology, is consistent with the Guizhou sedimentary rocks having reached "oil window" levels of maturity.

Biomarker proxies for redox conditions

For those samples from the Great Bank of Guizhou that could be measured, the average value of the homohopane index is 0.66. This is as high or higher than the value generally considered indicative of anoxic conditions in the sediments at the time of deposition. The ratio of 28,30 dinorhopane to C_{30} hopane was also relatively high with an average value of approximately 6.5% across the section (Seifert et al. 1978; Schoell et al. 1992). Although high values of the homohopane index have been associated with marine carbonate deposition under oxic conditions in previous studies (Connan et al. 1986; Mello et al. 1988), the moderately high values measured here at Guizhou are given added significance since they were deposited in shallow water settings and were measured with other biomarkers for anoxia.

Aryl isoprenoids with a 2,3,6 trimethyl substitution pattern were detected in every sample from the Great Bank of Guizhou, potentially indicates the presence of Chorobi, and therefore euxinic conditions that extended into the photic zone, as these sedimentary rocks were deposited. (See Table 5.1 and Figure 5.2.) The absence of the C_{40} carotenoids isorenieratane or chlorobactane, or $\delta^{13}C$ measurements, necessitates some caution in the identification of Chlorobi as the source of these compounds, though the presence of other biomarker proxies for anoxia supports the assumption that Chlorobi were present. The average total aryl isoprenoid content was ~12 mg/g total lipid extract throughout the section. In the Permian period, total aryl isoprenoid contents were slightly lower with an average of 10.8 mg/g total lipid extract. Average total aryl isoprenoid contents were higher in the Triassic sedimentary rocks with 12.4 mg/g total lipid extract. Although Chlorobi-derived biomarkers are commonly found in shales, the presence of aryl isoprenoids in shallow water marine carbonates suggests that ocean anoxia and sulfidic conditions were pervasive in shallow

sample	relative depth (Guandao base)	C_{35}/ C_{34}	28,30-DNH/ C_{30} hopane	AI ug/g TLE	hopane/ sterane	C_{30} 2-MHI	C_{30}/total sterane	C_{28}/C_{29} sterane	C_{27}/C_{29} sterane	C_{27} S/ (S+R)	C_{31} S/ (S+R)	C_{32} S/ (S+R)	Ts/ (Ts+Tm)	C_{29} ba/ab	C_{30} ba/ab
PUG-55	372.07			14.3											
PGD-221	282.38			5.5											
PGD-150	233.38			3.1											
PGD-110	163.48			9.8											
PGD-89	150.08			22.4											
PGD-76	118.83	0.51	0.06	20.5	0.83	0.03		1.00	1.28	0.50	0.51	0.54	0.55	0.093	0.073
PGD-84	114.03			12.3											
PDJ-200	77.59		0.06	2.9	1.06	0.03	0.016	1.00	1.41	0.45	0.56	0.54	0.57	0.088	0.094
PGD-35	70.73	0.69	0.09	19.6	0.78	0.06		0.89	1.97	0.57	0.54	0.57	0.57	0.096	0.076
PGD-29	61.33		0.02	7.1	1.40	0.03		0.76	0.85	0.52	0.56	0.58	0.48	0.100	0.096
PGD-11	46.53		0.05	17.8	0.72	0.03		1.11	2.10	0.58	0.49	0.54	0.54	0.057	0.072
PGD-5	4.3		0.11	8.6	0.73	0.08	0.014	0.78	1.45	0.58	0.51	0.52	0.53	0.087	0.100
PDJ-30	3.45	0.78	0.05	12.9	1.24	0.05		0.70	0.99	0.58	0.49	0.48	0.44	0.094	0.095

Table 5.1 Select biomarker data for the Great Bank of Guizhou. Biomarker samples are identified by the sample number within the individual section sampled. Depth is measured relative to the Guandao section. Biomarker proxies are grouped for redox sensitivity, microbial community and maturity.

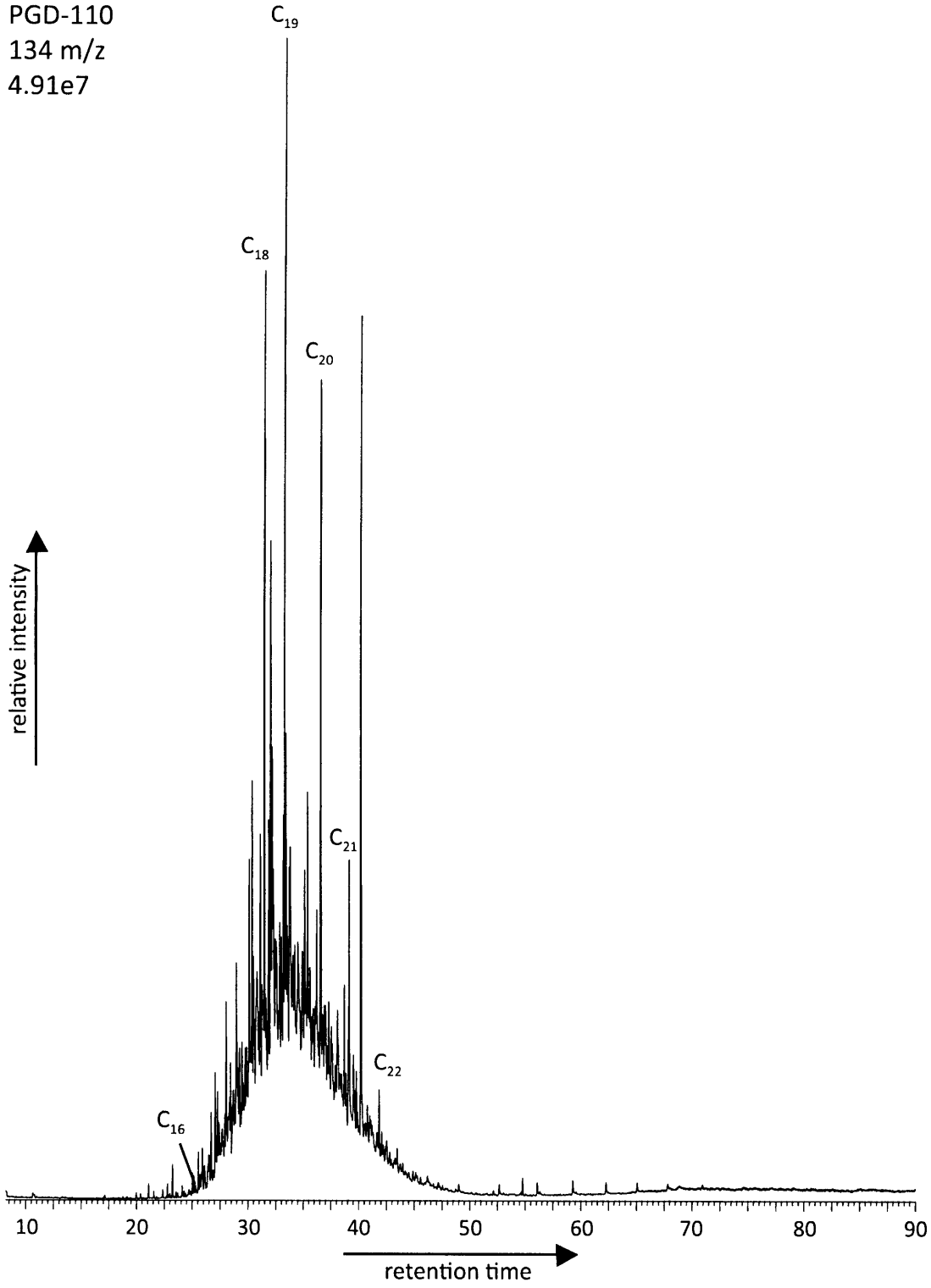

Figure 5.2 GC-MS select ion chromatogram of mass 134 from a sample aromatic hydrocarbon fraction from the Great Bank of Guizhou. Aryl isoprenoids from C_{16} to C_{22} have been identified.

environments during the late Permian period. The presence of marine fossils from organisms requiring oxygenated conditions, suggests that these conditions were intermittent, however.

Biomarkers for microbial community composition

Some biomarker ratios can be used to infer, in very general terms, the composition of the microbial community at the time of deposition. For example, the hopane/sterane ratio of ~1 throughout the section suggests balanced inputs from bacteria and eukaryotes. This value is considered typical for Phanerozoic sedimentary rocks and petroleum and is considerably lower than has been measured in other sections from the Permian-Triassic boundary. The 2-methylhopane index has average values of ~4.5%, which is typical for carbonate rocks in the Phanerozoic. The ratio of C_{27}/C_{29} sterane, a proxy for the ratio of red to green algal inputs to the sediments, was measured for a subset of samples from Guizhou, and had an average of ~1.5, which suggests a predominance of red algae. Red algae have a lower requirement for iron than green algae and might be expected to dominate input in marine environments with sulfidic deep waters, where the iron would be removed. The ratio of C_{28}/C_{29} steranes, a proxy for the input from prasinophyte algae, had a relatively high average value of 0.9 in this section. (See Table 5.1.) Studies of this parameter in a wide range of sedimentary rocks suggest that this value should be between 0.5 and 0.7 for this time period. However, this ratio has been observed to show short-lived increases corresponding to extinction events in the early Phanerozoic (Schwark and Empt 2006), and increased input from these microbes may be the explanation for the higher values observed here.

Summary

The biomarker data measured in the Great Bank of Guizhou represents a limited subset of the large

range of this carbonate section, and the samples had a low organic matter content. Nevertheless, the proxies give a general sense of the conditions that prevailed during deposition. Biomarker proxies such as the hopane/sterane ratio and 2-methylhopane index are generally within the values considered normal for the Phanerozoic, without any of the distinctly high values of these proxies that have been seen in other Permian-Triassic boundary sections worldwide. This may also be a reflection of the relatively sparse sampling density.

A carbonate reef is necessarily a shallow water environment, typically oxygenated and unfavorable for organic matter preservation. However, the biomarker proxies measured here, including a high C_{35}/C_{34} index and 28,30 bisnorhopane, indicate that anoxia was pervasive, if intermittent. Significantly, aryl isoprenoids were measured in all samples that were studied from the Guizhou section and indicate that photic zone euxinia was present throughout the deposition. Chlorobi-derived biomarkers are commonly found in well-laminated shales deposited beneath a stratified water column. Although the presence of these compounds has been reported for carbonate reef platforms (Bechtel et al. 2007; Marynowski et al. 2008), Chlorobi are generally rare in the typically oxic conditions of these environments. This suggests that the anoxia was regionally extensive but also present at all environments and at all depths in the water column, not only in the deep-water.

References

Bechtel, A., H. J. Gawlick, R. Gratzer, M. Tomaselli and W. Putmann (2007). "Molecular Indicators of Palaeosalinity and Depositional Environment of Small Scale Basins within Carbonate Platforms: The Late Triassic Hauptdolomite Wiestalstausee Section near Hallein (Northern Calcareous Alps, Austria)." Organic Geochemistry **38**(1): 92-111.

Cao, C., G. D. Love, L. E. Hays, W. Wang, S. Shen and R. E. Summons (2009). "Biogeochemical Evidence for Euxinic Oceans and Ecological Disturbance Presaging the End-Permian Mass Extinction Event." Earth and Planetary Science Letters **281**(3-4): 188-201.

Chen, J., T. W. Beatty, C. A. Henderson and H. Rowe (2009). "Conodont Biostratigraphy across the Permian-Triassic Boundary at the Dawen Section, Great Bank of Guizhou, Guizhou Province, South China: Implications for the Late Permian Extinction and Correlation with Meishan." Journal of Asian Earth Sciences **36**(6): 442-458.

Collin, P. Y., S. Kershaw, S. Crasquin-Soleau and Q. L. Feng (2009). "Facies Changes and Diagenetic Processes across the Permian-Triassic Boundary Event Horizon, Great Bank of Guizhou, South China: A Controversy of Erosion and Dissolution." Sedimentology **56**(3): 677-693.

Connan, J., J. Bouroullec, D. Dessort and P. Albrecht (1986). "The Microbial Input in Carbonate-Anhydrite Facies of a Sabkha Palaeoenvironment from Guatemala: A Molecular Approach." Organic Geochemistry **10**(1-3): 29-50.

Forel, M. B., S. Crasquin, S. Kershaw, Q. L. Feng and P. Y. Collin (2009). "Ostracods (Crustacea) and Water Oxygenation in the Earliest Triassic of South China: Implications for Oceanic Events at the End-Permian Mass Extinction." Australian Journal of Earth Sciences **56**(6): 815-823.

Knoll, A. H., R. K. Bambach, D. E. Canfield and J. P. Grotzinger (1996). "Comparative Earth History and Late Permian Mass Extinction." Science **273**: 452-457.

Lehrmann, D., P. Enos, J. Payne, P. Montgomery, J. Wei, Y. Yu, J. Xiao and M. J. Orchard (2005). "Permian and Triassic Depositional History of the Yangtze Platform and Great Bank of Guizhou in the Nanpanjiang Basin of Guizhou and Guangxi, South China." Albertiana **33**: 149-168.

Lehrmann, D. J., J. L. Payne, S. V. Felix, P. M. Dillett, H. Wang, Y. Y. Yu and J. Y. Wei (2003). "Permian-Triassic Boundary Sections from Shallow-Marine Carbonate Platforms of the Nanpanjiang Basin, South China: Implications for Oceanic Conditions Associated with the End-Permian Extinction and Its Aftermath." PALAIOS **18**(2): 138-152.

Lehrmann, D. J., Y. Wan, J. Y. Wei, Y. Y. Yu and J. F. Xiao (2001). "Lower Triassic Peritidal Cyclic Limestone: An Example of Anachronistic Carbonate Facies from the Great Bank of Guizhou, Nanpanjiang Basin, Guizhou Province, South China." Palaeogeography Palaeoclimatology Palaeoecology **173**(3-4): 103-123.

Lehrmann, D. J., Wei Jiayong and P. Enos (1998). "Controls on Facies Architecture of a Large Triassic Carbonate Platform; the Great Bank of Guizhou, Nanpanjiang Basin, South China." Journal of Sedimentary Research **68**(2): 311-326.

Marynowski, L., P. Filipiak and A. Pisarzowska (2008). "Organic Geochemistry and Palynofacies of the Early-Middle Frasnian Transition (Late Devonian) of the Holy Cross Mountains, Southern Poland." Palaeogeography Palaeoclimatology Palaeoecology **269**(3-4): 152-165.

Mello, M. R., N. Telnaes, P. C. Gaglianone, M. I. Chicarelli, S. C. Brassell and J. R. Maxwell (1988). "Organic Geochemical Characterisation of Depositional Palaeoenvironments of Source Rocks and Oils in Brazilian Marginal Basins." Organic Geochemistry **13**(1-3): 31-45.

Payne, J. L., D. J. Lehrmann, J. Wei and A. H. Knoll (2006a). "The Pattern and Timing of Biotic Recovery from the End-Permian Extinction on the Great Bank of Guizhou, Guizhou Province, China." PALAIOS **21**(1): 63-85.

Payne, J. L. and L. R. Kump (2007). "Evidence for Recurrent Early Triassic Massive Volcanism from Quantitative Interpretation of Carbon Isotope Fluctuations." Earth and Planetary Science Letters **256**(1-2): 264-277.

Payne, J. L., D. J. Lehrmann, S. Christensen, J. Y. Wei and A. H. Knoll (2006b). "Environmental and Biological Controls on the Initiation and Growth of a Middle Triassic (Anisian) Reef Complex on the Great Bank of Guizhou, Guizhou Province, China." PALAIOS **21**(4): 325-343.

Payne, J. L., D. J. Lehrmann, J. Wei, M. J. Orchard, D. P. Schrag and A. H. Knoll (2004). "Large Perturbations of the Carbon Cycle During Recovery from the End-Permian Extinction." Science **305**(5683): 506-509.

Pruss, S. B. and D. J. Bottjer (2005). "The Reorganization of Reef Communities Following the End-Permian Mass Extinction." Comptes Rendus Palevol **4**(6-7): 553-568.

Schoell, M., M. A. McCaffrey, F. J. Fago and J. M. Moldowan (1992). "Carbon Isotopic Compositions of 28,30-Bisnorhopanes and Other Biological Markers in a Monterey Crude Oil." Geochim. Cosmochim. Acta **56**(3): 1391-1399.

Schwark, L. and P. Empt (2006). "Sterane Biomarkers as Indicators of Palaeozoic Algal Evolution and Extinction Events." Palaeogeography, Palaeoclimatology, Palaeoecology **240**(1-2): 225-236.

Seifert, W. K., J. M. Moldowan, G. W. Smith and E. V. Whitehead (1978). "First Proof of Structure of a C_{28}-Pentacyclic Triterpane in Petroleum." Nature **271**(5644): 436-437.

Shao, L. Y., P. F. Zhang, J. W. Dou and S. Z. Shen (2000). "Carbon Isotope Compositions of the Late Permian Carbonate Rocks in Southern China: Their Variations between the Wujiaping and Changxing Formations." Palaeogeography Palaeoclimatology Palaeoecology **161**(1-2): 179-192.

Table 5.S1: Total biomarker data from the Great Bank of Guizhou, China

					Tricyclics						
Sample	**relative depth**	**TLE (mg)**	**extracted rock (g)**	**Hopane/ Sterane**	**C19/(Total Tricyclic)**	**C20/(Total Tricyclic)**	**C21/(Total Tricyclic)**	**C22/(Total Tricyclic)**	**C23/(Total Tricyclic)**	**C24/(Total Tricyclic)**	**C25/(Total Tricyclic)**
PUG-55 (N)	372.07	0.5	24.8931	ND	ND	0.112	0.373	0.043	0.371	0.101	ND
PGD-221 (M)	282.38	1	30.5341	ND	0.025	0.256	0.371	0.028	0.253	0.068	ND
PGD-150 (L)	233.38	0.6	28.5571	ND	ND	0.101	0.232	0.038	0.484	0.146	ND
PGD-110 (J)	163.48	0.4	17.3505	ND	ND	0.122	0.326	0.033	0.423	0.097	ND
PGD-89 (I)	150.08	0.2	21.9274	ND	ND	0.113	0.261	ND	0.488	0.138	ND
PGD-76(H)	118.83	0.1	13.8104	0.834	0.012	0.056	0.141	0.050	0.401	0.204	0.135
PGD-84 (K)	114.03	0.3	17.4679	ND	ND	0.212	0.428	ND	0.360	ND	ND
PDJ-200 (G)	77.59	0.1	22.1352	1.064	ND	0.031	0.110	0.039	0.391	0.217	0.211
PGD-35 (F)	70.73	0.1	20.9163	0.779	0.018	0.064	0.138	0.056	0.406	0.203	0.115
PGD-29 (C)	61.33	0.3	17.1363	1.395	0.020	0.081	0.175	0.048	0.351	0.186	0.138
PGD-11 (E)	46.53	0.2	17.2721	0.715	0.025	0.073	0.152	0.055	0.384	0.197	0.115
PGD-5 (B)	4.3	0.2	21.7201	0.726	0.023	0.091	0.232	0.069	0.366	0.148	0.071
PDJ-30 (A)	3.45	0.1	18.0626	1.242	ND	0.025	0.120	0.047	0.405	0.229	0.173

Table 5.S1: Total biomarker data from the Great Bank of Guizhou, China

		Tricyclics				Steranes						
Sample	**relative depth**	**C25 S/R**	**C19/C23**	**C22/C21**	**C24/C25**	**C27 Dia/Reg**	**C27 Dia S/R**	**C27 Reg abb/aaa**	**C27 Reg aaa S/(S+R)**	**C27 Reg abb S/R**	**C28 Dia/Reg**	**C28 Dia S/R**
PUG-55 (N)	372.07	ND	ND	0.115	ND	ND	ND	ND	ND	ND	ND	ND
PGD-221 (M)	282.38	ND	0.098	0.075	ND	ND	ND	ND	ND	ND	ND	ND
PGD-150 (L)	233.38	ND	ND	0.162	ND	ND	ND	ND	ND	ND	ND	ND
PGD-110 (J)	163.48	ND	ND	0.101	ND	ND	ND	ND	ND	ND	ND	ND
PGD-89 (I)	150.08	ND	ND	ND	ND	ND	ND	ND	ND	ND	ND	ND
PGD-76(H)	118.83	0.925	0.031	0.354	1.517	0.872	1.787	0.694	0.500	1.189	0.633	1.284
PGD-84 (K)	114.03	ND	ND	ND	ND	ND	ND	ND	ND	ND	ND	ND
PDJ-200 (G)	77.59	0.826	ND	0.357	1.029	0.526	1.665	0.685	0.452	0.921	0.507	1.074
PGD-35 (F)	70.73	0.952	0.044	0.408	1.762	1.442	1.877	1.094	0.568	0.704	1.608	1.253
PGD-29 (C)	61.33	0.873	0.057	0.275	1.347	0.540	1.886	0.614	0.505	1.137	0.458	1.265
PGD-11 (E)	46.53	0.971	0.064	0.364	1.715	1.055	1.885	0.891	0.576	0.938	0.905	1.407
PGD-5 (B)	4.3	0.983	0.063	0.297	2.069	1.385	1.695	1.023	0.576	0.830	1.576	1.349
PDJ-30 (A)	3.45	0.877	ND	0.396	1.324	1.644	1.748	1.124	0.578	0.735	1.235	1.871

Table 5.S1: Total biomarker data from the Great Bank of Guizhou, China

		Steranes										
Sample	**relative depth**	**C28 Reg abb/aaa**	**C28 Reg aaa S/R**	**C28 Reg abb S/R**	**C29 Dia/Reg**	**C29 Dia S/R**	**C29 Reg abb/aaa**	**C29 Reg aaa S/R**	**C29 Reg abb S/R**	**C27/total sterane**	**C28/total sterane**	**C29/total sterane**
PUG-55 (N)	372.07	ND	ND	ND	ND	ND	ND	ND	ND	ND	ND	ND
PGD-221 (M)	282.38	ND	ND	ND	ND	ND	ND	ND	ND	ND	ND	ND
PGD-150 (L)	233.38	ND	ND	ND	ND	ND	ND	ND	ND	ND	ND	ND
PGD-110 (J)	163.48	ND	ND	ND	ND	ND	ND	ND	ND	ND	ND	ND
PGD-89 (I)	150.08	ND	ND	ND	ND	ND	ND	ND	ND	ND	ND	ND
PGD-76(H)	118.83	1.320	0.930	0.959	0.516	0.786	0.892	0.495	1.804	0.432	0.295	0.273
PGD-84 (K)	114.03	ND	ND	ND	ND	ND	ND	ND	ND	ND	ND	ND
PDJ-200 (G)	77.59	1.123	0.645	0.757	0.377	0.722	0.903	0.404	2.873	0.420	0.295	0.268
PGD-35 (F)	70.73	1.620	0.695	0.769	0.990	1.505	1.300	0.582	1.631	0.527	0.255	0.218
PGD-29 (C)	61.33	1.204	0.962	0.864	0.320	0.765	0.856	0.509	1.918	0.350	0.297	0.353
PGD-11 (E)	46.53	1.530	0.742	0.843	0.852	0.915	0.998	0.539	1.779	0.520	0.256	0.224
PGD-5 (B)	4.3	1.458	1.006	0.737	0.921	1.143	1.324	0.561	1.784	0.461	0.269	0.256
PDJ-30 (A)	3.45	2.203	0.933	1.068	0.676	1.572	1.602	0.387	1.657	0.445	0.268	0.287

Table 5.S1: Total biomarker data from the Great Bank of Guizhou, China

		Steranes			Hopanes							
Sample	relative depth	C30/total sterane	C27/C29 sterane	C28/C29 sterane	Ts/ (Ts+Tm)	29,30-DNH/28,30-DNH	28,30-DNH/C30 hopane	29,30-DNH/C30 hopane	C29 Ts/ab	C29 ba/ab	C30 30-nor/ab	C30 ba/ab
PUG-55 (N)	372.07	ND	ND	ND	ND	ND	ND	ND	ND	ND	ND	ND
PGD-221 (M)	282.38	ND	ND	ND	ND	ND	ND	ND	ND	ND	ND	ND
PGD-150 (L)	233.38	ND	ND	ND	ND	ND	ND	ND	ND	ND	ND	ND
PGD-110 (J)	163.48	ND	ND	ND	ND	ND	ND	ND	ND	ND	ND	ND
PGD-89 (I)	150.08	ND	ND	ND	ND	ND	ND	ND	ND	ND	ND	ND
PGD-76(H)	118.83	0.000	1.280	1.003	0.547	0.865	0.057	0.050	0.373	0.093	0.115	0.073
PGD-84 (K)	114.03	ND	ND	ND	ND	ND	ND	ND	ND	ND	ND	ND
PDJ-200 (G)	77.59	0.016	1.412	1.005	0.568	0.641	0.061	0.039	0.558	0.088	0.158	0.094
PGD-35 (F)	70.73	0.000	1.968	0.894	0.566	1.401	0.094	0.132	0.456	0.096	0.200	0.076
PGD-29 (C)	61.33	0.000	0.849	0.760	0.483	2.111	0.019	0.040	0.494	0.100	0.223	0.096
PGD-11 (E)	46.53	0.000	2.096	1.113	0.539	1.133	0.053	0.060	0.451	0.057	0.196	0.072
PGD-5 (B)	4.3	0.014	1.448	0.782	0.529	0.879	0.114	0.100	0.350	0.087	0.348	0.100
PDJ-30 (A)	3.45	0.000	0.985	0.700	0.436	1.512	0.050	0.076	0.498	0.094	0.384	0.095

Table 5.S1: Total biomarker data from the Great Bank of Guizhou, China

		Hopanes										
Sample	relative depth	C30 2-MHI	C30 3-MHI	C31 S/(S+R)	C32 S/(S+R)	C33 S/R	C34 S/R	C35 S/R	C29 ab/ C30 ab	C29 ab/ (Total ab Hopane)	C30 ab/ (Total ab Hopane)	C31 ab/ (Total ab Hopane)
PUG-55 (N)	372.07	ND	ND	ND	ND	ND	ND	ND	ND	ND	ND	ND
PGD-221 (M)	282.38	ND	ND	ND	ND	ND	ND	ND	ND	ND	ND	ND
PGD-150 (L)	233.38	ND	ND	ND	ND	ND	ND	ND	ND	ND	ND	ND
PGD-110 (J)	163.48	ND	ND	ND	ND	ND	ND	ND	ND	ND	ND	ND
PGD-89 (I)	150.08	ND	ND	ND	ND	ND	ND	ND	ND	ND	ND	ND
PGD-76(H)	118.83	0.026	0.015	0.505	0.543	2.115	1.322	1.542	0.712	0.333	0.468	0.129
PGD-84 (K)	114.03	ND	ND	ND	ND	ND	ND	ND	ND	ND	ND	ND
PDJ-200 (G)	77.59	0.027	0.022	0.561	0.535	1.403	1.200	ND	0.618	0.289	0.467	0.155
PGD-35 (F)	70.73	0.060	0.043	0.543	0.567	1.604	1.628	1.469	0.859	0.305	0.355	0.193
PGD-29 (C)	61.33	0.033	0.018	0.560	0.581	1.175	1.057	ND	0.594	0.279	0.470	0.146
PGD-11 (E)	46.53	0.034	0.016	0.485	0.540	1.690	ND	ND	0.717	0.305	0.425	0.151
PGD-5 (B)	4.3	0.083	0.038	0.511	0.520	0.883	1.581	ND	1.080	0.370	0.342	0.150
PDJ-30 (A)	3.45	0.052	0.044	0.493	0.484	1.158	1.690	1.508	0.853	0.246	0.288	0.232

Table 5.S1: Total biomarker data from the Great Bank of Guizhou, China

		Hopanes								aromatics
Sample	relative depth	C32 ab/ (Total ab Hopane)	C33 ab/ (Total ab Hopane)	C34 ab/ (Total ab Hopane)	C35 ab/ (Total ab Hopane)	C35/C34	C29/C30 hopane	C31/C30 hopane	Gammacerane index	total AI ug/g TLE
PUG-55 (N)	372.07	ND	ND	ND	ND	ND	ND	ND	ND	14.283
PGD-221 (M)	282.38	ND	ND	ND	ND	ND	ND	ND	ND	5.547
PGD-150 (L)	233.38	ND	ND	ND	ND	ND	ND	ND	ND	3.060
PGD-110 (J)	163.48	ND	ND	ND	ND	ND	ND	ND	ND	9.782
PGD-89 (I)	150.08	ND	ND	ND	ND	ND	ND	ND	ND	22.372
PGD-76(H)	118.83	0.048	0.014	0.004	0.002	0.510	0.878	0.137	0.895	20.461
PGD-84 (K)	114.03	ND	ND	ND	ND	ND	ND	ND	ND	12.258
PDJ-200 (G)	77.59	0.054	0.023	0.011	ND	ND	0.812	0.146	1.125	2.866
PGD-35 (F)	70.73	0.084	0.031	0.018	0.013	0.686	1.045	0.249	1.189	19.546
PGD-29 (C)	61.33	0.061	0.029	0.015	ND	ND	0.718	0.137	0.858	7.072
PGD-11 (E)	46.53	0.085	0.034	ND	ND	ND	0.853	0.183	0.898	17.841
PGD-5 (B)	4.3	0.082	0.037	0.020	ND	ND	1.072	0.214	0.670	8.642
PDJ-30 (A)	3.45	0.146	0.047	0.023	0.018	0.778	0.918	0.663	1.015	12.941

Chapter 6

Biomarker and Isotopic Trends from Meishan, China

Abstract

The Late Permian sedimentary section at Meishan, in south China, includes the type section for the Permian-Triassic boundary. A broad array of biomarker proxies were analyzed from the Meishan outcrop and recently drilled core and reported in an earlier study, Cao et al. 2009; a subset of these are discussed here. Carotenoid derivatives from Chlorobi, such as 2,3,6 aryl isoprenoids, isorenieratane and crocetane, were quantified and peaks their abundances identified, including one centered at the Permian-Triassic boundary. The carbon isotopic compositions of *n*-C_{17} and *n*-C_{18} and the isoprenoids, pristane and phytane, were also measured enabling an evaluation of trends in the difference between the $\delta^{13}C$ values of these groups denoted by the parameter $\Delta\delta$. In Meishan, values of this proxy were overwhelmingly positive, considered anomalous isotopic ordering. Two intervals of more negative values were identified and these were negatively correlated to isorenieratane contents and the homohopane index. Trace amounts of carotenoid derivatives from anoxygenic phototrophic bacteria other than Chlorobi were also identified from samples with negative $\Delta\delta$ values. Together, the carotenoid derivatives and the pattern of $\Delta\delta$ suggest that at Meishan during the Permian-Triassic transition long-term pervasive oceanic anoxic conditions were punctuated by periods of chemocline upward excursions in which anoxygenic phototrophs had increased inputs into the sediments.

Locality and biostratigraphic information

The Global Stratotype Section and Point (GSSP) in Meishan, China, is the Permian-Triassic boundary section that best documents one of the most significant events in the history of life (Yin et al. 2001). (See Figure 6.1.) Even before it was proposed as the GSSP (Yin et al. 1996), the Meishan section was the subject of detailed geochemical and palynological studies (Shu and Utting 1990; Xu and Yan 1993), and these studies continued apace after the determination (Mei et al. 1998; Jin et al. 2000; Cao et al. 2002; Kaiho et al. 2006; Cao et al. 2009). Continuous deposition through the section, along with the presence of index fossils and a number of ash beds that could be precisely dated using the U/Pb isotope system (Mundil et al. 2004) solidified the Meishan section as a particularly good choice for the base-Triassic GSSP. Initially thought to have originated from Siberian Traps volcanism, recent studies have linked the critically important series of zircon-rich ash beds within the Meishan section to the more local Emeishan volcanism (Lo et al. 2002).

The section sampled in the early studies was collected from outcrop. This section allowed for the identification of a significant excursion of -6‰ in the carbon isotopic composition of carbonate as well as unique conodont zones present throughout. The conodont, *Hindeodus parvus*, which serves as the index fossil that defines the beginning of the Triassic period, was identified in bed 27c of the Meishan section (Yin et al. 1996). Unfortunately, the outcrop section has undergone significant weathering since its exposure. While samples collected from outcrop are usually sufficient for stratigraphic work and some geochemical measurements, weathering can complicate accurate measurements of organic geochemical proxies. As a result of these factors, a drilling project into the section was conducted so as to enable a more complete and unaltered sample set to be collected and

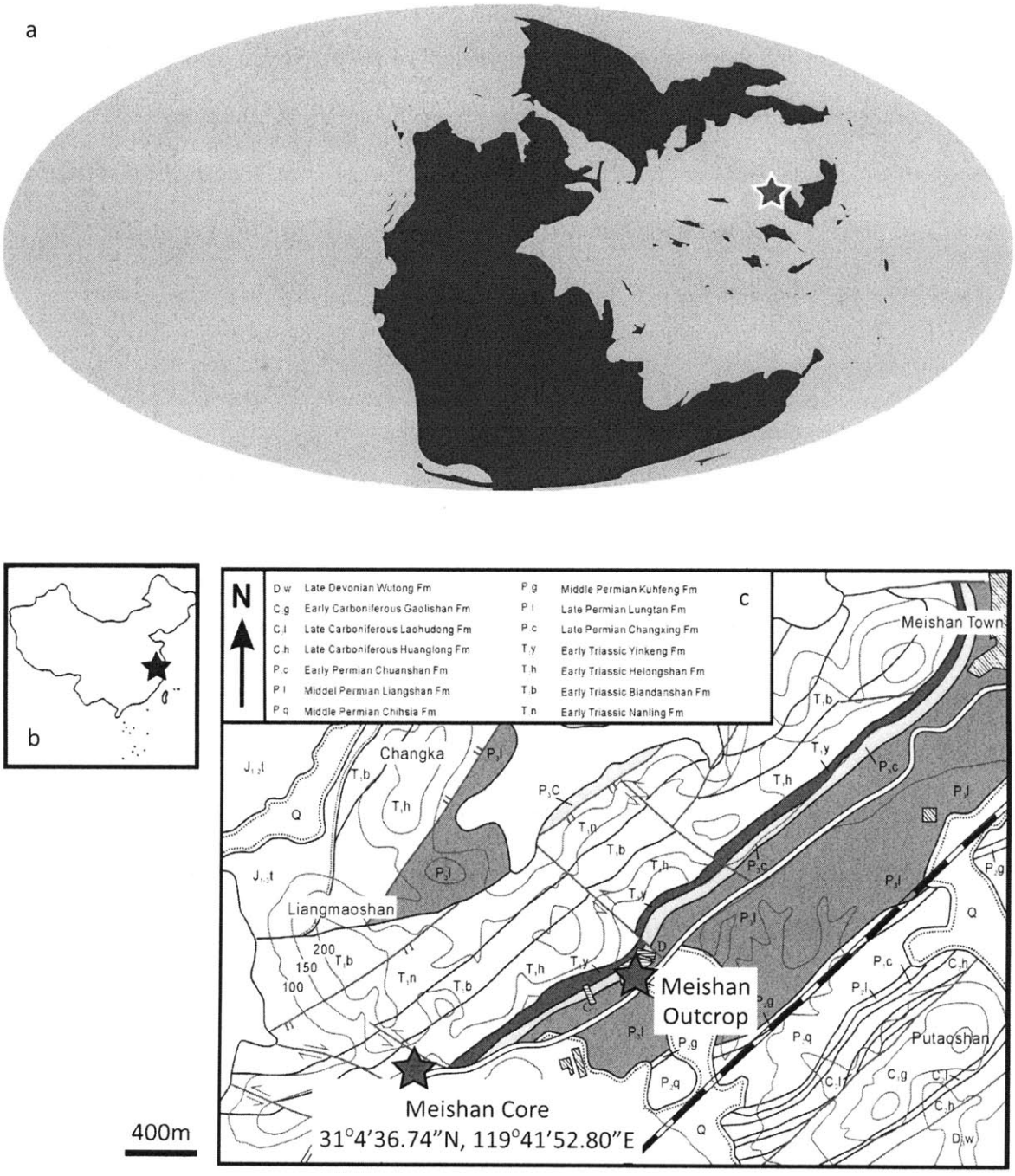

Figure 6.1 Locality of the Meishan, China section. (a) Global map from the Permian-Triassic boundary, with the depositional location of this section noted. Map modified from Scotese Paleomap Project website. (b) Map of modern China with relative location of Meishan section noted. (c) Detailed geological map showing the Meishan Core and Outcrop sections sampled for this study. (b) and (c) modified from Cao et al. 2009.

analyzed. As part of the project, which was proposed by the late Professor Jin Yugan of the Nanjing Institute of Geology and Paleontology, two cores were drilled in 2005 from a site a few kilometers to the west of the original outcrop. These cores sampled a portion of the Wuchiapingian and the entire Changhsingian, the final stages of the Permian period, as well as the entire Induan, the first stage of the Triassic period (Cao et al. 2009). Data from a combination of samples from the drill core and outcrop are presented in this thesis.

Results and Discussion

Cao et al. 2009 - EPSL

In core samples from Meishan, high-density sampling for $\delta^{13}C$ of carbonate identified a single significant negative excursion in this section between Beds 24e and 25, just below the "boundary ash clay." The $\delta^{13}C$ of organic carbon reaches its minimum at the top of Bed 26. That these signals do not co-vary is one indication that the carbon cycle was not in a steady state during this interval. This offset in excursions may instead be a result of mixing from a number of carbon sources with different $\delta^{13}C$ values, such as that between marine and weathered terrestrial components (Foster et al. 1997; Cao et al. 2002). Other observed features such as an overall drift to more negative values and significant bed-to-bed variation may also be consistent with this mixing.

Although biomarkers that reveal a combination of maturity, lithology and source were reported to be among the most enigmatic within the Meishan core section, the isomerization ratio for the C_{31} homohopanes and C_{27} steranes suggest that the sedimentary rocks deposited in the Meishan section are within the early stages of the oil window. A "moretane anomaly" beginning at the boundary and continuing through the earliest Triassic was observed hydrocarbon samples from Meishan and

attributed to increased terrestrial inputs (Tsuzuki et al. 2001; Xie et al. 2007). However, the identification of an elevation in the βα-isomers in the complete range of the hopane series indicates that this "anomaly" is, instead, a result of diagenetic conditions preferential to the formation and preservation of this stereoisomer of the hopanoid molecule. (See Appendix 1 for uncertainties in biomarker measurements.)

Biomarker evidence for redox conditions in the Meishan section, such as the pristane/phytane ratio, the homohopane index and the 28,30-bisnorhopane index, suggest that anoxic-reducing conditions persisted throughout the section, supporting hypotheses for a long-term "superanoxic event" previously described in Permian-Triassic boundary global oceans (Isozaki 1995; Isozaki 1997). For further information on the Meishan locality and the biomarker proxies measured there, see the full text of Cao et al. 2009, Appendix 3.

Biomarkers for Chlorobi

Carotenoid-derived biomarkers, isorenieratane and a suite of 2,3,6 aryl isoprenoids (C_{14} to C_{27}), were identified in all samples from the Meishan section. (See Figure 6.2.) Since Chlorobi are obligate phototrophs with a requirement of sulfide as an electron donor (Summons and Powell 1987; Imhoff 2003; Bryant and Frigaard 2006), the presence of these compounds indicate that conditions of photic zone euxinia were present during the deposition of these samples. Although the aryl isoprenoid contents were very low in the samples from the Late Permian Wuchiapingian stage and Early Triassic Dienerian stage, values initially begin to rise in the Changhsignian, and peaks are seen through the early Griesbachian. (See Figure 6.3.) A similar pattern is seen in isorenieratane contents, with low concentrations found in Wuchiapingian, Dienerian and Griesbachian sedimentary rocks and higher values throughout the Changhsingian. Two major intervals of increased aryl

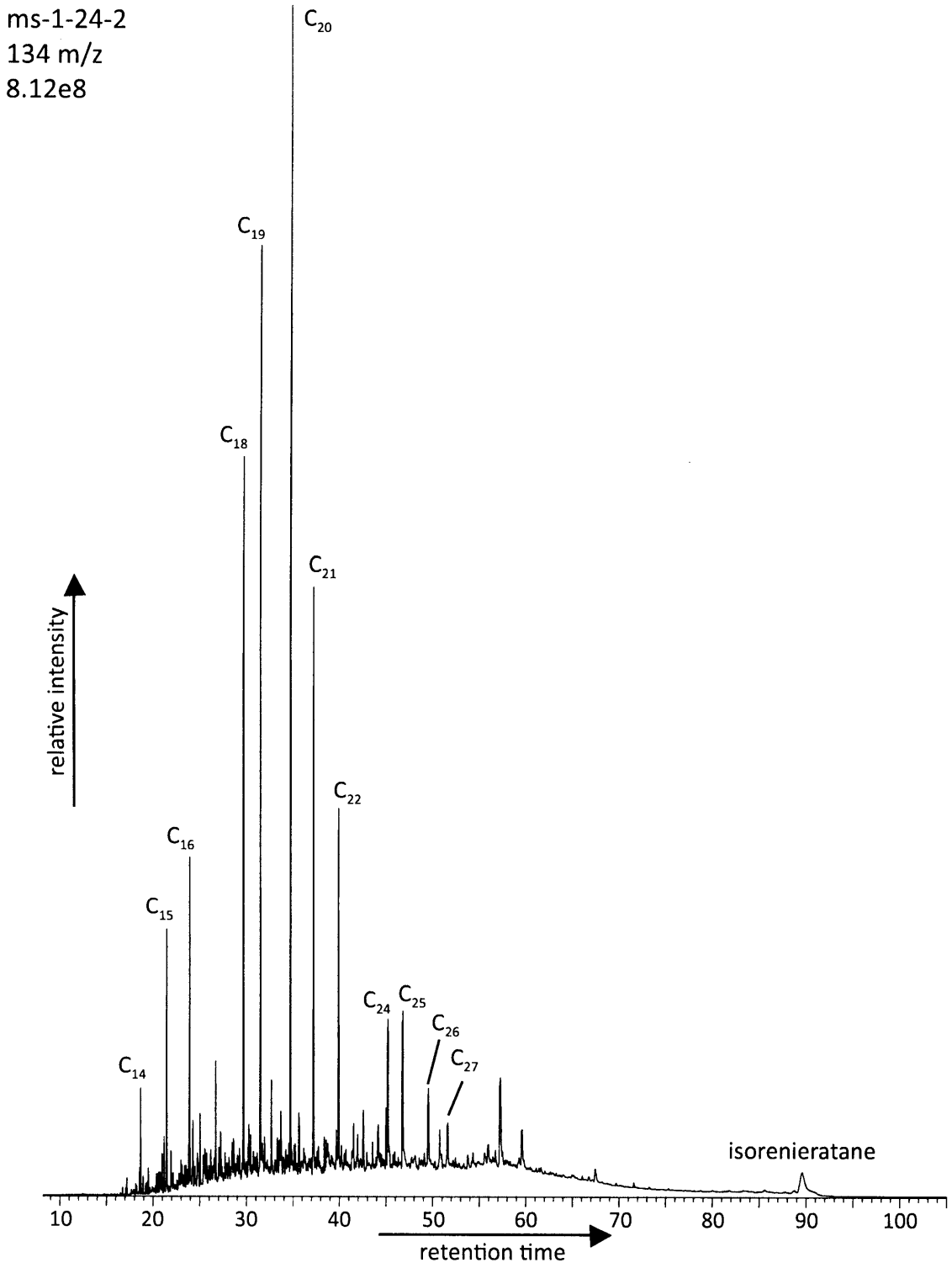

Figure 6.2 GC-MS select ion chromatogram of mass 134 from a sample aromatic hydrocarbon fraction from Meishan. Aryl isoprenoids from C_{14} to C_{27} have been identified, as well as the extended C_{40} carotenoid derivative isorenieratane.

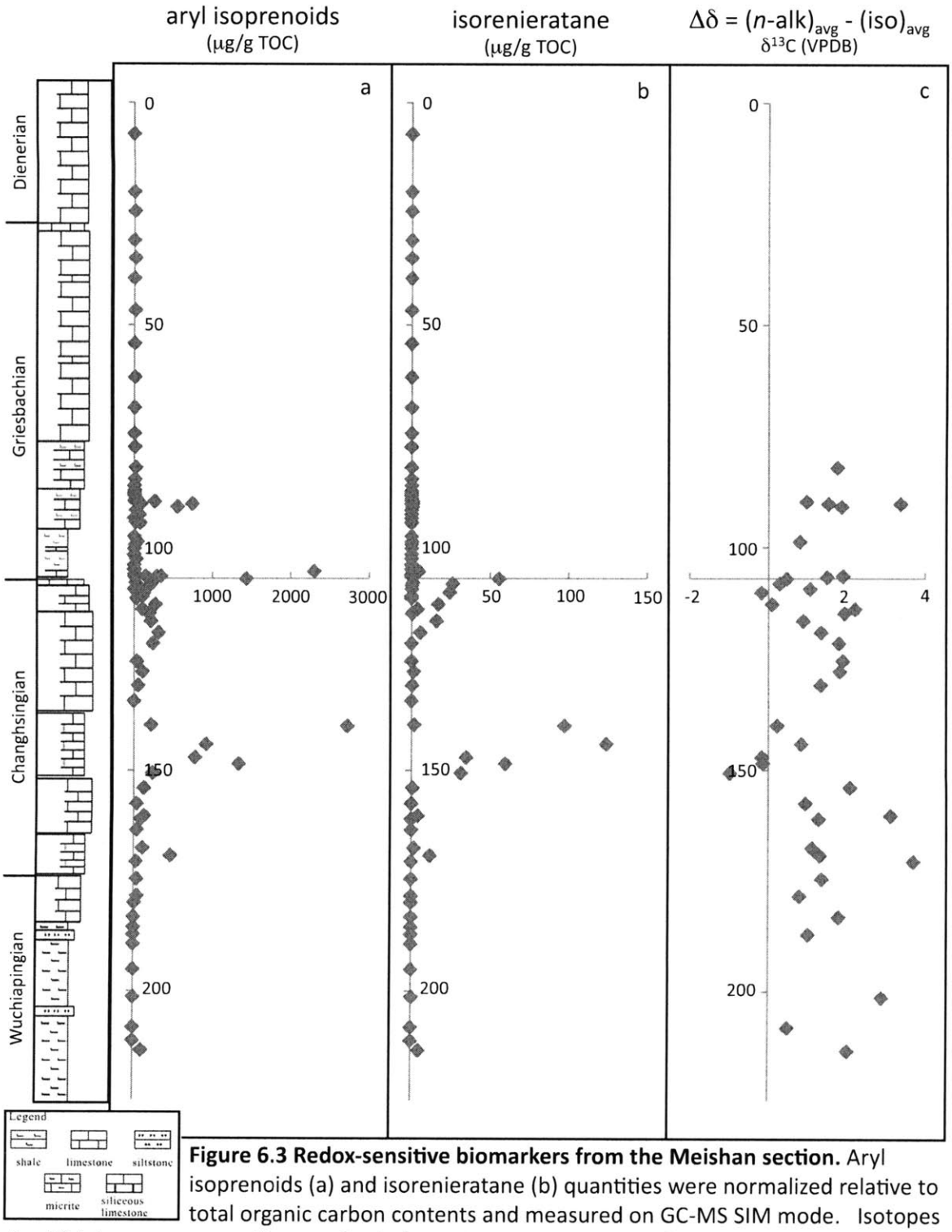

Figure 6.3 Redox-sensitive biomarkers from the Meishan section. Aryl isoprenoids (a) and isorenieratane (b) quantities were normalized relative to total organic carbon contents and measured on GC-MS SIM mode. Isotopes for Δδ (c) were measured in permil relative to VPDB on GC-irMS. All parameters are plotted relative to depth. Litholog adapted from Cao et al. 2009.

isoprenoid and isorenieratane contents are seen first in the mid-Changhsingian and then later concentrated around the boundary itself. One additional peak in aryl isoprenoid occurs above the boundary in the early Griesbachian, but the isorenieratane content remains low.

Previous studies have reported an absence of crocetane in samples from Meishan outcrop rocks (Maslen et al. 2009). However, when sedimentary rocks from the Meishan core were examined, a few samples were found to have small amounts of crocetane. (See Figure 6.4.) Crocetane was measured almost exclusively in the interval between the two peaks of aryl isoprenoid abundance in the mid-Changhsingian and early Griesbachian, an interval that includes the boundary itself. Outside of this interval, at the very bottom of the section, there was a single sample where crocetane was measured, and this sample also had higher aryl isoprenoid contents than surrounding sedimentary rocks. The $\delta^{13}C$ of the crocetane was not measured. In this section with abundant aryl isoprenoid and isorenieratane contents, the crocetane may have been derived from the carotenoids of Chlorobi in the sedimentary rocks as has been suggested previously (Maslen et al. 2009).

Stable Carbon Isotopes in Hydrocarbons

In Phanerozoic environments, the isoprenoids pristane and phytane, produced primarily by photoautotrophs, generally have greater $\delta^{13}C$ values than the *n*-alkanes heptadecane and octadecane, which are produced by a wide range of organisms. This pattern is considered 'normal' isotopic ordering because it conforms to what is observed in cultured phytoplankton (Hayes 2001). The term $\Delta\delta$, as used here, refers to the difference between the average $\delta^{13}C$ values of the *n*-alkanes *n*-C_{17} and *n*-C_{18} and average value for the isoprenoids pristane and phytane. The value of $\Delta\delta$ in samples from the Meishan section was overwhelmingly positive, indicating anomalous isotopic ordering

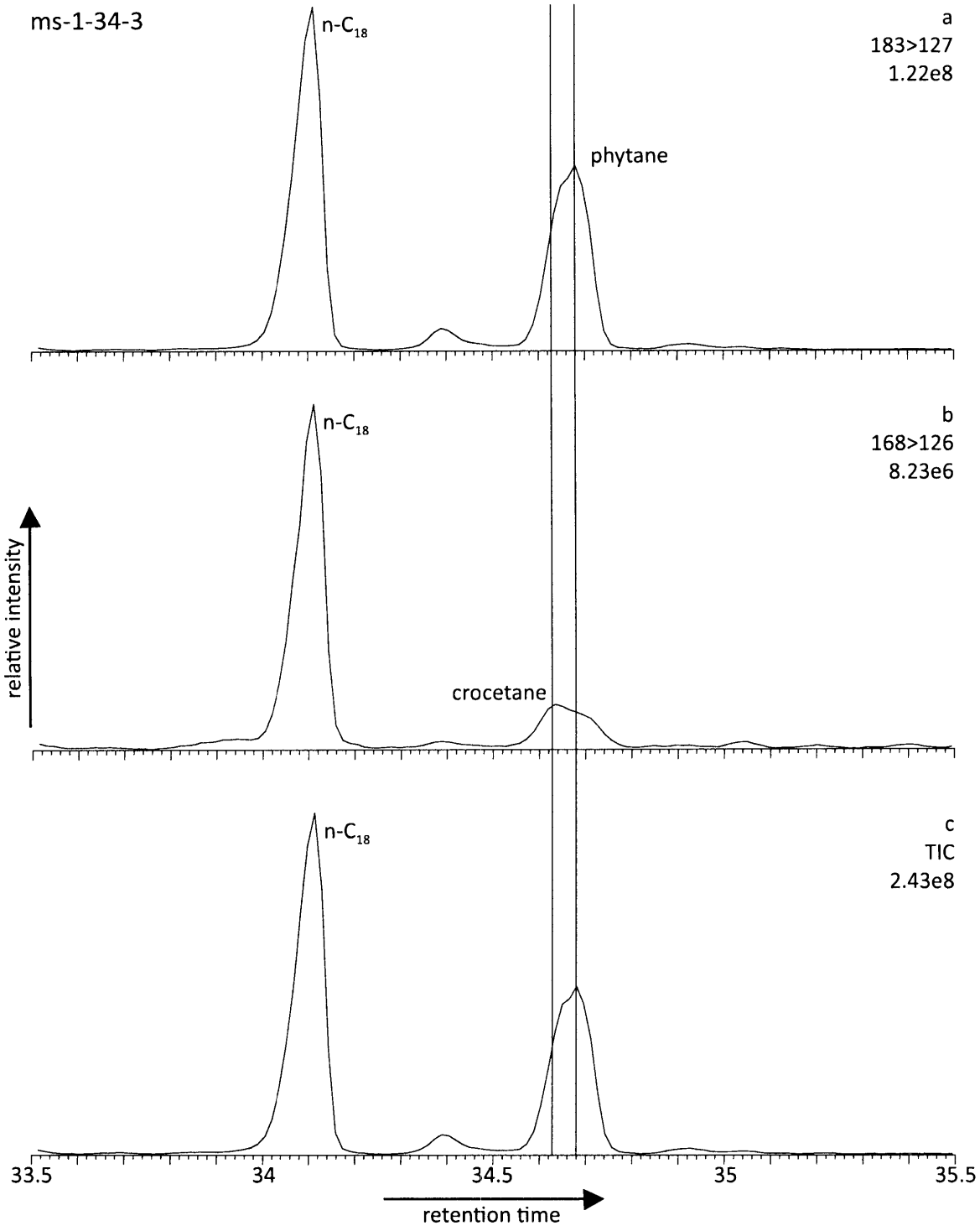

Figure 6.4 GC-MS MRM chromatograms from a select saturated hydrocarbon fraction from Meishan. (a) and (b) are transitions that separate the co-eluting phytane and crocetane peaks, respectively.

where pristane and phytane were depleted relative to the *n*-alkanes. (See Figure 6.5.) There is good agreement between the $\delta^{13}C$ values of each of the isoprenoids and also between the $\delta^{13}C$ values of each of the *n*-alkanes. (See Figure A1.2 in Appendix 1.) This suggests that no individual compound is representative of an isotopically peculiar source and that no individual compound is driving the pattern in $\Delta\delta$ values. (See Appendix 1 for uncertainties in isotope measurements.)

The average $\Delta\delta$ value throughout the section was close to 1.3‰, and there were only two intervals in which this value was less than 0.5‰. (See Figure 6.5.) One interval near the boundary had $\Delta\delta$ values below the average, although only one sample had a negative value. In a second, younger interval, the $\Delta\delta$ values were even lower. Here, the lowest value, ~-1‰, was measured from the mid-Changhsingian, earlier than the major fluctuations in $\delta^{13}C$ values for organic and carbonate carbon. In both of the more negative $\Delta\delta$ intervals, all four measured compounds show a significant positive excursion in $\delta^{13}C$ values and individual values converge. (See Figure 6.5.) There is no enrichment of one group over another.

Correlation coefficients were calculated between the $\Delta\delta$ pattern and all other parameters measured, and values > |0.4| indicate a relationship exists between the variables 99% of the time based on the Pearson Correlation Coefficient for these number of samples. (See Appendix 1 for methods.) Positive correlations of 0.58, 0.44 and 0.49 were measured between the $\Delta\delta$ pattern and the C_{27} and C_{29} Dia/Reg sterane ratios and the C_{31} hopane 22S/(22S+22R) ratio, respectively. (See Table A1.1 in Appendix 1.) Since these compounds are indicative of maturity of the organic material in the rocks and show only very minor changes throughout the section, this correlation is not likely consequential for the understanding of the $\Delta\delta$ pattern. Significant negative correlations were measured to the patterns of isorenieratane content (-0.47) and the homohopane index (-0.52). This

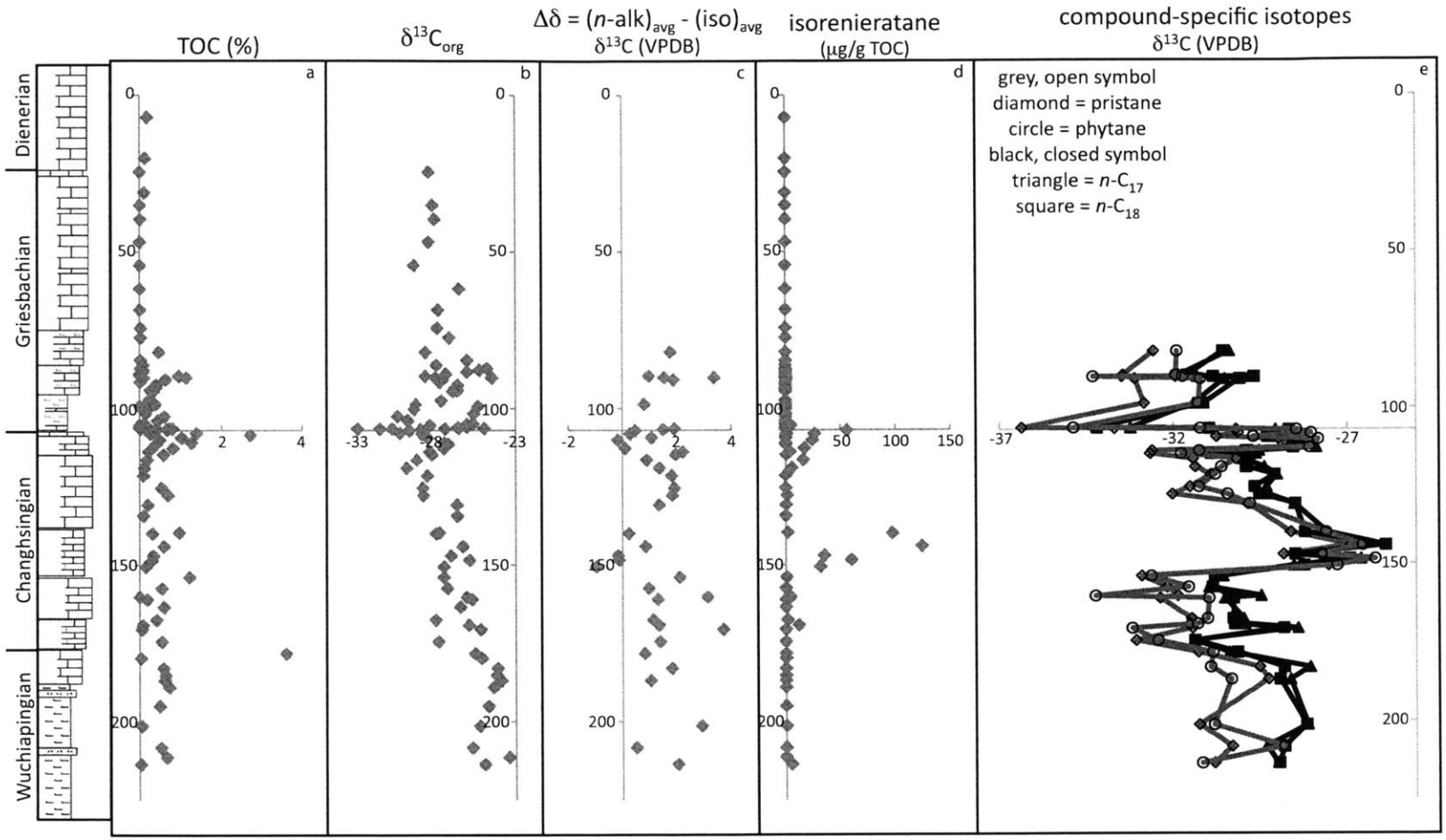

Figure 6.5 Δδ-related biomarkers from the Meishan section. Isotopes for $\delta^{13}C$ (b), Δδ (c) and compound-specific (e) were measured in permil relative to VPDB on GC-irMS. Isorenieratane (d) quantities were normalized relative to total organic carbon contents and measured on GC-MS SIM mode. All parameters are plotted relative to depth. Litholog adapted from Cao et al. 2009.

demonstrates that in the intervals in which the Δδ pattern was more negative, there was an increase in inputs from Chlorobi and strong evidence for anoxia. No other significant correlations were observed.

The positive Δδ values measured throughout the section, and when viewed with respect to the hypothesis in the original work on Δδ (Logan et al. 1995), indicate that for the significant majority of deposition, sedimentary input was dominated by heterotrophic organisms and fueled by an increase of organic material reworking in a restricted oxic zone within the stratified water column. The interpretation proposed by a more recent study of modern samples (Close et al. 2008) suggests that positive Δδ seen throughout the section may have been the result of an increased sedimentary input from prokaryotic organisms. Evidence from the biomarker proxies for redox (such as the pristane/phytane ratio, homohopane index, 28,30 DNH and Chlorobi-derived biomarkers) as well as biomarker proxies for microbial community (such as the hopane/sterane ratio and 2-methylhopane index) suggest that both of these interpretations may be correct, and that the Meishan section was deposited during a period of prolonged euxinia with a significant bacterial component to the plankton.

However, the two intervals in which the Δδ value had a negative excursion were unexpected. Although Δδ values of greater than ~-3‰ may still be considered anomalous, as this is the typical difference between the values of these compound in primary producers (Schouten et al. 1998; Hayes 2001), the trend toward more negative Δδ values indicated a change in the carbon cycling during these intervals. The observation that the negative Δδ values were accompanied by a positive shift in $\delta^{13}C$ values of the compounds measured, as well as a converging of $\delta^{13}C$ values of both the isoprenoids and *n*-alkanes, indicates that this carbon cycle disruption pervaded the microbial

community. Trace quantities of chlorobactane, produced by green pigmented Chlorobi that differ physiologically from the brown pigmented strains that preferentially make isorenieratene (Montesinos et al. 1983; Frigaard et al. 2004; Bryant and Frigaard 2006) and 2,3,4 aryl isoprenoids, produced by other anoxygenic phototrophs, were identified in some of the samples with negative $\Delta\delta$ values. A significant increase in Chlorobi-derived biomarkers in these samples suggests that perhaps these intervals were a time of extreme shoaling of the chemocline, such that there were increased inputs from anoxygenic phototrophs and decreased input from oxygenic phototrophs. This change in primary producers may have had the observed effect on the isotopes measured here. The presence of one of the intervals with negative $\Delta\delta$ values immediately preceding the Permian-Triassic boundary suggests that ocean conditions may have affected the extinction itself. However, with atmospheric oxygen contents close to modern (Berner 2005), a very shallow chemocline would be stable only for short, intermittent periods.

Summary

Biomarker proxies for the Meishan section carry particular importance because of the significance of the GSSP as well as the benefit of the context provided by the well-documented previous works. With the addition of more pristine samples available from the newly drilled cores, the potential information that may be collected from this section has only increased. It is in this context that the research into carotenoid diagenetic products from Chlorobi and carbon isotopic differences described here is presented.

The presence of aryl isoprenoids and isorenieratane in nearly all samples measured (and crocetane in a few of the samples closest to the boundary) is a strong indication that conditions of photic zone

euxinia presaged the main pulse of extinction and continued for an extended period afterwards. The trends in the two carotenoid derivatives are roughly parallel, indicating that the aryl isoprenoids were likely derived from Chlorobi biomolecules. The double-peak feature, one shortly before the boundary that corresponds to an increase in other biomarkers for anoxia (Cao et al. 2009), and the other at the boundary, which corresponds to the peak seen in other sections, indicates that although photic zone euxinia was present throughout, there were periods where the Chlorobi had an even greater input to the sediments.

Carbon isotopic values of *n*-alkanes and isoprenoids were measured and used to calculate the value of $\Delta\delta$ in the samples from this section. A predominant trend of positive values was found throughout, suggesting the presence of a stratified water column with high prokaryotic input. The two intervals with negative values of $\Delta\delta$ in this section correspond to the highest inputs of Chlorobi-derived biomarkers, suggesting further perturbation of carbon cycle dynamics at these periods.

The biomarker data collected from the Meishan section outcrop and core shows that the extinction event at the Permian-Triassic boundary occurred in the midst of a long-term pervasive anoxic event, at least in the paleo-Tethys ocean, where the carbon cycle was significantly different than normal Phanerozoic cycling.

References

Berner, R. A. (2005). "The Carbon and Sulfur Cycles and Atmospheric Oxygen from Middle Permian to Middle Triassic." Geochimica et Cosmochimica Acta **69**(13): 3211-3217.

Bryant, D. A. and N.-U. Frigaard (2006). "Prokaryotic Photosynthesis and Phototrophy Illuminated." Trends in Microbiology **14**(11): 488-496.

Cao, C., G. D. Love, L. E. Hays, W. Wang, S. Shen and R. E. Summons (2009). "Biogeochemical Evidence for Euxinic Oceans and Ecological Disturbance Presaging the End-Permian Mass Extinction Event." Earth and Planetary Science Letters **281**(3-4): 188-201.

Cao, C. Q., W. Wang and Y. G. Jin (2002). "Carbon Isotope Excursions across the Permian-Triassic Boundary in the Meishan Section, Zhejiang Province, China." Chinese Science Bulletin **47**(13): 1125-1129.

Close, H., A. Diefendorf, K. H. Freeman and A. Pearson (2008). "A Modern Analogue for Proterozoic Inverse Carbon Isotope Signatures." Eos Trans. AGU **89**(53): Fall Meet. Suppl., Abstract PP14A-07.

Foster, C., G. Logan, R. E. Summons, J. Gorter and D. Edwards (1997). "Carbon Isotopes, Kerogen Types and the Permian-Triassic Boundary in Australia: Implications for Exploration." Australian Petroleum Production and Exploration Association Journal **37**: 442-459.

Frigaard, N. U., J. A. Maresca, C. E. Yunker, A. D. Jones and D. A. Bryant (2004). "Genetic Manipulation of Carotenoid Biosynthesis in the Green Sulfur Bacterium Chlorobium Tepidum." Journal of Bacteriology **186**(16): 5210-5220.

Hayes, J. M. (2001). Fractionation of the Isotopes of Carbon and Hydrogen in Biosynthetic Processes. Stable Isotope Geochemistry, Reviews in Mineralogy and Geochemistry. J. W. Valley and D. R. Cole. Washington, DC, Mineralogical Society of America**:** 225-278.

Imhoff, J. F. (2003). "Phylogenetic Taxonomy of the Family Chlorobiaceae on the Basis of 16s Rrna and Fmo (Fenna-Matthews-Olson Protein) Gene Sequences." Int J Syst Evol Microbiol **53**(4): 941-951.

Isozaki, Y. (1995). "Superanoxia across the Permo-Triassic Boundary: Record in Accreted Deep-Sea Pelagic Chert in Japan. ." Canadian Society of Petroleum Geologists, Memoir 17: 805-812.

Isozaki, Y. (1997). "Permo-Triassic Boundary Superanoxia and Stratified Superocean: Records from Lost Deep Sea." Science **276**(5310): 235-238.

Jin, Y., Y. Wang, W. Wang, Q. H. Shang, C. Cao and D. H. Erwin (2000). "Pattern of Marine Mass Extinction near the Permian-Triassic Boundary in South China." Science **289**: 432-436.

Kaiho, K., Z.-Q. Chen, H. Kawahata, Y. Kajiwara and H. Sato (2006). "Close-up of the End-Permian Mass Extinction Horizon Recorded in the Meishan Section, South China: Sedimentary, Elemental, and Biotic Characterization and a Negative Shift of Sulfate Sulfur Isotope Ratio." Palaeogeography, Palaeoclimatology, Palaeoecology **239**(3-4): 396-405.

Lo, C. H., S. L. Chung, T. Y. Lee and G. Y. Wu (2002). "Age of the Emeishan Flood Magmatism and Relations to Permian-Triassic Boundary Events." Earth and Planetary Science Letters **198**(3-4): 449-458.

Logan, G. A., J. M. Hayes, G. B. Hieshima and R. E. Summons (1995). "Terminal Proterozoic Reorganization of Biogeochemical Cycles." Nature **376**(6535): 53-56.

Maslen, E., K. Grice, J. D. Gale, C. Hallmann and B. Horsfield (2009). "Crocetane: A Potential Marker of Photic Zone Euxinia in Thermally Mature Sediments and Crude Oils of Devonian Age." Organic Geochemistry **40**(1): 1-11.

Mei, S., K. Zhang and B. R. Wardlaw (1998). "A Refined Zonation of Changhsingian and Griesbachian Gondolellid Conodonts from the Meishan Section, Candidate of the Global Stratotype Section and Point of the Permian-Triassic Boundary." Palaeogeography, Palaeoclimatology, Palaeoecology **143**(4): 213-226.

Montesinos, E., R. Guerrero, C. Abella and I. Esteve (1983). "Ecology and Physiology of the Competition for Light between Chlorobium Limicola and Chlorobium Phaeobacteroides in Natural Habitats." Appl. Environ. Microbiol. **46**(5): 1007-1016.

Mundil, R., K. R. Ludwig, I. Metcalfe and P. R. Renne (2004). "Age and Timing of the Permian Mass Extinctions: U/Pb Dating of Closed-System Zircons." Science **305**(5691): 1760-1763.

Schouten, S., W. C. M. Klein Breteler, P. Blokker, N. Schogt, W. I. C. Rijpstra, K. Grice, M. Baas and J. S. Sinninghe Damstè (1998). "Biosynthetic Effects on the Stable Carbon Isotopic

Compositions of Algal Lipids: Implications for Deciphering the Carbon Isotopic Biomarker Record." Geochimica et Cosmochimica Acta **62**(8): 1397-1406.

Shu, O. and J. Utting (1990). "Palynology of Upper Permian and Lower Triassic Rocks, Meishan, Changxing County, Zhejiang Province, China." Review of Palaeobotany and Palynology **66**(1-2): 65-103.

Summons, R. E. and T. G. Powell (1987). "Identification of Aryl Isoprenoids in Source Rocks and Crude Oils : Biological Markers for the Green Sulphur Bacteria." Geochimica et Cosmochimica Acta **51**: 557-566.

Tsuzuki, K., A. Ôhashi, Y. Arai, K. Masuda, A. Takano, K. Shiojima, H. Ageta and S.-Q. Cai (2001). "Triterpenoids from Adiantum Caudatum." Phytochemistry **58**(2): 363-367.

Xie, S., R. D. Pancost, J. Huang, P. B. Wignall, J. Yu, X. Tang, L. Chen, X. Huang and X. Lai (2007). "Changes in the Global Carbon Cycle Occurred as Two Episodes During the Permian-Triassic Crisis." Geology **35**(12): 1083-1086.

Xu, D.-Y. and Z. Yan (1993). "Carbon Isotope and Iridium Event Markers near the Permian/Triassic Boundary in the Meishan Section, Zhejiang Province, China." Palaeogeography, Palaeoclimatology, Palaeoecology **104**(1-4): 171-176.

Yin, H., K. Zhang, J. Tong, Z. Yang and S. Wu (2001). "The Global Stratotype Section and Point (Gssp) of the Permian-Triassic Boundary." Episodes **24**(2): 102-114.

Yin, H. F., S. B. Wu, M. H. Ding, K. X. Zhang, J. N. Tong, F. Q. Yang and X. L. Lai (1996). The Meishan Section, Candidate for the Global Stratotype Section and Point of the Permian-Triassic Boundary. The Palaeozoic-Mesozoic Boundary Candidates for Global Stratotype Section and Point of the Permian-Triassic Boundary: . H. F. Yin. Wuhan, China University of Geosciences Press, Natural Science Foundation of China Project: 31-48.

Table 6.S1: Total biomarker and isotopic data from Meishan, China

sample name	depth	extracted rock (g)	TLE (mg)	TOC	sats (mg)	aros (mg)	Total AI (ug/g TOC)	isorenieratane (ug/g TOC)
MS05-140	7.05	13.3158	0.1	0.01	0.1	0.4	0.231	ND
MS05-150	20.14	14.0776	0.2	0.01	0.1	0.1	0.597	ND
MS05-160	24.5	14.3876	0.2	0.01	0.3	1.9	10.123	ND
MS05-165	31.05	13.1666	0.8	-	0.1	0.2	0.609	ND
MS05-168	35.06	13.5079	0.9	0.01	0.9	0.1	17.898	ND
MS05-170	39.56	13.835	0.2	0.02	0.1	0.3	2.865	ND
MS05-175	46.79	13.6346	0.2	0.01	1.1	0.1	12.951	ND
MS05-177	54.23	13.6372	3.1	0.01	0.2	0.1	6.254	ND
MS05-180	61.77	12.9274	1.1	0.01	0.1	0.1	11.963	ND
MS05-183	68.57	13.7867	0.3	0.01	0.2	0.1	5.552	ND
MS05-185	74.38	13.7049	0.2	0.03	0.1	0.1	5.521	ND
MS05-187	77.44	14.6749	0.8	0.03	0.6	0.1	10.969	ND
MS05-191	82.07	14.0752	1.1	0.48	0.2	0.9	22.901	0.045
MS05-193	84.66	13.6327	0.3	0.03	0.1	0.3	11.113	ND
MS05-195b	86.17	11.3635	7	0.09	0.1	0.1	0.860	ND
MS05-197	87.27	14.2022	7.4	0.03	0.1	0.1	7.044	ND
ms-1-39-1	87.77	12.6126	0.8	0.09	0.3	0.4	2.824	ND
ms-1-38-2	88.32	12.9608	1.2	0.09	0.3	0.1	5.509	ND
MS05-199	89.02	13.7572	1.1	0.01	0.1	0.4	22.108	ND
ms-1-37-5	89.53	12.2813	0.9	0.01	0.7	0.6	9.329	ND
MS05-200	89.71	14.5005	5	0.96	2.2	2.8	264.099	0.613
MS37-3a	90.22	14.0864	6.7	1.14	2.8	3.9	744.435	0.586
MS37-3b	90.23	14.4724	0.3	0.1	0.1	0.2	87.514	ND
ms-1-37-2	90.88	13.8216	17.4	0.64	0.1	0.2	554.884	0.615
MS37-1	91.65	14.3455	0.1	0.02	-	0.1	23.773	ND
ms-1-36-3	92.61	12.5044	2.2	0.41	0.4	0.1	68.279	ND
ms-1-36-1	93.43	12.7101	1.2	0.41	0.3	0.5	1.082	ND
ms-1-35-2	94.28	10.5857	4.3	0.27	0.7	0.8	19.457	ND
ms-1-35-1	94.53	12.8983	1.6	0.35	0.5	0.1	78.141	ND
ms-1-34-12	97.55	12.499	0.5	0.23	0.3	0.2	1.766	ND
MS34-10	98.73	14.2496	1.2	0.39	0.3	0.9	44.684	0.223
ms-1-34-8	99.39	11.8133	8.4	0.01	-	0.5	14.558	ND
MS34-7	100.28	13.6582	20.5	0.2	0.5	1.3	2.435	ND
ms-1-34-5	101.63	12.2496	0.5	0.16	0.1	0.1	0.303	ND
ms-1-34-3	102.59	12.2669	3.7	0.61	0.6	0.1	29.360	ND
ms-1-34-1	103.93	13.0052	3.2	0.45	-	0.2	3.457	ND
ms-1-32-3	104.59	13.8379	1.4	0.12	0.3	0.4	0.393	ND
ms-1-32-1	105.09	13.5873	1	0.12	0.3	0.4	1.754	ND
ms-1-30-3	105.43	13.409	2.2	0.01	0.3	0.1	2301.411	4.616
ms-1-29-2	105.93	11.3949	0.8	0.15	0.6	0.1	7.358	ND
ms-1-29-1	106.08	13.379	0.6	0.04	0.2	0.5	10.895	ND
ms-1-27-3	106.16	13.5852	0.9	0.01	0.1	1.1	25.839	ND
ms-1-27-2	106.38	12.9188	1.2	0.03	-	0.4	8.741	ND
ms-1-27-1 p1	106.39	13.2968	0.5	0.02	0.4	0.3	5.846	ND
ms-1-27-1 p2	106.49	13.364	1.9	0.03	0.7	0.3	22.641	ND
ms-1-26-3	106.52	13.5318	14.1	0.81	1	0.5	342.956	0.658
ms-1-26-2	106.56	13.4376	9.9	0.72	0.9	0.3	150.141	ND
ms-1-26-1	106.6	13.8409	9.3	0.43	1.4	0.1	290.366	ND

Table 6.S1: Total biomarker and isotopic data from Meishan, China

sample name	depth	extracted rock (g)	TLE (mg)	TOC	sats (mg)	aros (mg)	Total AI (ug/g TOC)	isorenieratane (ug/g TOC)
ms-1-24-8	106.74	13.2261	12	0.67	1.5	0.1	19.386	0.829
ms-1-24-2	107.1	12.692	14	0.3	3.8	0.3	1432.929	55.825
ms-1-24-6	107.94	13.2847	27.2	1.39	-	0.7	17.365	0.934
MS23-2a	108.2	15.125	8	0.27	3.9	4.1	220.220	26.302
ms-1-23-1	108.56	15.4098	16.1	1.04	5.4	10.8	48.035	0.317
ms-1-23-4	109.4	12.3571	14.3	1.03	4.6	0.5	1.296	0.154
ms-1-22-1	110.15	13.8821	8.4	0.18	2.3	6.1	126.493	24.393
ms-1-22-3	111.04	12.1236	30.8	1.27	1.7	0.1	106.853	ND
MS05-02b	111.44	14.1398	2.6	0.08	0.7	1.9	31.427	0.055
MS05-04	112.8	14.0818	14.9	0.72	3.6	5.6	272.992	17.147
MS05-5	113.9	13.2376	7.3	0.23	0.4	0.6	108.009	3.808
MS05-08	114.81	14.0085	6	1.18	2	4	195.537	0.401
MS05-10	116.51	13.2263	9.9	0.19	0.3	1.6	217.991	16.051
MS05-15	119.09	13.7947	7.1	0.12	1	2.4	314.157	5.650
MS05-20	121.52	13.5358	5.9	0.1	0.9	1.3	241.327	ND
MS05-25	125.46	12.9272	10.9	0.54	0.1	2.9	38.166	0.020
MS05-30	127.82	13.2254	22.8	0.7	1.5	4	109.203	1.410
MS05-35	130.88	14.443	5.4	0.21	1.1	2.5	53.431	0.422
MS05-40	134.38	-	0.7	-	-	0.1	0.796	ND
MS05-49	139.74	-	-	-	-	-	220.054	1.714
MS05-50	140.01	13.4933	29.9	0.32	6.4	14.3	2723.021	97.438
MS05-55	144.13	13.9711	22.5	0.6	9	13.5	921.903	124.182
MS05-60	147.08	13.0458	12.7	0.34	5.6	5.2	780.857	35.016
MS05-63	148.5	14.047	8.3	0.31		5.2	1339.162	59.932
MS05-65	150.62	14.0947	1.3	0.16	0.5	0.8	239.203	31.631
MS05-70	153.95	13.5217	112.1	1.22	5.6	10.5	128.717	0.761
MS05-76	157.48	14.3528	10.7	0.55	1.9	4.4	36.366	0.071
MS05-80	160.27	13.3414	0.9	0.01	0.2	1.9	131.233	4.144
MS05-81	161.02	15.0807	4.1	0.19	1.1	3	90.425	ND
MS05-86	163.45	14.4117	4.8	0.6	-	3.3	40.932	0.075
MS05-90	167.55	13.0873	38.6	0.42	1.4	4.9	114.402	1.610
MS05-92b	169.24	14.2209	3.4	0.09	1.3	2.1	471.300	12.008
MS05-95	170.59	14.9159	2.5	0.06	0.7	0.7	33.607	ND
MS05-100	174.5	13.1751	43.2	3.61	3.7	8.5	40.617	ND
MS05-105	178.3	13.2783	68.3	6	11	15.2	46.138	0.103
MS05-107	179.8	15.3319	1	0.04	0.4	0.6	10.383	ND
MS05-112	183.02	14.2913	3.4	0.59	-	1.2	3.691	ND
MS05-115	185.3	13.4753	5.8	0.64	0.1	0.8	1.792	ND
MS05-117	186.91	14.5044	2.1	0.62	0.6	1.5	2.147	ND
MS05-120	189.05	13.2611	65.9	0.73	0.3	1.7	1.202	ND
MS05-125	195.05	13.5108	2.6	0.5	0.1	0.3	0.786	ND
MS05-130	201.35	13.1272	1.8	0.06	0.2	0.1	2.557	0.363
MS05-134	208.22	13.2155	2.7	0.53	-	2.3	1.447	0.045
MS05-136c	211.3	13.6291	22.5	0.67	0.1	0.1	0.419	ND
MS05-138	213.52	14.1109	15.3	0.04	11	4.3	108.012	4.999

Table 6.S1: Total biomarker and isotopic data from Meishan, China

		isotopes				isotopes		
sample name	depth	$\delta^{13}C_{org}$	$\delta^{15}N$	farnesane	pristane	phytane	n-C17	n-C18
MS05-140	7.05	-	-	ND	-	-	-	-
MS05-150	20.14	-	-	ND	-	-	-	-
MS05-160	24.5	-28.29	-	ND	-	-	-	-
MS05-165	31.05	-	-	ND	-	-	-	-
MS05-168	35.06	-28.06	-	ND	-	-	-	-
MS05-170	39.56	-27.94	-	ND	-	-	-	-
MS05-175	46.79	-28.30	-	ND	-	-	-	-
MS05-177	54.23	-29.27	-	ND	-	-	-	-
MS05-180	61.77	-26.44	-	ND	-	-	-	-
MS05-183	68.57	-27.72	-	ND	-	-	-	-
MS05-185	74.38	-27.77	-	ND	-	-	-	-
MS05-187	77.44	-27.04	-0.446	ND	-	-	-	-
MS05-191	82.07	-26.47	1.281	ND	-32.565	-31.886	-30.381	-30.562
MS05-193	84.66	-25.41	-	ND	-	-	-	-
MS05-195b	86.17	-27.82	-	ND	-	-	-	-
MS05-197	87.27	-24.74	-	ND	-	-	-	-
ms-1-39-1	87.77	-25.20	1.154	ND	-	-	-	-
ms-1-38-2	88.32	-25.95	-	ND	-	-	-	-
MS05-199	89.02	-27.25	-	ND	-	-	-	-
ms-1-37-5	89.53	-	-	ND	-	-	-	-
MS05-200	89.71	-27.94	0.366	ND	-33.441	-31.923	-31.833	-31.588
MS37-3a	90.22	-27.88	-1.032	ND	-33.481	-31.721	-31.302	-30.842
MS37-3b	90.23	-	-	ND	-31.929	-34.303	-29.823	-29.667
ms-1-37-2	90.88	-27.46	-0.630	ND	-33.102	-31.218	-30.515	-30.082
MS37-1	91.65	-27.62	0.655	ND	-	-	-	-
ms-1-36-3	92.61	-25.73	-	ND	-	-	-	-
ms-1-36-1	93.43	-26.69	-	ND	-	-	-	-
ms-1-35-2	94.28	-26.53	-1.382	ND	-	-	-	-
ms-1-35-1	94.53	-26.82	-	ND	-	-	-	-
ms-1-34-12	97.55	-27.53	1.280	ND	-	-	-	-
MS34-10	98.73	-27.36	0.891	ND	-32.835	-31.276	-31.398	-31.124
ms-1-34-8	99.39	-25.28	-	ND	-	-	-	-
MS34-7	100.28	-27.47	0.848	ND	-	-	-	-
ms-1-34-5	101.63	-25.54	-	ND	-	-	-	-
ms-1-34-3	102.59	-30.30	0.110	ND	-	-	-	-
ms-1-34-1	103.93	-29.66	0.310	ND	-	-	-	-
ms-1-32-3	104.59	-25.59	-	ND	-	-	-	-
ms-1-32-1	105.09	-25.97	-	ND	-	-	-	-
ms-1-30-3	105.43	-28.23	-	ND	-	-	-	-
ms-1-29-2	105.93	-25.95	0.260	ND	-	-	-	-
ms-1-29-1	106.08	-26.50	-	ND	-	-	-	-
ms-1-27-3	106.16	-24.60	-	ND	-	-	-	-
ms-1-27-2	106.38	-24.91	-	ND	-	-	-	-
ms-1-27-1 p1	106.39	-26.47	-	ND	-	-	-	-
ms-1-27-1 p2	106.49	-27.30	-	ND	-	-	-	-
ms-1-26-3	106.52	-32.79	0.280	ND	-36.352	-34.863	-33.228	-34.192
ms-1-26-2	106.56	-31.40	-0.510	ND	-	-	-	-
ms-1-26-1	106.6	-30.63	0.316	ND	-	-	-	-

Table 6.S1: Total biomarker and isotopic data from Meishan, China

		isotopes				isotopes		
sample name	depth	δ^{13}Corg	δ^{15}N	farnesane	pristane	phytane	n-C17	n-C18
ms-1-24-8	106.74	-28.82	2.220	ND	-33.690	-31.221	-30.956	-30.961
ms-1-24-2	107.1	-29.56	1.440	ND	-30.190	-28.458	-29.056	-28.663
ms-1-24-6	107.94	-30.17	1.740	ND	-	-	-	-
MS23-2a	108.2	-28.74	2.165	ND	-30.142	-28.033	-29.042	-28.560
ms-1-23-1	108.56	-	-	ND	-	-	-	-
ms-1-23-4	109.4	-28.38	2.410	ND	-30.754	-29.700	-29.039	-29.294
ms-1-22-1	110.15	-	-	ND	-28.976	-27.828	-28.721	-28.436
ms-1-22-3	111.04	-27.34	2.830	ND	-	-	-	-
MS05-02b	111.44	-27.09	2.956	ND	-	-	-	-
MS05-04	112.8	-27.37	2.314	ND	-28.536	-28.080	-27.878	-28.549
MS05-5	113.9	-28.24	-	ND	-32.601	-31.245	-29.534	-29.896
MS05-08	114.81	-28.11	1.612	ND	-32.660	-31.767	-29.628	-30.911
MS05-10	116.51	-29.08	-	ND	-31.431	-30.151	-29.994	-29.816
MS05-15	119.09	-29.73	-	ND	-31.360	-30.615	-29.383	-29.904
MS05-20	121.52	-28.39	-	ND	-30.911	-30.791	-29.019	-29.085
MS05-25	125.46	-28.69	1.975	ND	-31.513	-31.254	-29.320	-29.659
MS05-30	127.82	-28.65	1.184	ND	-32.017	-30.440	-29.291	-29.526
MS05-35	130.88	-26.56	0.981	ND	-29.867	-29.806	-28.516	-28.490
MS05-40	134.38	-26.55	-	ND	-	-	-	-
MS05-49	139.74	-	-	ND	-	-	-	-
MS05-50	140.01	-27.86	-	ND	-28.620	-27.607	-27.572	-28.206
MS05-55	144.13	-26.22	1.573	ND	-26.896	-26.558	-25.885	-25.890
MS05-60	147.08	-26.94	-	ND	-28.829	-27.738	-28.395	-28.497
MS05-63	148.5	-25.81	0.798	ND	-27.064	-26.197	-26.603	-26.931
MS05-65	150.62	-27.38	-	ND	-27.533	-27.286	-28.535	-28.233
MS05-70	153.95	-27.38	2.202	ND	-32.906	-32.634	-30.571	-30.806
MS05-76	157.48	-27.16	3.495	ND	-32.175	-31.558	-30.967	-30.868
MS05-80	160.27	-25.98	-	ND	-31.868	-34.237	-29.479	-30.390
MS05-81	161.02	-25.67	2.875	-30.900	-32.380	-30.976	-30.518	-30.270
MS05-86	163.45	-27.88	2.402	ND	-	-	-	-
MS05-90	167.55	-27.87	-	ND	-31.470	-31.016	-29.980	-30.276
MS05-92b	169.24	-25.85	-	ND	-31.519	-31.298	-29.945	-30.232
MS05-95	170.59	-25.14	3.257	ND	-31.447	-33.184	-28.415	-28.824
MS05-100	174.5	-27.70	2.194	-30.800	-33.071	-32.438	-31.407	-31.376
MS05-105	178.3	-27.16	2.008	ND	-31.283	-30.868	-30.396	-30.160
MS05-107	179.8	-25.07	-	ND	-	-	-	-
MS05-112	183.02	-24.11	2.709	ND	-29.532	-30.929	-28.062	-28.815
MS05-115	185.3	-24.15	-	ND	-	-	-	-
MS05-117	186.91	-23.89	3.221	ND	-29.273	-30.338	-28.635	-28.937
MS05-120	189.05	-24.34	-	ND	-	-	-	-
MS05-125	195.05	-24.66	-	ND	-	-	-	-
MS05-130	201.35	-25.18	-	ND	-31.254	-30.829	-28.135	-28.168
MS05-134	208.22	-24.52	3.070	ND	-30.315	-28.813	-29.329	-28.814
MS05-136c	211.3	-24.20	3.527	ND	-	-	-	-
MS05-138	213.52	-24.89	-	ND	-30.823	-31.171	-28.998	-28.964

Table 6.S1: Total biomarker and isotopic data from Meishan, China

						Tricyclic			
sample name	depth	Δδ	cr/ph %	Pr/Ph (%)	Ster/ Hop	C19/C23	C22/C21	C24/C23	C26/C25
MS05-140	7.05	-	-	-	0.217	0.023	0.671	0.654	0.970
MS05-150	20.14	-	-	0.43	0.156	0.051	0.431	0.565	0.866
MS05-160	24.5	-	-	0.85	0.219	0.105	0.359	0.586	0.694
MS05-165	31.05	-	-	-	0.146	0.000	1.487	0.474	0.645
MS05-168	35.06	-	-	0.36	0.188	0.087	0.326	0.472	0.784
MS05-170	39.56	-	-	-	0.325	0.000	0.397	0.517	1.475
MS05-175	46.79	-	-	-	0.290	0.000	0.537	0.620	1.253
MS05-177	54.23	-	-	0.5	0.151	0.112	0.311	0.448	0.643
MS05-180	61.77	-	-	0	0.136	0.034	0.352	0.480	0.870
MS05-183	68.57	-	-	0.43	0.216	0.181	0.352	0.516	0.981
MS05-185	74.38	-	-	0.24	0.198	0.200	0.202	0.374	1.399
MS05-187	77.44	-	-	0.88	0.122	0.679	0.319	0.392	0.810
MS05-191	82.07	1.754	-	4.76	0.041	0.499	0.087	0.446	1.243
MS05-193	84.66	-	-	1.49	0.318	3.629	0.834	5.157	5.855
MS05-195b	86.17	-	-	0	0.239	0.000	0.504	0.545	1.026
MS05-197	87.27	-	-	0.44	0.095	0.239	0.171	0.313	0.772
ms-1-39-1	87.77	-	-	-	0.211	1.018	0.173	0.365	0.629
ms-1-38-2	88.32	-	-	3.66	-	-	-	-	-
MS05-199	89.02	-	-	-	0.176	1.205	0.021	0.572	0.894
ms-1-37-5	89.53	-	-	0.34	-	-	-	-	-
MS05-200	89.71	0.971	1.318	4.73	0.078	0.254	0.112	0.439	1.275
MS37-3a	90.22	1.529	1.409	4.37	0.061	0.312	0.119	0.303	0.967
MS37-3b	90.23	3.371		3.97	0.055	0.150	0.125	0.455	1.241
ms-1-37-2	90.88	1.861	1.428	5.23	-	-	-	-	-
MS37-1	91.65	-	-	-	-	-	-	-	-
ms-1-36-3	92.61	-	-	5.36	-	-	-	-	-
ms-1-36-1	93.43	-	-	-	0.019	0.572	0.104	0.542	0.675
ms-1-35-2	94.28	-	-	-	0.014	1.037	0.075	0.351	0.753
ms-1-35-1	94.53	-	-	4.61	-	-	-	-	-
ms-1-34-12	97.55	-	-	0.58	0.034	0.244	0.210	0.402	0.548
MS34-10	98.73	0.794	1.848	4.62	0.024	0.481	0.080	0.421	1.195
ms-1-34-8	99.39	-	-	-	0.542	0.020	0.347	0.512	0.670
MS34-7	100.28	-	-	1.14	0.041	0.670	0.168	0.425	0.741
ms-1-34-5	101.63	-	-	-	0.088	0.149	0.204	0.405	0.641
ms-1-34-3	102.59	-	-	4.18	0.068	0.269	0.243	0.451	0.755
ms-1-34-1	103.93	-	1.853	3.38	-	-	-	-	-
ms-1-32-3	104.59	-	2.015	0.42	0.108	0.789	0.226	0.429	0.564
ms-1-32-1	105.09	-	-	1.55	0.056	1.321	0.076	0.252	0.659
ms-1-30-3	105.43	-	-	2.34	-	-	-	-	-
ms-1-29-2	105.93	-	-	-	-	-	-	-	-
ms-1-29-1	106.08	-	-	1.07	-	-	-	-	-
ms-1-27-3	106.16	-	-	0.94	0.081	0.691	0.200	0.381	0.744
ms-1-27-2	106.38	-	-	1.29	0.420	0.157	0.182	0.536	1.015
ms-1-27-1 p1	106.39	-	-	0.36	-	-	-	-	-
ms-1-27-1 p2	106.49	-	1.556	1.41	-	-	-	-	-
ms-1-26-3	106.52	1.898	1.529	3.41	-	-	-	-	-
ms-1-26-2	106.56	-	1.594	2.85	-	-	-	-	-
ms-1-26-1	106.6	-	1.366	2.4	-	-	-	-	-

Table 6.S1: Total biomarker and isotopic data from Meishan, China

						Tricyclic			
sample name	depth	Δδ	cr/ph %	Pr/Ph (%)	Ster/ Hop	C19/C23	C22/C21	C24/C23	C26/C25
ms-1-24-8	106.74	1.497	1.331	2.31	-	-	-	-	-
ms-1-24-2	107.1	0.464	1.319	0.94	-	-	-	-	-
ms-1-24-6	107.94	-	-	0.77	-	-	-	-	-
MS23-2a	108.2	0.286	1.546	0.87	0.152	0.026	0.779	0.437	0.652
ms-1-23-1	108.56	-	-	-	0.223	0.252	0.227	0.598	0.672
ms-1-23-4	109.4	1.061	1.384	1.42	-	-	-	-	-
ms-1-22-1	110.15	-0.176	-	-	0.131	0.027	0.760	0.416	0.656
ms-1-22-3	111.04	-	1.397	1.54	-	-	-	-	-
MS05-02b	111.44	-	-	1.38	0.294	0.206	0.237	0.616	0.637
MS05-04	112.8	0.094	-	0.59	0.155	0.051	0.657	0.393	0.608
MS05-5	113.9	2.208	-	1.33	0.242	0.125	0.238	0.713	0.685
MS05-08	114.81	1.944	1.273	1.67	0.406	0.155	0.199	0.719	0.651
MS05-10	116.51	0.886	1.490	0.87	0.202	0.102	0.435	0.536	0.645
MS05-15	119.09	1.344	1.449	0.85	0.230	0.151	0.444	0.450	0.546
MS05-20	121.52	1.799	1.231	0.67	0.231	0.237	0.385	0.641	0.611
MS05-25	125.46	1.894	1.441	0.74	0.224	0.281	0.468	0.556	0.525
MS05-30	127.82	1.820	1.319	1.56	0.307	0.227	0.199	0.650	0.643
MS05-35	130.88	1.333	-	0.67	0.142	0.167	0.668	0.446	0.543
MS05-40	134.38	-	-	-	-	-	-	-	-
MS05-49	139.74	-	-	-	0.042	0.088	0.904	0.357	0.523
MS05-50	140.01	0.224	1.605	0.71	0.062	0.077	0.867	0.360	0.606
MS05-55	144.13	0.840	-	0.72	0.050	0.099	0.741	0.389	0.653
MS05-60	147.08	-0.163	1.594	0.54	0.059	0.107	0.664	0.414	0.665
MS05-63	148.5	-0.136	1.506	-	0.030	0.104	0.583	0.575	0.652
MS05-65	150.62	-0.975	-	0.45	0.064	0.048	0.653	0.555	0.718
MS05-70	153.95	2.081	1.457	0.81	0.306	0.140	0.346	0.590	0.653
MS05-76	157.48	0.949	-	1.07	0.234	0.206	0.285	0.568	0.606
MS05-80	160.27	3.118	-	0.84	0.310	0.267	0.262	0.601	0.728
MS05-81	161.02	1.284	1.231	3.81	0.281	0.177	0.202	0.605	0.735
MS05-86	163.45	-	-	-	0.304	0.222	0.177	0.517	0.747
MS05-90	167.55	1.115	1.234	0.89	0.279	0.273	0.289	0.548	0.611
MS05-92b	169.24	1.320	1.534	1.01	0.358	0.133	0.257	0.580	0.650
MS05-95	170.59	3.696	1.553	1.35	0.335	0.254	0.260	0.663	0.712
MS05-100	174.5	1.363	-	3.17	0.315	0.130	0.207	0.482	0.889
MS05-105	178.3	0.797	1.329	1.96	0.360	0.070	0.227	0.435	0.940
MS05-107	179.8	-	-	0.94	0.308	0.935	0.233	0.532	0.861
MS05-112	183.02	1.792	1.877	-	0.138	0.732	0.130	0.465	1.330
MS05-115	185.3	-	-	1.4	0.158	0.837	0.120	0.515	1.279
MS05-117	186.91	1.020	-	2.81	0.117	0.819	0.118	0.462	1.321
MS05-120	189.05	-	-	0.58	0.098	0.541	0.113	0.412	1.159
MS05-125	195.05	-	-	1.03	0.051	0.967	0.125	0.450	1.269
MS05-130	201.35	2.890	-	0.93	0.193	0.459	0.197	0.523	1.238
MS05-134	208.22	0.493	-	-	0.055	1.611	0.118	0.437	1.087
MS05-136c	211.3	-	-	2.87	0.147	1.062	0.187	0.464	1.068
MS05-138	213.52	2.016	1.559	1.91	0.603	0.396	0.237	0.780	1.006

Table 6.S1: Total biomarker and isotopic data from Meishan, China

				Steranes			
sample name	depth	tet/C23	tricyclics/ C30 Hopane	%C27 Steranes (C27-C29)	%C28 Steranes (C27-C29)	%C29 Steranes (C27-C29)	% C27 abb steranes
MS05-140	7.05	1.649	0.203	0.226	0.247	0.527	0.186
MS05-150	20.14	1.106	0.386	0.219	0.258	0.523	0.176
MS05-160	24.5	1.102	0.498	0.267	0.186	0.547	0.234
MS05-165	31.05	1.069	0.529	0.265	0.234	0.501	0.235
MS05-168	35.06	0.827	0.450	0.230	0.243	0.527	0.203
MS05-170	39.56	3.161	0.062	0.222	0.222	0.556	0.184
MS05-175	46.79	1.683	0.144	0.274	0.231	0.495	0.229
MS05-177	54.23	1.470	0.251	0.254	0.213	0.533	0.213
MS05-180	61.77	1.621	0.163	0.237	0.232	0.531	0.208
MS05-183	68.57	1.453	0.280	0.257	0.254	0.489	0.223
MS05-185	74.38	3.216	0.090	0.253	0.216	0.531	0.213
MS05-187	77.44	1.365	0.341	0.258	0.250	0.492	0.227
MS05-191	82.07	1.272	0.239	0.263	0.211	0.525	0.198
MS05-193	84.66	0.623	11.841	0.233	0.289	0.477	0.305
MS05-195b	86.17	0.848	0.240	0.324	0.269	0.408	0.280
MS05-197	87.27	1.224	0.905	0.322	0.231	0.447	0.238
ms-1-39-1	87.77	0.943	2.332	0.417	0.218	0.366	0.315
ms-1-38-2	88.32	-	-	-	-	-	-
MS05-199	89.02	2.600	2.038	0.328	0.253	0.419	0.293
ms-1-37-5	89.53	-	-	-	-	-	-
MS05-200	89.71	0.710	0.273	0.297	0.219	0.484	0.231
MS37-3a	90.22	0.849	0.509	0.323	0.231	0.446	0.275
MS37-3b	90.23	0.470	0.372	0.291	0.215	0.494	0.212
ms-1-37-2	90.88	-	-	-	-	-	-
MS37-1	91.65	-	-	-	-	-	-
ms-1-36-3	92.61	-	-	-	-	-	-
ms-1-36-1	93.43	2.318	0.770	0.298	0.185	0.517	0.199
ms-1-35-2	94.28	2.533	0.832	0.297	0.202	0.501	0.182
ms-1-35-1	94.53	-	-	-	-	-	-
ms-1-34-12	97.55	1.935	0.496	0.352	0.192	0.456	0.266
MS34-10	98.73	1.350	0.354	0.255	0.188	0.557	0.183
ms-1-34-8	99.39	0.371	2.422	0.462	0.228	0.310	0.324
MS34-7	100.28	1.822	0.437	0.306	0.196	0.497	0.267
ms-1-34-5	101.63	1.886	0.592	0.396	0.254	0.350	0.275
ms-1-34-3	102.59	0.206	4.977	0.327	0.274	0.399	0.219
ms-1-34-1	103.93	-	-	-	-	-	-
ms-1-32-3	104.59	1.147	2.186	0.365	0.218	0.417	0.250
ms-1-32-1	105.09	1.355	4.608	0.348	0.223	0.429	0.217
ms-1-30-3	105.43	-	-	-	-	-	-
ms-1-29-2	105.93	-	-	-	-	-	-
ms-1-29-1	106.08	-	-	-	-	-	-
ms-1-27-3	106.16	3.406	0.354	0.397	0.188	0.415	0.269
ms-1-27-2	106.38	0.845	0.465	0.367	0.231	0.402	0.274
ms-1-27-1 p1	106.39	-	-	-	-	-	-
ms-1-27-1 p2	106.49	-	-	-	-	-	-
ms-1-26-3	106.52	-	-	-	-	-	-
ms-1-26-2	106.56	-	-	-	-	-	-
ms-1-26-1	106.6	-	-	-	-	-	-

Table 6.S1: Total biomarker and isotopic data from Meishan, China

				Steranes			
sample name	depth	tet/C23	tricyclics/ C30 Hopane	%C27 Steranes (C27-C29)	%C28 Steranes (C27-C29)	%C29 Steranes (C27-C29)	% C27 abb steranes
ms-1-24-8	106.74	-	-	-	-	-	-
ms-1-24-2	107.1	-	-	-	-	-	-
ms-1-24-6	107.94	-	-	-	-	-	-
MS23-2a	108.2	0.529	0.969	0.360	0.140	0.500	0.355
ms-1-23-1	108.56	1.159	0.563	0.340	0.124	0.535	0.316
ms-1-23-4	109.4	-	-	-	-	-	-
ms-1-22-1	110.15	0.493	1.218	0.354	0.156	0.489	0.354
ms-1-22-3	111.04	-	-	-	-	-	-
MS05-02b	111.44	1.275	0.550	0.313	0.119	0.568	0.294
MS05-04	112.8	0.539	1.258	0.359	0.152	0.489	0.354
MS05-5	113.9	0.978	0.461	0.298	0.139	0.563	0.288
MS05-08	114.81	0.765	0.825	0.340	0.134	0.527	0.322
MS05-10	116.51	0.851	0.739	0.309	0.135	0.556	0.297
MS05-15	119.09	0.766	1.448	0.320	0.145	0.535	0.310
MS05-20	121.52	1.799	0.570	0.279	0.136	0.585	0.252
MS05-25	125.46	1.753	0.678	0.294	0.159	0.547	0.262
MS05-30	127.82	0.934	0.828	0.304	0.139	0.557	0.282
MS05-35	130.88	1.490	0.822	0.304	0.131	0.564	0.264
MS05-40	134.38	-	-	-	-	-	-
MS05-49	139.74	1.092	1.334	0.343	0.163	0.494	0.344
MS05-50	140.01	0.891	1.532	0.360	0.171	0.469	0.354
MS05-55	144.13	0.992	1.485	0.403	0.165	0.432	0.398
MS05-60	147.08	1.057	1.242	0.377	0.174	0.449	0.378
MS05-63	148.5	1.374	0.935	0.376	0.173	0.451	0.394
MS05-65	150.62	0.881	0.863	0.344	0.155	0.501	0.336
MS05-70	153.95	0.930	0.842	0.316	0.174	0.510	0.295
MS05-76	157.48	1.264	0.545	0.298	0.147	0.555	0.284
MS05-80	160.27	1.760	0.238	0.289	0.137	0.574	0.279
MS05-81	161.02	0.711	0.398	0.289	0.144	0.568	0.278
MS05-86	163.45	0.768	0.361	0.276	0.138	0.585	0.276
MS05-90	167.55	1.394	0.607	0.286	0.154	0.560	0.275
MS05-92b	169.24	0.836	0.631	0.302	0.148	0.550	0.291
MS05-95	170.59	1.398	0.334	0.300	0.133	0.567	0.286
MS05-100	174.5	0.460	0.416	0.293	0.157	0.550	0.296
MS05-105	178.3	0.295	0.494	0.344	0.188	0.469	0.322
MS05-107	179.8	0.905	0.720	0.303	0.236	0.461	0.256
MS05-112	183.02	2.838	0.101	0.182	0.207	0.611	0.162
MS05-115	185.3	3.254	0.147	0.201	0.203	0.596	0.184
MS05-117	186.91	2.787	0.134	0.228	0.180	0.592	0.189
MS05-120	189.05	4.516	0.109	0.153	0.208	0.639	0.138
MS05-125	195.05	6.503	0.076	0.216	0.169	0.615	0.184
MS05-130	201.35	1.561	0.318	0.266	0.228	0.506	0.237
MS05-134	208.22	5.071	0.145	0.242	0.162	0.596	0.211
MS05-136c	211.3	2.883	0.190	0.164	0.204	0.632	0.147
MS05-138	213.52	0.870	0.643	0.167	0.244	0.589	0.155

Table 6.S1: Total biomarker and isotopic data from Meishan, China

						Steranes	
sample name	depth	% C28 abb steranes	% C29 abb steranes	C29 St abb/ (aaa+abb)	C27 St abb/ (aaa+abb)	C29 aaa St S/(S+R)	C27 aaa St S/(S+R)
MS05-140	7.05	0.259	0.555	0.416	0.363	0.268	0.303
MS05-150	20.14	0.257	0.567	0.516	0.445	0.206	0.251
MS05-160	24.5	0.190	0.576	0.506	0.464	0.242	0.256
MS05-165	31.05	0.245	0.520	0.451	0.410	0.258	0.269
MS05-168	35.06	0.249	0.548	0.500	0.458	0.256	0.250
MS05-170	39.56	0.249	0.567	0.378	0.311	0.282	0.313
MS05-175	46.79	0.244	0.527	0.433	0.375	0.266	0.339
MS05-177	54.23	0.200	0.587	0.444	0.380	0.264	0.253
MS05-180	61.77	0.246	0.546	0.383	0.363	0.293	0.321
MS05-183	68.57	0.231	0.546	0.475	0.449	0.253	0.256
MS05-185	74.38	0.226	0.561	0.343	0.282	0.320	0.336
MS05-187	77.44	0.247	0.526	0.401	0.341	0.278	0.325
MS05-191	82.07	0.217	0.585	0.226	0.161	0.376	0.393
MS05-193	84.66	0.221	0.475	0.570	0.719	0.155	0.109
MS05-195b	86.17	0.249	0.471	0.448	0.412	0.279	0.262
MS05-197	87.27	0.244	0.518	0.364	0.275	0.243	0.338
ms-1-39-1	87.77	0.242	0.444	0.384	0.246	0.241	0.426
ms-1-38-2	88.32	-	-	-	-	-	-
MS05-199	89.02	0.234	0.472	0.411	0.387	0.271	0.292
ms-1-37-5	89.53	-	-	-	-	-	-
MS05-200	89.71	0.220	0.549	0.252	0.197	0.396	0.359
MS37-3a	90.22	0.249	0.477	0.320	0.287	0.296	0.333
MS37-3b	90.23	0.210	0.578	0.267	0.190	0.358	0.356
ms-1-37-2	90.88	-	-	-	-	-	-
MS37-1	91.65	-	-	-	-	-	-
ms-1-36-3	92.61	-	-	-	-	-	-
ms-1-36-1	93.43	0.171	0.629	0.398	0.281	0.146	0.344
ms-1-35-2	94.28	0.207	0.611	0.300	0.180	0.172	0.398
ms-1-35-1	94.53	-	-	-	-	-	-
ms-1-34-12	97.55	0.189	0.544	0.441	0.337	0.131	0.336
MS34-10	98.73	0.206	0.611	0.272	0.193	0.368	0.369
ms-1-34-8	99.39	0.255	0.420	0.420	0.263	0.198	0.408
MS34-7	100.28	0.212	0.521	0.357	0.335	0.315	0.311
ms-1-34-5	101.63	0.304	0.421	0.358	0.243	0.151	0.421
ms-1-34-3	102.59	0.246	0.535	0.239	0.123	0.304	0.410
ms-1-34-1	103.93	-	-	-	-	-	-
ms-1-32-3	104.59	0.249	0.501	0.455	0.285	0.196	0.394
ms-1-32-1	105.09	0.241	0.542	0.343	0.223	0.185	0.364
ms-1-30-3	105.43	-	-	-	-	-	-
ms-1-29-2	105.93	-	-	-	-	-	-
ms-1-29-1	106.08	-	-	-	-	-	-
ms-1-27-3	106.16	0.193	0.538	0.420	0.238	0.208	0.413
ms-1-27-2	106.38	0.253	0.473	0.398	0.280	0.215	0.308
ms-1-27-1 p1	106.39	-	-	-	-	-	-
ms-1-27-1 p2	106.49	-	-	-	-	-	-
ms-1-26-3	106.52	-	-	-	-	-	-
ms-1-26-2	106.56	-	-	-	-	-	-
ms-1-26-1	106.6	-	-	-	-	-	-

Table 6.S1: Total biomarker and isotopic data from Meishan, China

						Steranes	
sample name	depth	% C28 abb steranes	% C29 abb steranes	C29 St abb/ (aaa+abb)	C27 St abb/ (aaa+abb)	C29 aaa St S/(S+R)	C27 aaa St S/(S+R)
ms-1-24-8	106.74	-	-	-	-	-	-
ms-1-24-2	107.1	-	-	-	-	-	-
ms-1-24-6	107.94	-	-	-	-	-	-
MS23-2a	108.2	0.147	0.499	0.527	0.545	0.246	0.232
ms-1-23-1	108.56	0.125	0.559	0.534	0.520	0.253	0.258
ms-1-23-4	109.4	-	-	-	-	-	-
ms-1-22-1	110.15	0.166	0.480	0.512	0.528	0.262	0.241
ms-1-22-3	111.04	-	-	-	-	-	-
MS05-02b	111.44	0.118	0.588	0.518	0.514	0.243	0.250
MS05-04	112.8	0.158	0.488	0.514	0.511	0.250	0.248
MS05-5	113.9	0.134	0.578	0.519	0.518	0.259	0.238
MS05-08	114.81	0.137	0.542	0.530	0.520	0.242	0.245
MS05-10	116.51	0.128	0.575	0.536	0.531	0.248	0.235
MS05-15	119.09	0.138	0.552	0.531	0.518	0.245	0.236
MS05-20	121.52	0.121	0.627	0.525	0.508	0.241	0.234
MS05-25	125.46	0.146	0.591	0.505	0.481	0.251	0.243
MS05-30	127.82	0.129	0.589	0.535	0.511	0.256	0.252
MS05-35	130.88	0.111	0.625	0.525	0.488	0.236	0.266
MS05-40	134.38	-	-	-	-	-	-
MS05-49	139.74	0.171	0.485	0.472	0.485	0.251	0.229
MS05-50	140.01	0.170	0.476	0.511	0.494	0.243	0.233
MS05-55	144.13	0.176	0.427	0.499	0.496	0.243	0.238
MS05-60	147.08	0.173	0.449	0.509	0.512	0.243	0.224
MS05-63	148.5	0.192	0.413	0.446	0.515	0.229	0.224
MS05-65	150.62	0.156	0.508	0.521	0.525	0.232	0.234
MS05-70	153.95	0.168	0.537	0.527	0.515	0.245	0.244
MS05-76	157.48	0.145	0.571	0.526	0.518	0.237	0.254
MS05-80	160.27	0.130	0.591	0.525	0.526	0.247	0.234
MS05-81	161.02	0.139	0.583	0.536	0.524	0.237	0.242
MS05-86	163.45	0.140	0.584	0.490	0.500	0.269	0.263
MS05-90	167.55	0.142	0.582	0.528	0.521	0.246	0.238
MS05-92b	169.24	0.144	0.565	0.533	0.530	0.236	0.243
MS05-95	170.59	0.128	0.586	0.539	0.541	0.236	0.238
MS05-100	174.5	0.150	0.554	0.492	0.499	0.281	0.259
MS05-105	178.3	0.183	0.495	0.436	0.414	0.312	0.305
MS05-107	179.8	0.243	0.501	0.446	0.360	0.253	0.282
MS05-112	183.02	0.213	0.625	0.314	0.288	0.299	0.341
MS05-115	185.3	0.205	0.612	0.309	0.285	0.342	0.336
MS05-117	186.91	0.181	0.629	0.321	0.264	0.293	0.364
MS05-120	189.05	0.202	0.661	0.305	0.282	0.356	0.347
MS05-125	195.05	0.165	0.651	0.295	0.245	0.320	0.375
MS05-130	201.35	0.219	0.544	0.383	0.368	0.324	0.320
MS05-134	208.22	0.177	0.612	0.269	0.243	0.349	0.356
MS05-136c	211.3	0.218	0.635	0.332	0.318	0.322	0.332
MS05-138	213.52	0.243	0.601	0.519	0.534	0.254	0.239

Table 6.S1: Total biomarker and isotopic data from Meishan, China

				Hopanes			
sample name	depth	C29 Dia/Reg	C27 Dia/Reg	C31(R+S) Hopane/ C30Hopane	C29Hopane/ C30Hopane	Ts/Tm	Ts/(Ts+Tm)
MS05-140	7.05	0.203	0.350	0.749	0.913	0.503	0.335
MS05-150	20.14	0.243	0.452	0.785	0.979	0.524	0.344
MS05-160	24.5	0.343	0.476	0.870	0.883	0.743	0.426
MS05-165	31.05	0.229	0.310	0.839	1.347	0.590	0.371
MS05-168	35.06	0.183	0.277	0.747	0.922	0.458	0.314
MS05-170	39.56	0.347	0.361	0.824	0.745	0.186	0.157
MS05-175	46.79	0.326	0.459	0.692	0.736	0.699	0.411
MS05-177	54.23	0.667	0.872	0.805	0.771	0.472	0.321
MS05-180	61.77	0.393	0.544	0.764	0.696	0.405	0.288
MS05-183	68.57	0.274	0.544	0.831	0.850	0.631	0.387
MS05-185	74.38	0.384	0.427	0.954	0.686	0.154	0.133
MS05-187	77.44	0.355	0.403	0.717	0.815	0.094	0.086
MS05-191	82.07	0.358	0.436	0.725	0.745	0.093	0.085
MS05-193	84.66	0.412	0.359	15.526	0.000	0.293	0.227
MS05-195b	86.17	0.655	1.027	0.947	1.111	1.114	0.527
MS05-197	87.27	0.258	0.493	0.920	0.924	0.054	0.052
ms-1-39-1	87.77	0.389	0.430	0.811	0.957	0.134	0.118
ms-1-38-2	88.32	-	-	-	-	-	-
MS05-199	89.02	0.474	0.750	0.745	0.890	0.069	0.064
ms-1-37-5	89.53	-	-	-	-	-	-
MS05-200	89.71	0.737	0.975	0.615	0.576	0.815	0.449
MS37-3a	90.22	0.276	0.439	0.428	0.686	0.064	0.060
MS37-3b	90.23	0.643	0.872	0.664	0.641	0.880	0.468
ms-1-37-2	90.88	-	-	-	-	-	-
MS37-1	91.65	-	-	-	-	-	-
ms-1-36-3	92.61	-	-	-	-	-	-
ms-1-36-1	93.43	0.190	0.530	0.436	1.366	0.078	0.072
ms-1-35-2	94.28	0.150	0.369	0.482	1.136	0.044	0.042
ms-1-35-1	94.53	-	-	-	-	-	-
ms-1-34-12	97.55	0.265	0.524	0.410	1.367	0.083	0.076
MS34-10	98.73	0.180	0.279	0.747	0.886	0.036	0.034
ms-1-34-8	99.39	0.478	0.791	0.562	1.126	0.371	0.271
MS34-7	100.28	0.172	0.324	0.539	0.952	0.094	0.086
ms-1-34-5	101.63	0.399	0.640	0.341	1.445	0.072	0.067
ms-1-34-3	102.59	0.247	0.285	1.080	1.026	0.095	0.086
ms-1-34-1	103.93	-	-	-	-	-	-
ms-1-32-3	104.59	0.553	0.708	0.406	1.171	0.058	0.055
ms-1-32-1	105.09	0.337	0.753	0.478	1.155	0.036	0.035
ms-1-30-3	105.43	-	-	-	-	-	-
ms-1-29-2	105.93	-	-	-	-	-	-
ms-1-29-1	106.08	-	-	-	-	-	-
ms-1-27-3	106.16	0.267	0.371	0.592	1.086	0.051	0.049
ms-1-27-2	106.38	0.255	0.391	0.624	0.782	0.432	0.302
ms-1-27-1 p1	106.39	-	-	-	-	-	-
ms-1-27-1 p2	106.49	-	-	-	-	-	-
ms-1-26-3	106.52	-	-	-	-	-	-
ms-1-26-2	106.56	-	-	-	-	-	-
ms-1-26-1	106.6	-	-	-	-	-	-

Table 6.S1: Total biomarker and isotopic data from Meishan, China

				Hopanes			
sample name	depth	C29 Dia/Reg	C27 Dia/Reg	C31(R+S) Hopane/ C30Hopane	C29Hopane/ C30Hopane	Ts/Tm	Ts/(Ts+Tm)
ms-1-24-8	106.74	-	-	-	-	-	-
ms-1-24-2	107.1	-	-	-	-	-	-
ms-1-24-6	107.94	-	-	-	-	-	-
MS23-2a	108.2	0.236	0.290	1.019	1.000	0.671	0.402
ms-1-23-1	108.56	0.570	0.718	0.869	0.513	1.056	0.514
ms-1-23-4	109.4	-	-	-	-	-	-
ms-1-22-1	110.15	0.150	0.162	1.070	1.148	0.569	0.363
ms-1-22-3	111.04	-	-	-	-	-	-
MS05-02b	111.44	0.516	0.663	0.917	0.578	1.326	0.570
MS05-04	112.8	0.191	0.202	0.959	1.010	0.784	0.439
MS05-5	113.9	0.445	0.528	0.772	0.565	1.938	0.660
MS05-08	114.81	0.435	0.527	0.732	0.577	1.252	0.556
MS05-10	116.51	0.540	0.643	0.953	0.812	1.091	0.522
MS05-15	119.09	0.516	0.575	0.819	0.894	1.160	0.537
MS05-20	121.52	0.801	1.064	0.800	0.825	1.433	0.589
MS05-25	125.46	0.640	0.893	0.744	0.747	1.568	0.611
MS05-30	127.82	0.551	0.685	0.832	0.523	1.127	0.530
MS05-35	130.88	0.745	1.076	0.848	1.009	1.572	0.611
MS05-40	134.38	-	-	-	-	-	-
MS05-49	139.74	0.055	0.064	0.995	1.381	0.952	0.488
MS05-50	140.01	0.090	0.086	0.950	1.855	0.472	0.321
MS05-55	144.13	0.050	0.047	0.971	1.664	0.253	0.202
MS05-60	147.08	0.105	0.108	0.977	1.556	0.525	0.344
MS05-63	148.5	0.057	0.064	1.121	1.304	0.321	0.243
MS05-65	150.62	0.224	0.278	1.074	1.183	0.679	0.404
MS05-70	153.95	0.404	0.550	0.878	0.714	1.243	0.554
MS05-76	157.48	0.492	0.588	0.841	0.677	1.133	0.531
MS05-80	160.27	0.551	0.660	0.727	0.636	1.221	0.550
MS05-81	161.02	0.819	0.897	0.545	0.483	1.369	0.578
MS05-86	163.45	1.091	1.131	0.582	0.590	0.550	0.355
MS05-90	167.55	0.596	0.705	0.837	0.697	1.128	0.530
MS05-92b	169.24	0.416	0.502	0.909	0.631	1.015	0.504
MS05-95	170.59	0.736	0.890	0.780	0.501	1.809	0.644
MS05-100	174.5	0.938	0.955	0.387	0.517	0.876	0.467
MS05-105	178.3	1.129	1.269	0.518	0.426	1.478	0.596
MS05-107	179.8	0.634	0.697	0.709	0.669	0.736	0.424
MS05-112	183.02	0.546	0.619	0.781	0.782	0.082	0.075
MS05-115	185.3	0.355	0.408	0.882	0.956	0.050	0.048
MS05-117	186.91	0.342	0.409	0.856	0.832	0.044	0.042
MS05-120	189.05	0.270	0.349	0.772	0.992	0.029	0.029
MS05-125	195.05	0.202	0.241	0.764	0.947	0.031	0.030
MS05-130	201.35	0.434	0.660	0.719	0.926	0.089	0.082
MS05-134	208.22	0.190	0.263	0.673	0.937	0.035	0.033
MS05-136c	211.3	0.418	0.522	0.805	0.835	0.053	0.050
MS05-138	213.52	0.630	0.839	0.607	0.575	0.525	0.344

Table 6.S1: Total biomarker and isotopic data from Meishan, China

			Hopanes			
sample name	depth	29,30 dinorhopane/ C30 Hopane	28,30 dinorhopane/ C30 Hopane	28,30BNH/ 29,30BNH	C29Ts/C29 Hopane	C30-norhopane/ C30 Hopane
MS05-140	7.05	0.187	0.013	0.069	0.164	0.071
MS05-150	20.14	0.162	0.010	0.063	0.126	0.076
MS05-160	24.5	0.157	0.007	0.043	0.244	0.065
MS05-165	31.05	0.176	0.018	0.102	0.121	0.084
MS05-168	35.06	0.107	0.011	0.102	0.101	0.046
MS05-170	39.56	0.030	0.009	0.317	0.103	0.008
MS05-175	46.79	0.048	0.014	0.282	0.174	0.046
MS05-177	54.23	0.074	0.007	0.100	0.199	0.096
MS05-180	61.77	0.056	0.005	0.087	0.074	0.042
MS05-183	68.57	0.116	0.019	0.166	0.124	0.060
MS05-185	74.38	0.032	0.008	0.248	0.137	0.010
MS05-187	77.44	0.043	0.008	0.176	0.094	0.010
MS05-191	82.07	0.023	0.003	0.112	0.034	0.005
MS05-193	84.66	2.214	1.102	0.498	ND	38.133
MS05-195b	86.17	0.051	0.027	0.516	0.329	0.040
MS05-197	87.27	0.052	0.012	0.225	0.057	0.020
ms-1-39-1	87.77	0.053	0.027	0.516	0.059	0.025
ms-1-38-2	88.32	-	-	-	-	-
MS05-199	89.02	0.048	0.021	0.451	0.078	0.015
ms-1-37-5	89.53	-	-	-	-	-
MS05-200	89.71	0.011	0.003	0.302	0.347	0.005
MS37-3a	90.22	0.031	0.004	0.129	0.089	0.021
MS37-3b	90.23	0.012	0.004	0.294	0.413	0.037
ms-1-37-2	90.88	-	-	-	-	-
MS37-1	91.65	-	-	-	-	-
ms-1-36-3	92.61	-	-	-	-	-
ms-1-36-1	93.43	0.055	0.005	0.094	0.033	0.014
ms-1-35-2	94.28	0.043	0.004	0.083	0.026	0.016
ms-1-35-1	94.53	-	-	-	-	-
ms-1-34-12	97.55	0.070	0.007	0.096	0.066	0.000
MS34-10	98.73	0.024	0.003	0.125	0.041	0.021
ms-1-34-8	99.39	0.085	0.060	0.703	0.153	0.058
MS34-7	100.28	0.044	0.006	0.128	0.045	0.023
ms-1-34-5	101.63	0.081	0.016	0.197	0.064	0.000
ms-1-34-3	102.59	0.040	0.015	0.371	0.049	0.014
ms-1-34-1	103.93	-	-	-	-	-
ms-1-32-3	104.59	0.081	0.018	0.218	0.000	0.000
ms-1-32-1	105.09	0.054	0.010	0.179	0.034	0.021
ms-1-30-3	105.43	-	-	-	-	-
ms-1-29-2	105.93	-	-	-	-	-
ms-1-29-1	106.08	-	-	-	-	-
ms-1-27-3	106.16	0.059	0.011	0.186	0.072	0.076
ms-1-27-2	106.38	0.054	0.018	0.329	0.167	0.059
ms-1-27-1 p1	106.39	-	-	-	-	-
ms-1-27-1 p2	106.49	-	-	-	-	-
ms-1-26-3	106.52	-	-	-	-	-
ms-1-26-2	106.56	-	-	-	-	-
ms-1-26-1	106.6	-	-	-	-	-

Table 6.S1: Total biomarker and isotopic data from Meishan, China

			Hopanes			
sample name	depth	29,30 dinorhopane/ C30 Hopane	28,30 dinorhopane/ C30 Hopane	28,30BNH/ 29,30BNH	C29Ts/C29 Hopane	C30-norhopane/ C30 Hopane
ms-1-24-8	106.74	-	-	-	-	-
ms-1-24-2	107.1	-	-	-	-	-
ms-1-24-6	107.94	-	-	-	-	-
MS23-2a	108.2	0.087	0.008	0.097	0.225	0.088
ms-1-23-1	108.56	0.023	0.006	0.251	0.685	0.025
ms-1-23-4	109.4	-	-	-	-	-
ms-1-22-1	110.15	0.113	0.013	0.116	0.155	0.111
ms-1-22-3	111.04	-	-	-	-	-
MS05-02b	111.44	0.034	0.006	0.170	0.594	0.027
MS05-04	112.8	0.093	0.008	0.091	0.205	0.059
MS05-5	113.9	0.032	0.005	0.143	0.462	0.021
MS05-08	114.81	0.033	0.007	0.200	0.457	0.019
MS05-10	116.51	0.058	0.007	0.118	0.362	0.056
MS05-15	119.09	0.083	0.008	0.093	0.303	0.054
MS05-20	121.52	0.096	0.007	0.075	0.275	0.058
MS05-25	125.46	0.068	0.008	0.122	0.314	0.044
MS05-30	127.82	0.016	0.008	0.475	0.659	0.022
MS05-35	130.88	0.126	0.009	0.069	0.182	0.077
MS05-40	134.38	-	-	-	-	-
MS05-49	139.74	0.343	0.015	0.042	0.235	0.206
MS05-50	140.01	0.378	0.016	0.042	0.110	0.176
MS05-55	144.13	0.360	0.018	0.051	0.054	0.162
MS05-60	147.08	0.238	0.012	0.052	0.080	0.126
MS05-63	148.5	0.338	0.012	0.035	0.142	0.169
MS05-65	150.62	0.110	0.008	0.076	0.160	0.101
MS05-70	153.95	0.057	0.009	0.153	0.229	0.042
MS05-76	157.48	0.047	0.007	0.141	0.231	0.027
MS05-80	160.27	0.047	0.007	0.140	0.264	0.022
MS05-81	161.02	0.017	0.004	0.224	0.447	0.029
MS05-86	163.45	0.019	0.006	0.311	0.231	0.023
MS05-90	167.55	0.044	0.007	0.161	0.240	0.022
MS05-92b	169.24	0.043	0.009	0.198	0.269	0.033
MS05-95	170.59	0.031	0.006	0.207	0.509	0.043
MS05-100	174.5	0.008	0.005	0.666	0.253	0.018
MS05-105	178.3	0.005	0.006	1.182	0.537	0.022
MS05-107	179.8	0.034	0.012	0.349	0.220	0.045
MS05-112	183.02	0.024	0.011	0.466	0.066	0.020
MS05-115	185.3	0.032	0.010	0.297	0.030	0.010
MS05-117	186.91	0.028	0.010	0.375	0.034	0.020
MS05-120	189.05	0.032	0.008	0.261	0.019	0.010
MS05-125	195.05	0.033	0.005	0.142	0.007	0.008
MS05-130	201.35	0.040	0.009	0.233	0.039	0.017
MS05-134	208.22	0.033	0.000	0.008	0.029	0.015
MS05-136c	211.3	0.032	0.009	0.285	0.040	0.030
MS05-138	213.52	0.032	0.013	0.420	0.175	0.034

Table 6.S1: Total biomarker and isotopic data from Meishan, China

						Hopanes
sample name	depth	C31 2+3MeHopane/ C30 Hopane	C31 22S/S+R	C31 R homohopane/ C30 hopane	C31 2-Methyl/3-Methyl	Homohopane Index %
MS05-140	7.05	0.135	0.577	0.317	1.597	4.947
MS05-150	20.14	0.129	0.581	0.329	1.767	5.742
MS05-160	24.5	0.135	0.578	0.367	0.976	7.434
MS05-165	31.05	0.117	0.550	0.378	1.778	10.211
MS05-168	35.06	0.134	0.580	0.314	2.371	5.732
MS05-170	39.56	0.143	0.591	0.336	2.143	2.943
MS05-175	46.79	0.141	0.582	0.289	2.401	4.017
MS05-177	54.23	0.161	0.583	0.335	3.153	3.791
MS05-180	61.77	0.132	0.594	0.311	2.437	3.326
MS05-183	68.57	0.181	0.595	0.337	1.487	5.672
MS05-185	74.38	0.143	0.594	0.387	2.054	2.091
MS05-187	77.44	0.141	0.584	0.298	1.422	3.744
MS05-191	82.07	0.094	0.586	0.300	2.383	1.700
MS05-193	84.66	13.201	0.022	15.187	4.259	3.215
MS05-195b	86.17	0.150	0.629	0.351	2.067	5.566
MS05-197	87.27	0.150	0.589	0.378	1.816	3.926
ms-1-39-1	87.77	0.125	0.581	0.340	1.355	2.324
ms-1-38-2	88.32	-	-	-	-	-
MS05-199	89.02	0.116	0.593	0.303	1.920	4.021
ms-1-37-5	89.53	-	-	-	-	-
MS05-200	89.71	0.140	0.582	0.257	5.563	2.884
MS37-3a	90.22	0.071	0.587	0.177	2.605	2.171
MS37-3b	90.23	0.501	0.582	0.277	27.685	3.066
ms-1-37-2	90.88	-	-	-	-	-
MS37-1	91.65	-	-	-	-	-
ms-1-36-3	92.61	-	-	-	-	-
ms-1-36-1	93.43	0.147	0.579	0.183	5.919	0.781
ms-1-35-2	94.28	0.138	0.595	0.195	4.734	0.619
ms-1-35-1	94.53	-	-	-	-	-
ms-1-34-12	97.55	0.180	0.578	0.173	5.610	1.482
MS34-10	98.73	0.235	0.587	0.308	8.506	1.417
ms-1-34-8	99.39	0.103	0.578	0.237	2.213	3.630
MS34-7	100.28	0.163	0.574	0.230	3.172	3.235
ms-1-34-5	101.63	0.090	0.586	0.141	1.043	1.413
ms-1-34-3	102.59	0.061	0.584	0.450	0.123	1.370
ms-1-34-1	103.93	-	-	-	-	-
ms-1-32-3	104.59	0.118	0.589	0.167	1.178	1.806
ms-1-32-1	105.09	0.190	0.578	0.202	1.872	1.595
ms-1-30-3	105.43	-	-	-	-	-
ms-1-29-2	105.93	-	-	-	-	-
ms-1-29-1	106.08	-	-	-	-	-
ms-1-27-3	106.16	0.119	0.592	0.242	2.590	1.320
ms-1-27-2	106.38	0.062	0.589	0.256	0.869	1.729
ms-1-27-1 p1	106.39	-	-	-	-	-
ms-1-27-1 p2	106.49	-	-	-	-	-
ms-1-26-3	106.52	-	-	-	-	-
ms-1-26-2	106.56	-	-	-	-	-
ms-1-26-1	106.6	-	-	-	-	-

Table 6.S1: Total biomarker and isotopic data from Meishan, China

						Hopanes
sample name	depth	C31 2+3MeHopane/ C30 Hopane	C31 22S/S+R	C31 R homohopane/ C30 hopane	C31 2-Methyl/3-Methyl	Homohopane Index %
ms-1-24-8	106.74	-	-	-	-	-
ms-1-24-2	107.1	-	-	-	-	-
ms-1-24-6	107.94	-	-	-	-	-
MS23-2a	108.2	0.075	0.567	0.442	1.009	11.718
ms-1-23-1	108.56	0.134	0.590	0.357	0.568	7.974
ms-1-23-4	109.4	-	-	-	-	-
ms-1-22-1	110.15	0.070	0.559	0.472	1.157	12.036
ms-1-22-3	111.04	-	-	-	-	-
MS05-02b	111.44	0.142	0.590	0.376	0.560	7.975
MS05-04	112.8	0.072	0.564	0.418	0.989	11.224
MS05-5	113.9	0.091	0.588	0.318	0.699	7.443
MS05-08	114.81	0.120	0.587	0.303	0.554	8.626
MS05-10	116.51	0.127	0.583	0.397	0.788	11.856
MS05-15	119.09	0.099	0.577	0.346	0.833	9.651
MS05-20	121.52	0.127	0.577	0.338	0.895	10.030
MS05-25	125.46	0.156	0.572	0.319	0.781	9.871
MS05-30	127.82	0.127	0.588	0.343	0.618	8.451
MS05-35	130.88	0.142	0.567	0.367	0.836	12.135
MS05-40	134.38	-	-	-	-	-
MS05-49	139.74	0.116	0.541	0.457	1.995	11.894
MS05-50	140.01	0.091	0.533	0.444	1.729	14.159
MS05-55	144.13	0.062	0.542	0.444	1.308	13.118
MS05-60	147.08	0.061	0.557	0.433	1.266	13.084
MS05-63	148.5	0.042	0.561	0.492	1.241	10.954
MS05-65	150.62	0.056	0.580	0.451	0.835	14.465
MS05-70	153.95	0.121	0.583	0.366	0.955	7.160
MS05-76	157.48	0.167	0.585	0.349	0.877	6.198
MS05-80	160.27	0.146	0.587	0.300	0.647	5.039
MS05-81	161.02	0.125	0.594	0.221	0.864	5.876
MS05-86	163.45	0.152	0.579	0.245	1.237	6.075
MS05-90	167.55	0.161	0.585	0.347	0.804	5.535
MS05-92b	169.24	0.136	0.582	0.381	0.776	6.833
MS05-95	170.59	0.144	0.592	0.319	0.577	5.332
MS05-100	174.5	0.122	0.582	0.162	1.912	0.105
MS05-105	178.3	0.073	0.569	0.223	2.024	7.140
MS05-107	179.8	0.107	0.571	0.304	0.930	6.281
MS05-112	183.02	0.104	0.583	0.325	1.651	2.910
MS05-115	185.3	0.097	0.585	0.366	0.577	2.224
MS05-117	186.91	0.093	0.582	0.358	0.540	2.443
MS05-120	189.05	0.080	0.585	0.320	0.660	1.947
MS05-125	195.05	0.092	0.581	0.320	0.415	1.500
MS05-130	201.35	0.112	0.572	0.308	0.512	4.681
MS05-134	208.22	0.102	0.590	0.276	0.562	1.576
MS05-136c	211.3	0.103	0.584	0.335	0.567	2.550
MS05-138	213.52	0.077	0.571	0.260	2.503	4.889

Table 6.S1: Total biomarker and isotopic data from Meishan, China

sample name	depth	C35(S+R)/ C34(S+R)	C35S/C34S homohopane	C31 22S/(S+R)	C32 22S/(S+R)	C33 22S/(S+R)	C34 22S/(S+R)
MS05-140	7.05	0.621	0.631	0.577	0.576	0.588	0.593
MS05-150	20.14	0.607	0.592	0.581	0.607	0.607	0.606
MS05-160	24.5	0.745	0.719	0.578	0.591	0.588	0.627
MS05-165	31.05	1.030	1.070	0.550	0.571	0.606	0.585
MS05-168	35.06	0.627	0.668	0.580	0.587	0.591	0.599
MS05-170	39.56	0.491	0.464	0.591	0.571	0.596	0.598
MS05-175	46.79	0.560	0.582	0.582	0.586	0.599	0.594
MS05-177	54.23	0.522	0.495	0.583	0.608	0.600	0.609
MS05-180	61.77	0.469	0.470	0.594	0.591	0.592	0.607
MS05-183	68.57	0.751	0.695	0.595	0.589	0.592	0.616
MS05-185	74.38	0.388	0.373	0.594	0.590	0.593	0.614
MS05-187	77.44	0.651	0.528	0.584	0.562	0.609	0.588
MS05-191	82.07	0.349	0.336	0.586	0.574	0.584	0.610
MS05-193	84.66	0.410	0.411	0.022	0.429	0.653	0.594
MS05-195b	86.17	0.731	0.717	0.629	0.601	0.618	0.645
MS05-197	87.27	0.760	0.738	0.589	0.596	0.589	0.626
ms-1-39-1	87.77	0.554	0.537	0.581	0.581	0.575	0.612
ms-1-38-2	88.32	-	-	-	-	-	-
MS05-199	89.02	0.731	0.707	0.593	0.555	0.587	0.624
ms-1-37-5	89.53	-	-	-	-	-	-
MS05-200	89.71	0.411	0.403	0.582	0.570	0.582	0.615
MS37-3a	90.22	0.525	0.490	0.587	0.570	0.579	0.621
MS37-3b	90.23	0.431	0.422	0.582	0.574	0.581	0.610
ms-1-37-2	90.88	-	-	-	-	-	-
MS37-1	91.65	-	-	-	-	-	-
ms-1-36-3	92.61	-	-	-	-	-	-
ms-1-36-1	93.43	0.392	0.370	0.579	0.576	0.592	0.605
ms-1-35-2	94.28	0.331	0.297	0.595	0.585	0.599	0.622
ms-1-35-1	94.53	-	-	-	-	-	-
ms-1-34-12	97.55	0.619	0.645	0.578	0.591	0.618	0.657
MS34-10	98.73	0.360	0.334	0.587	0.578	0.579	0.601
ms-1-34-8	99.39	0.756	1.113	0.578	0.590	0.537	0.553
MS34-7	100.28	0.778	0.754	0.574	0.576	0.584	0.596
ms-1-34-5	101.63	0.556	0.699	0.586	0.573	0.612	0.607
ms-1-34-3	102.59	0.374	0.364	0.584	0.581	0.589	0.608
ms-1-34-1	103.93	-	-	-	-	-	-
ms-1-32-3	104.59	0.644	0.573	0.589	0.617	0.644	0.708
ms-1-32-1	105.09	0.544	0.514	0.578	0.586	0.590	0.616
ms-1-30-3	105.43	-	-	-	-	-	-
ms-1-29-2	105.93	-	-	-	-	-	-
ms-1-29-1	106.08	-	-	-	-	-	-
ms-1-27-3	106.16	0.456	0.403	0.592	0.601	0.611	0.646
ms-1-27-2	106.38	0.439	0.462	0.589	0.587	0.582	0.599
ms-1-27-1 p1	106.39	-	-	-	-	-	-
ms-1-27-1 p2	106.49	-	-	-	-	-	-
ms-1-26-3	106.52	-	-	-	-	-	-
ms-1-26-2	106.56	-	-	-	-	-	-
ms-1-26-1	106.6	-	-	-	-	-	-

Table 6.S1: Total biomarker and isotopic data from Meishan, China

sample name	depth	C35(S+R)/ C34(S+R)	C35S/C34S homohopane	C31 22S/(S+R)	C32 22S/(S+R)	C33 22S/(S+R)	C34 22S/(S+R)
ms-1-24-8	106.74	-	-	-	-	-	-
ms-1-24-2	107.1	-	-	-	-	-	-
ms-1-24-6	107.94	-	-	-	-	-	-
MS23-2a	108.2	1.192	1.206	0.567	0.587	0.593	0.619
ms-1-23-1	108.56	0.863	0.845	0.590	0.584	0.592	0.619
ms-1-23-4	109.4	-	-	-	-	-	-
ms-1-22-1	110.15	1.214	1.245	0.559	0.590	0.592	0.606
ms-1-22-3	111.04	-	-	-	-	-	-
MS05-02b	111.44	0.793	0.810	0.590	0.586	0.591	0.596
MS05-04	112.8	1.145	1.166	0.564	0.589	0.593	0.616
MS05-5	113.9	0.738	0.728	0.588	0.591	0.590	0.624
MS05-08	114.81	0.869	0.842	0.587	0.589	0.592	0.626
MS05-10	116.51	1.081	1.086	0.583	0.583	0.598	0.612
MS05-15	119.09	0.997	0.988	0.577	0.593	0.602	0.618
MS05-20	121.52	0.896	0.908	0.577	0.587	0.596	0.606
MS05-25	125.46	0.993	1.010	0.572	0.576	0.588	0.605
MS05-30	127.82	0.828	0.829	0.588	0.586	0.576	0.612
MS05-35	130.88	1.108	1.065	0.567	0.597	0.599	0.617
MS05-40	134.38	-	-	-	-	-	-
MS05-49	139.74	1.224	1.153	0.541	0.597	0.597	0.621
MS05-50	140.01	1.348	1.339	0.533	0.584	0.598	0.614
MS05-55	144.13	1.326	1.237	0.542	0.601	0.597	0.620
MS05-60	147.08	1.269	1.271	0.557	0.587	0.599	0.609
MS05-63	148.5	1.130	1.113	0.561	0.605	0.602	0.596
MS05-65	150.62	1.319	1.343	0.580	0.606	0.597	0.614
MS05-70	153.95	0.826	0.834	0.583	0.592	0.600	0.607
MS05-76	157.48	0.730	0.742	0.585	0.600	0.595	0.616
MS05-80	160.27	0.582	0.578	0.587	0.592	0.599	0.620
MS05-81	161.02	0.657	0.649	0.594	0.591	0.596	0.623
MS05-86	163.45	0.609	0.600	0.579	0.583	0.587	0.613
MS05-90	167.55	0.730	0.717	0.585	0.594	0.595	0.624
MS05-92b	169.24	0.732	0.723	0.582	0.597	0.597	0.615
MS05-95	170.59	0.652	0.643	0.592	0.590	0.603	0.614
MS05-100	174.5	0.026	0.014	0.582	0.580	0.586	0.961
MS05-105	178.3	0.651	0.650	0.569	0.572	0.577	0.610
MS05-107	179.8	0.684	0.664	0.571	0.570	0.600	0.603
MS05-112	183.02	0.425	0.408	0.583	0.584	0.588	0.609
MS05-115	185.3	0.391	0.379	0.585	0.584	0.574	0.605
MS05-117	186.91	0.401	0.388	0.582	0.580	0.583	0.603
MS05-120	189.05	0.393	0.377	0.585	0.582	0.598	0.605
MS05-125	195.05	0.365	0.358	0.581	0.574	0.570	0.605
MS05-130	201.35	0.749	0.749	0.572	0.583	0.572	0.580
MS05-134	208.22	0.405	0.360	0.590	0.587	0.587	0.613
MS05-136c	211.3	0.455	0.425	0.584	0.590	0.592	0.602
MS05-138	213.52	0.606	0.576	0.571	0.591	0.595	0.620

Table 6.S1: Total biomarker and isotopic data from Meishan, China

			Hopanes			
sample name	depth	C35 22S/(S+R)	C31(R+S) Hopane/ C29Hopane	C32(R+S) Hopane/ C29Hopane	C33(R+S) Hopane/ C29Hopane	C34(R+S) Hopane/ C29Hopane
MS05-140	7.05	0.603	0.821	0.503	0.262	0.145
MS05-150	20.14	0.591	0.802	0.495	0.261	0.174
MS05-160	24.5	0.605	0.985	0.617	0.333	0.234
MS05-165	31.05	0.608	0.623	0.363	0.256	0.154
MS05-168	35.06	0.638	0.810	0.436	0.259	0.162
MS05-170	39.56	0.564	1.106	0.491	0.246	0.121
MS05-175	46.79	0.618	0.940	0.512	0.263	0.138
MS05-177	54.23	0.577	1.044	0.494	0.257	0.147
MS05-180	61.77	0.608	1.097	0.538	0.275	0.151
MS05-183	68.57	0.570	0.977	0.543	0.302	0.159
MS05-185	74.38	0.591	1.390	0.603	0.281	0.133
MS05-187	77.44	0.477	0.879	0.363	0.173	0.090
MS05-191	82.07	0.586	0.972	0.392	0.161	0.079
MS05-193	84.66	0.596	ND	ND	ND	ND
MS05-195b	86.17	0.632	0.852	0.471	0.244	0.137
MS05-197	87.27	0.608	0.996	0.407	0.197	0.091
ms-1-39-1	87.77	0.594	0.848	0.289	0.124	0.057
ms-1-38-2	88.32	-	-	-	-	-
MS05-199	89.02	0.604	0.837	0.407	0.164	0.086
ms-1-37-5	89.53	-	-	-	-	-
MS05-200	89.71	0.604	1.068	0.569	0.276	0.149
MS37-3a	90.22	0.580	0.624	0.285	0.097	0.044
MS37-3b	90.23	0.597	1.036	0.570	0.306	0.152
ms-1-37-2	90.88	-	-	-	-	-
MS37-1	91.65	-	-	-	-	-
ms-1-36-3	92.61	-	-	-	-	-
ms-1-36-1	93.43	0.572	0.319	0.096	0.027	0.009
ms-1-35-2	94.28	0.558	0.424	0.122	0.034	0.011
ms-1-35-1	94.53	-	-	-	-	-
ms-1-34-12	97.55	0.685	0.300	0.100	0.033	0.011
MS34-10	98.73	0.557	0.843	0.348	0.128	0.055
ms-1-34-8	99.39	0.815	0.499	0.243	0.110	0.045
MS34-7	100.28	0.577	0.566	0.238	0.091	0.040
ms-1-34-5	101.63	0.763	0.236	0.081	0.026	0.009
ms-1-34-3	102.59	0.592	1.052	0.388	0.144	0.061
ms-1-34-1	103.93	-	-	-	-	-
ms-1-32-3	104.59	0.630	0.346	0.141	0.044	0.016
ms-1-32-1	105.09	0.583	0.414	0.136	0.044	0.018
ms-1-30-3	105.43	-	-	-	-	-
ms-1-29-2	105.93	-	-	-	-	-
ms-1-29-1	106.08	-	-	-	-	-
ms-1-27-3	106.16	0.571	0.545	0.173	0.057	0.023
ms-1-27-2	106.38	0.631	0.797	0.375	0.141	0.055
ms-1-27-1 p1	106.39	-	-	-	-	-
ms-1-27-1 p2	106.49	-	-	-	-	-
ms-1-26-3	106.52	-	-	-	-	-
ms-1-26-2	106.56	-	-	-	-	-
ms-1-26-1	106.6	-	-	-	-	-

Table 6.S1: Total biomarker and isotopic data from Meishan, China

			Hopanes			
sample name	depth	C35 22S/(S+R)	C31(R+S) Hopane/ C29Hopane	C32(R+S) Hopane/ C29Hopane	C33(R+S) Hopane/ C29Hopane	C34(R+S) Hopane/ C29Hopane
ms-1-24-8	106.74	-	-	-	-	-
ms-1-24-2	107.1	-	-	-	-	-
ms-1-24-6	107.94	-	-	-	-	-
MS23-2a	108.2	0.626	1.019	0.664	0.496	0.273
ms-1-23-1	108.56	0.606	1.695	1.095	0.564	0.374
ms-1-23-4	109.4	-	-	-	-	-
ms-1-22-1	110.15	0.621	0.932	0.618	0.473	0.257
ms-1-22-3	111.04	-	-	-	-	-
MS05-02b	111.44	0.609	1.587	1.026	0.534	0.386
MS05-04	112.8	0.627	0.950	0.621	0.446	0.250
MS05-5	113.9	0.615	1.367	0.860	0.421	0.324
MS05-08	114.81	0.607	1.269	0.824	0.424	0.307
MS05-10	116.51	0.616	1.174	0.801	0.544	0.358
MS05-15	119.09	0.612	0.916	0.608	0.355	0.225
MS05-20	121.52	0.615	0.970	0.650	0.369	0.283
MS05-25	125.46	0.615	0.996	0.692	0.372	0.255
MS05-30	127.82	0.612	1.591	1.059	0.532	0.399
MS05-35	130.88	0.594	0.840	0.583	0.366	0.255
MS05-40	134.38	-	-	-	-	-
MS05-49	139.74	0.585	0.720	0.425	0.339	0.184
MS05-50	140.01	0.610	0.512	0.299	0.264	0.150
MS05-55	144.13	0.578	0.583	0.346	0.302	0.158
MS05-60	147.08	0.610	0.628	0.384	0.307	0.177
MS05-63	148.5	0.588	0.859	0.535	0.427	0.222
MS05-65	150.62	0.626	0.907	0.619	0.538	0.304
MS05-70	153.95	0.612	1.230	0.764	0.389	0.245
MS05-76	157.48	0.626	1.242	0.812	0.390	0.243
MS05-80	160.27	0.614	1.143	0.714	0.337	0.220
MS05-81	161.02	0.615	1.128	0.727	0.373	0.234
MS05-86	163.45	0.603	0.986	0.574	0.322	0.223
MS05-90	167.55	0.613	1.201	0.744	0.340	0.199
MS05-92b	169.24	0.607	1.441	0.932	0.466	0.316
MS05-95	170.59	0.605	1.556	1.043	0.474	0.290
MS05-100	174.5	0.522	0.747	0.436	0.254	0.060
MS05-105	178.3	0.610	1.216	0.754	0.527	0.335
MS05-107	179.8	0.585	1.060	0.716	0.392	0.235
MS05-112	183.02	0.584	0.998	0.570	0.238	0.137
MS05-115	185.3	0.587	0.923	0.493	0.177	0.098
MS05-117	186.91	0.584	1.029	0.512	0.199	0.116
MS05-120	189.05	0.580	0.778	0.394	0.133	0.069
MS05-125	195.05	0.592	0.806	0.367	0.118	0.056
MS05-130	201.35	0.581	0.777	0.392	0.162	0.093
MS05-134	208.22	0.546	0.718	0.327	0.107	0.047
MS05-136c	211.3	0.562	0.964	0.572	0.195	0.106
MS05-138	213.52	0.589	1.055	1.069	0.409	0.235

Table 6.S1: Total biomarker and isotopic data from Meishan, China

						Hopanes
sample name	depth	C35(R+S) Hopane/ C29Hopane	gamma/ C30H	2aMeC31H/ (C30H+2aMe C31H)%	3bMeC31H/ (C30H+3bMe C31H)%	C31 2aMe H/ (C31 2+3Me H)
MS05-140	7.05	0.090	0.113	0.077	0.049	0.615
MS05-150	20.14	0.106	0.029	0.076	0.045	0.639
MS05-160	24.5	0.174	0.042	0.063	0.064	0.494
MS05-165	31.05	0.159	0.071	0.070	0.040	0.640
MS05-168	35.06	0.101	0.051	0.086	0.038	0.703
MS05-170	39.56	0.060	0.049	0.089	0.044	0.682
MS05-175	46.79	0.078	0.051	0.091	0.040	0.706
MS05-177	54.23	0.077	0.010	0.109	0.037	0.759
MS05-180	61.77	0.071	0.032	0.086	0.037	0.709
MS05-183	68.57	0.119	0.031	0.098	0.068	0.598
MS05-185	74.38	0.051	0.034	0.088	0.045	0.673
MS05-187	77.44	0.059	0.026	0.076	0.055	0.587
MS05-191	82.07	0.028	0.031	0.062	0.027	0.704
MS05-193	84.66	ND	13.153	0.914	0.715	0.810
MS05-195b	86.17	0.100	0.135	0.092	0.046	0.674
MS05-197	87.27	0.069	0.026	0.088	0.051	0.645
ms-1-39-1	87.77	0.031	0.038	0.067	0.050	0.575
ms-1-38-2	88.32	-	-	-	-	-
MS05-199	89.02	0.063	0.028	0.071	0.038	0.658
ms-1-37-5	89.53	-	-	-	-	-
MS05-200	89.71	0.061	0.031	0.106	0.021	0.848
MS37-3a	90.22	0.023	0.023	0.049	0.019	0.723
MS37-3b	90.23	0.065	0.044	0.326	0.017	0.965
ms-1-37-2	90.88	-	-	-	-	-
MS37-1	91.65	-	-	-	-	-
ms-1-36-3	92.61	-	-	-	-	-
ms-1-36-1	93.43	0.004	0.032	0.111	0.021	0.855
ms-1-35-2	94.28	0.004	0.020	0.102	0.024	0.826
ms-1-35-1	94.53	-	-	-	-	-
ms-1-34-12	97.55	0.007	0.069	0.133	0.027	0.849
MS34-10	98.73	0.020	0.015	0.174	0.024	0.895
ms-1-34-8	99.39	0.034	0.068	0.066	0.031	0.689
MS34-7	100.28	0.031	0.044	0.110	0.038	0.760
ms-1-34-5	101.63	0.005	0.058	0.044	0.042	0.510
ms-1-34-3	102.59	0.023	0.156	0.007	0.052	0.110
ms-1-34-1	103.93	-	-	-	-	-
ms-1-32-3	104.59	0.010	0.026	0.060	0.052	0.541
ms-1-32-1	105.09	0.010	0.030	0.110	0.062	0.652
ms-1-30-3	105.43	-	-	-	-	-
ms-1-29-2	105.93	-	-	-	-	-
ms-1-29-1	106.08	-	-	-	-	-
ms-1-27-3	106.16	0.011	0.019	0.079	0.032	0.721
ms-1-27-2	106.38	0.024	0.083	0.028	0.032	0.465
ms-1-27-1 p1	106.39	-	-	-	-	-
ms-1-27-1 p2	106.49	-	-	-	-	-
ms-1-26-3	106.52	-	-	-	-	-
ms-1-26-2	106.56	-	-	-	-	-
ms-1-26-1	106.6	-	-	-	-	-

Table 6.S1: Total biomarker and isotopic data from Meishan, China

						Hopanes
sample name	depth	C35(R+S) Hopane/ C29Hopane	gamma/ C30H	2aMeC31H/ (C30H+2aMe C31H)%	3bMeC31H/ (C30H+3bMe C31H)%	C31 2aMe H/ (C31 2+3Me H)
ms-1-24-8	106.74	-	-	-	-	-
ms-1-24-2	107.1	-	-	-	-	-
ms-1-24-6	107.94	-	-	-	-	-
MS23-2a	108.2	0.325	0.061	0.036	0.036	0.502
ms-1-23-1	108.56	0.323	0.038	0.046	0.079	0.362
ms-1-23-4	109.4	-	-	-	-	-
ms-1-22-1	110.15	0.312	0.055	0.036	0.032	0.536
ms-1-22-3	111.04	-	-	-	-	-
MS05-02b	111.44	0.306	0.027	0.049	0.084	0.359
MS05-04	112.8	0.287	0.053	0.035	0.035	0.497
MS05-5	113.9	0.239	0.038	0.036	0.051	0.411
MS05-08	114.81	0.267	0.030	0.041	0.072	0.356
MS05-10	116.51	0.387	0.040	0.053	0.066	0.441
MS05-15	119.09	0.225	0.041	0.043	0.051	0.455
MS05-20	121.52	0.253	0.029	0.056	0.063	0.472
MS05-25	125.46	0.254	0.047	0.064	0.081	0.439
MS05-30	127.82	0.331	0.047	0.046	0.073	0.382
MS05-35	130.88	0.282	0.021	0.061	0.072	0.455
MS05-40	134.38	-	-	-	-	-
MS05-49	139.74	0.225	0.100	0.072	0.037	0.666
MS05-50	140.01	0.202	0.081	0.054	0.032	0.634
MS05-55	144.13	0.210	0.068	0.034	0.026	0.567
MS05-60	147.08	0.225	0.052	0.033	0.026	0.559
MS05-63	148.5	0.251	0.039	0.023	0.019	0.554
MS05-65	150.62	0.400	0.024	0.025	0.029	0.455
MS05-70	153.95	0.203	0.029	0.056	0.058	0.489
MS05-76	157.48	0.178	0.014	0.072	0.082	0.467
MS05-80	160.27	0.128	0.019	0.054	0.081	0.393
MS05-81	161.02	0.154	0.012	0.055	0.063	0.463
MS05-86	163.45	0.136	0.017	0.077	0.064	0.553
MS05-90	167.55	0.146	0.018	0.067	0.082	0.446
MS05-92b	169.24	0.231	0.017	0.056	0.071	0.437
MS05-95	170.59	0.189	0.012	0.050	0.084	0.366
MS05-100	174.5	0.002	0.014	0.074	0.040	0.657
MS05-105	178.3	0.218	0.023	0.047	0.024	0.669
MS05-107	179.8	0.161	0.060	0.049	0.053	0.482
MS05-112	183.02	0.058	0.015	0.061	0.038	0.623
MS05-115	185.3	0.038	0.019	0.034	0.058	0.366
MS05-117	186.91	0.046	0.011	0.031	0.057	0.351
MS05-120	189.05	0.027	0.012	0.031	0.046	0.398
MS05-125	195.05	0.021	0.011	0.026	0.061	0.293
MS05-130	201.35	0.070	0.026	0.037	0.069	0.339
MS05-134	208.22	0.019	0.013	0.035	0.061	0.360
MS05-136c	211.3	0.048	0.014	0.036	0.061	0.362
MS05-138	213.52	0.142	0.014	0.052	0.022	0.715

Table 6.S1: Total biomarker and isotopic data from Meishan, China

sample name	depth	C32 2a-MeH/ C32 3b-MeH	C33 2a-MeH/ C33 3b-MeH	C34 2a-MeH/ C34 3b-MeH	C35 2a-MeH/ C35 3b-MeH	C36 2a-MeH/ C36 3b-MeH
MS05-140	7.05	2.704	2.292	2.322	1.973	1.289
MS05-150	20.14	2.604	2.226	2.453	1.663	1.497
MS05-160	24.5	1.355	1.177	1.072	1.022	1.040
MS05-165	31.05	2.536	2.442	2.397	1.555	1.129
MS05-168	35.06	2.340	2.451	1.741	1.070	2.797
MS05-170	39.56	2.688	1.937	2.545	2.111	2.370
MS05-175	46.79	3.081	2.383	2.755	4.185	1.471
MS05-177	54.23	3.328	3.266	2.717	2.818	3.301
MS05-180	61.77	3.167	2.260	2.650	2.371	1.991
MS05-183	68.57	2.221	2.511	1.945	1.216	1.074
MS05-185	74.38	2.877	2.493	2.363	2.398	2.558
MS05-187	77.44	1.688	1.083	1.340	1.102	0.825
MS05-191	82.07	3.545	2.484	2.293	2.286	3.079
MS05-193	84.66	0.900	1.538	1.641	1.504	1.664
MS05-195b	86.17	5.894	4.698	4.991	3.405	2.312
MS05-197	87.27	2.474	1.746	1.553	1.459	1.267
ms-1-39-1	87.77	2.037	1.614	1.615	1.979	1.414
ms-1-38-2	88.32	-	-	-	-	-
MS05-199	89.02	2.750	2.455	3.256	3.145	1.843
ms-1-37-5	89.53	-	-	-	-	-
MS05-200	89.71	14.749	9.116	7.169	6.019	5.304
MS37-3a	90.22	3.789	2.627	2.257	2.446	2.930
MS37-3b	90.23	111.951	51.003	32.632	21.312	41.170
ms-1-37-2	90.88	-	-	-	-	-
MS37-1	91.65	-	-	-	-	-
ms-1-36-3	92.61	-	-	-	-	-
ms-1-36-1	93.43	7.500	4.983	3.746	4.420	2.946
ms-1-35-2	94.28	6.745	4.581	4.114	4.851	4.270
ms-1-35-1	94.53	-	-	-	-	-
ms-1-34-12	97.55	8.041	7.068	5.265	6.358	2.467
MS34-10	98.73	13.136	9.067	10.354	9.406	9.831
ms-1-34-8	99.39	4.230	2.262	3.691	1.898	1.722
MS34-7	100.28	4.967	3.592	3.097	2.916	2.260
ms-1-34-5	101.63	1.774	1.912	3.408	3.010	0.801
ms-1-34-3	102.59	0.282	0.196	0.217	0.277	0.302
ms-1-34-1	103.93	-	-	-	-	-
ms-1-32-3	104.59	1.818	1.322	2.244	2.982	1.040
ms-1-32-1	105.09	2.579	2.017	1.704	2.936	2.298
ms-1-30-3	105.43	-	-	-	-	-
ms-1-29-2	105.93	-	-	-	-	-
ms-1-29-1	106.08	-	-	-	-	-
ms-1-27-3	106.16	4.469	2.893	5.189	4.951	1.186
ms-1-27-2	106.38	1.822	1.342	2.039	1.271	1.727
ms-1-27-1 p1	106.39	-	-	-	-	-
ms-1-27-1 p2	106.49	-	-	-	-	-
ms-1-26-3	106.52	-	-	-	-	-
ms-1-26-2	106.56	-	-	-	-	-
ms-1-26-1	106.6	-	-	-	-	-

Table 6.S1: Total biomarker and isotopic data from Meishan, China

sample name	depth	C32 2a-MeH/ C32 3b-MeH	C33 2a-MeH/ C33 3b-MeH	C34 2a-MeH/ C34 3b-MeH	C35 2a-MeH/ C35 3b-MeH	C36 2a-MeH/ C36 3b-MeH
ms-1-24-8	106.74	-	-	-	-	-
ms-1-24-2	107.1	-	-	-	-	-
ms-1-24-6	107.94	-	-	-	-	-
MS23-2a	108.2	1.822	1.643	1.852	1.100	1.033
ms-1-23-1	108.56	0.742	0.705	0.588	0.565	0.487
ms-1-23-4	109.4	-	-	-	-	-
ms-1-22-1	110.15	2.309	1.938	2.205	1.165	1.220
ms-1-22-3	111.04	-	-	-	-	-
MS05-02b	111.44	0.648	0.647	0.570	0.572	0.539
MS05-04	112.8	1.688	1.509	1.543	1.005	0.892
MS05-5	113.9	0.823	0.860	0.783	0.727	0.689
MS05-08	114.81	0.638	0.635	0.557	0.531	0.463
MS05-10	116.51	1.037	1.001	0.992	0.672	0.657
MS05-15	119.09	1.040	1.089	0.983	0.791	0.644
MS05-20	121.52	0.976	1.025	0.848	0.688	0.595
MS05-25	125.46	0.904	0.950	0.699	0.608	0.447
MS05-30	127.82	0.800	0.834	0.732	0.696	0.644
MS05-35	130.88	1.152	1.114	0.804	0.764	0.581
MS05-40	134.38	-	-	-	-	-
MS05-49	139.74	3.848	3.519	3.165	2.034	1.836
MS05-50	140.01	3.011	2.728	2.420	1.419	1.288
MS05-55	144.13	2.529	2.330	2.060	1.110	1.118
MS05-60	147.08	2.014	1.863	1.872	1.042	0.914
MS05-63	148.5	2.405	2.060	2.134	1.268	1.279
MS05-65	150.62	1.371	1.270	1.269	0.802	0.673
MS05-70	153.95	1.030	1.062	0.990	0.790	0.548
MS05-76	157.48	0.863	0.869	0.729	0.690	0.546
MS05-80	160.27	0.747	0.759	0.677	0.665	0.642
MS05-81	161.02	0.936	0.858	0.832	0.649	0.647
MS05-86	163.45	1.407	1.149	1.182	1.031	0.831
MS05-90	167.55	0.779	0.842	0.709	0.698	0.560
MS05-92b	169.24	0.834	0.878	0.882	0.751	0.629
MS05-95	170.59	0.621	0.662	0.595	0.481	0.466
MS05-100	174.5	2.148	1.947	15.974	20.716	12.634
MS05-105	178.3	2.925	2.126	2.644	2.053	2.021
MS05-107	179.8	1.312	1.070	1.478	1.000	1.395
MS05-112	183.02	2.095	1.231	2.330	1.933	2.171
MS05-115	185.3	0.884	0.510	1.007	0.911	1.074
MS05-117	186.91	0.794	0.537	0.924	0.854	0.728
MS05-120	189.05	1.030	0.580	1.125	1.034	1.263
MS05-125	195.05	0.663	0.436	0.747	0.745	0.785
MS05-130	201.35	0.825	0.780	1.393	1.185	1.110
MS05-134	208.22	0.885	0.627	0.922	0.903	1.007
MS05-136c	211.3	0.935	0.561	1.134	0.782	0.945
MS05-138	213.52	3.054	1.058	3.317	7.123	2.044

Chapter 7

Global Patterns in Biomarkers and Isotopes at the Permian-Triassic Boundary

Abstract

The Permian-Triassic boundary extinction, the largest in the Phanerozoic, has been the subject of many studies, yet the causes of this event remain controversial. Long-term ocean anoxia and massive trap volcanism are two trigger mechanisms, in combination, that best agree with current observations. Hydrocarbon biomarkers were measured from marine sedimentary rocks in Peace River, Canada; Kap Stosch, Greenland; the Great Bank of Guizhou, China; and Meishan, China locations and are compared to previously reported sections to provide insight into global ocean conditions at the Permian-Triassic boundary. Although a suite of biomarkers was measured at each of these locations, only four are compared here for their worldwide distribution: the ratio of C_{33} *n*-alkylcyclohexane to *n*-C_{34}, carotenoid derivatives from Chlorobi, the hopane/sterane ratio and the parameter $\Delta\delta$, a measure of the difference between the $\delta^{13}C$ values of the *n*-alkanes *n*-C_{17} and *n*-C_{18} and the isoprenoids pristane and phytane. The first biomarker proxy, an abundance of C_{33} *n*-ACH, is a potential age marker for the boundary and was identified in the Kap Stosch and Peace River sections from sedimentary rocks at and immediately following the identified Permian-Triassic transition. Carotenoid derivatives from Chlorobi were identified in sedimentary rocks from all sections. Hopane/sterane ratios higher than the average for the Phanerozoic were measured in the Peace River, Kap Stosch and Meishan sections. Anomalously high values of $\Delta\delta$ were measured in

the Peace River and Meishan sections. Together, these last three parameters indicate global marine conditions dominated by bacterial inputs where photic zone euxinia was prevalent for extended time periods. An intermittent shoaling of the chemocline, as suggested by $\Delta\delta$ values and carotenoid derivatives from anoxygenic phototrophic bacteria other than Chlorobi, may have brought euxinia higher in the photic zone, and the biomarker patterns observed here indicate a correlation with the main pulse of extinction.

Extinction at the Permian-Triassic Boundary

The causes and duration of the Permian-Triassic boundary event, the largest extinction in the Phanerozoic, remain controversial (Erwin 2006). Evidence from the terrestrial and marine realms suggests that although ecosystem disruption extended over millions of years, the major species loss was relatively sudden (Bowring et al. 1999; Jin et al. 2000; Ward et al. 2005). At the Global Stratotype Section and Point in Meishan, the defining section of the boundary, the extinction occurred on the relatively short timescale of thousands of years (Cao et al. 2009).

Measurements of carbon and sulfur isotopic fluctuations in sections that encompass the Permian-Triassic boundary suggest the presence of a stagnant ocean with anoxic and euxinic conditions (Cao et al. 2002; Kaiho et al. 2006). Hypercapnia in this anoxic ocean has been proposed to account for the selectivity against certain physiological groups during the extinction in the marine realm (Knoll et al. 1996; Knoll et al. 2007).

Siberian Traps volcanism, which was roughly contemporaneous with the Permian-Triassic boundary, may have been a factor in the extinction event. The release of significant concentrations of carbon

dioxide from this massive igneous province would have certainly affected the global carbon cycle and subsequently been a factor in the protracted recovery period (Wignall 2001; Payne and Kump 2007). It has also been hypothesized that the Siberian volcanics were emplaced into extensive and hydrocarbon-rich salt basins, thereby releasing sulfate aerosols and other climate-perturbing materials into the atmosphere (Visscher et al. 1996; Visscher et al. 2004). To have been a factor the initiation of Siberian volcanism must not have post-dated the extinctions, and currently equivocal age constraints prevent a precise temporal correlation.

This report focuses on measurements of biomarker proxies that are indicative of microbial community and redox conditions in stratigraphic sections from a wide range of paleoenvironments at the Permian-Triassic boundary. While the studied sections have individual limitations in coverage, collectively they give insight to patterns of environmental change that appear to be worldwide. Hydrocarbon biomarkers collected from marine sedimentary rocks suggest conditions of oceanic anoxia, but are not suited to directly address the effects of massive trap volcanism.

Studied Localities

Four stratigraphic sections were examined for hydrocarbon biomarkers studied here: Peace River, Canada; Kap Stosch, Greenland; Meishan, China; and the Great Bank of Guizhou, China. Data from additional sections are included in the discussion to make the coverage as globally representative as possible. These additional sections are from the Schuchert Dal formation, Eastern Greenland; the Perth Basin, Australia; the Kupfersheifer Basin, Germany; Lusitaniadalen, Spitsbergen, Norway; present day Tibet; the Sverdrup Basin in Blind Fiord, Canada; and the Western Canada Basin in Opal Creek, Canada

The Montney Formation of the Peace River Basin in western Canada was deposited near the northwestern region of Pangaea during the Late Permian to Early Triassic periods in the eastern margin of the Panthalassic Ocean (Henderson 1997). A composite section of the Permian-Triassic transition was constructed from four petroleum exploration drill cores which were correlated using gamma-ray wire logs and conodont biostratigraphy (Hays et al. 2007). Only one core had late Permian conodonts in the lower portion and fossils of the conodont *Hindeodus parvus*, the index fossil for the Permian-Triassic boundary. The other cores sample the early Triassic period exclusively.

A Permian-Triassic section from the Kap Stosch locality was deposited on the margin of the Boreal Sea, an epicontinental basin forming in the northwest region of Pangaea (Teichert and Kummel 1972, 1976). The Kap Stosch section was assembled into a single column from outcrops at four localities correlated using stratigraphic relationships and fossil assemblages. Although the Permian-Triassic boundary is not exposed at Kap Stosch and the event has appears to be further obscured through erosion and reworking, sedimentary rocks with distinct fossils from the Permian and Triassic periods, respectively, have been identified.

The Great Bank of Guizhou in modern-day South China was formed within the Paleo-Tethys Ocean, an ocean basin bordered on three sides by the continent Pangaea and a number of smaller continental blocks to the east. On the southern margin of one of these blocks the carbonate platform of the Great Bank of Guizhou was deposited. The stratigraphic context for this section has been well established, and indicates that this section is a significantly expanded record of this period (Lehrmann et al. 1998; Lehrmann et al. 2005). It further demonstrates its relatively constant

deposition except for a minor dissolution surface at the Permian-Triassic boundary itself. Biostratigraphy from Guizhou shows that the high-diversity of the Permian reef environment gave way to the low-diversity of the Triassic period, dominated by mollusk beds and small relative fossil size (Lehrmann et al. 2005). A small subset of the large outcrop has been examined here, assembled from three different sampled localities (Payne et al. 2006).

A single outcrop section in Meishan, South China, is the Global Stratotype Section and Point of the Permian-Triassic boundary, and as such, defines the boundary (Yin et al. 2001). This section has provided an age for the extinction event, 252 Ma (Bowring et al. 1998; Mundil et al. 2004), as well as been a source to study the pace and characteristics of the extinction event itself (Jin et al. 2000). This section was deposited within the Paleo-Tethys Ocean, on the inner margin of one of the blocks forming its eastern edge. A core drilled through the section, just to the west of the original outcrop, provides a continuous record of this section from the Wuchiapingian through the Dinerian, and capturing the Permian-Triassic boundary itself (Cao et al. 2009).

Biomarkers

Although a large suite of biomarker proxies was measured from the four locations described above, this work examines only a subset of these in order to focus on global patterns at the time of the Permian-Triassic boundary.

C_{33} *n*-alkylcyclohexane

Prior research has identified anomalous absolute and relative abundances of the biomarker C_{33} *n*-alkylcyclohexane (*n*-heptacosylcyclohexane, C_{33} *n*-ACH) in sediments spanning the Permian-Triassic

transition. There appears to be a unique relationship between this hydrocarbon feature and the PT event as it is absent in sedimentary rocks from other time periods regardless of thermal maturity (McIldowie and Alexander 2005). In this study, elevated levels of C_{33} *n*-ACH were identified in the Peace River and Kap Stosch sections but were not measured in the Meishan and Guizhou sections. In the Kap Stosch and Peace River sections, the highest values of the ratio of C_{33} *n*-ACH/*n*-C_{34} were measured in samples close to the identified Permian-Triassic boundary. Elevated levels of C_{33} *n*-ACH extended further into the Triassic period than they did into the Permian period, but did not extend many meters in either direction. (See Figure 7.1.)

In the report of this compound from Grice et al. (2005b), elevated levels were identified in the Perth Basin in Western Australia, where this compound had been identified previously (Thomas and Barber 2004), as well as the Schuchert Dal formation from Eastern Greenland. (See Figure 7.2) The identification of the C_{33} *n*-ACH in the Kap Stosch section is an anticipated observation, since it was deposited in the same epicontinental basin as the Schuchert Dal formation. The paleolocation of the Peace River section was also very close to the two Greenland sections, though it was sampling the Panthalassic Ocean, the global ocean, which was not restricted like the Boreal Sea. The identification of this compound in samples from the global Panthalassic Ocean, in addition to the previously sampled Paleo-Tethys, strengthens the argument that this compound is an indicator for the Permian-Triassic boundary.

The biological source of the C_{33} *n*-ACH remains unknown, and its identification is outside the purpose of this study. The absence of this compound in the Meishan and Guizhou sections may give some clue as to the source, such as its potential limitation to higher-latitude environments. Regardless of the source, the non-uniform distribution of elevated C_{33} *n*-ACH levels strengthens the

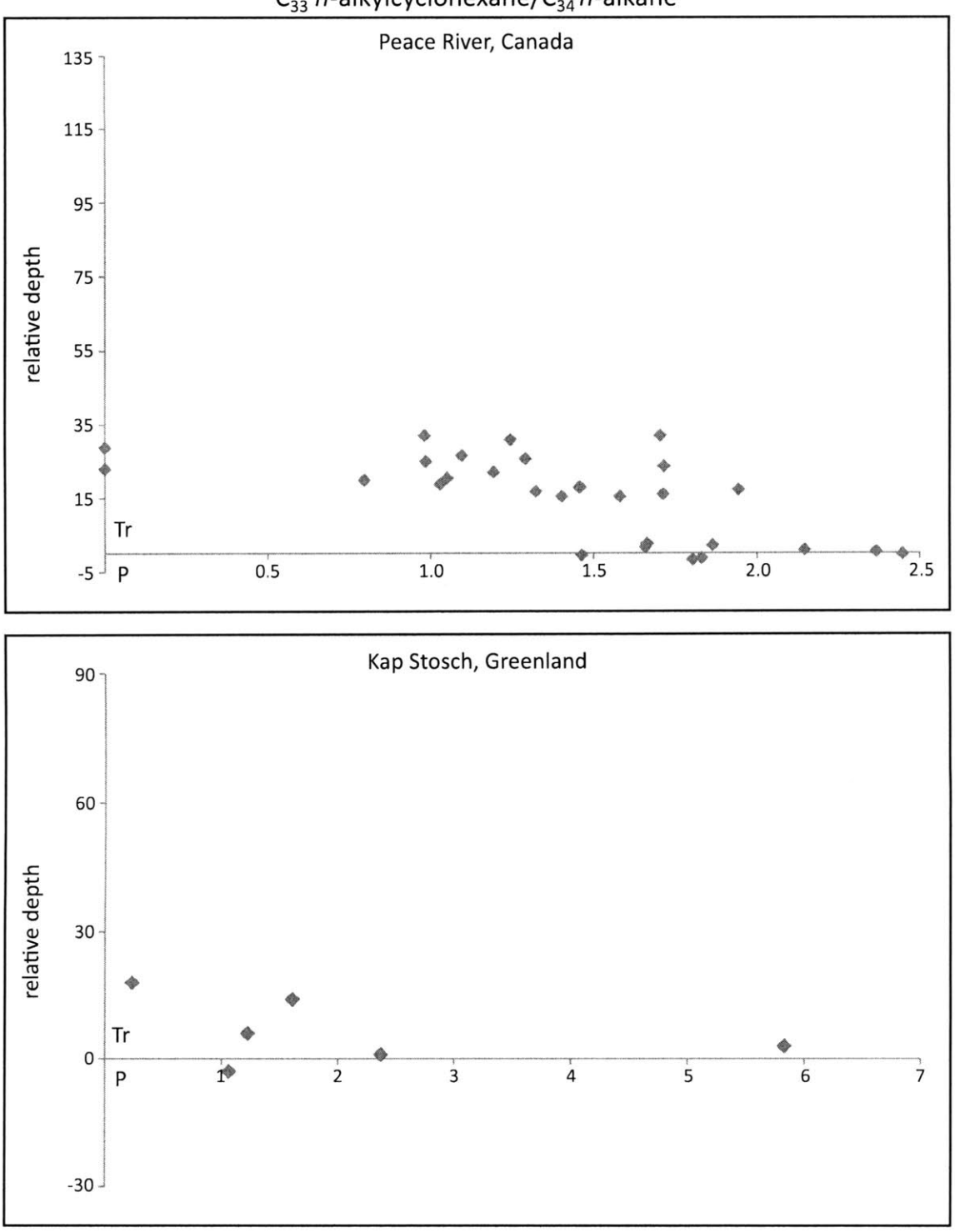

Figure 7.1 The ratio of C_{33} n-alkylcyclohexane to C_{34} n-alkanes for Peace River, Canada and Kap Stosch, Greenland. Compounds were measured by GC-MS in SIM mode and are plotted relative to depth for each section.

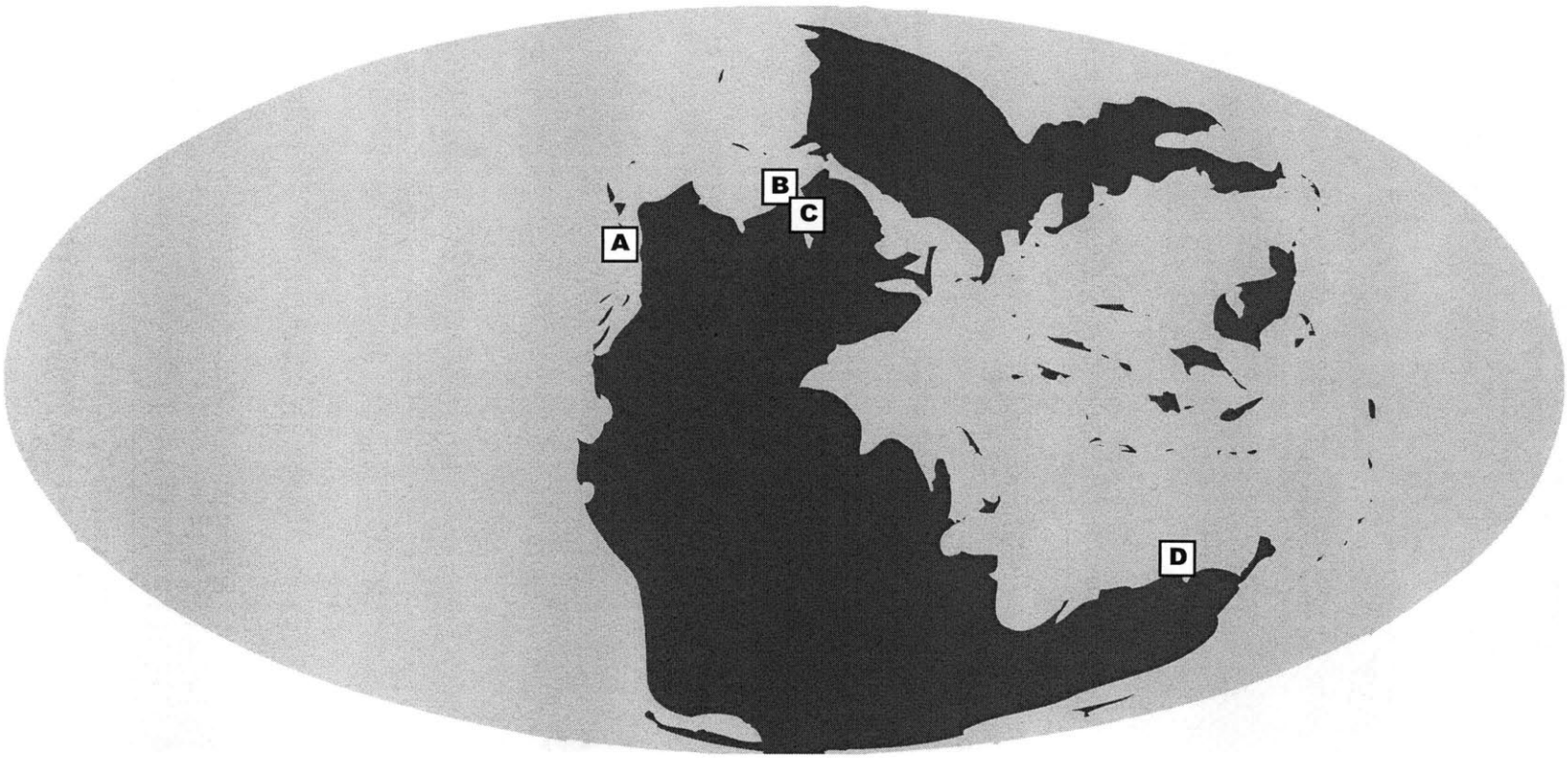

Figure 7.2 Global map from the Permian-Triassic boundary. Elevated abundances of C_{33} *n*-alkylcyclohexane have been identified in the sites noted. (a) Peace River, Canada. (b) Kap Stosch, Greenland. (c) Schuchert Dal, Greenland. (d) Perth Basin, Australia. Map modified from Scotese Paleomap Project website.

argument for examining a wide range of sections to understand global changes in environmental conditions.

Carotenoid Derivatives

Aryl isoprenoids with a 2,3,6 trimethyl substitution pattern and the precursor C_{40} compounds isorenieratane and chlorobactane are derived from the carotenoids of Green Sulfur Bacteria or Chlorobi (Summons and Powell 1986). These organisms are obligate phototrophs that utilize hydrogen sulfide as an electron donor. The identification of these carotenoid derivatives in sedimentary rocks suggests that conditions of photic zone euxinia were present during deposition. In all sections 2,3,6 aryl isoprenoids were measured, including Peace River, Kap Stosch, the Great Bank of Guizhou and Meishan. (See Figure 7.3.) An alternative origin of these compounds has been suggested through sedimentary diagenetic processes from other carotenoids (Koopmans et al. 1996). However, isorenieratane was identified in the Kap Stosch section and measured in the Peace River and Meishan sections. Chlorobactane was also measured in the Peace River sedimentary rocks – the first time it has been reported from a Permian-Triassic boundary section. The $\delta^{13}C$ of the aryl isoprenoids was also measured in the Peace River sedimentary rocks and values were enriched relative to the *n*-alkanes and isoprenoids. The presence of these extended carotenoids and the more positive $\delta^{13}C$ values, where measured, suggests that the aryl isoprenoids were indeed derived from the lipids of Chlorobi.

The distribution pattern of the carotenoid derivatives were similar in the Peace River, Greenland and Meishan sections, with a peak in measured abundances at the identified Permian-Triassic transition. There are other peaks in these sections as well, although in the Kap Stosch and Peace River sections,

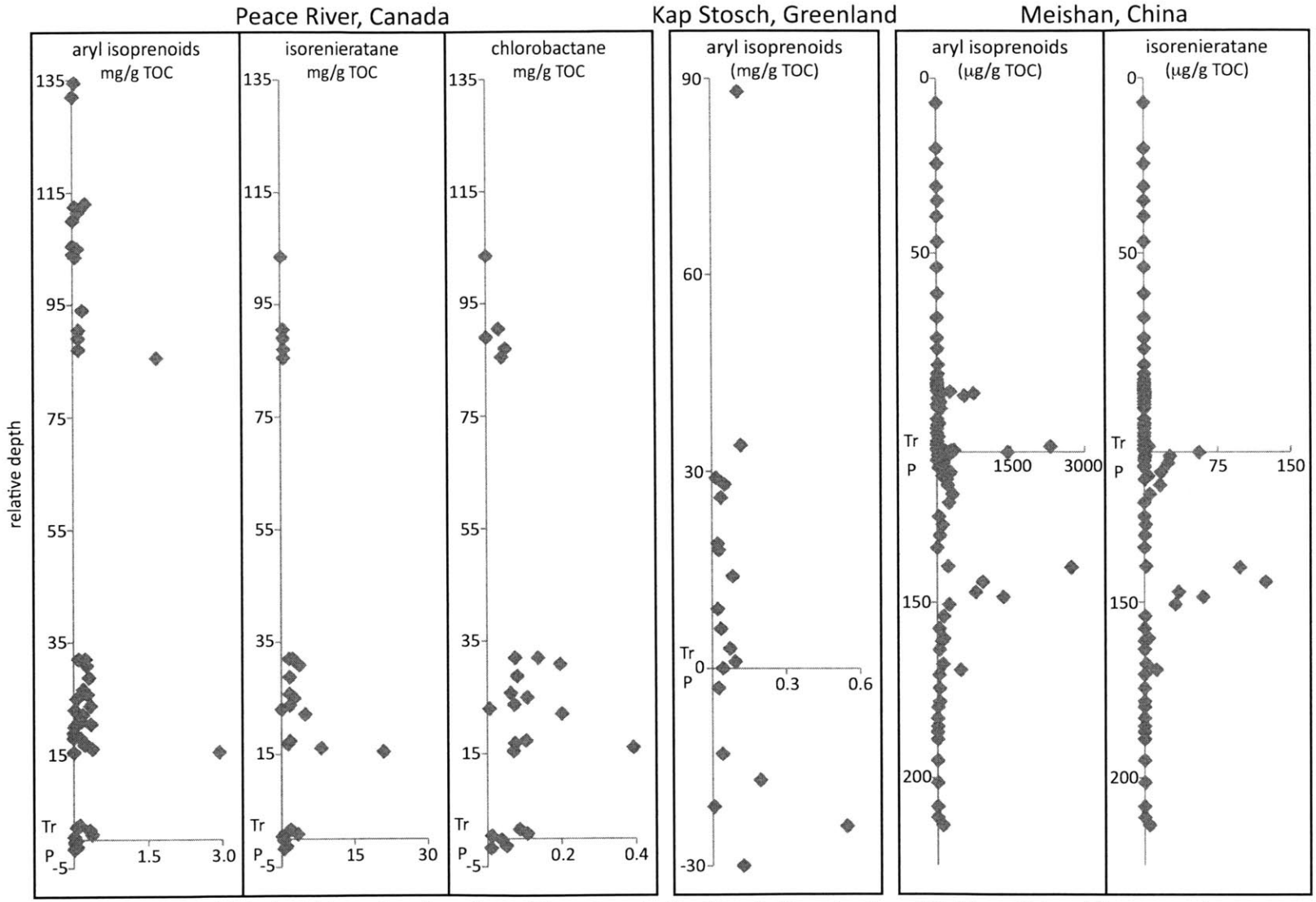

Figure 7.3 Carotenoid-derived biomarkers from Peace River, Canada, Kap Stosch, Greenland, and Meishan, China. All compounds were normalized relative to total organic carbon contents and measured in GC-MS SIM mode. Parameters are plotted relative to depth section.

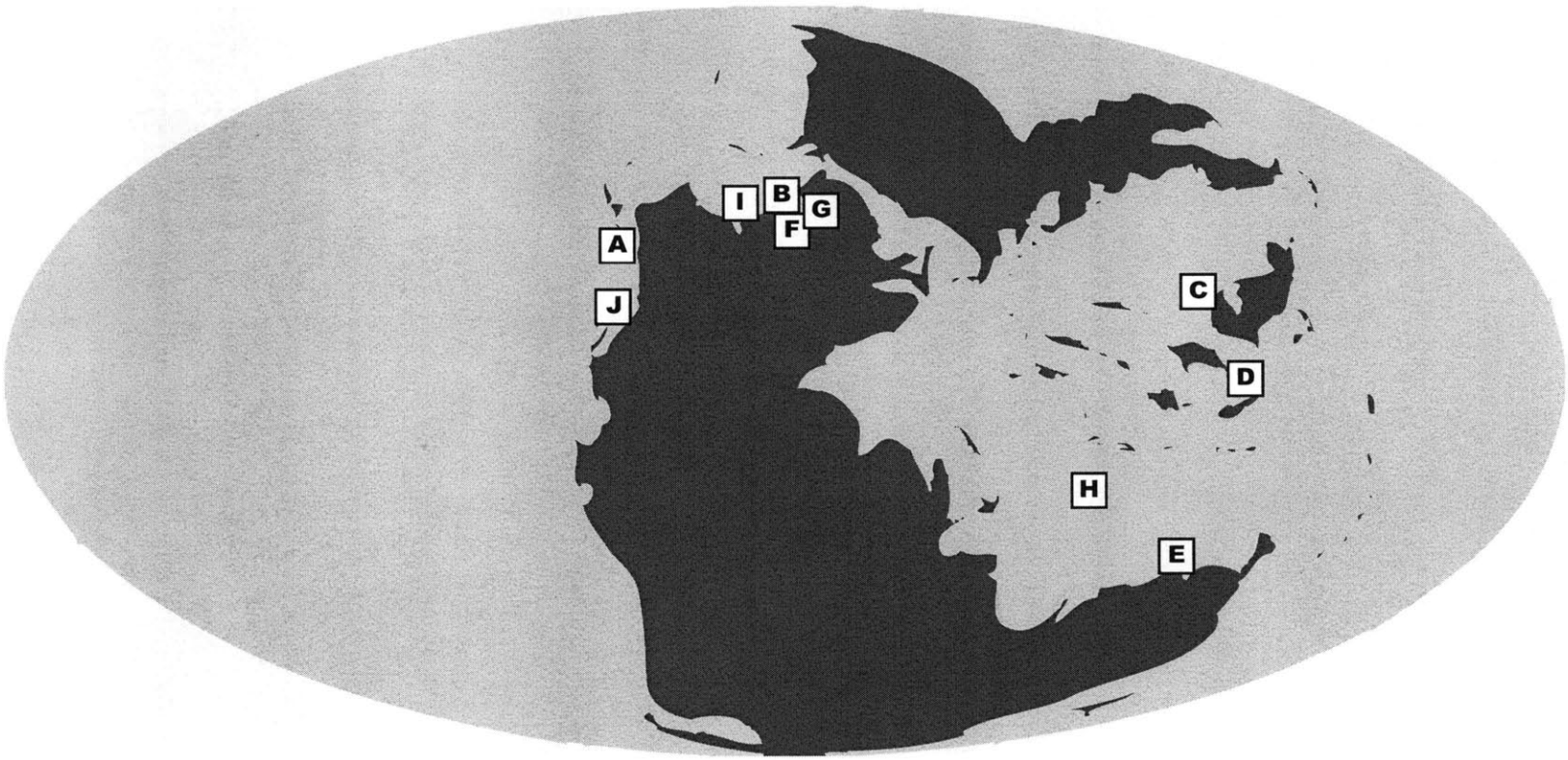

Figure 7.4 Global map from the Permian-Triassic boundary. Chlorobi-derived biomarkers have been identified in the sites noted. (a) Peace River, Canada. (b) Kap Stosch, Greenland. (c) Meishan, China. (d) Great Bank of Guizhou, China. (e) Perth Basin, Australia. (f) Kupfershiefer Basin, Germany. (g) Spitsbergen, Norway. (h) Tibet. (i) Blind Fiord, Canada. (j) Opal Creek, Canada. Map modified from Scotese Paleomap Project website.

these peaks are in the early Triassic period, whereas the peak in the Meishan section is in the late Permian period. Peaks in aryl isoprenoid concentrations normalized to total organic contents of the sedimentary rocks are indicative of a relative increase of Chlorobi-derived biomass during deposition.

In addition to the sections studied for this report, aryl isoprenoids and other carotenoid derivatives have been identified in a number of other global sections spanning the Permian-Triassic boundary, and generally show an increase in these compounds through the Late Permian with a maximum at or near the boundary. In Late Permian and Early Triassic sedimentary rocks from the Perth Basin, Australia, aryl isoprenoids and isorenieratane were measured (Grice et al. 2005a). Aryl isoprenoids and isorenieratane were also measured in Late Permian sedimentary rocks from the Kupfersheifer Basin, Germany (Grice et al. 1996). From a Late Permian section in Lusitaniadalen, Spitsbergen, Norway, aryl isoprenoids were measured (Nabbefeld et al. 2010). Sedimentary rocks spanning the Permian-Triassic transition from present day Tibet contained aryl isoprenoids (Twitchett and Grice, personal communication), as did those from the Sverdrup Basin in Blind Fiord, Canada and the Western Canada Basin in Opal Creek, Canada (Hays, unpublished data). (See Figure 7.4.)

Hopane/Sterane Ratio

The hopane to sterane ratio is used as a generalized proxy of the inputs of bacteria to eukaryotes (Moldowan et al. 1985). The average for the Phanerozoic is generally between 0.5 and 2; higher values were measured in the Peace River, Kap Stosch and Meishan sections. In the Great Bank of Guizhou section, values are closer to an average of ~1. Different ranges of values for this proxy were measured in the different sections, with highest values in the Meishan section where this ratio

reached ~70. Lower peaks of ~4 and ~6.4 were measured in the Peace River and Kap Stosch sections, respectively. (See Figure 7.5.)

In all three sections intervals with high hopane/sterane ratio roughly corresponded to peaks in aryl isoprenoid concentrations. In the Peace River and Meishan sections an increase immediately following the boundary was measured in both biomarker proxies, which then began to decrease into the Triassic period. The hopane/sterane ratio remained much higher at Meishan, where the last interval has a value of ~5, than at Peace River, where the ratio returned to values normal for the Phanerozoic at the top of the section. In the Kap Stosch section, peaks in the hopane/sterane ratio and aryl isoprenoid concentrations were measured near the identified Permian-Triassic boundary as well. A decrease in the hopane/sterane ratio in younger sedimentary rocks was not seen in Kap Stosch, but this section does not extend as far into the Triassic period as the other two, and this signal may not have been recorded.

Although the ratio of total hopanes to total steranes gives a measure of the relative input of bacterial to eukaryotic biomass, specific values can be affected by maturity of sedimentary rocks (Seifert and Moldowan 1978). The maturity is relatively constant throughout Meishan and Peace River, and in these sections the hopane/sterane ratio is suggestive of a marine microbial community dominated by bacteria. In the Greenland section, higher values of the hopane/sterane ratio correspond to higher aryl isoprenoid contents; however, higher values also correspond to changes in a number of biomarker proxies for maturity and source. Since the hopane/sterane ratio is lowered by increased terrestrial inputs and the Greenland section contains other evidence for increased terrestrial input in the early Triassic period, it is possible that this may be the source of some of the lowest values of the ratio in this section.

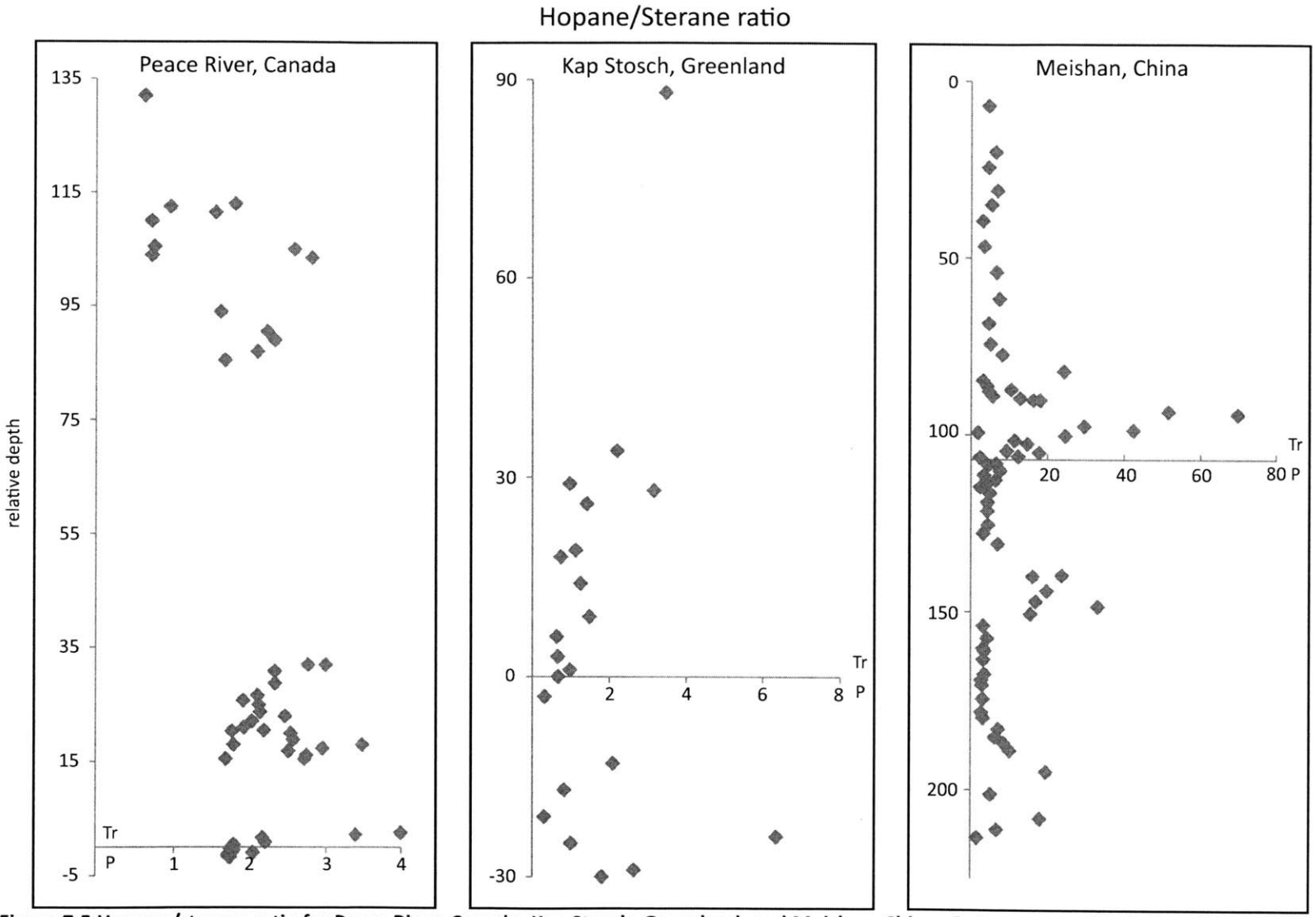

Figure 7.5 Hopane/sterane ratio for Peace River, Canada, Kap Stosch, Greenland, and Meishan, China. Ratio measured including all identified hopane and steranes in the section. All ratios were measured by GC-MS in MRM mode and plotted relative to depth in each section.

The hopane/sterane ratio was also measured in the Hovea-3 core from the Perth Basin in Western Australia, although this ratio was unreported in the initial publication of the biomarker data from this section (Grice et al. 2005a). However as with the sections reported in this paper, values for this parameter were uniformly high, with an average of ~4.6. Immediately following the identified Permian-Triassic transition, and coincident with the highest values of aryl isoprenoids and isorenieratane, the ratio of hopane/sterane reaches a peak of 15.2. Values for this proxy are higher in the Permian sedimentary rocks than in the Triassic rocks, but they remain elevated relative to normal in the Phanerozoic throughout the measured section.

Stable Carbon Isotopes of Hydrocarbons

The term, $\Delta\delta$, refers to the difference between the $\delta^{13}C$ values of the *n*-alkanes *n*-C_{17} and *n*-C_{18} and the isoprenoids pristane and phytane. In the Phanerozoic, values for this proxy are primarily negative, and enrichment of pristane and phytane relative to the *n*-alkanes is considered normal isotopic ordering. In the Proterozoic, and a number of Phanerozoic oceanic anoxic events, the value of $\Delta\delta$ is positive, considered anomalous isotopic ordering (Logan et al. 1995).

In Neoproterozic sections where $\Delta\delta$ was measured, hypotheses were proposed for the cause of the transition from anomalous to normal isotopic ordering. One hypothesis put forth suggested that changing carbon cycle dynamics in an ocean where the DOC pool was significantly higher than in modern oceans led to increased heterotrophic activity (Rothman et al. 2003). Possible causes for depletion of this DOC pool include the evolution of animals with guts producing fecal pellets (Logan et al. 1995) or sponges (Love et al. 2009) or other organisms that were able to filter out this

organic matter and produce recalcitrant biomolecules. Nevertheless, having evolved and radiated into many of the modern groups by the Permian-Triassic boundary, these organisms are unlikely to be the cause of the anomalous $\Delta\delta$ values in these samples.

For this study, the value of $\Delta\delta$ was calculated for the Peace River and Meishan sections. (See Figure 7.6.) In the Peace River section, the average value of $\Delta\delta$ is close to zero. In the Meishan section, values measured for the $\Delta\delta$ proxy are significantly more positive. Both signals are considered anomalous isotopic ordering, indicative of an enrichment of *n*-alkanes relative to isoprenoids not generally seen in the Phanerozoic. In both sections there are measured intervals in which values are more negative than the rest of the section, and in the Meishan section, these excursions are inversely correlated to the isorenieratane content. The compound chlorobactane, as well as a suite of 2,3,4 aryl isoprenoids, were also identified in Meishan at these intervals; the later is likely derived from the carotenoids of Chromatiaceae – anoxygenic phototrophic sulfur bacteria with higher light requirements than Chlorobi. In the more negative interval immediately following the boundary in Peace River, the highest quantities of chlorobactane from this section were measured.

In the Perth Basin, Australia, (See Figure 7.7) compound specific isotopes of *n*-alkanes and isoprenoids were measured and the value of $\Delta\delta$ was calculated for sedimentary rocks spanning the Permian-Triassic transition (Grice et al. 2005a). In this section, as in both Peace River and Meishan, the $\Delta\delta$ values were positive, or showed reverse isotopic ordering in the Late Permian sedimentary rocks, followed by a more negative $\Delta\delta$ excursion immediately followed the identified boundary. This pattern of a negative excursion in $\Delta\delta$ co-occurred with a peak in isorenieratane, although other carotenoid derivatives were not identified.

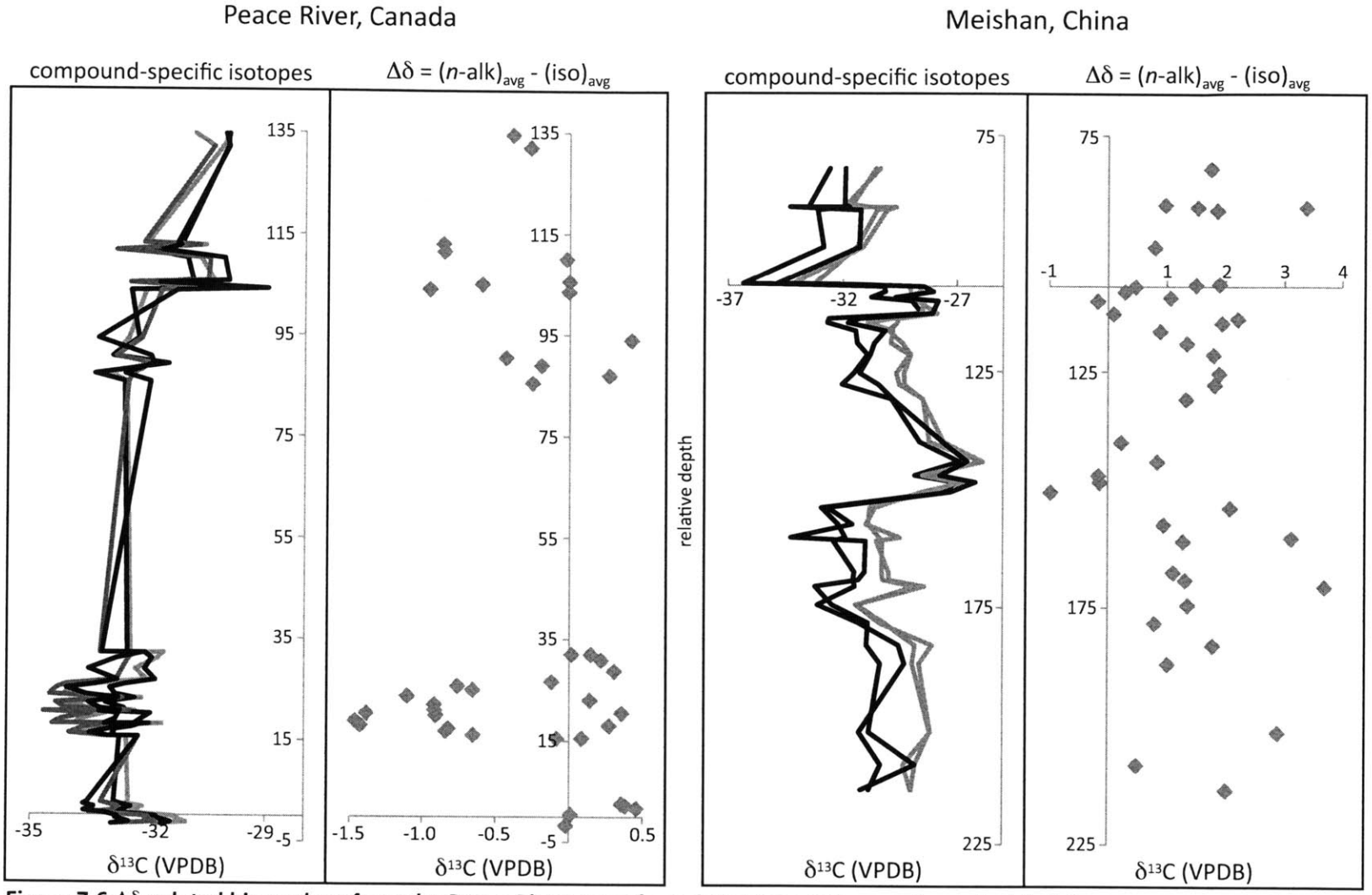

Figure 7.6 Δδ-related biomarkers from the Peace River, Canada and Meishan, China sections. In Δδ plots, grey represents the individual *n*-alkane measurements (*n*-C_{17} and *n*-C_{18}) and black represents individual isoprenoid measurements (pristane and phytane). Isotopes were measured in permil relative to VPDB on GC-irMS. All parameters are plotted relative to depth.

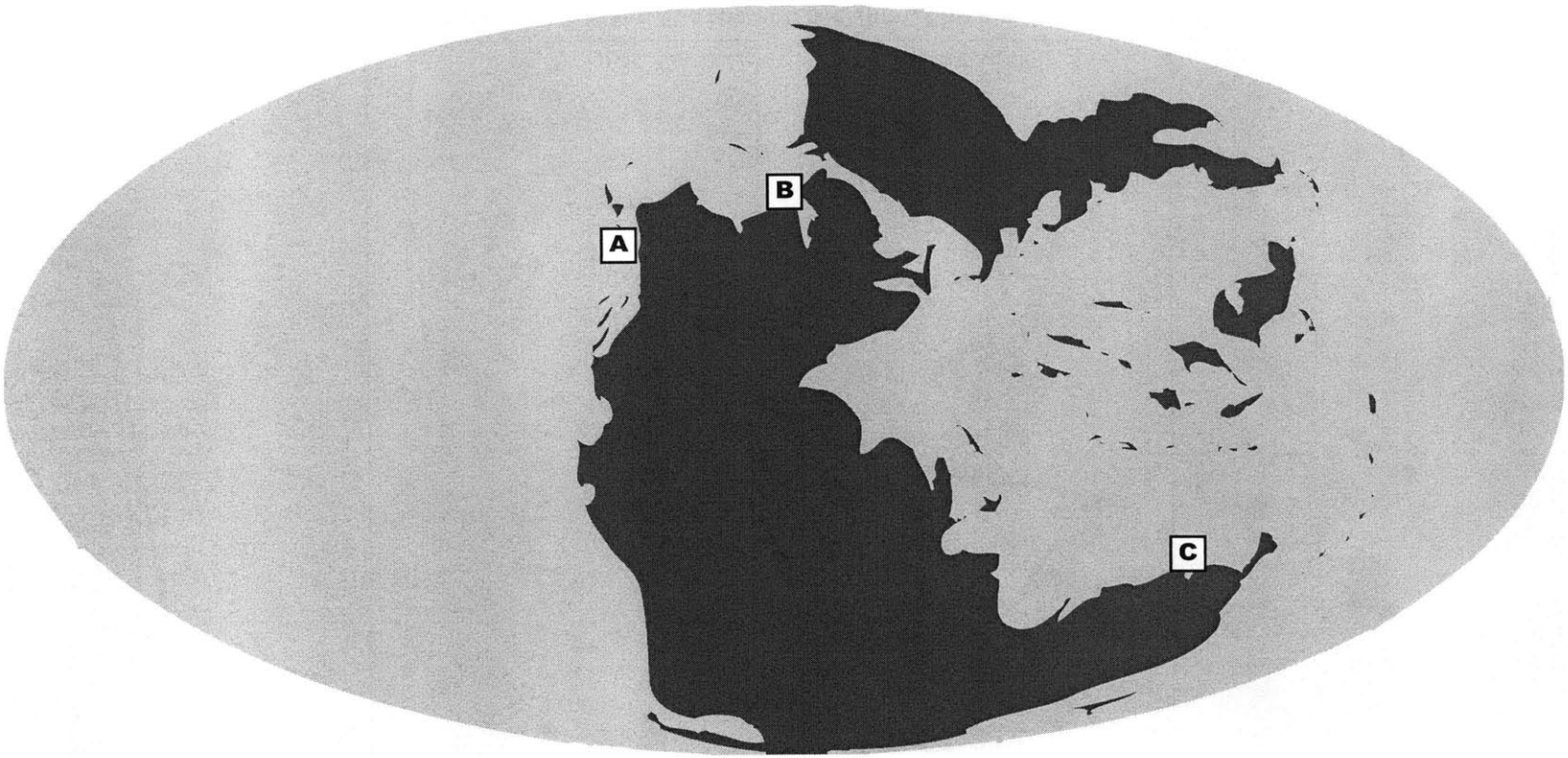

Figure 7.7 Global map from the Permian-Triassic boundary. Compound-specific isotopes for the measurement of $\Delta\delta$ were measured in the sites noted. (a) Peace River, Canada. (b) Kap Stosch, Greenland. (c) Perth Basin, Australia. Map modified from Scotese Paleomap Project website.

Conclusions

Aryl isoprenoids, isorenieratane and chlorobactane were measured in the Peace River, Kap Stosch, Meishan and Great Bank of Guizhou sections from the Changsingian, across the Permian-Triassic boundary and continuing through Greisbachian and into the Dienerian. Aryl isoprenoids have also been reported from Permian-Triassic transition rocks from Perth Basin, Australia (Grice et al. 2005a); the Kupfersheifer Basin, Germany (Grice et al. 1996); Spitsbergen, Norway (Nabbefeld et al. 2010); present day Tibet (Twitchett and Grice, personal communication); as well as the Sverdrup Basin in Blind Fiord, Canada and the Western Canada Basin in Opal Creek, Canada (Hays, unpublished data). The measurement of these carotenoid derivatives indicates that conditions of photic zone euxinia were global in the shelf and near-shore environments leading up to the Permian-Triassic boundary and presaged the main extinction event. Lithological evidence for euxinia beginning at the Guadalupian-Lopingian boundary from a Japanese chert suggests that anoxic conditions were present in the global ocean for millions of years (Isozaki 1997). The long-term and widespread nature of these anoxic and euxinic conditions indicates that they must have been caused by factors that occurred on long time scales. The final assembly of Pangaea would have affected weathering, oceanic circulation and nutrient cycling, bringing about changes that allowed for the development of anoxic conditions and prevented the full ventilation of the oceans, and these processes would have operated on appropriate time scales.

The corresponding peaks in hopane/sterane ratio and carotenoid derivatives indicate that the broadly euxinic ocean intervals were also periods of heightened bacterial significance within the microbial community. This hypothesis is supported by other biomarker proxies as well.

In the original work on the $\Delta\delta$ proxy for sections throughout the Proterozoic and Phanerozoic, it was proposed that positive values, or anomalous isotopic ordering, resulted from increased heterotrophic reworking of biomass in a stratified water column (Logan et al. 1995). Another hypothesis proposed recently and based on modern ocean sediments suggested that anomalous isotopic ordering is caused by increased sedimentary input from organisms such as bacteria that dominate the small size fractions (Close et al. 2008). Therefore, the measurement of predominantly positive $\Delta\delta$ values throughout the Peace River and Meishan sections, in conjunction with the prevalence of carotenoid derivatives and high hopane/sterane ratios, suggest long-term conditions of euxinia and heightened bacterial productivity in the disrupted ecosystems.

However, two intervals of negative excursions in $\Delta\delta$ values from the Peace River and Meishan sections argue that the ocean carbon cycle dynamics are more complicated. In both sections, negative $\Delta\delta$ values correspond to enriched $\delta^{13}C$ values of the constituent compounds. In these intervals, trace quantities of 2,3,4 aryl isoprenoids and chlorobactane were identified in the Meishan section, and in the Peace River section peaks in the chlorobactane contents were measured. These carotenoid-derived biomarkers are produced by anoxygenic phototrophic bacteria that thrive at higher light intensities than Chlorobi, suggesting perhaps an extreme shoaling of the chemocline during these intervals. Although these conditions would have been unstable in the Phanerozoic oxygenated atmosphere, they may have served to disrupt the carbon cycle and produce the observed changes in isotopes. Although these compounds were not identified in the Perth Basin sedimentary rocks, the peak in isorenieratane in conjunction with the negative excursions in $\Delta\delta$ values supports the hypothesis of a shoaling of the chemocline.

The Permian-Triassic boundary section from Meishan, the only section that includes data from a single core, provides for the clearest insight into the changes in carbon cycling. There are two distinct negative excursions in $\Delta\delta$ values at Meishan, where measured carotenoid derivatives suggest chemocline excursions. However, only one of these excursions is coincident with the extinction – at the other there is no significant change in biodiversity of metazoans (Jin et al. 2000; Yin et al. 2007). The hopane/sterane ratio has two peaks in this section, and while the first coincides with the first negative $\Delta\delta$ interval, the second peak post-dates the second negative $\Delta\delta$ interval, indicating a different pattern of interaction between changing conditions in the microbial community and changes in carbon cycling at these two intervals. This suggests perhaps that an external factor – perhaps the influence of another trigger mechanism such as the eruption of the Siberian traps – may have combined with the chemocline upward excursion and affected the global conditions more profoundly at the boundary itself, leading to the mass extinction.

Biomarker evidence presented here gives a picture of the global oceanic conditions before the Permian-Triassic boundary and in the aftermath of the largest extinctions of the Phanerozoic. These proxies suggest an environment dominated by bacteria, where deep-water anoxia was present for a period of millions of years, and an intermittent shoaling of the chemocline brought euxinic waters well within the photic zone, which would have certainly been deleterious for metazoa in the oceans. Emissions of hydrogen sulfide from the oceans during chemocline upward excursions (Kump et al. 2005; Meyer et al. 2008), with the potential addition of volatiles from Siberian Traps volcanism, may have been more damaging than either trigger mechanism individually (Lamarque et al. 2007), and provide a mechanism to account for the extinction in the terrestrial environments as well. The long-standing anoxic and euxinic oceanic conditions and the more short-term volcanism, both the result

of tectonic processes, would have together created a globally hostile environment that could have persisted for millions of years, affecting the survival taxa and lengthening the recovery period.

References:

Bowring, S. A., D. H. Erwin and Y. Isozaki (1999). "The Tempo of Mass Extinction and Recovery: The End-Permian Example." Proceedings of the National Academy of Sciences **96**(16): 8827-8828.

Bowring, S. A., D. H. Erwin, Y. G. Jin, M. W. Martin, K. Davidek and W. Wang (1998). "U/Pb Zircon Geochronology and Tempo of the End-Permian Mass Extinction." Science **280**(5366): 1039-1045.

Cao, C., G. D. Love, L. E. Hays, W. Wang, S. Shen and R. E. Summons (2009). "Biogeochemical Evidence for Euxinic Oceans and Ecological Disturbance Presaging the End-Permian Mass Extinction Event." Earth and Planetary Science Letters **281**(3-4): 188-201.

Cao, C. Q., W. Wang and Y. G. Jin (2002). "Carbon Isotope Excursions across the Permian-Triassic Boundary in the Meishan Section, Zhejiang Province, China." Chinese Science Bulletin **47**(13): 1125-1129.

Close, H., A. Diefendorf, K. H. Freeman and A. Pearson (2008). "A Modern Analogue for Proterozoic Inverse Carbon Isotope Signatures." Eos Trans. AGU **89**(53): Fall Meet. Suppl., Abstract PP14A-07.

Erwin, D. H. (2006). Extinction: How Life on Earth Nearly Ended 250 Million Years Ago. Princeton, Princeton University Press.

Grice, K., C. Cao, G. D. Love, M. E. Bottcher, R. J. Twitchett, E. Grosjean, R. E. Summons, S. C. Turgeon, W. Dunning and Y. Jin (2005a). "Photic Zone Euxinia During the Permian-Triassic Superanoxic Event." Science **307**(5710): 706-709.

Grice, K., P. Schaeffer, L. Schwark and J. R. Maxwell (1996). "Molecular Indicators of Palaeoenvironmental Conditions in an Immature Permian Shale (Kupferschiefer, Lower Rhine Basin, North-West Germany) from Free and S-Bound Lipids." Organic Geochemistry **25**(3-4): 131-147.

Grice, K., R. J. Twitchett, R. Alexander, C. B. Foster and C. Looy (2005b). "A Potential Biomarker for the Permian-Triassic Ecological Crisis." Earth and Planetary Science Letters **236**(1-2): 315-321.

Hays, L., T. Beatty, C. M. Henderson, G. D. Love and R. E. Summons (2007). "Evidence for Photic Zone Euxinia through the End-Permian Mass Extinction in the Panthalassic Ocean (Peace River Basin, Western Canada)." Palaeoworld **16**(1-3): 39-50

Henderson, C. M. (1997). "Uppermost Permian Conodonts and the Permian-Triassic Boundary in the Western Canada Sedimentary Basin." Bulletin of Canadian Petroleum Geology **45**(4): 693-707.

Isozaki, Y. (1997). "Permo-Triassic Boundary Superanoxia and Stratified Superocean: Records from Lost Deep Sea." Science **276**(5310): 235-238.

Jin, Y., Y. Wang, W. Wang, Q. H. Shang, C. Cao and D. H. Erwin (2000). "Pattern of Marine Mass Extinction near the Permian-Triassic Boundary in South China." Science **289**: 432-436.

Kaiho, K., Y. Kajiwara, Z.-Q. Chen and P. Gorjan (2006). "A Sulfur Isotope Event at the End of the Permian." Chemical Geology **235**(1-2): 33-47.

Knoll, A. H., R. K. Bambach, D. E. Canfield and J. P. Grotzinger (1996). "Comparative Earth History and Late Permian Mass Extinction." Science **273**: 452-457.

Knoll, A. H., R. K. Bambach, J. L. Payne, S. Pruss and W. W. Fischer (2007). "Paleophysiology and End-Permian Mass Extinction." Earth and Planetary Science Letters **256**(3-4): 295-313.

Koopmans, M. P., S. Schouten, M. E. L. Kohnen and J. S. S. Damste (1996). "Restricted Utility of Aryl Isoprenoids as Idicators for Photic Zone Anoxia." Geochemica et Cosmochimica Acta **60**(23): 4873-4876.

Kump, L. R., A. Pavlov and M. A. Arthur (2005). "Massive Release of Hydrogen Sulfide to the Surface Ocean and Atmosphere During Intervals of Oceanic Anoxia." Geology **33**: 397–400.

Lamarque, J. F., J. T. Kiehl and J. J. Orlando (2007). "Role of Hydrogen Sulfide in a Permian-Triassic Boundary Ozone Collapse." Geophys. Res. Lett. **34**(2): L02801.

Lehrmann, D., P. Enos, J. Payne, P. Montgomery, J. Wei, Y. Yu, J. Xiao and M. J. Orchard (2005). "Permian and Triassic Depositional History of the Yangtze Platform and Great Bank of Guizhou in the Nanpanjiang Basin of Guizhou and Guangxi, South China." Albertiana **33**: 149-168.

Lehrmann, D. J., Wei Jiayong and P. Enos (1998). "Controls on Facies Architecture of a Large Triassic Carbonate Platform; the Great Bank of Guizhou, Nanpanjiang Basin, South China." Journal of Sedimentary Research **68**(2): 311-326.

Logan, G. A., J. M. Hayes, G. B. Hieshima and R. E. Summons (1995). "Terminal Proterozoic Reorganization of Biogeochemical Cycles." Nature **376**(6535): 53-56.

Love, G. D., E. Grosjean, C. Stalvies, D. A. Fike, J. P. Grotzinger, A. S. Bradley, A. E. Kelly, M. Bhatia, W. Meredith, C. E. Snape, S. A. Bowring, D. J. Condon and R. E. Summons (2009). "Fossil Steroids Record the Appearance of Demospongiae During the Cryogenian Period." Nature **457**(7230): 718-721.

McIldowie, M. and R. Alexander (2005). "Identification of a Novel C33 N-Alkylcyclohexane Biomarker in Permian-Triassic Sediments." Organic Geochemistry **36**(10): 1454-1458.

Meyer, K. M., L. R. Kump and A. Ridgwell (2008). "Biogeochemical Controls on Photic-Zone Euxinia During the End-Permian Mass Extinction." Geology **36**(9): 747-750.

Moldowan, J. M., W. K. Seifert and E. J. Gallegos (1985). "Relationship between Petroleum Composition and Depositional Environment of Petroleum Source Rocks." AAPG Bulletin **69**(8): 1255-1268.

Mundil, R., K. R. Ludwig, I. Metcalfe and P. R. Renne (2004). "Age and Timing of the Permian Mass Extinctions: U/Pb Dating of Closed-System Zircons." Science **305**(5691): 1760-1763.

Nabbefeld, B., K. Grice, R. J. Twitchett, R. E. Summons, L. Hays, M. E. Bottcher and M. Asif (2010). "An Integrated Biomarker, Isotopic and Palaeoenvironmental Study through the Late Permian Event at Lusitaniadalen, Spitsbergen." Earth and Planetary Science Letters **291**(1-4): 84-96.

Payne, J. L. and L. R. Kump (2007). "Evidence for Recurrent Early Triassic Massive Volcanism from Quantitative Interpretation of Carbon Isotope Fluctuations." Earth and Planetary Science Letters **256**(1-2): 264-277.

Payne, J. L., D. J. Lehrmann, S. Christensen, J. Y. Wei and A. H. Knoll (2006). "Environmental and Biological Controls on the Initiation and Growth of a Middle Triassic (Anisian) Reef Complex on the Great Bank of Guizhou, Guizhou Province, China." PALAIOS **21**(4): 325-343.

Rothman, D. H., J. M. Hayes and R. E. Summons (2003). "Dynamics of the Neoproterozoic Carbon Cycle." Proceedings of the National Academy of Sciences of the United States of America **100**(14): 8124-8129.

Seifert, W. K. and M. J. Moldowan (1978). "Applications of Steranes, Terpanes and Monoaromatics to the Maturation, Migration and Source of Crude Oils." Geochimica et Cosmochimica Acta **42**(1): 77-95.

Summons, R. E. and T. Powell (1986). "Chlorobiaceae in Paleozoic Seas Revealed by Biological Markers, Isotopes and Geology." Nature **319**(6056): 763-765.

Teichert, C. and B. Kummel (1972). "Permian-Triassic Boundary in the Kap Stosch Area, East Greenland." Bulletin of Canadian Petroleum Geology **20**(4): 659-675.

Teichert, C. and B. Kummel (1976). "Permian-Triassic Boundary in the Kap Stosch Area, East Greenland." Meddelelser om Gronland **197**(5): 2-49.

Thomas, B. M. and C. J. Barber (2004). "A Re-Evaluation of the Hydrocarbon Habitat of the Northern Perth Basin." Australian Petroleum Production and Exploration Association Journal **44**: 59-92.

Visscher, H., H. Brinkhuis, D. L. Dilcher, W. C. Elsik, Y. Eshet, C. V. Looy, M. R. Rampino and A. Traverse (1996). "The Terminal Paleozoic Fungal Event: Evidence of Terrestrial Ecosystem Destabilization and Collapse." Proceedings of the National Academy of Sciences of the United States of America **93**(5): 2155-2158.

Visscher, H., C. V. Looy, M. E. Collinson, H. Brinkhuis, J. H. A. van Konijnenburg-van Cittert, W. M. Kurschner and M. A. Sephton (2004). "Environmental Mutagenesis During the End-Permian Ecological Crisis." Proceedings of the National Academy of Sciences of the United States of America **101**(35): 12952-12956.

Ward, P. D., J. Botha, R. Buick, M. De Kock, D. H. Erwin, G. Garrison, J. Kirschvink and R. Smith (2005). "Abrupt and Gradual Extinction among Late Permian Land Vertebrates in the Karoo Basin, South Africa." Science **307**: 709-714.

Wignall, P. B. (2001). "Large Igneous Provinces and Mass Extinctions." Earth-Science Reviews **53**(1-2): 1-33.

Yin, H., Q. Feng, X. Lai, A. Baud and J. Tong (2007). "The Protracted Permo-Triassic Crisis and Multi-Episode Extinction around the Permian-Triassic Boundary." Global and Planetary Change **55**(1-3): 1-20.

Yin, H., K. Zhang, J. Tong, Z. Yang and S. Wu (2001). "The Global Stratotype Section and Point (Gssp) of the Permian-Triassic Boundary." Episodes **24**(2): 102-114.

Appendix 1

Experimental Methods

Sample Preparation

Samples analyzed throughout this thesis were prepared using a set of methods. The basic steps for sample preparation included rock cleaning and crushing, lipid extraction, sample separation, and finally analysis. The solvents used throughout this process were organic-free solvents from OmniSolv. Also, all glass and aluminum products that came in contact with samples during the preparation process were fired to remove organic compounds before the sample preparation process.

Sand was fired at 850°C for 8h; glass wool, pipettes and silica gel were fired at 450°C for 8h; and all other products were fired at 550°C for 8h. In the samples where they were measured, RockEval and TOC data were provided by Humble Geochemical Services in Humble, Texas, with the exception of the Kap Stosch sample set.

Rock Cleaning and Crushing

For all samples, pieces of rock were cleaned with a wire brush in DI water to remove any contaminating particulate organic matter (OM). The outsides of the samples were then cleaned with three washes of methanol (MeOH), six washes of dichloromethane (DCM) and

three washes of hexane to remove external bitumen contamination. From this point forward, the sample only came in contact with glass or aluminum that had either been fired or had been cleaned with the same process of three washes of MeOH, six washes of DCM and three washes of hexane. If the whole rock was large (pieces larger than $1cm^3$) the rock was wrapped in fired aluminum foil and struck with a hammer in order to break off smaller pieces, and then these pieces were cleaned. Next, the smaller rock fragments were crushed to a fine powder using a SPEX 8510 Shatterbox ceramic puck mill for three, one-minute periods. Between samples, the puck mill was be cleaned by crushing fired sand three times for one-minute periods each followed by washing with the same solvent sequence.

Lipid Extraction

For the samples with high or unknown organic content, a fraction of the powdered sample, between 15-25g, was then placed in an extraction cell for processing with a DIONEX ASE 200 Accelerated Solvent Extractor. This instrument extracted the sample using a solvent mixture of 9:1 DCM to MeOH (v:v) at 1000psi and 100°C. This process was repeated three times, and the solutions pooled in a single vial.

An alternative method of extraction for small samples (<10g) was manual extraction. The powdered rock fraction was combined in a centrifuge tube along with ~40mL of a 9:1 dichloromethane (DCM) to methanol (MeOH) solution and sonicated in a VWR Aquasonic 150HT and vortexed with VWR Mini Vortexer MV-1. The samples were then centrifuged in a Eppendorf Centrifuge 5804 at 3500 rpm for 10 minutes, and the supernatant was poured off. The samples were extracted three times and the solutions pooled. This extract

was then filtered to remove any particulates still in suspension, using a small pipette with glass wool and a small amount of sand and silica gel.

The lipid extracts were then treated with activated copper to remove any elemental sulfur, and weighed as the total lipid extract.

Sample Separation

The total lipid extract was then separated by column chromatography on a silica gel column affording saturated hydrocarbons, an aromatic hydrocarbon fraction and a polar lipid fraction, by elution with solutions of increasing polarity comprising, respectively, hexane, hexane:DCM (4:1 v:v) and DCM:MeOH (4:1 v:v) solution. Different column sizes were used for different quantities of extract. The saturated fraction and aromatic fractions were gently dried, weighed and re-suspended in hexane. Then 50 ng of D4 20R stigmastane standard was added to the saturated fraction, and 100 ng of D14 p-terphenyl standard was added to the aromatic fraction for quantification.

Sample Analysis

Both the saturated and aromatic fractions were analyzed by gas chromatography-mass spectrometry (GC-MS) on a HP 6890 GC fitted with split/splitless injector and a 60 m J&W Scientific DB-1 fused silica capillary column (60 m x 0.32 mm; 0.25 um film thickness) attached to an Agilent 5973 mass selective detector (MSD). Injections were 1 ul from a total of 100 ul for both fractions. For the saturated fraction, samples were injected at 60°C and held for two minutes prior to a constant pressure (20.3 psi) programmed temperature ramp

of 10°C/min to 100°C, 4°C/min to 320°C and followed by a hold period of 20 minutes. Similar conditions were used for the aromatic fraction except that the temperature was raised from an initial 60°C at 20°C/min to 150°C followed by 2°C/minute to 320°C and a hold of 15 minutes. Saturated hydrocarbons were analyzed in the full scan mode while aromatics were run in selected ion monitoring (SIM) mode for the following ions: 91, 105, 119, 125, 133, 134, 178, 191, 192, 231, 237, 244, 245, 253, 287 and 365 Da. Individual compounds were semi-quantified by comparison of their peak areas to that of the D_{14}-terphenyl internal standard (244 Da) without correcting for individual response factors.

Saturated and aromatic hydrocarbon fractions were also analyzed in GC-MS using a Waters AutoSpec Ultima operated at 70eV in the multiple reaction monitoring (MRM) mode. Samples were injected onto a J&W Scientific DB-1 fused silica capillary column (60 m x 0.25 mm; 0.25μm film thickness) via the split/splitless injector operated in splitless mode with helium as the carrier gas. For the saturated fraction, the oven was programmed from 60°C (held for 2 min) to 150°C at 10°C/min, and then at 3°C/min to 315°C with a final hold of 24 min. A suite of C_{26}-C_{30} steranes, C_{27}-C_{35} hopanes, C_{31} methylhopanes and C_{26}-C_{30} cheilanthanes were quantified via their specific precursor-product reactions and using the D_4-aaa-ethylcholestane (D4) as internal standard without taking into account response factors. For the aromatic fraction to measure the carotenoids, the oven was programmed from 60°C (held for two minutes) and then ramped to 300°C at 10°C/min held for 30 minutes and finally ramped at 5°C/min to 320°C. During this oven schedule, the MS was effectively run in selected ion monitoring (SIM) mode for the 133 and 134 Da ions.

Compound-specific isotope results for lipids were obtained with a ThermoFinniganTraceGC equipped with a J&W DB-1MS column (60 m x 32 mm, 0.25 mm film). Chromatographic conditions were initially 60°C for three minutes, ramped from 60 - 180°C at 10°C/min, then 180 - 320°C at 4°C/min, and finally held at 320°C for 40 minutes. The GC was coupled to a combustion furnace interfaced to a Finnigan MAT DeltaPlus XP isotope ratio monitoring mass spectrometer operated with Isodat 2.0. Precision of isotope results were measured with standards and found to be better than 0.25‰ vs. VPDB, and sample replicates produced average errors of ~ 0.7‰ vs. VPDB.

Measurement of Uncertainties

Biomarker Measurements

For biomarker analyses on the AutoSpec, a standard oil (produced by the Australian Geological Survey Organization) was prepared using the same methods of separation as is used on samples. The saturated hydrocarbon fraction was further separated using a 5Å molecular sieve to trap the n-alkanes, leaving behind the branched saturated hydrocarbons, including biomarkers. This standard was used before every sample run and served to provide retention times for the known biomarker compounds it contains. A fraction of this molecular sieve non-adduct was run repeatedly on the AutoSpec to test accuracy and reproducibility of the measurements. Two biomarker proxies were measured. The first was the C_{27} Dia/Reg sterane ratio, involving the sum of two compounds (C_{27} diasterane βα 20S and C_{27} diasterane βα 20R) divided by the sum another four compounds (C_{27} sterane ααα 20S, C_{27} sterane αββ 20S, C_{27} sterane ααα 20R and C_{27} sterane αββ 20S). The other biomarker proxy measured was the C_{29} moretane/hopane ratio, the ratio of C_{29} βα hopane

divided by C_{29} $\alpha\beta$ hopane. The compounds for these proxies were measured a total of ~70 times from the single standard; the ratios were calculated, and the standard deviations as a percent of the ratios were low – 1σ was 2.6% of the mean for the C_{27} Dia/Reg sterane ratio and 5.2% of the mean for the C_{29} moretane/hopane ratio. However, the maximum outliers of these ratios were for both biomarkers was relatively large: ~2.5σ from the mean for the C_{27} Dia/Reg sterane ratio and 3.6σ from the mean for the C_{29} moretane/hopane ratio. The data, however, were not normally distributed about a single mean value: both biomarker proxies varied systematically in time. Since the concentration of the compounds, as indicated by their signal size, increased monotonically due to evaporation, this provides a convenient explanation for the observed drift. When the sample is more concentrated and there is a higher signal to noise ratio, the dispersion decreases. There seems to be a minimum concentration above which the dispersion no longer decreases. For the C_{27} Dia/Reg sterane ratio, the six component compounds are of similar concentrations in the sample. For this ratio, when the average "counts" of the component compounds ranged from ~4e5 to ~1.4e6, and if the ratios calculated for averages less than ~5.5e5 are excluded from the measurement, the standard deviation drops to 1.7% of the mean. For the C_{29} moretane/hopane ratio, the concentration of the hopane is significantly higher than the moretane, but the average of these two compounds ranged from ~1.5e6 to 5e6. When the ratios of moretane/hopane calculated for averages less than ~2.5e6 are excluded, the standard deviation drops to 3.2% of the mean. It is difficult to put a specific number on how concentrated a sample needs to be to minimize this effect, since it is affected by the number of component compounds in a proxy as well as the general proportions of these compounds. The different concentrations required to minimize this effect will be different for each proxy and different in each sample as these ratios differ. One solution may be to

run standards more frequently, interspersed with samples, so that biomarker concentrations can be measured and ratios used for proxies can be calculated and compared from throughout the run, and the statistics of these can be used to guide the uncertainties for the samples. This clearly emphasizes the importance of using samples as concentrated as possible for making measurements.

Isotope Measurements

For biomarker analysis on the DeltaPlus XP, a mix of *n*-alkanes from C_{16} to C_{30} was produced using compounds of known $\delta^{13}C$ values (compounds prepared and measured by Arndt Schimmelmann of the University of Indiana). This standard is analyzed before every sample run, as well as multiple times during the sample run to test the accuracy and reproducibility of the instrument. Sample data is only used if the average error from the known values is less than 0.25‰ vs. VPDB. A comparison of the isotopic values from this standard run over a period of two years was compared to obtain statistics for uncertainties within the samples. The error between the measured and known values had an average of 0.24% of the known values, and the 1σ standard deviation was 1.5% of the known values. The only significant trend observed was a decrease in the difference between the known and measured $\delta^{13}C$ values with an increase in carbon number, but the total difference was only between 0.5% and 0.05% of the known standard values.

From this analysis it can be concluded that these uncertainties are very small, and are consistent with the 1σ standard deviation of 0.5% to 0.8% (equivalent to <0.25‰ for most samples, except for a few where values were >0.5‰) within repeat measurements of

compounds in the samples. The higher standard deviation in sample data may be a result of slight interference from other close-eluting compounds, as whole saturated fractions were used for compound-specific *n*-alkanes and isoprenoids in the Peace River and Meishan sections and whole aromatic fractions were used for aryl isoprenoid measurements in the Peace River.

Calculations

Isotope data are measured in delta notation and values are given in permil, using the equation:

$$\delta^{13}C = 1000 * (R_{sample} - R_{standard})/R_{standard}$$

where R_{sample} is the $^{13}C/^{12}C$ ratio of the sample and $R_{standard}$ is the $^{13}C/^{12}C$ ratio for the standard Vienna Pee Dee Belemnite (VPDB).

To calculate correlation coefficients a vector of the $\Delta\delta$ values was created and the corrcoef function of MATLAB was run comparing this vector to vectors comprised of data from the other proxies. This function calculates the correlation coefficient as defined:

$$\rho = cov(X,Y)/(\sigma_x\sigma_y)$$

where cov(X,Y) is the covariance between X and Y, and σ is the standard deviation. See Table A1.1 for all measured correlation coefficients.

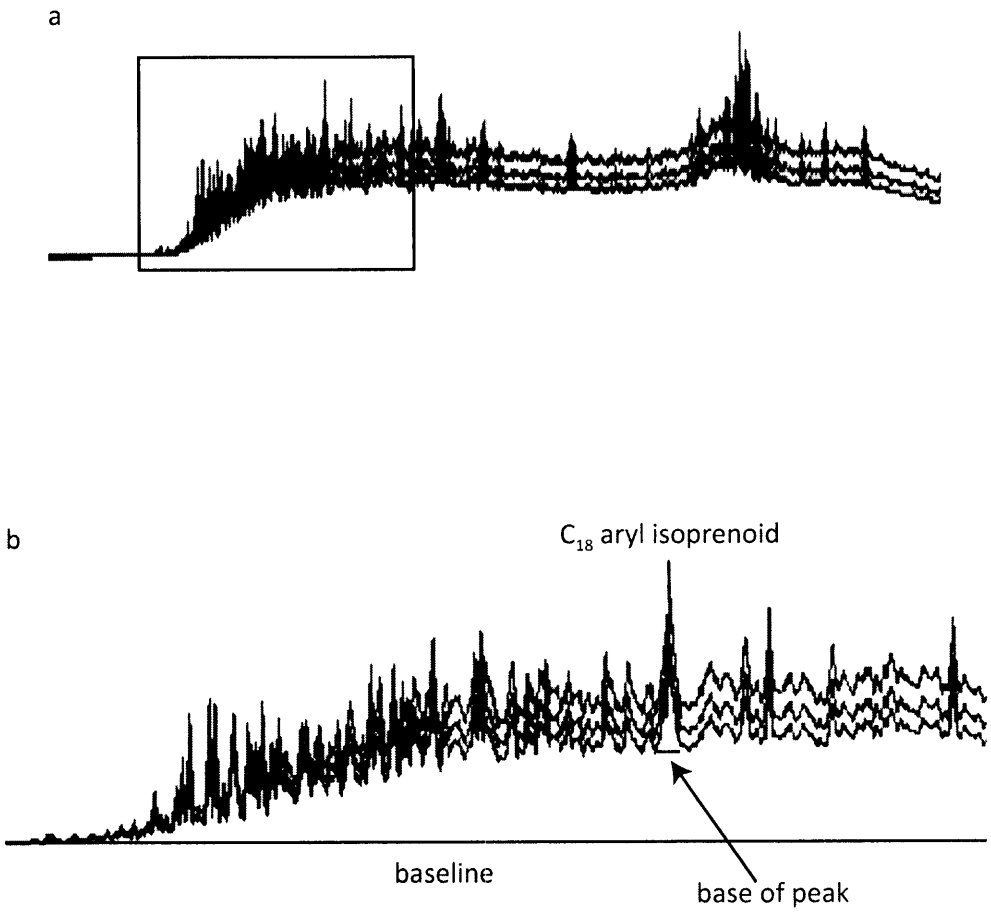

Figure A1.1 Gas chromatogram for a select Peace River, Canada sample prepared for aryl isoprenoid isotope analysis. Three masses of carbon dioxide produced from combustion of the sample, 44, 45 and 46, are measured simultaneously. (a) Total chromatogram where the high background of complex mixture can be observed. (b) Inset from (a) with the C_{18} aryl isoprenoid identified. The $\delta^{13}C$ value of this compound is calculated by measuring the area under the peak for all three carbon masses. Different values result from using either the baseline for the section or the base of the peak as the bottom of the calculated area.

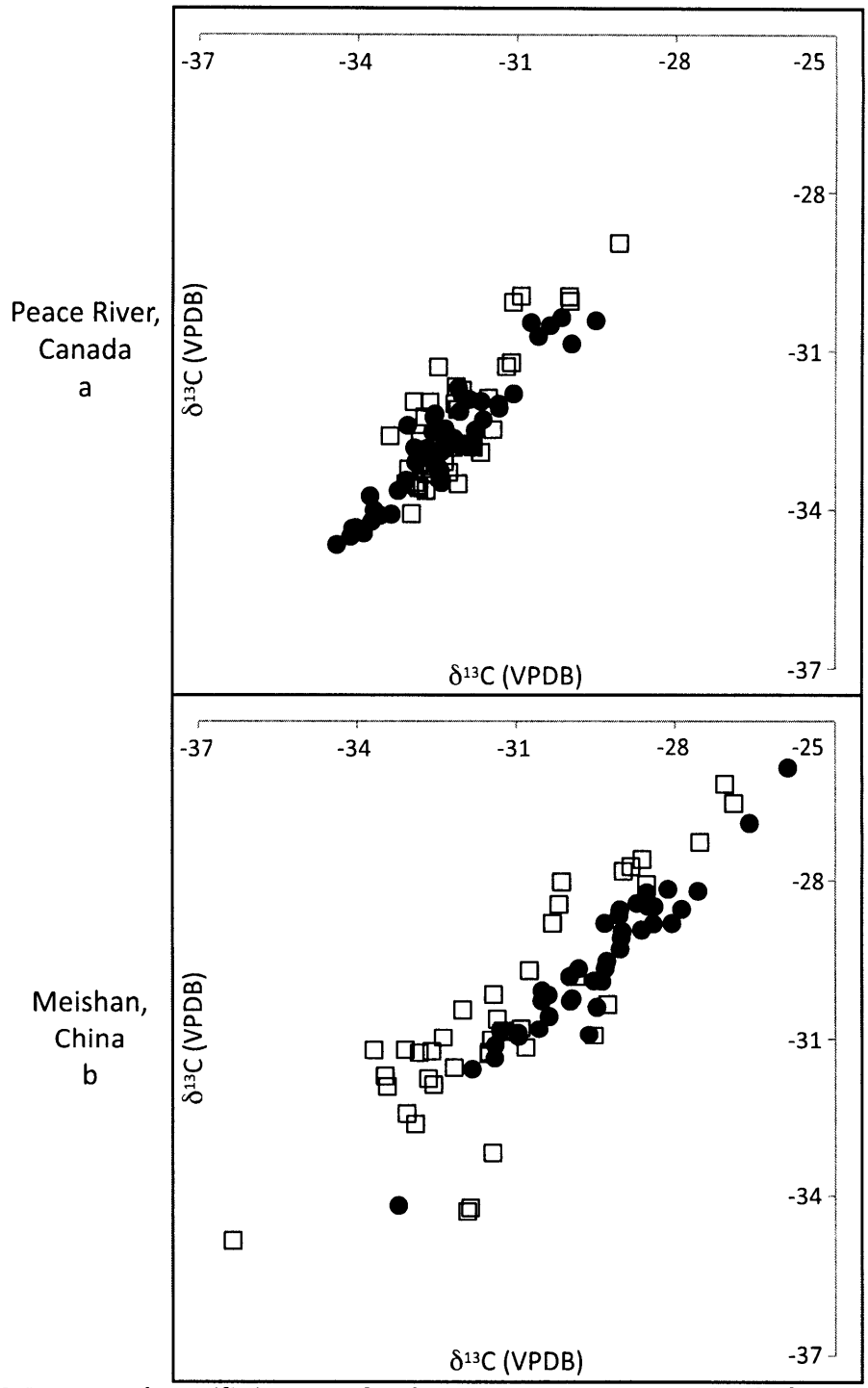

Figure A1.2 Compound-specific isotopes for the component compounds of Δδ. For both Peace River (a) and Meishan (b) closed circles represent the *n*-alkanes *n*-C_{17} and *n*-C_{18} and open squares represent the isoprenoids pristane and phytane. The horizontal axis is the lower-mass compound (*n*-C_{17} or pristane) and the vertical axis is the higher-mass compound (*n*-C_{18} or phytane).

Peace River	
Pr/Ph	0.343
Hopane/ Sterane	-0.075
C19/C23 tricyclic	0.060
C22/C21 tricyclic	-0.165
C24/C25 tricyclic	0.172
C26/C25 tricyclic	0.051
Tet/C23 tricyclic	0.170
C27 Dia/Reg	0.169
C29 Dia/Reg	0.203
C27 Reg aaa S/(S+R)	-0.066
C27/(total)	0.009
C28/(total)	-0.262
C29/(total)	0.173
C30/(total)	-0.224
C27/C29 sterane	0.016
C28/C29 sterane	-0.212
Ts/Tm	0.030
29,30-DNH/C30 hopane	-0.055
C29 ba/ab	-0.087
C30 ba/ab	-0.086
C30 2-MHI	-0.135
C30 3-MHI	0.151
C31 S/(S+R)	-0.047
C35/C34 hopane	0.278
C29/C30 hopane	0.258
C31(R) /C30 hopane	-0.098
AI (mg/ g TOC)	0.081

Meishan	
Delta org Carb	-0.156
TOC %	-0.147
Pr/Ph	0.215
C35 HHI %	**-0.523**
28,30-DNH/C30 Hopane %	-0.297
isorenieratane (ppmTOC)	**-0.471**
total AI (ppmTOC)	-0.371
Hopane/ Sterane	-0.332
% C27 Sterane	-0.338
% C28 Sterane	0.199
Gamma/C30 H	-0.358
3b-MHI %	0.380
2a-MHI %	0.129
Ts/(Ts+Tm)	0.090
C29 Dia/Reg	**0.443**
C30 H ba/ (ba+ab) %	0.198
C31 hopane S/(S+R) %	**0.494**
C27 S/(S+R) aaa Sterane%	0.084
C27 Dia/(Dia+Reg) Sterane	**0.577**
% C29 Sterane	0.316
% C30 Sterane	**-0.544**

Table A1.1 Table of correlation coefficients measured relative to Δδ for various biomarker parameters in the Peace River, Canada and Meishan, China sections. Significant correlations are highlighted.

Appendix 2

Reprinted from Palaeoworld 16 1-3, Lindsay E. Hays, Tyler Beatty, Charles M. Henderson, Gordon D. Love, Roger E. Summons, Evidence for Photic Zone Euxinia Though the End-Permian Mass Extinction in the Panthalassic Ocean (Peace River Basin, Western Canada), p39-50, Copyright (2007), with permission from Elsevier.

Evidence for Photic Zone Euxinia through the End-Permian Mass Extinction in the Panthalassic Ocean (Peace River Basin, Western Canada)

Lindsay Hays[1], Tyler Beatty[2], Charles M. Henderson[2], Gordon D. Love[1, 3] and Roger E. Summons[1*]

[1] Massachusetts Institute of Technology, Department of Earth, Atmospheric and Planetary Sciences, 77 Massachusetts Avenue, Cambridge MA 02139 USA

[2] Department of Geology and Geophysics, University of Calgary, 2500 University Drive, NW Calgary, Alberta T2N1N4, Canada

[3]Present address: Department of Earth Sciences, University of California, Riverside, CA 92521, USA

Key Words:

Permian Triassic Extinction, biomarkers, biostratigraphy, photic zone euxinia, Panthalassic Ocean, Peace River Basin, Alberta, Canada

Abstract

A combination of sequence stratigraphic and conodont biostratigraphic analyses of sediment cores from five petroleum exploration wells, together with reference to nearby outcrops, has allowed us to construct a composite geological section through the Permian-Triassic transition in the Peace River Basin of Western Canada. The cores contain significant contents of organic matter comprising kerogen and bitumen of low to moderate thermal maturity. Extraction and analysis of the bitumens has revealed patterns of biomarker hydrocarbons consistent with marine deposition and photic zone euxinia. In particular isorenieratane and aryl isoprenoids, derived from the carotenoid pigments of green sulfur bacteria (Chlorobiaceae), are abundant and pervasive throughout the section and indicate that hydrogen sulfide must have been present in the photic zone for significant periods of time. These findings mirror the geochemical results obtained for other Permian-Triassic boundary sections of the Tethys realm (e.g. Western Australia, East Greenland and South China) and suggest that euxinic conditions prevailed widely, though perhaps periodically, and that hydrogen sulfide toxicity could have been an important factor in the extinction of marine invertebrates.

1. Introduction

The end-Permian mass extinction of 252 million years ago (Bowring et al., 1998; Mundil et al., 2004) is the most profound and best documented of the Phanerozoic (Erwin, 2006). Over a period of less than half a million years, the marine ecosystem is thought to have lost close to 94% of its invertebrate and vertebrate fauna (Jin et al., 2000) while, on land, there was a significant loss of animals and plants (Retallack, 1995; Looy et al., 2001; Retallack et al., 2003; Ward et al., 2005). This extinction event is also the most enigmatic with numerous postulated

causes and a low degree of consensus on their respective merits. Although a comprehensive understanding has proven elusive, various lines of evidence indicate a close association between the faunal extinction and major perturbations to both ocean chemistry (Holser, 1977; Holser et al., 1989; Magaritz et al., 1992; Isozaki, 1995; Payne et al., 2004; Grice et al., 2005), and sea-level (Simberloff, 1974). Hypercapnia, following overturn of an anoxic and CO_2-rich water column, best explains the selective extinction of organisms with susceptible physiologies in both the terrestrial and marine realms according to one hypothesis (Knoll et al., 1996; Wignall and Twitchett, 1996; Huey and Ward, 2005; Knoll et al., 2007 (In Press)). In a recent paper, Wagner et al (2006) concluded that the Permian-Triassic boundary (PTB) event caused permanent changes to the structure of the marine ecosystem based on the distribution of fossil assemblages across the boundary. Additional postulated factors and/or causes of extinction include a lowering of atmospheric pO_2 (Berner, 2005; Huey and Ward, 2005), rapid climate change following widespread collapse of methane hydrates (Krull and Retallack, 2000; Krull et al., 2000) and terrestrial ecosystem breakdown possibly as a consequence of Siberian traps volcanism (Visscher et al., 1996; Visscher et al., 2004; Sephton et al., 2005). A bolide impact (Becker et al., 2001; Basu et al., 2003; Becker et al., 2004) is the most controversial postulated extinction mechanism (Koeberl et al., 2004). Ultimately, the mass extinction may never be attributable to a single cause but, rather, to a 'tangled web of causality' (Erwin, 1994; Erwin, 2006).

Multiple sets of stable carbon and sulfur isotopic data, together with other geochemical and mineralogical characteristics, associate the Permian-Triassic extinction with an extreme and protracted perturbation of the marine carbon cycle with the attributes of an oceanic anoxic event

(OAE) or events (Holser, 1977; Holser et al., 1989; Magaritz et al., 1992; Knoll et al., 1996; Wignall and Twitchett, 1996; Payne et al., 2004; Riccardi et al., 2006). Enhanced burial of pyrite and patterns of sulfur isotopes suggest that the marine sulfate inventory was depleted through organic matter respiration and that euxinia was widespread in the open ocean (Holser et al., 1989; Isozaki, 1995; Kato et al., 2002; Nielsen and Shen, 2004; Grice et al., 2005). Furthermore, molecular evidence from sediment cores spanning the boundary in Australia, and at the type section in Meishan, China (Grice et al., 2005), show that these localities were prone to photic zone euxinia (PZE), that is, a situation where concentrations of sulfide, sufficient to support anoxygenic photosynthesis, were prevalent in the realm of light penetration. Evasion of highly toxic hydrogen sulfide to the very surface of the ocean, thence into the atmosphere, has been proposed as a mechanism for bringing about mass mortality simultaneously in the sea and on land during the Permian extinction (Kump et al., 2005; Riccardi et al., 2006). Ready saturation, and a tendency to slow regeneration of the atmospheric hydroxyl radical sink for hydrogen sulfide while ever sulfide is upwelling to the surface, would account for the protracted biotic recovery (Kump et al., 2005).

In the modern world, PZE persists in salinity-stratified bodies of water, such as the Black Sea and fjords of the Arctic and Antarctic (Overmann et al. 1992; Smittenberg et al. 2004) but has, so far, not been reported in open ocean waters. However, sulfide eruptions with fish kills have been observed during periods of intense upwelling off the Namibian coastline (Weeks et al., 2002) showing that even an oxygenated ocean can be prone to sulfide formation. Geochemical records of several Mesozoic OAEs suggest that PZE was prevalent in narrow seaways such as those of the Tethys realm and proto-Atlantic ocean (Wagner et al., 2004; van Breugel et al., 2006).

Molecular signals that indicate PZE conditions in both recent and ancient sedimentary environments trace their origins to the aromatic pigments of planktonic green (Chlorobiaceae) and purple (Chromatiaceae) sulfur bacteria of which the former are most often found. While Chlorobiaceae can inhabit benthic microbial mat communities in acidic, high sulfide hydrothermal settings (Castenholz et al., 1990; Madigan, 2003), the geologic record of their biomarkers suggests the majority of well-preserved ancient occurrences were in salinity-or thermally-stratified anoxic basins (Summons and Powell, 1986; Summons and Powell, 1987; Koopmans et al., 1996; Schouten et al., 2001; Pancost et al., 2004; Smittenberg et al., 2004; Brocks et al., 2005). It is only in these aquatic environments that anoyxgenic phototrophs can reach sufficient standing biomass for their lipids to make a significant contribution to total organic carbon contents and be detected in the resultant biomarker pool.

One particular pigment, isorenieratene, common to the brown strains of the Chlorobiaceae, is particularly diagnostic and found in high abundance at chemoclines in the Black Sea and in meromictic fjords and lakes (Overmann et al., 1992; Schouten et al., 2001; Smittenberg et al., 2004). During diagenesis isorenieratene is reduced to isorenieratane – a diaromatic C_{40} hydrocarbon with both aromatic rings having a 2,3,6-trimethyl substitution pattern. Also formed is a suite of C_{10}-C_{31} 1-alkyl-2,3,6-trimethyl aryl isoprenoids whose relative abundances are controlled by the loci of methyl branching along the chain bridging the two aromatic rings (Summons and Powell, 1987). While it has been suggested that 2,3,6-trimethyl aryl isoprenoids can arise from other carotenoid precursors (Koopmans et al., 1996), the vast majority of occurrences are accompanied by isorenieratane and/or isotopic data showing characteristically

high $\delta^{13}C$ values. Chlorobiaceae also contain bacteriochlorophylls *c*, *d* and *(e)* which have distinctive farnesyl side chains and patterns of alkylation of the tetrapyrrole rings. The diagenetic products of these pigments include the C_{15} isoprenoid farnesane and *n*-Pr and iso-Bu maleimides which identify them as potential biomarkers for Chlorobiaceae (Grice et al., 1996; Grice et al., 1997; Pancost et al., 2002). The utility of isorenieratane, aryl isoprenoids, farnesane and the *n*-Pr and iso-Bu maleimides is confirmed by their $\delta^{13}C$ values which have characteristically low values due to the fact that Chlorobiaceae fix carbon by the reverse tricarboxylic acid cycle. This confers a significant ^{13}C-enrichment on them relative to lipids from photosynthetic organisms that fix carbon via the Benson-Calvin cycle (Summons and Powell, 1987; Grice et al., 1996; Koopmans et al., 1996; Koopmans et al., 1996).

In this study we report biomarker distributions for sediments from a series of petroleum exploration drill cores from the latest Permian to Lower Triassic Montney Formation of the Peace River Basin of Western Canada. The biomarker patterns are presented together with a sequence biostratigraphic framework based on conodonts for the purpose of evaluating oxygen conditions in shallow marine waters during the PTB interval and Early Triassic. Furthermore, the data presented in this paper are the first to establish the existence of euxinic conditions in the Panthalassic Ocean at the end of the Permian.

2. Geologic Setting and Biostratigraphic Framework

The latest Permian and Early Triassic Montney Formation was deposited in a block-faulted embayment of the Ishbel Trough (Henderson, 1997) that was located along the northwestern margin of Pangaea at about 35°N paleolatitude (Figure 1). Previous studies have documented the

sequence stratigraphy, lithofacies distribution and conodont biostratigraphy for the Peace River Basin (Henderson, 1997; Markhasin, 1997; Kendall, 1999; Panek, 2000). Five drill cores were selected for this investigation based on their stratigraphic coverage from latest Changhsingian to Dienerian (late Induan) within lithofacies representative of an offshore transition to lower shoreface environments. The lithofacies consist of shale, ripple-laminated siltstone with shale drapes, low angle inclined cross-stratified coarse siltstone and very fine-grained sandstone, and lam-scram indicating storm deposition in the offshore transition zone with occasional bioturbation. The relatively depauperate ichnofauna primarily consists of *Planolites*, *Palaeophycus*, *Helminthopsis*, and rare *Cylindrichnus* and *Lingulichnus* indicating at least sporadic, short-lived, oxygenated conditions. The presence of fish scales, rare lingulid brachiopods and conodonts point to the marine setting. Parasequence G1b represents a sharp-based shoreface including high-angle cross-bedding in very fine-grained sandstone with ripped up intraclasts at the base. Samples for biomarker analysis are from the shale lithofacies associated with flooding surfaces and mud drapes in sandstone-siltstone lithofacies.

The lower Montney Formation represents a transgressive-regressive sequence comprising eight parasequences correlated throughout the subsurface of the Peace River Embayment using gamma-ray wire-line logs and sequence stratigraphic principles (Figure 2). These correlations have been tested biostratigraphically wherever core was available thereby providing relative age control to the parasequences. The initial transgressive deposits (G1, Figure 3) of the lower Montney Formation, which unconformably overlie the Middle Permian upper Belloy Formation, are correlated with the Late Changhsingian although conodonts of that age have not been recovered from the cores in this study. Elsewhere in outcrop sections (Henderson 1997)

Clarkina meishanensis together with *Clarkina hauschkei* indicate that the transgression began during the Late Permian as it does in other locations (Henderson and Baud, 1997; Korte et al., 2003). Furthermore, carbon isotopic analyses confirm that the negative excursion associated with the P-T boundary interval (Yin et al., 2001) occurs in the lower part of this transgressive succession (Garrison et al., 2005). The Permian-Triassic boundary occurs within parasequence G1, but the position cannot be precisely defined (Fig. 3). The upper part of parasequence G1 includes *Clarkina taylorae*, *C. tulongensis*, *C. nevadensis* and *Hindeodus parvus* which correlate with the earliest Triassic. Parasequences G1b and G2 include *Clarkina carinata* and *C. planata* indicating a well developed Griesbachian succession. There are no subsurface cores that penetrate parasequences G3-G5 in the immediate study area, but elsewhere in the basin parasequences G4 and G5 include *Clarkina krystyni* and *C.* cf. *kazi* that correlate with the Upper Griesbachian (Orchard & Krystyn 1998). The occurrence of *Sweetospathodus kummeli* in the top of G5 points to the Griesbachian-Dienerian boundary at approximately this level. Parasequences D2 to D5 include *Neospathodus cristagalli* and *N. dieneri* indicating correlation with the Upper Dienerian.

3. Materials and Methods

The sampled cores are geographically located in Figure 1 and placed within a sequence stratigraphic and environmental context in Figure 2 (latitudes and longitudes are provided in the caption). The individual samples from the five cores are stratigraphically arranged in Figure 3. The relative position of those samples is also reflected in the depiction of geochemical data in Figure 5.

Core pieces of 8-15 cm^3 were cleaned with a wire brush in DI water to remove any contaminating particulate organic matter (OM). The outsides of the cores were then cleaned with 3 washes of methanol (MeOH), 6 washes of dichloromethane (DCM) and 3 washes of hexane to remove external bitumen contamination. From this point forward, the rock was only in contact with glass or aluminum that had either been fired for 10 hours at 550°C or cleaned with the same process of 3 washes of MeOH, 6 washes of DCM and 3 washes of hexane. The whole rock fragments were then crushed to a fine powder in the SPEX 8510 Shatterbox ceramic puck mill for three 1-minute periods. Between samples, the puck mill was cleaned by crushing fired sand three times for 1-minute periods each followed by washing with the same solvent sequence. RockEval and TOC data were provided by Humble Geochemical Services in Humble, Texas.

Each powdered sample (ca. 15g) was then placed in an extraction cell for processing with a DIONEX ASE 200 Accelerated Solvent Extractor using a solvent mixture of 9:1 DCM to MeOH (v:v) at 1000psi and 100°C. This process was repeated three times, the solutions pooled in a single vial and then treated with activated copper to remove any elemental sulfur. This total lipid extract (TLE) was then separated by column chromatography on a silica gel column affording saturated hydrocarbons, an aromatic hydrocarbon fraction and a polar lipid fraction, by elution with solutions of increasing polarity comprising, respectively, hexane, hexane:DCM (4:1 v:v) and DCM:MeOH (4:1 v:v) solution. The saturated fraction and aromatic fractions were gently dried, weighed and re-suspended in hexane. 50 ng of D4 20R stigmastane standard was added to the saturated fraction and 100 ng of D14 p-terphenyl standard was added to the aromatic fraction for quantification.

Both the saturated and aromatic fractions were analyzed by gas chromatography-mass spectrometry (GC-MS) on a HP 6890 GC fitted with split/splitless injector and a 60 m J&W Scientific DB-1 fused silica capillary column (60 m x 0.32 mm; 0.25 μm film thickness) attached to an Agilent 5973 mass selective detector (MSD). Injections were 1 μl from a total of 100 μl for both fractions. For the saturated fraction, samples were injected at 60°C and held for 2 min prior to a constant pressure (20.3 psi) programmed temperature ramp of 10°C/min to 100°C, 4°C/min to 320°C and followed by a hold period of 20 min. Similar conditions were used for the aromatic fraction except that the temperature was raised from an initial 60°C at 20°C/min to 150°C followed by 2°C/minute to 320°C and a hold of 15 minutes. Saturated hydrocarbons were analyzed in the full scan mode while aromatics were run in selected ion monitoring (SIM) mode for the following ions: 91, 105, 119, 125, 133, 134, 178, 191, 192, 231, 237, 244, 245, 253, 287 and 365 Da. Individual compounds were semi-quantified by comparison of their peak areas to that of the D_{14}-terphenyl internal standard (244 Da) without correcting for individual response factors.

Saturated hydrocarbon fractions were also analyzed in GC-MS using a Waters AutoSpec Ultima operated at 70eV in the multiple reaction monitoring (MRM) mode. Samples were injected onto a J&W Scientific DB-1 fused silica capillary column (60 m x 0.25 mm; 0.25μm film thickness) via the split/splitless injector operated in splitless mode with helium as the carrier gas. The oven was programmed from 60°C (held for 2 min) to 150°C at 10°C/min, and then at 3°C/min to 315°C with a final hold of 24 min. A suite of C_{26}-C_{30} steranes, C_{27}-C_{35} hopanes, C_{31} methylhopanes and

C_{26}-C_{30} cheilanthanes were quantified via their specific precursor-product reactions and using the D_4-ααα-ethylcholestane (D_4) as internal standard without taking into account response factors.

4. Results and Discussion

4.1 Bulk Geochemical Parameters

Core samples from five petroleum exploration wells from the Peace River region were analyzed for their organic carbon contents and the average values for each well are given in Table 1. The TOC contents were quite low and varied between 0.5 and 2.0 wt% for most samples in the Permian and earliest Triassic, and the values range from 0 to 3.0 wt% in the Dienerian samples (Table 1).

Results of RockEval analyses, supported by the biomarker data discussed below, show that maturity levels within all 5 wells were early oil window for the Clouston and Apexco wells and middle oil window for the Kandex and Chevron wells. Lowest TOC contents were observed in the Kandex well where most of the organic carbon was present as bitumen. The relatively high production indices of 0.3 to 0.6 indicate that the hydrocarbons may have migrated somewhat and that the Tmax values of 420-430 °C were probably suppressed.

4.2 Biomarkers in the Aromatic Hydrocarbon Fractions

Isorenieratane and the 1-alkyl-2,3,6-trimethyl monoaromatic degradation products were present in all of the analyzed samples and their identities were confirmed by comparison of retention times with authentic standards as reported previously (Summons and Powell, 1987; Brocks et al., 2005; Grice et al., 2005). Figure 4 shows a typical 134 Da trace bearing the characteristic

relative abundance pattern where the C_{17} and C_{22} members of the series have reduced relative abundances. When referenced to the TOC (Figure 5) it can be seen that samples that traverse the boundary into the earliest Triassic have values of 0.4 mg/g (mg isorenieratane derivatives per g TOC) or higher. However, there is a significantly lower range of abundances in the younger samples, where values rarely rise above 0.2 mg/g. While the monoaromatic aryl isoprenoids have been questioned as being biomarkers for PZE (Koopmans et al., 1996) their prevalence and the consistency of their detection together with the parent C_{40} precursor isorenieratane leaves no doubt about their origin from Chlorobiaceae.

4.3 Biomarkers from Saturated Hydrocarbon Fractions

The depositional environments of sedimentary rocks can be inferred from their lithologies and patterns of sedimentation. In hydrocarbon-producing basins, where sedimentary organic matter is abundant and of appropriate maturity, hydrocarbon biomarkers can provide an independent means of reconstructing paleoenvironmental conditions (Seifert and Moldowan, 1981; Zumberge, 1987; Brocks and Summons, 2004; Peters et al., 2004). For example, the ratio of C_{26}/C_{25} tricyclic terpanes to C_{31}/C_{30} hopanes can be used to differentiate marine from lacustrine source-rocks, as these compounds are produced in different ratios by microorganisms from these environments. It has been empirically demonstrated that marine source rocks typically have low (<1) C_{26}/C_{25} tricyclic ratios and high (> 0.25) C_{31}/C_{30} hopane ratios (Zumberge, 1987; Peters et al., 2004). In the Peace River samples, the C_{26}/C_{25} tricyclic ratios vary from 0.4 to just under 1, and the C_{31}/C_{30} hopane ratios range from 0.3 to 0.6 consistent with sedimentation under marine conditions.

The C_{30} sterane index is the ratio of C_{30} steranes (24-*n*-propylcholestanes) to total C_{27}-C_{30} steranes. This index facilitates the identification of sedimentary rocks with high marine OM input due to the observation that marine Chrysophyte algae biosynthesize 24-*n*-propylcholesterol which is diagenetically altered to 24-n-propylcholestane isomers in sediments (Moldowan, 1984). Empirical analysis of a large suite of oil samples has shown that C_{30} sterane abundances in excess of 4% of total C_{27}-C_{30} steranes indicates significant contribution from these organisms to OM deposition (Peters et al., 2004). The values for the C_{30} sterane index for most of the Peace River samples range from 3.5 to 5.5%, providing additional evidence of their deposition within a marine setting.

Pristane and phytane in sediments are derived primarily from the diagenetic alteration of the phytol side chain of chlorophyll *a* and bacteriochlorophyll *a* and *b* from algae and cyanobacteria (Brooks et al., 1969) and their relative abundance is broadly used as proxy for the redox conditions prevailing during sediment deposition (Peters et al., 2004). A pristane/phytane ratio of <1 has been used to indicate marine anoxic OM deposition conditions while values of 2.0 or more are indicative for oxic conditions or deposition in a non-marine environment. In the Peace River data set, the ratio of pristane/phytane is uniformly low with values less than 0.8 for the end of the Permian and Early Triassic. It reaches values of 1 in the early Dienerian and increases to 1.5 in some of the youngest Triassic samples. Taken at face value, these data are consistent with the aforementioned C_{30} sterane, tricyclic terpane and C_{31}/C_{30} hopane proxies for marine deposition.

Final confirmation comes from the relative abundances of C_{31}-C_{35} homohopanes – hopanes derived from polyfunctional C_{35} hopanoids present in bacteria (Ourisson et al., 1979). High values of C_{35} relative to C_{34} hopanes (~1) are interpreted as an indicator of bottom water anoxic deposition (Peters and Moldowan, 1991) and/or signify early catagenetic release of hopane skeletons bound into the parent kerogens with thermally labile poly-, di- or mono-sulfide linkages in their alkyl side-chain (Köster et al., 1997) The ratio of C_{35}/C_{34} homohopanes is relatively high throughout these samples, varying between 0.75 and 1.25 with a few exceptions in the Dienerian where the value increases to 2 or greater.

The 2-methylhopane index (2-MeHI) has been proposed as a proxy for cyanobacterial contributions to sedimentary organic matter (Summons et al., 1999). Further, it has been observed that this index can be exceptionally high during OAEs (Kuypers et al., 2004; Knoll et al., 2007 (In Press)). In the Peace River sample set, the 2-MeHI is low compared to the high values seen in Cretaceous OAEs (Kuypers et al., 2004). Across the boundary and into the earliest Triassic, the values range from 0.015 to 0.05 consistent with the presence of cyanobacteria in abundances typical of marine clastic sediments and their derived oils (Knoll et al., 2007 (In Press)). The index increases into the Dienerian where it is in the range of 0.035 to 0.13 – indicative of an increased importance of cyanobacterial primary producers. Because some cyanobacteria are able to independently fix N_2, enhanced values of the 2-MeHI during OAEs have been attributed to disruption of the normal marine N-cycle and curtailment of nitrification during periods of intense euxinia (Kuypers et al., 2004). In fact, this hypothesis is supported by a very strong correlation between high values of the 2-MeHI and high abundances of aryl isoprenoids in Phanerozoic oils and their source rocks (Knoll et al., 2007 (In Press)).

MRM chromatograms for the steranes and triterpanes of a typical Peace River Basin sample are shown in Figure 6. The low ratios of diasteranes to steranes and high abundances of 30-norhopanes suggest that this rock has a low content of acidic clays. The values of parameters such as the 20S/20S+20R, Ts/Tm and moretane/hopane ratios indicate a middle oil window maturity level. The pattern of C_{30} desmethyl steranes are characteristic of marine sedimentation and dinosteranes are present in significant abundance in the Early Triassic sediment.

4.4 Possible Effects of Maturity and Bitumen Migration

The RockEval data, especially the high production indices and suppressed T_{max} values indicate that a significant fraction of the kerogen has been converted to bitumen and that migration of these hydrocarbons may have attenuated the stratigraphic variations of the biomarker ratios. Vertical migration of bitumen would tend to homogenize the geochemical variations that would otherwise allow us to identify the true scale of redox and biota fluctuations in our sample set. The lower maturity levels of the Clouston and Apexco samples, as well as the relatively low TOC contents, suggest that the biomarker hydrocarbons from these wells are most likely to be *in-situ*. This is confirmed by the wide span and variation in biomarker proxies for redox conditions and lithology such as Pr/Ph, diasteranes/sterane, 29,30-DNH/hopane and 28,30-DNH/hopane ratios, that exist in these two wells. Thus, while some of the natural variability in biomarker parameters may be lost to vertical mixing of bitumens, evidence of dynamic change in the microbial community over the section is still preserved.

5. Summary

Conodont biostratigraphy indicates that rocks that transition the Permian Triassic Boundary are present in the Peace River Basin of Western Canada. Using this information, combined with sequence stratigraphic analysis, has allowed us to piece together a partial composite Late Permian to Early Triassic section using cores from five petroleum exploration wells. Organic matter from this section then allowed us to examine aspects of the prevailing paleoenvironmental conditions and microbiota.

Biomarker parameters indicative of euxinia and water column stratification are present through the PTB and into the early Triassic in these samples from the Peace River Basin. These biomarkers decrease or are absent in samples from the Dienerian, indicating some measure of recovery to a more oxygenated water column. The parameters measured in this study indicate that euxinia extending into the photic zone was present at the PTB in this region of the eastern Panthalassic Ocean. This is the first evidence of these conditions in the greater Panthalassic Ocean and indicates that this phenomenon was not limited to the Tethys and inland seas such as the Permian Zechstein at the PTB (Pancost et al 2002; Grice et al 1997). The geochemical data from this Peace River sample set supports an overall model of carbon cycling that has been previously presented for the PTB in other regions (Payne et al., 2004; Grice et al., 2005). Significant fluctuations in a range of geochemical parameters presage the boundary and continue well into the recovery period. This suggests that the microbiota at this location were in dynamic flux and that the carbon cycle continued to be unstable for some time after the main extinction event.

The evidence for PZE conditions and rapid transgression form a pattern similar to that proposed by Grice et al (2005) for euxinic waters in the Tethys realm. The presence of these conditions in the eastern Panthalassic Ocean strengthens the argument for sulfide toxicity as a global driver of the Permian-Triassic extinction.

6. References.

Basu, A. R., M. I. Petaev, R. J. Poreda, S. B. Jacobsen and L. Becker (2003). "Chondritic Meteorite Fragments Associated with the Permian-Triassic Boundary in Antarctica." *Science* **302**(5649): 1388-1392.

Becker, L., R. J. Poreda, A. R. Basu, K. O. Pope, T. M. Harrison, C. Nicholson and R. Iasky (2004). "Bedout: A Possible End-Permian Impact Crater Offshore of Northwestern Australia." *Science* **304**(5676): 1469-1476.

Becker, L., R. J. Poreda, A. G. Hunt, T. E. Bunch and M. Rampino (2001). "Impact event at the Permian-Triassic boundary: evidence from extraterrestrial noble gases in fullerenes." *Science* **291**: 1530-1533.

Berner, R. A. (2005). "The carbon and sulfur cycles and atmospheric oxygen from middle Permian to middle Triassic." *Geochimica et Cosmochimica Acta* **69**(13): 3211-3217.

Bowring, S. A., D. H. Erwin, Y. G. Jin, M. W. Martin, K. Davidek and W. Wang (1998). "U/Pb Zircon Geochronology and Tempo of the End-Permian Mass Extinction." *Science* **280**(5366): 1039-1045.

Brocks, J. J., G. D. Love, R. E. Summons, A. H. Knoll, G. A. Logan and S. A. Bowden (2005). "Biomarker evidence for green and purple sulphur bacteria in a stratified Palaeoproterozoic sea." *Nature* **437**(7060): 866.

Brocks, J. J. and R. E. Summons (2004). Sedimentary hydrocarbons, biomarkers for early life. Biogeochemistry. W. H. Schlesinger. Oxford, Elsevier. **8:** 63-116.

Brooks, J., K. Gould and J. Smith (1969). "Isoprenoid Hydrocarbons in Coal and Petroleum." *Nature* **222**(5190): 257-259.

Castenholz, R. W., J. Bauld and B. B. Jorgenson (1990). "Anoxygenic microbial mats of hot springs: thermophilic Chlorobium sp." *FEMS Microbiology Letters* **74**(4): 325-336.

Erwin, D. H. (1994). "The Permo-Triassic extinction." *Nature* **367**: 231-236.

Erwin, D. H. (2006). Extinction: how life on earth nearly ended 250 million years ago. Princeton, Princeton University Press.

Garrison, G. H., P. D. Ward and C. M. Henderson (2005). Stable isotope chemostratigraphy across the conformable Permian-Triassic Boundary at Opal Creek, Alberta. American Association of Petroleum Geologists Annual Convention, A49.

Grice, K., C. Cao, G. D. Love, M. E. Bottcher, R. J. Twitchett, E. Grosjean, R. E. Summons, S. C. Turgeon, W. Dunning and Y. Jin (2005). "Photic Zone Euxinia During the Permian-Triassic Superanoxic Event." *Science* **307**(5710): 706-709.

Grice, K., R. Gibbison, J. E. Atkinson, L. Schwark, C. B. Eckardt and J. R. Maxwell (1996). "Maleimides (1H-pyrrole-2,5-diones) as molecular indicators of anoxygenic

photosynthesis in ancient water columns." *Geochimica et Cosmochimica Acta* **60**(20): 3913-3924.

Grice, K., P. Schaeffer, L. Schwark and J. R. Maxwell (1997). "Changes in palaeoenvironmental conditions during deposition of the Permian Kupferschiefer (Lower Rhine Basin, northwest Germany) inferred from molecular and isotopic compositions of biomarker components." *Organic Geochemistry* **26**(11-12): 677.

Henderson, C. M. (1997). "Uppermost Permian conodonts and the Permian-Triassic boundary in the Western Canada sedimentary basin." *Bulletin of Canadian Petroleum Geology* **45**(4): 693-707.

Henderson, C. M. and A. Baud (1997). Correlation of the Permian-Triassic boundary in Arctic Canada and comparison with Meishan, China. Proceedings of the 30th International Geological Congress.

Holser, W. T. (1977). "Catastrophic chemical events in the history of the ocean." *Nature* **267**(5610): 403.

Holser, W. T., H.-P. Schonlaub, M. Attrep, K. Boeckelmann, P. Klein, M. Magaritz, C. J. Orth, A. Fenninger, C. Jenny, M. Kralik, H. Mauritsch, E. Pak, J.-M. Schramm, K. Stattegger and R. Schmoller (1989). "A unique geochemical record at the Permian/Triassic boundary." *Nature* **337**(6202): 39.

Huey, R. B. and P. D. Ward (2005). "Hypoxia, Global Warming, and Terrestrial Late Permian Extinctions." *Science* **308**(5720): 398-401.

Isozaki, Y. (1995). "Superanoxia across the Permo-Triassic boundary: record in accreted deep-sea pelagic chert in Japan." *Canadian Society of Petroleum Geologists, Memoir 17*: 805-812.

Jin, Y., Y. Wang, W. Wang, Q. H. Shang, C. Cao and D. H. Erwin (2000). "Pattern of Marine Mass Extinction Near the Permian-Triassic Boundary in South China." *Science* **289**: 432-436.

Kato, Y., K. Nakao and Y. Isozaki (2002). "Geochemistry of late Permian to early Triassic pelagic cherts from southwest Japan: Implications for an oceanic redox change." *Chemical Geology* **182**: 15–34.

Kendall, D. R. (1999). Sedimentology and Stratigraphy of the Lower Triassic Montney Formation, Peace River Basin, subsurface of northwestern Alberta. Calgary, University of Calgary. **M.Sc.:** 368.

Knoll, A. H., R. K. Bambach, D. E. Canfield and J. P. Grotzinger (1996). "Comparative Earth History and Late Permian Mass Extinction." *Science* **273**(5274): 452-457.

Knoll, A. H., R. E. Summons, J. Waldbauer and J. Zumberge (2007 (In Press)). The Geological Succession of Primary Producers in the Oceans. The Evolution of Photosynthetic Organisms in the Oceans. F. P. a. K. A.H.

Koeberl, C., K. A. Farley, B. Peucker-Ehrenbrink and M. A. Sephton (2004). "Geochemistry of the end-Permian extinction event in Austria and Italy: No evidence for an extraterrestrial component." *Geology* **32**(12): 1053-1056.

Koopmans, M. P., J. Koster, H. M. E. Van Kaam-Peters, F. Kenig, S. Schouten, W. A. Hartgers, J. W. de Leeuw and J. S. Sinninghe Damste (1996). "Diagenetic and catagenetic products of isorenieratene: Molecular indicators for photic zone anoxia." *Geochimica et Cosmochimica Acta* **60**(22): 4467.

Koopmans, M. P., S. Schouten, M. E. L. Kohnen and J. S. Sinninghe Damste (1996). "Restricted utility of aryl isoprenoids as indicators for photic zone anoxia." *Geochimica et Cosmochimica Acta* **60**(23): 4873.

Korte, C., H. W. Kozur, P. Bruckschen and J. Veizer (2003). "Strontium isotope evolution of Late Permian and Triassic seawater." *Geochimica et Cosmochimica Acta* **67**(1): 47.

Köster, J., H. M. E. Van Kaam-Peters, M. P. Koopmans, J. W. De Leeuw and J. S. Sinninghe Damste (1997). "Sulphurisation of homohopanoids: Effects on carbon number distribution, speciation, and 22S/22R epimer ratios." *Geochimica et Cosmochimica Acta* **61**(12): 2431-2452.

Krull, E. S. and G. J. Retallack (2000). "$\delta^{13}C$ depth profiles from paleosols across the Permian–Triassic boundary: evidence for methane release." *Geological Society of America Bulletin* **112**(9): 1459-1472.

Krull, E. S., G. J. Retallack, I. H. Campbell and G. L. Lyon (2000). "$\delta^{13}Corg$ chemostratigraphy of the Permian–Triassic boundary in the Maitai Group, New Zealand: evidence for high latitudinal methane release." *New Zealand Journal of Science* **43**: 23–32.

Kump, L. R., A. Pavlov and M. A. Arthur (2005). "Massive release of hydrogen sulfide to the surface ocean and atmosphere during intervals of oceanic anoxia." *Geology* **33**: 397–400.

Kuypers, M. M. M., Y. van Breugel, S. Schouten, E. Erba and J. S. S. Damste (2004). "N2-fixing cyanobacteria supplied nutrient N for Cretaceous oceanic anoxic events." *Geology* **32**(10): 853-856.

Looy, C. V., R. J. Twitchett, D. L. Dilcher, J. H. A. Van Konijnenburg-Van Cittert and H. Visscher (2001). "Life in the end-Permian dead zone." *PNAS* **98**(14): 7879-7883.

Madigan, M. T. (2003). "Anoxygenic phototrophic bacteria from extreme environments." *Photosynthesis Research* **76**(Numbers 1-3): 157-171.

Magaritz, M., R. V. Krishnamurthy and W. T. Holser (1992). "Parallel trends in organic and inorganic carbon isotopes across the Permian/Triassic boundary." *American Journal of Science* **292**(10): 727-739.

Markhasin, B. (1997). Sedimentology and Stratigraphy of the Lower Triassic Montney Formation, subsurface of northwestern Alberta. Calgary, University of Calgary. **M.Sc:** 153.

Moldowan, J. M. (1984). "C30-steranes, novel markers for marine petroleums and sedimentary rocks." *Geochimica et Cosmochimica Acta* **48**(12): 2767-2768.

Mundil, R., K. R. Ludwig, I. Metcalfe and P. R. Renne (2004). "Age and Timing of the Permian Mass Extinctions: U/Pb Dating of Closed-System Zircons." *Science* **305**(5691): 1760-1763.

Nielsen, J. K. and Y. Shen (2004). "Evidence for sulfidic deep water during the late Permian in the East Greenland Basin." *Geology* **32**: 1037–1040.

Ourisson, G., P. Albrecht and M. Rohmer (1979). "The Hopanoids. Palaeochemistry and Biochemistry of a Group of Natural Products." *Pure and Applied Chemistry* **51**(4): 709-729.

Overmann, J., H. Cypionka and N. Pfenning (1992). "An extremely low-light-adapted phototrophic sulfur bacterium from the Black Sea." *Limnology and Oceanography* **37**(1): 150-155.

Pancost, R. D., N. Crawford, S. Magness, A. Turner, H. C. Jenkyns and J. R. Maxwell (2004). "Further evidence for the development of photic-zone euxinic conditions during Mesozoic oceanic anoxic events." *Journal of the Geological Society* **161**(3): 353-364.

Pancost, R. D., N. Crawford and J. R. Maxwell (2002). "Molecular evidence for basin-scale photic zone euxinia in the Permian Zechstein Sea." *Chemical Geology* **188**(3-4): 217.

Panek, R. (2000). The Sedimentology and Stratigraphy of the Lower Triassic Montney Formation in the subsurface of the Peace River area, northwestern Alberta. Calgary, University of Calgary. **M.Sc.:** 275.

Payne, J. L., D. J. Lehrmann, J. Wei, M. J. Orchard, D. P. Schrag and A. H. Knoll (2004). "Large Perturbations of the Carbon Cycle During Recovery from the End-Permian Extinction." *Science* **305**(5683): 506-509.

Peters, K. and J. Moldowan (1991). "Effects of source, thermal maturity, and biodegredation on the distribution and isomerization of homohopanes in petroleum." *Organic Geochemistry* **17**(1): 47-61.

Peters, K. E., C. C. Walters and J. M. Moldowan (2004). The Biomarker Guide. Cambridge, Cambridge University Press.

Retallack, G. J. (1995). "Permian-Triassic Life Crisis on Land." *Science* **267**(5194): 77-80.

Retallack, G. J., R. M. H. Smith and P. D. Ward (2003). "Vertebrate extinction across Permian-Triassic boundary in Karoo Basin, South Africa." *Geological Society of America Bulletin* **115**(9): 1133-1152.

Riccardi, A. L., M. A. Arthur and L. R. Kump (2006). "Sulfur isotopic evidence for chemocline upward excursions during the end-Permian mass extinction." *Geochimica et Cosmochimica Acta*(70): 5740-5752.

Schouten, S., W. I. C. Rijpstra, M. Kok, E. C. Hopmans, R. E. Summons, J. K. Volkman and J. S. Sinninghe Damste (2001). "Molecular organic tracers of biogeochemical processes in a saline meromictic lake (Ace Lake)." *Geochimica et Cosmochimica Acta* **65**(10): 1629.

Seifert, W. K. and J. M. Moldowan (1981). "Paleoreconstruction by biological markers." *Geochimica et Cosmochimica Acta* **45**(6): 783-798.

Sephton, M. A., C. V. Looy, H. Brinkhuis, P. B. Wignall, J. W. de Leeuw and H. Visscher (2005). "Catastrophic soil erosion during the end-Permian biotic crisis." *Geology* **33**(12): 941-944.

Simberloff, D. S. (1974). "Permo-Triassic extinction: effects of area on biotic equilibrium." *Journal of Geology* **82**: 267-274.

Smittenberg, R. H., Pancost R.D., E. C. Hopmans, M. Paetzel and J. S. Sinninghe Damsté (2004). "A 400-year record of environmental change in an euxinic fjord as revealed by the sedimentary biomarker record." *Palaeogeography, Palaeoclimatology, Palaeoecology* **202**: 331-351.

Summons, R. E., L. L. Jahnke, J. M. Hope and G. A. Logan (1999). "2-methylhopanoids as biomarkers for cyanobacterial oxygenic photosynthesis." *Nature* **400**(6744): 554-556.

Summons, R. E. and T. Powell (1986). "Chlorobiaceae in Paleozoic Seas Revealed by Biological Markers, Isotopes and Geology." *Nature* **319**(6056): 763-765.

Summons, R. E. and T. G. Powell (1987). "Identification of aryl isoprenoids in source rocks and crude oils: Biological markers for the green sulphur bacteria." *Geochimica et Cosmochimica Acta* **51**: 557-566.

van Breugel, Y., M. Baas, S. Schouten, E. Mattioli and J. S. Sinninghe Damsté (2006). "Isorenieratane record in black shales from the Paris Basin, France: Constraints on recycling of respired CO2 as a mechanism for negative carbon isotope shifts during the Toarcian oceanic anoxic event." *Paleoceanography* **21**: PA4220.

Visscher, H., H. Brinkhuis, D. L. Dilcher, W. C. Elsik, Y. Eshet, C. V. Looy, M. R. Rampino and A. Traverse (1996). "The terminal Paleozoic fungal event: Evidence of terrestrial ecosystem destabilization and collapse." *PNAS* **93**(5): 2155-2158.

Visscher, H., C. V. Looy, M. E. Collinson, H. Brinkhuis, J. H. A. van Konijnenburg-van Cittert, W. M. Kurschner and M. A. Sephton (2004). "Environmental mutagenesis during the end-Permian ecological crisis." *PNAS* **101**(35): 12952-12956.

Wagner, P., M. Kosnik and S. Lidgard (2006). "Abundance Distributions Imply Elevated Complexity of Post-Paleozoic Marine Ecosystems." *Science* **314**(5803): 1289-1292.

Wagner, T., P. Hofmann, B. Beckmann and J. Sinninghe Damsté (2004). "Euxinia and primary production in Upper Cretaceous eastern equatorial Atlantic surface waters fostered orbital-driven formation of marine black shales in the Deep Ivory Basin, ODP Site 959." *Paleoceanography* **19**: PA3009.

Ward, P. D., J. Botha, R. Buick, M. De Kock, D. H. Erwin, G. Garrison, J. Kirschvink and R. Smith (2005). "Abrupt and Gradual Extinction Among Late Permian Land Vertebrates in the Karoo Basin, South Africa." *Science* **307**: 709-714.

Weeks, S. J., B. Currie and A. Bakun (2002). "Satellite imaging: Massive emissions of toxic gas in the Atlantic." *Nature* **415**: 493-494.

Wignall, P. B. and R. J. Twitchett (1996). "Oceanic Anoxia and the End Permian Mass Extinction." *Science* **272**(5265): 1155-1158.

Yin, H., K. Zhang, J. Tong, Z. Yang and S. Wu (2001). "The Global Stratotype Section and Point (GSSP) of the Permian-Triassic Boundary." *Episodes* **24**(2): 102-114.

Zumberge, J. E. (1987). "Prediction of source rock characteristics based on terpane biomarkers in crude oils: A multivariate statistical approach." *Geochimica et Cosmochimica Acta* **51**(6): 1625-1637.

Figure 1. Location of study area. A) Location of study area with respect to the Pangean super continent. B) Extent of the Peace River Embayment in western Alberta, Canada. C) Location of sampled drill core on the Alberta township and range grid; 1: Puskwa 16-10-73-26W5 (Lat: 55.31279; Long:-117.903855); 2: Clouston 16-1-71-25W5 (55.124233; -117.698059); 3: Apexco 2/7-20-70-24W5(55.073307; -11761852) ; 4: Kandex 15-6-71-22W5 (55.125067; -117.365387); 5: Chevron 4-17-74-22W5 (55.405549; -117355726).

Figure 2. Stratigraphic cross section A-A^{1}, Montney Formation in the southern Peace River Embayment, showing depositional sequences and stratigraphic position of sampled drill cores. Sequence framework based on Kendall (1999) and Panek (2000). Sequence prefixes represent substage position, G = Griesbachian, D = Dienerian, S = Smithian, Sp = Spathian.

Figure 3. Correlation and lithology of sampled drill cores from the lower Montney Formation in the subsurface of the Western Canadian Sedimentary Basin. Horizons sampled for biomarker analyses indicated by black arrows. Depositional sequences G1 to D3 follow those described as parasequence sets by Markhasin (1997), Kendall (1999), and Panek (2000) and correspond to figure 2. Precise well locations shown in figure 1.

Figure 4. GC-MS chromatogram for the 134 m/z ion fragment of a typical sample. Numbered peaks represent depicted aryl isoprenoids of given carbon numbers. Peak labeled "i" is isorenieratane.

Figure 5. Biomarker Parameters. In all figures, wells are indicated by: (-) Puskwa, (□) Apexco, (△) Clouston, (◊) Chevron, and (○) Kandex. (a-g) Parameters measured against relative sample depth; parameters are ratios except when indicated by units. (h) Cross-plot of hopane to tricyclic ratios.

Figure 6. Chromatograms from GC-MS MRM mode for a typical sample close to the boundary. Steranesare on the left, triterpanesare on the right. Quantified biomarkers are labeled.

Table 1. Average values for each well of some RockEval parameters.

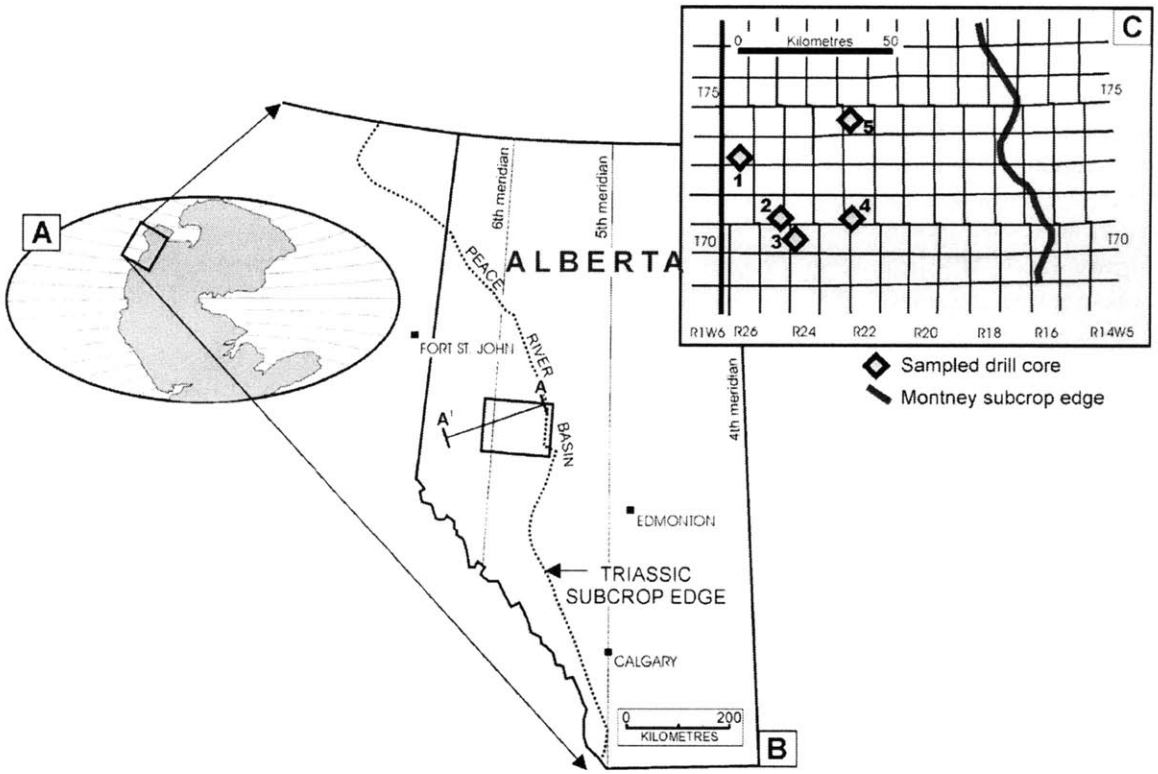

Fig. 1. Location of study area. (A) Location of study area with respect to the Pangean super continent. (B) Extent of the Peace River Embayment in western Alberta, Canada. (C) Location of sampled drill core on the Alberta township and range grid; 1: Puskwa 16-10-73-26W5 (lat: 55.31279; long: −117.903855); 2: Clouston 16-1-71-25W5 (lat: 55.124233; long: −117.698059); 3: Apexco 2/7-20-70-24W5 (lat: 55.073307; long: −117.61852); 4: Kandex 15-6-71-22W5 (lat: 55.125067; long: −117.365387); 5: Chevron 4-17-74-22W5 (lat: 55.405549; long: −117.355726).

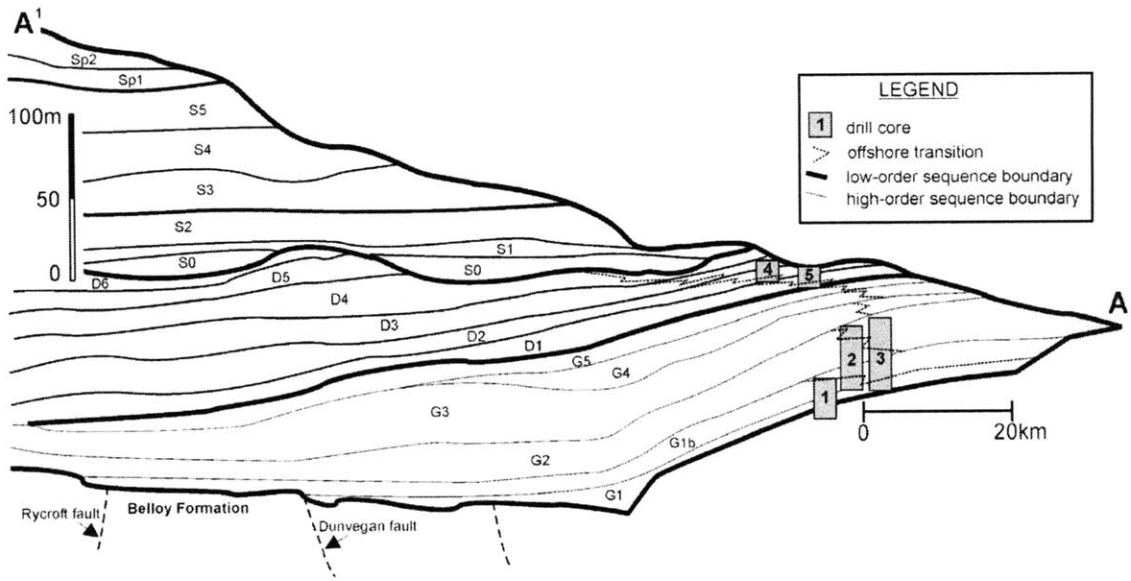

Fig. 2. Stratigraphic cross-section A–A^1, Montney Formation in the southern Peace River Embayment, showing depositional sequences and stratigraphic position of sampled drill cores. Sequence framework based on Kendall (1999) and Panek (2000). Sequence prefixes represent substage position; G = Griesbachian, D = Dienerian, S = Smithian, Sp = Spathian.

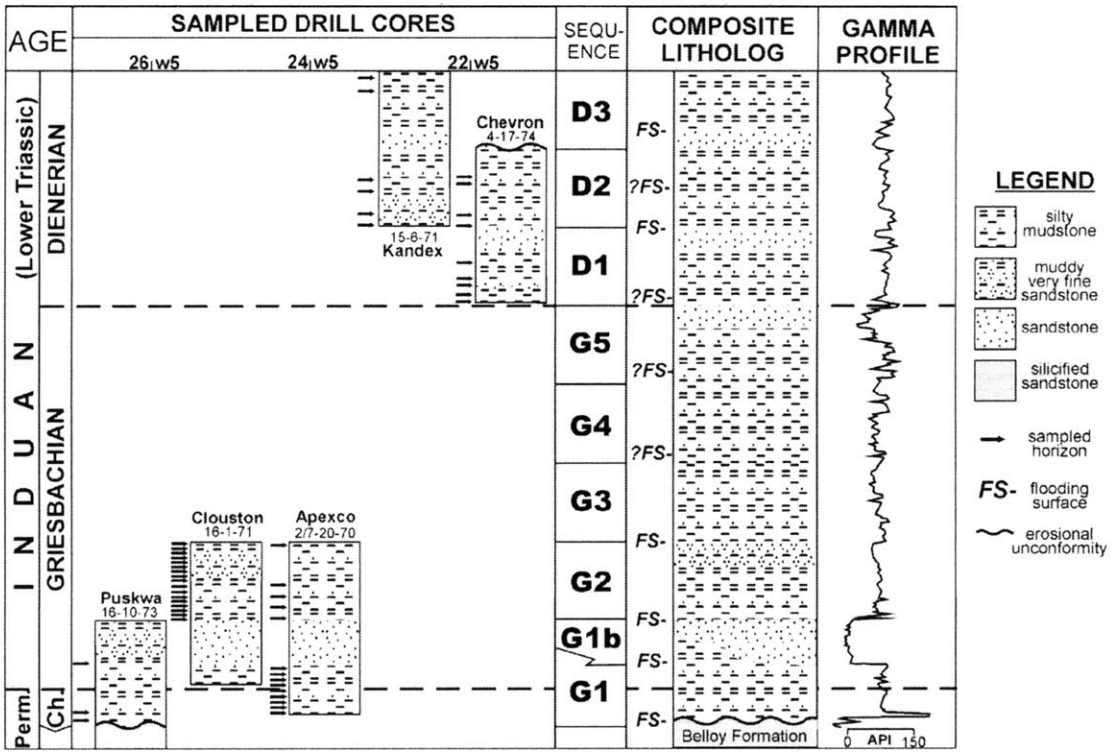

Fig. 3. Correlation and lithology of sampled drill cores from the lower Montney Formation in the subsurface of the Western Canadian Sedimentary Basin. Horizons sampled for biomarker analyses indicated by black arrows. Depositional sequences G1 to D3 follow those described as parasequence sets by Markhasin (1997), Kendall (1999), and Panek (2000) and correspond to Fig. 2. Precise well locations shown in Fig. 1.

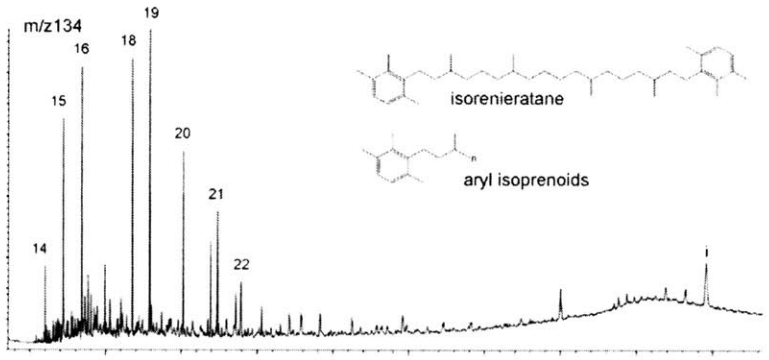

Fig. 4. GC–MS chromatogram for the 134 *m/z* ion fragment of a typical sample. Numbered peaks represent depicted aryl isoprenoids of given carbon numbers. Peak labeled "i" is isorenieratane.

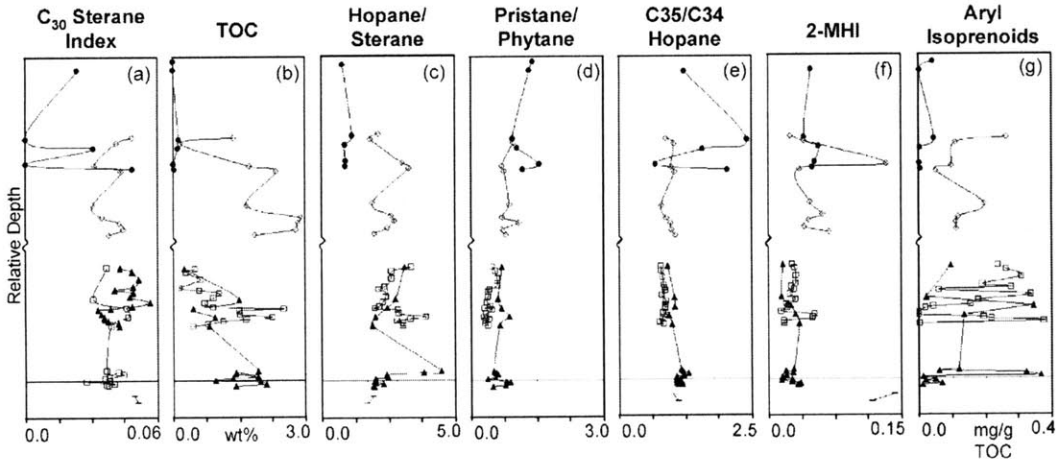

Fig. 5. Stratigraphic variability in organic carbon content and biomarker parameters. In all columns, wells are indicated by: (—) Puskwa, (▲) Apexco, (□) Clouston, (◊) Chevron, and (●) Kandex. (a–g) Parameters measured against relative sample depth; parameters are ratios except when indicated by units.

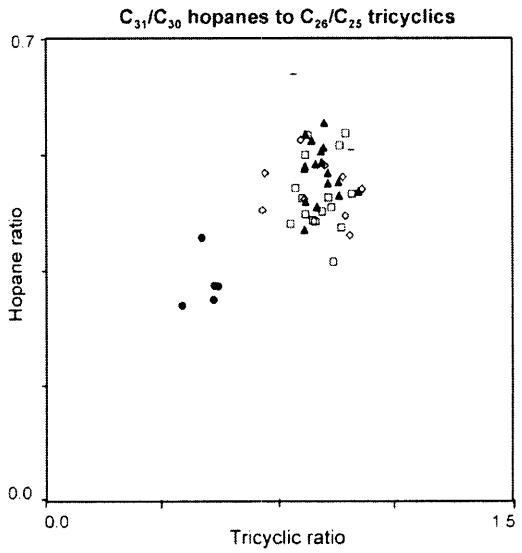

Fig. 6. Cross-plot of C_{31}/C_{30} hopane to C_{26}/C_{25} tricyclic ratios for the Peace River sediments.

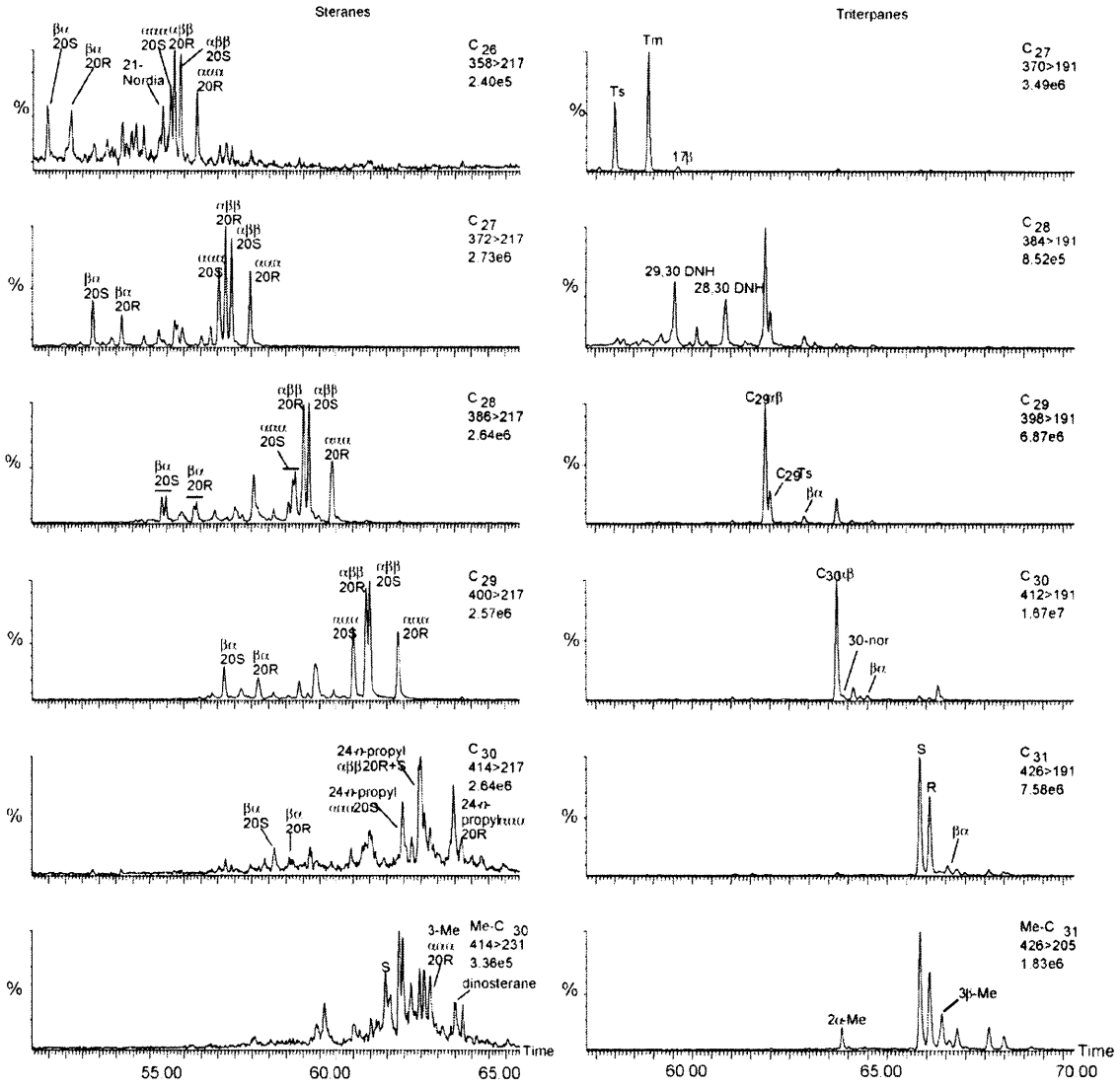

Fig. 7. Chromatograms from GC–MS MRM mode for a typical sample close to the boundary. Steranes appear in the left panel and triterpanes in the right. Quantified biomarkers are labeled according to structure and stereochemistry.

Table 1
Average values for each well of some RockEval parameters

Well name	# Samples	TOC (wt.%)	S1	S2	S3	HI	OI	T_{max}	PI
Puskwa	2	ND	ND	ND	ND	ND	ND	ND	ND
Kandex	6	0.05	0.04	0.05	0.17	60	185	302	0.64
Chevron	9	1.99	1.65	1.99	0.30	294	59	420	0.49
Clouston	17	1.03	0.35	1.03	0.25	210	61	431	0.29
Apexco	16	1.32	0.54	1.32	0.27	220	57	432	0.31

Appendix 3

Reprinted from Earth and Planetary Science Letters, 281 3-4, Changqun Cao, Gordon D. Love, Lindsay E. Hays, Wei Wang, Shuzhong Shen, Roger E. Summons, Biogeochemical Evidence for Euxinic Oceans and Ecological Disturbance Presaging the end-Permian Mass Extinction Event, p188-201, Copyright (2009), with permission from Elsevier.

Biogeochemical Evidence for Euxinic Oceans and Ecological Disturbance Presaging the end-Permian Mass Extinction Event

Changqun Cao[a], Gordon D. Love[b, c], Lindsay E. Hays[b], Wei Wang[a], Shuzhong Shen[a] and Roger E. Summons[b]*

[a] State Key Laboratory of Palaeobiology and Stratigraphy, Nanjing Institute of Geology and Palaeontology, Chinese Academy of Sciences, 39 East Beijing Road, Nanjing, Jiangsu, 210008, China.

[b]Massachusetts Institute of Technology, Department of Earth, Atmospheric and Planetary Sciences, 77 Massachusetts Avenue, Cambridge MA 02139 USA

[c]Present address: Department of Earth Sciences, University of California, Riverside, CA 92521, USA

Abstract

The Permian-Triassic Boundary event at 252.2 Ma marks the largest extinction of marine fauna in the Phanerozoic and there is a wide consensus that the extinction coincided with an intense oceanic anoxic event. The stratotype of the Changhsingian Stage, precisely constrained by the PTB Global Stratotype Section and Point (GSSP) and the GSSP for the Wuchiapingian - Changhsingian Boundary, both at Meishan in southern China, is well-documented in respect to geochronology and the pattern of extinction. Here we report secular trends in bulk isotopic parameters and lipid biomarkers in a core spanning 214 m of stratigraphic section across the PTB and through the entire Changhsingian interval. Our analysis of these data, viewed in the context of relative sea level change and strontium isotopes, reveals distinct shifts in paleoenvironmental conditions and profound changes in plankton ecology well before and following the biological extinction event. Specifically, patterns of steroids and triterpenoids indicate a marine plankton community that was heavily dominated by bacteria during the late Wuchiapingian, middle Changhsingian and early Griesbachian stages. Secular trends in aromatic hydrocarbons diagnostic for anoxygenic green sulphur bacteria (Chlorobiaceae) identify periods when euxinic conditions extended into the photic zone during the entire Changhsingian stage. Here also, the $\delta^{15}N$ of organic nitrogen progressively shifted from positive values around +2 or +3 ‰ to -1 ‰ coincident with a sharp negative excursion in $\delta^{13}C_{org}$ and slightly postdating the sharp minimum in $\delta^{13}C$ values of inorganic carbon that occurs at the top of Bed 24. These results, together the published chronology indicate that conditions unfavourable for aerobiosis existed in the marine photic zone at Meishan for 1.5 million years prior to the main phase of the biological extinction. The induction of marine euxinic conditions, worldwide, at the end of the Permian was likely a consequence of the aggregation of Pangea and the uplift, weathering and transport of nutrients to the ocean well in advance of the PTB. The protracted and widespread nature of the ensuing oceanic anoxic event suggests a causal association with the mass extinction.

Key Words: Permian Triassic, Extinction, Meishan, South China, euxinia, Chlorobiaceae, biomarker hydrocarbons, stable carbon isotopes, strontium

1. Introduction

The Permian-Triassic Boundary (PTB) event culminated at 252.2 Ma with the largest extinction of marine fauna in the Phanerozoic (Erwin, 2006; Raup & Sepkoski, 1982). The pattern of extinction at the Meishan D section with the PTB and Changhsingian-base GSSPs in south China (Jin *et al.*, 2006; Yin *et al.*, 2001), where there are robust geochronological constraints (Bowring *et al.*, 1998; Crowley *et al.*, 2006; Mundil *et al.*, 2004), has been especially well documented (Jin *et al.*, 2000). Further, the main extinction beginning at the base of Bed 25 took place abruptly and, possibly, in as little as 100 kyr (Bowring *et al.*, 1999). The paleontological manifestation of the end-Permian mass extinction is also well known for being accompanied by geochemical evidence for a significant disturbance to ocean chemistry (Holser, 1977). Studies of marine PTB sections worldwide have provided many illustrations of the extinction, marked co-eval negative shifts in the carbon isotopic compositions of carbonates and organic carbon, as well as anomalies in the isotopic compositions of sulfur species (Algeo *et al.*, 2007; Berner, 2006; Cao *et al.*, 2002; Faure *et al.*, 1995; Foster *et al.*, 1997; Grice *et al.*, 2005a; Grice *et al.*, 2005b; Holser *et al.*, 1989; Korte *et al.*, 2004; Newton *et al.*, 2004; Payne *et al.*, 2004; Riccardi *et al.*, 2006; Sephton *et al.*, 2002). At Meishan, $\delta^{13}C$ values for both carbonate and organic carbon show sharp negative spikes coincident with the abrupt faunal change. This study was undertaken to examine the trends in molecular fossils that might provide insight into the biogeochemical processes that accompanied the mass extinction at Meishan.

1.1 Factors underlying the PTB event

There is no consensus on the underlying cause(s) of the PTB event (Benton, 2003; Erwin, 2006). A scenario favoured by many is that the extinction resulted from oceanic and atmospheric disturbances triggered by the eruption of the Siberian flood basalts (Benton, 2003; Bowring *et al.*, 1998; Campbell *et al.*, 1992; Kamo *et al.*, 2003; Kamo *et al.*, 1996; Knoll *et al.*, 2007a; Visscher *et al.*, 2004). In one well-documented variant of this idea, volatiles from the intense volcanism (Visscher *et al.*, 2004) destabilised terrestrial ecosystema leading to unprecedented rates of soil erosion and the transport of the plant debris to the ocean (Sephton *et al.*, 2005; Visscher *et al.*, 2004; Wang & Visscher, 2007). Another scenario, the overturn of a stagnant or anoxic ocean (Isozaki, 1995; Isozaki, 1997; Knoll *et al.*, 1996; Wignall & Twitchett, 1996), is consistent with the concurrence of geochemical anomalies and the selective aspects of mass

77 extinction (Knoll *et al.*, 2007a; Valentine & Jablonski, 1986). C-cycle modelling (Berner, 2006;
78 Payne & Kump, 2007) appears to confirm that multiple factors must be responsible for the
79 magnitude and duration of ^{13}C-anomalies.
80
81 Various geological, geochemical, paleoceanographic and biological processes have been
82 explored in an effort to test the linkages between perturbed ocean chemistry, mass extinction and
83 subsequent radiation of organisms. A promising approach toward addressing the problem of the
84 PTB has been to document the physiological attributes of particularly vulnerable and surviving
85 taxa e.g. (Knoll *et al.*, 1996; Knoll *et al.*, 2007a). Other researchers (Kump *et al.*, 2005; Riccardi
86 *et al.*, 2006) have specifically proposed that sulfide escaping to the atmosphere during shoaling
87 of the chemocline of a euxinic ocean would provide an effective killing mechanism on land as
88 well as in the marine realm. Regional and global biostratigraphic and chemostratigraphic
89 correlation (Erwin, 1994; Erwin, 2006) and dramatic improvements in the measurements of the
90 rates of change through isotope geochronology (Bowring *et al.*, 1998; Crowley *et al.*, 2006;
91 Mundil *et al.*, 2004) can help constrain the possible mechanisms behind these geochemical
92 perturbations and their biological consequences.
93
94 *1.2 Biomarkers as paleoenvironmental and paleobiological indicators at the PTB*
95 Time series of changes in biomarkers provide a window onto the plankton successions and
96 geomicrobiological processes which accompany C- and S-isotopic excursions (Grice *et al.*,
97 2005a; Hays *et al.*, 2007; Knoll *et al.*, 2007b; Sephton *et al.*, 2005; Wang, 2007; Wang &
98 Visscher, 2007; Watson *et al.*, 2005; Xie *et al.*, 2005). Molecular fossils, in the form of
99 recalcitrant hydrocarbon skeletons of biogenic compounds, are preserved in sedimentary rocks of
100 low to moderate metamorphic grade over geologic time. These biomarkers, which are largely
101 derived from membranes and photosynthetic pigments, and biosynthesised via highly conserved
102 pathways, are modified *post mortem* according to known diagenetic processes and convey, with
103 varying degrees of specificity, information about the identities and physiologies of their source
104 organisms (Brassell *et al.*, 1983; Brocks & Summons, 2003; Ourisson *et al.*, 1987; Peters *et al.*,
105 2004).
106

Biomarker studies of PTB sediments reveal a diversity of biogeochemical evidence for dramatic events. Sephton and others, for example, have measured trends in $\delta^{13}C$ of sedimentary carbonate and leaf wax-derived *n*-alkanes and abundances of oxygen-containing aromatic compounds in Permian sedimentary strata from northern Italy that suggest an end-Permian terrestrial ecosystem collapse and transport of this soil-derived organic matter to the ocean (Sephton *et al.*, 2005; Sephton *et al.*, 2002; Watson *et al.*, 2005). Similar aromatic abundance data has been reported in an expanded section from Eastern Greenland (Fenton *et al.*, 2007) where samples from the pre-collapse interval in this section were characterised by high abundances of dibenzofuran (DBF), dibenzothiophene (DBT) and biphenyl thought to be derived from phenolic compounds of lignin from defunct woody plants. Enhanced sedimentation of soil-derived organics was also recently reported in a study of outcrop samples from Beds 24-26 and 29-31 of the Meishan section where the distributions and isotopic compositions of hopanoid triterpanes (Wang, 2007) were invoked as evidence. Enrichment in the contents of dibenzofurans and lignin-derived alkyl phenols has also been reported for Meishan (Wang & Visscher, 2007). Bacterial biomarker anomalies at Meishan, specifically two episodes of enhancement in the abundances of 2-methylhopanoids, which potentially reflect cyanobacterial productivity (Summons *et al.*, 1999), were reported by both Wang and Xie (Wang, 2007; Xie *et al.*, 2007; Xie *et al.*, 2005). These occurred in Beds 26 and 34 following the main documented extinction horizon at the base of Bed 25 at Meishan.

Prime examples of taxonomically and physiologically diagnostic biomarkers are the aromatic carotenoids produced abundantly by the green and purple sulfur bacteria. Isorenieratene and chlorobactene are two distinctive aromatic carotenoid pigments essential to light-harvesting by the brown and green strains of green sulfur bacteria (Chlorobiaceae) respectively. The Chlorobiaceae biosynthesise pigments with a 2,3,6-trimethyl aromatic substitution pattern and utilise the reversed TCA cycle for carbon assimilation leading to their biochemicals being enriched in ^{13}C compared to those produced by most other phototrophs (Grice *et al.*, 1996; Grice *et al.*, 1997; Hartgers *et al.*, 1993; Summons & Powell, 1986a). Further, these compounds are well preserved as the molecular fossils isorenieratane and chlorobactane, together with their derivative aryl isoprenoids (Brocks & Summons, 2003; Koopmans *et al.*, 1996; Sinninghe Damsté *et al.*, 2001).

Chlorobiaceae are strictly anaerobic, obligate phototrophs using mainly H_2S as an electron donor for photosynthesis; as plankton, they abound where euxinic conditions extend into the photic zone such as in the modern-day Black Sea (Overmann *et al.*, 1992). Furthermore, the presence of environmental sulfide promotes their initial preservation as organo-sulfur compounds (OSC) which ultimately become reduced to the more stable hydrocarbons that have been used extensively as paleoenvironmental indicators of photic zone euxinia (PZE) (Grice *et al.*, 1996; Hartgers *et al.*, 1993; Koopmans *et al.*, 1996; Pancost *et al.*, 2002; Summons & Powell, 1986b; Summons & Powell, 1987). Chlorobiaceae biomarkers have been shown to be present in PTB sediments from the Perth Basin, Meishan (Grice *et al.*, 2005a) and in a section in the Peace River Basin (Hays *et al.*, 2007).

In most PTB biomarker studies conducted to date, emphasis has been placed on events near to the main extinction horizon and its aftermath and this has been particularly enlightening in respect to documenting the 'soil crisis' and phytoplankton transitions (Fenton *et al.*, 2007; Sephton *et al.*, 2005; Wang, 2007; Wang & Visscher, 2007; Xie *et al.*, 2005). However, few biomarker investigations have sought to unravel events occurring on longer timescales, especially in respect to examining paleoenvironmental conditions presaging the extinction. Accordingly, when samples became available as part of the Meishan Drilling Project, we undertook a detailed investigation of trends in biomarker and isotopic lipids through 214m of section covering the late Wuchiapingian through Dienerian stages in the Lungtan, Changxing, Yinkeng and Helongshan formations.

2. The Meishan Drilling Project

The PTB succession exposed in quarries at Meishan, South China (Figure 1), has been the focus of more than twenty years of detailed research into the paleontology and geochemistry of the mass extinction (Cao *et al.*, 2002; Jin *et al.*, 2000; Yin *et al.*, 2001). Nevertheless, there remains a considerable amount of ambiguous and conflicting data that, in part, reflects the exposure of these rocks to intense surface weathering. In order to obtain a complete succession of rock samples unaffected by atmospheric exposure and free from outcrop contamination, a drilling project was instigated by the Nanjing Institute of Geology and Paleontology under the leadership of the late Professor Jin Yugan. Two cores, drilled at a site 550 m to the west of the Meishan

Section D, afforded the best possible geochemical record of the environmental evolution at the GSSP, not only for the Permian-Triassic transition, but also for the entire Changhsingian Stage and post-extinction Induan Stage of Early Triassic. Details of the samples and analytical methods are provided as supplementary online material.

3. Results and Discussion

3.1 Isotopic data

Bulk geochemical parameters for the samples analysed in this study are plotted in the context of stratigraphic and lithologic relationships and relative sea-level (Fig. 2) (Zhang *et al.*, 1996). The $\delta^{13}C_{carb}$ data (Fig. 2B) reported here are mostly those collected in the outcrop of Section D prior to drilling (Cao *et al.*, 2002). A total of 371 samples span 158 m of section from the bottom of the Permian Changxing Fm. through the Triassic Helongshan Fm. Of these, 94 samples were from just 1.28 m of section across the Permian-Triassic boundary interval comprising Beds 24 to 27. This carefully conducted, high density sampling reveals that a minimum $\delta^{13}C_{carb}$ value of -3.23‰ is encountered only once at the topmost unit of Bed 24e just below the "boundary ash clay" of Bed 25 and not in Beds 26 and 27 and previously reported (Xu & Yan, 1993).

Some black sediment samples were collected for comparison of $\delta^{13}C_{carb}$ in selected horizons in the Changxing Fm. (Fig. 2B) and have more positive values. Considering the trends in $\delta^{13}C_{carb}$ in the Changhsingian stage from other sites, such as the Shangsi Section, where these more negative values are not encountered, this strongly suggests that these samples are diagenetically altered. Additional negative $\delta^{13}C_{carb}$ values measured in the basal part of Changxing Fm. are either in, or near, the calcite veins. They too likely contain diagenetically-altered carbonate.

The TOC and the organic carbon, nitrogen and strontium isotopic data shown in Figure 2 are all from the Meishan-1 core. A number of clear and informative trends can be discerned. The very sharp negative excursion $\delta^{13}C_{carb}$ (Fig. 2B) culminates at the top of Bed 24 while the $\delta^{13}C_{org}$ values reach their minimum at the top of Bed 26 (Fig. 2C). Thus, the $\delta^{13}C_{org}$ minimum postdates the $\delta^{13}C_{carb}$ minimum and the signals do not co-vary as one would expect from a carbon cycle operating in steady state. If not due to factors reflecting C-cycle dynamics, the offset and large variability in $\delta^{13}C_{org}$ values might be a reflection of the mixing of some organic matter sources

200 of different isotopic compositions. An overall drift to slightly more negative values in $\delta^{13}C_{carb}$
201 (ca. 1‰) and $\delta^{13}C_{org}$ (ca. 2‰) can be discerned over the entire sampled section. The $\delta^{13}C_{carb}$
202 data show two negative excursions corresponding to the maximum flooding surfaces through the
203 intervals of Beds 34-35, Beds 21-22 and Beds 11-13 which are quite subtle. The major
204 excursion extends from Bed 24 and continues through Bed 37, with the sharp spike at the top of
205 Bed 24. In contrast to these progressive 'excursions' we observe much larger and apparently
206 chaotic bed-to-bed variation in the $\delta^{13}C_{org}$ values. This is most readily explained by mixing of
207 organic components of differing $\delta^{13}C_{org}$ compositions and possibly comprising end-member
208 marine and weathered terrestrial components as described previously (Cao *et al.*, 2002). A
209 similar phenomenon can be seen in the organic carbon isotopic trends of the PTB sections of the
210 Perth, Carnarvon and Bonaparte Basins of Western Australia (Foster *et al.*, 1997; Foster *et al.*,
211 1998; Gorter *et al.*, 1995). A terrestrial component may include recently defunct plant-derived
212 biomass from breakdown of terrestrial productivity (Sephton *et al.*, 2005) but would most likely
213 be dominated by weathered and re-worked fossil carbon including coal fragments (Faure *et al.*,
214 1995; Foster *et al.*, 1997).
215
216 Seawater $^{87}Sr/^{86}Sr$ values reflect a balance of radiogenic strontium inputs from both continental
217 silicate weathering and the hydrothermal circulation at mid oceanic ridges (Palmer & Edmond,
218 1993). It is a useful proxy for tracking tectonic evolution (Veizer & Compston, 1976) and for
219 Late Permian stratigraphic correlations worldwide (Faure *et al.*, 1995; McArthur *et al.*, 2001;
220 Wang *et al.*, 2007). The values of $^{87}Sr/^{86}Sr$ in Meishan carbonates (Fig. 2D) generally parallel the
221 background seawater values suggested by McArthur et al. (2001) with values near 0.7072 for the
222 Changhsingian stage and moving to more positive values around 0.7075 in lower Triassic strata.
223 This accords with earlier findings (Faure *et al.*, 1995; Korte *et al.*, 2006; Korte *et al.*, 2003). A
224 small decrease in the claystone Beds 6-7 suggests volcanic input to the ocean while the
225 progressive increase evident from Bed 15 onwards indicates a strong dominance of continental
226 detritus during the latest Permian regression. Overall, the long-term trends in carbon and
227 strontium isotopes are consistent with an extended period of enhanced weathering of both
228 silicates and organic matter with the coincidence of strong opposing trends in $^{87}Sr/^{86}Sr$ and
229 $\delta^{13}C_{carb}$ (Fig. 2B) starting at Bed 23 being particularly profound.
230

231 The trend in $\delta^{15}N$ of organic matter is also informative. Positive values of $\delta^{15}N_{org}$ (Fig. 2E) in
232 the Lungtan Fm. reflect a normal and complex trophic structure and N-cycling through nitrate
233 and are typical of values recorded for organic nitrogen formed in the modern ocean (Altabet &
234 Francois, 1994). There is a progressive decrease through the Changhsingian stage and the
235 positive values of the Permian then give way to zero and negative values at the top of Bed 24.
236 Negative $\delta^{15}N_{org}$ persist into the Early Triassic Yinkeng Fm. although low contents of organic
237 matter precluded $\delta^{15}N_{org}$ measurements above Bed 37. As with other Mesozoic Oceanic Anoxic
238 Events (OAEs), a trend to zero and negative values of $\delta^{15}N_{org}$ is widely thought to reflect
239 ecological disturbance and a nitrogen cycle with reduced involvement of oxidised species (nitrate
240 and nitrite) and increased nitrogen fixation (Altabet & Francois, 1994). Based on strong
241 correlations with increased abundances of hopanoid hydrocarbons, these 'light' nitrogen isotopic
242 data are hypothesised to signal significantly enhanced cyanobacterial N-fixation (Dumitrescu &
243 Brassell, 2006; Kuypers *et al.*, 2004; Ohkouchi *et al.*, 2006).
244
245 *4.2 Redox-sensitive biomarkers*
246 The patterns of biomarker trends in the Meishan-1 core indicate that biogeochemical changes
247 that presaged the PTB extinction were both profound and prolonged. Trends in biomarker
248 hydrocarbons (Fig. 3) that are considered diagnostic for water column redox conditions, such as
249 the ratio of pristane to phytane (Pr/Ph), C_{35} homohopane index (C_{35}HHI) and relative abundance
250 of 28,30-dinorhopane (28,30-DNH), are empirically linked to organic matter deposited in marine
251 environments under strongly reducing conditions (Peters *et al.*, 2004). However, these indices
252 also reflect a complex interplay of diagenetic conditions, specific source inputs and sediment
253 maturity that vary somewhat independently. As reported previously (Wang *et al.*, 2005) a
254 protracted interval with persistently low Pr/Ph (<1) values in the Changxing Fm. gives way to
255 one with large fluctuations at and above Bed 25. The very low TOC and extract yield of samples
256 from the Helongshan Formation precluded exact Pr/Ph measurements in this unit. However, in
257 the Changxing Fm., the low Pr/Ph values are directly correlated with other parameters diagnostic
258 of reducing and sulfidic conditions. The C_{35}HHI (Fig. 3B) records selective preservation of the
259 intact C_{35} carbon skeleton of bacteriohopanepolyols under highly reducing conditions (Köster *et*
260 *al.*, 1997). The elevated (> 5%) values of this parameter correlate well with low Pr/Ph ratios (Fig.
261 3A) and show that strongly reducing conditions persisted in the sediments from the top of the

Lungtan Fm. and throughout the entire Changxing Fm. The relative abundance of 28,30-DNH as reflected by the value of the 28,30-DNH/C_{30}-hopane index shows somewhat higher values at maximum flooding (cf. Fig 2A and Fig 3C). Although the specific source of 28,30-DNH remains unknown, and the index is dependent on maturity and sediment lithology (Brincat & Abbott, 2001), its values in the range 0.5 to 2% suggests the entire cored section represents a reducing sedimentary environment (Grantham *et al.*, 1980; Schoell *et al.*, 1992; Seifert *et al.*, 1978).

In contrast to the redox proxies based on acyclic isoprenoids (Pr/Ph) and bacteriohopanes (28, 30-DNH and C_{35}HHI), whose origins are multiple and complex, the aromatic carotenoid-derived biomarkers are very well established indicators for the physiological requirements (i.e. sunlight and H_2S) of the green sulphur bacteria (Brocks & Summons, 2003; Summons & Powell, 1987) and have previously been detected in the boundary section at Meishan (Grice *et al.*, 2005a) and other oceanic anoxic events (Ohkouchi *et al.*, 2006; Pancost *et al.*, 2004; van Breugel *et al.*, 2006). Isorenieratane and $C_{14\text{-}27}$ aryl isoprenoids are present in the Meishan core samples through the entire section (Fig. 3D and 3E) from the Wuchiapingian Lungtan Fm., where they are in relatively low abundances, throughout the Changhsingian and Griesbachian stages. Notably, highest absolute abundances of isorenieratane (>5 ppm TOC) and the C_{14}-C_{27} aryl isoprenoids, and presumably the most persistent euxinic episodes, occur in zones encompassing Beds 11-15 - well in advance of the main extinction horizon and at Beds 24-25. Aryl isoprenoids then persist into the Triassic until the early Dienerian. The sediments encountered in the Meishan core alternate between shelf, slope and basinal environments and the *Chlorobium* biomarkers (Fig. 3D and 3E) are present at all stages of eustatic sea-level variation with maxima during the highstands (Fig. 2A). Modelling studies (Meyer *et al.*, 2008) suggest that there would be spatial and secular variability in the intensity of shoaling of sulfidic waters into the photic zone and that this will be governed by bathymetry, nutrient fluxes and numerous other factors. Overall, PZE must have existed locally in the Eastern Tethys Ocean, at least intermittently, from c.254 Ma (Bowring *et al.*, 1998) until ~251.4 Ma (Galfetti *et al.*, 2007).

The biomarker data gathered from the Meishan sediments shows that the processes leading to euxinic conditions were protracted and persistent. This is consistent with sedimentological, paleontological and geochemical evidence for a widespread 'superanoxic' event (Isozaki, 1995;

293 Wignall & Twitchett, 2002). Nevertheless, there are sections such as the carbonate reef sections
294 at Ziyun and Laolongdong in South China and the Jiangyema section in Tibet that contain
295 abundant benthic faunas not indicative of anoxic conditions in the Changhsingian and
296 Wuchiapingian. Evidently, local topography and geography conferred variability in how
297 anoxic/euxinic conditions affected shallow water environments.
298
299 *4.3 Biomarkers indicative of the microbial community structure*
300 Figure 4 compares the distributions of a range of biomarkers that are often associated with
301 specific taxonomic or physiological categories of microbes (Peters *et al.*, 2004) The
302 hopane/sterane ratio (H/S; Fig. 4A), a generalised proxy for the relative contributions of bacterial
303 versus eukaryotic biomass shows exceedingly high values, throughout the entire section,
304 compared to typical Phanerozoic values (0.5 to 2). In particular, the peaks in hopane/sterane in
305 the Changxing (H/S=31) and Yinkeng (H/S=70) formations point to an ocean dominated by
306 bacterial biomass and more resembling conditions recorded in Mesoproterozoic basins (Brocks
307 *et al.*, 2005). The proportions of steranes are also diagnostic for variability in the types of
308 photosynthetic eukaryotes contributing organic matter to the sediments (Peters *et al.*, 2004;
309 Volkman *et al.*, 1998; Volkman, 1986). In the marine realm, the proportion of C_{27} steranes (Fig.
310 4B) is generally higher than in non-marine environments and records variation in the balance of
311 red over green algal communities. Low values can also be suggestive of significant inputs of
312 vascular plant debris. This could be the case for samples from the Permian section where they
313 are accompanied by elevated abundances of other plant-derived organic compound such as
314 dibenzofurans (data not shown). A comparison of the $C_{27}/C_{27\text{-}30}$ sterane ratio with the lithologies
315 and sea-level curves of different orders suggests that an increase in the ratio, indicating a higher
316 proportion of marine algal biomass, parallels the transitional phases of the 3rd-order sea-level
317 (Haq *et al.*, 1988; Zhang *et al.*, 1996) in the Changhsingian stage. Here, the $C_{27}/C_{27\text{-}30}$ sterane
318 ratio shows similar trends to the relative abundance of gammacerane (Fig 4C). Tetrahymanol,
319 the precursor of gammacerane, is known to be produced by both purple non-sulfur bacteria and
320 bacterivorous marine ciliates (Harvey & McManus, 1991; Kleemann *et al.*, 1990; Ten Haven *et*
321 *al.*, 1989). Increased concentrations of its precursor, tetrahymanol, at the chemocline of
322 stratified water columns appears to support a predominant origin from non-photosynthetic
323 organisms, that is, ciliated protozoa that graze on algae and bacteria (Wakeham *et al.*, 2007). In

the late Permian H/S, $C_{27}/C_{27\text{-}30}$ sterane and gammacerane/C_{30} hopane ratios peak together with the redox indicators C_{35}HHI, 28,30-DNH and aryl isoprenoids through Beds 10-14 of the Changxing Formation identifying this as a period where stratification and euxinia were most stable. In contrast, the values of most biomarker proxies fluctuate dramatically through the main extinction zone (Beds 22-26) and its immediate aftermath (Beds 27-35).

Increases in the proportion of C_{28} steranes (Fig 4C) can record the relative importance of the chlorophyll C-containing plankton (dinoflagellates, diatoms and coccolithophorids); this is particularly evident in long timescale datasets when they rise to prominence during the Cenozoic (Knoll *et al.*, 2007b). Here at Meishan, the proportion of C_{28} steranes is slightly elevated in Wuchiapingian, but significantly higher in the Griesbachian and Dienerian where values reach 25%, almost double the Changhsingian average. Although these sediments pre-date the middle Triassic dinoflagellate radiation, the traces of dinosteranes in these sediments record a presence of dinoflagellates around the PTB at Meishan. However, the abundances of dinosteranes are too low to discern any secular or paleoenvironmental trends. It is more likely that the overt increase in the C_{28} sterane signal through the Griesbachian records proliferation of prasinophytes in response to nitrate-N depletion and, possibly, other aspects of peturbed water column chemistry as observed elsewhere in the aftermath of OAEs (Prauss, 2007). Members of the Chlorodendrales, the most derived prasinophyte lineage, generally have a strong predominance of C_{28} sterols (Kodner *et al.*, 2008).

It is also during this interval that carbonate deposition practically ceased and gave way to the clastic sedimentation recorded by the Yinkeng Fm. At the base of the Griesbachian stage, we observe the existence of conditions favourable for deposition of organic matter-rich and pyritic black shales during the basal Triassic transgressive phase (Fig 2F). Very similar conditions are recorded in other basins at this time (Wignall & Twitchett, 2002) and, in the case of the Perth Basin, coincide with the development of thin intervals of petroleum-prone source rocks (Grice *et al.*, 2005b). The co-eval and rapid fluctuations all the biomarker signals suggests an unstable and rapidly changing microbial community throughout the post-extinction flooding event (Fig. 2A).

354 Methylhopanes can be particularly useful for discerning specific bacterial physiologies (Talbot &
355 Farrimond, 2007). As far as is known, 3β-methylbacteriohopanepolyols (3-MeBHP), precursors
356 of 3β-methylhopanes, are derived from aerobic proteobacteria comprising methanotrophs and
357 acetic acid bacteria (Rohmer *et al.*, 1984; Zundel & Rohmer, 1985a; Zundel & Rohmer, 1985b).
358 This is consistent with the prevalence of 3-MeBHP in environmental samples where methane-
359 cycling is a significant biogeochemical process and observation of abundant 3β-methylhopanes
360 in alkaline saline lakes (Collister *et al.*, 1992; Farrimond *et al.*, 2004; Talbot & Farrimond, 2007;
361 Talbot *et al.*, 2003). The abundances of both 2- and 3-methyl hopanes are generally measured
362 relative to their non-methylated hopane equivalents using the 2-methylhopane index 2-MeHI
363 (Summons *et al.*, 1999) and analogous 3-MeHI. Values for the 3-MeHI at Meishan (Fig. 4E) are
364 very high (1.6 > 3-MeHI <7) and elevated relative to values (1-3) typical of marine petroleum
365 source rocks (Farrimond *et al.*, 2004). Values of 3-MeHI (Fig. 4E) are highest in Beds 5-7 and
366 Beds 15-18. However, there seems to be no direct relationship between high values for the 3-
367 MeHI and the negative trends in $\delta^{13}C_{org}$ and $\delta^{13}C_{carb}$ suggesting that methane oxidation may be
368 coupled to active methanogenesis associated with organic matter decay in a strongly oxygen- and
369 sulfate-depleted environment, rather than being tied to any catastrophic release (Weidlich *et al.*,
370 2003).
371
372 The 2-MeHI was originally proposed as a proxy for cyanobacterial input to sedimentary organic
373 matter based on a combination of observations of the hopanoid contents for cultured organisms,
374 natural environmental samples and the pattern of 2-methylhopane variations in the geological
375 record (Knoll *et al.*, 2007b; Kuypers *et al.*, 2004; Sinninghe Damsté *et al.*, 2008; Summons *et al.*,
376 1999). Although alternative sources of 2-methylhopanoids are known, and specifically in a
377 purple non-sulfur bacterium *Rhodopseudomonas palustris* (Rashby *et al.*, 2007) and some other
378 typically non-marine soil bacteria (Bisseret *et al.*, 1985), these do not account for the patterns
379 seen at Meishan or elsewhere in marine rocks and oils (Knoll *et al.*, 2007b). Although tolerant of
380 low concentrations of sulfide (Imhoff, 2006), *R. palustris* are not favoured by the euxinic
381 conditions present at Meishan. Furthermore, *R. palustris* produces an abundance of methylated
382 triterpenoids of the gammacerane type (Bravo *et al.*, 2001; Rashby *et al.*, 2007) which, so far,
383 have not been reported in geological samples. Values of 2-MeHI (Fig. 4F) vary within a tight
384 range from 5-7% for most of the late Permian section at Meishan. Dramatic fluctuations in the

385 index are first seen at the PTB extinction horizon at Beds 24-25 as reported earlier (Xie *et al.*,
386 2005) and continue during the Yinkeng Fm. In contrast to the earlier report, however, data from
387 the Meishan-1 core show that the enhancement of the 2-MeHI occurs with numerous maxima
388 with the highest being in Bed 37 (2-MeHI = 32.6).
389
390 The data for $\delta^{15}N_{org}$ (Fig. 2C) have their lowest values through Beds 24-37, the same interval as
391 fluctuating 2-MeHI. This is consistent with the episodic loss of N-cycling through nitrate and,
392 when this happens, a switch to N-fixing cyanobacterial primary producers (Dumitrescu &
393 Brassell, 2006; Ohkouchi *et al.*, 2006). At maximum flooding in the basal Triassic, we postulate
394 a shoaling chemocline with greater utilization of newly fixed nitrogen and ^{15}N-depleted
395 ammonium (Junium, 2007). The highest values in the H/S ratio (Fig 4A) also occur here.
396 Following the boundary event, in the interval of low $\delta^{15}N_{org}$, rapid fluctuations in redox (Pr/Ph)
397 and repeated episodes of euxinia are evident as shown by the patterns of aryl isoprenoids (Fig 3D
398 and 3E). Therefore, we question whether there is a robust coupling between the 2-MeHI index
399 and faunal extinction that was reported earlier (Xie *et al.*, 2005). Rather, the fluctuating value
400 for this parameter is likely yet another reflection of the instability of the Griesbachian microbial
401 communities depicted in Figures 2-5. Proliferation of various kinds of bacteria, including
402 nitrogen-fixing cyanobacteria, and consequent elevation in the 2-MeHI index in the Griesbachian
403 shales (Fig. 6 C), was almost certainly a response to the paucity of nitrate in the water column
404 following the extended euxinic conditions of the Late Permian.
405
406 *4.4 Biomarker parameters influenced by maturity and lithology*
407 The most enigmatic trends in the biomarkers of the Meishan-1 core occur in the ratios of
408 compounds whose distributions depend on a combination of maturity, lithology and source (Figs
409 5 and 6). The maturity of organic matter in samples from the Meishan-1 core is most reliably
410 reflected in the ratio of the 22S/22S+22R for C_{31} homohopanes (Fig. 5D). This parameter is an
411 expression of isomerization at C-22 of the hopane side-chain and a stable end-point (~58-60%) is
412 reached before the main phase of petroleum generation (Peters *et al.*, 2004). The Meishan-1
413 values between 54 and 59% are highly consistent. Coupled to the range of the 20S/20S+20R
414 epimer ratio of the C_{27} steranes (45-50%), which measures a comparable isomerization, these
415 suggest the entire sediment column is uniformly in the earliest stages of the 'oil window'.

The ratio of βα-hopanes (moretanes) to αβ-hopanes involves a more difficult isomerization in the hopane ring system and takes place at higher maturities than side-chain the side-chain epimerizations discussed above. When organic matter is immature for oil generation, with vitrinite reflectance values below 0.6 - 0.7, the ratio βα/αβ+βα of C_{30}-hopanes does not correlate with depth of burial and does not approach an end-point until the main phase of petroleum generation (Grantham, 1986; Seifert & Moldowan, 1980). Therefore, in the Meishan samples the ratio βα/αβ+βα C_{30}-hopanes is a reflection of diagenetic conditions. Thus the step down in βα/αβ+βα C_{30}-hopanes near the top of the Lungtan Fm., and the step up again at the base of the Yinkeng Fm., are evidence of rapid transitions in paleoenvironment, organic matter source and diagenetic conditions.

During catagenesis, the abundance of the less stable C_{27} 17α-trisnorhopane (Tm or 17α-22,29,30-trisnorhopane) decreases relative to the more stable C_{27} 18α-trisnorneohopane (Ts) isomer as a function of burial depth (Peters *et al.*, 2004; Seifert & Moldowan, 1978). However, the Ts/(Ts+Tm) ratio, like the relative abundance of moretanes, is also profoundly influenced by paleoenvironment and organic matter sources at low-moderate levels of thermal maturity (Moldowan *et al.*, 1986). The Ts/(Ts+Tm) ratio is, therefore, most useful as a maturity indicator when samples are mature and of a common organofacies. The Ts/(Ts+Tm) ratio can also be a powerful indicator of changing environmental conditions and source biota, that is, organic matter inputs and sediment lithologies, as appears to be the case with the Meishan-1 core. Interestingly, the highest values of Ts/(Ts+Tm) are seen in the carbonate-dominated Permian section from the upper Lungtan Fm. and through most of the Changxing Fm. (Fig 5A). Further, low values in the shale below 180m in the Lungtan Fm. coincide with high values for βα/αβ+βα C_{30}-hopanes (Fig. 5B), as would be expected if maturity was the dominant control. This phenomenon is further illustrated in the cross-plot of Figure 6B. However, for a sediment column that has only experienced relatively shallow burial, and which shows no evidence of volcanic intrusion, the presence of an apparent 'mature' interval sandwiched between two 'less mature' ones is difficult to rationalise.

446 Anomalies in hopanoid maturity parameters for the Changxing and Yinkeng formations, and
447 specifically the enhanced presence of βα-hopanes at Meishan have been noted previously
448 (Wang, 2007; Xie *et al.*, 2007) and attributed to input of terrestrial organic matter. However,
449 these studies were conducted on outcrop samples and did not include detailed examination of the
450 Lungtan Formation. Our data provide little support for this and, instead, suggest a more complex
451 and long-lived scenario. Enhancement of βα-hopane abundances occurs in the Wuchiapingian
452 and again at the PTB. High βα-hopane abundances occur more or less continuously starting
453 from Bed 25 and show a more complex character with multiple maxima between Bed 26 and
454 Bed 39. Some of the differences among studies might reflect local variation in organic matter
455 inputs and differences in preservation between core and outcrop samples. Regardless, the
456 observed 'anomalous' behaviour of hopanoid maturity parameters, specifically the βα/βα+αβ-
457 hopane and Ts/Ts+Tm ratios are best accounted for by secular change in diagenetic conditions.
458 For example, Xie et al. (2007) suggested that the moretane anomaly could be a signal of
459 increased terrestrial plant inputs resulting from enhanced continental weathering. This infers an
460 origin of moretane from the array of C_{30} triterpenoids from ferns and, possibly, other primitive
461 plants (Tsuzuki *et al.*, 2001). However, the elevated moretane/hopane ratio is almost as high in
462 the extended (C_{31+}) hopane series as it is in the C_{29} and C_{30} compounds (data not shown). In
463 samples with very high βα/βα+αβ-hopane ratio, we observe a comparable elevation in the βα-
464 isomers of the 2α-methylhopanes and the 3β-methylhopanes and their C_{32+} pseudohomologues.
465 Thus, the 'moretane anomaly' is reflected in all three forms (desmethyl, 2-methyl and 3-methyl)
466 of the extended hopanes and must, therefore, be a result of diagenetic conditions conducive to
467 enhanced preservation of all βα-hopanoids.
468
469 **5. Synthesis and Conclusions**
470 The biomarker and isotopic data gathered from Meishan-1 core point to a pattern of ecological
471 disturbance and profound biogeochemical change that significantly predates the faunal transition
472 marking the Permian Triassic boundary. Overt changes in biomarker distributions correspond to
473 distinct lithological transitions toward the top of the Lungtan Fm. and, again, at the base of the
474 Yinkeng Fm. Organic matter below 180m in the core (Lungtan Fm.) is characterized by a
475 predominance of C_{29} regular steranes, high hopane/sterane ratios and elevated relative
476 abundances of βα-hopanes. Organic carbon and nitrogen isotopic values in this section record

their highest values of -23.4 and + 3.5 ‰ respectively. It appears feasible that, at this time of predominantly clastic sedimentation, the organic matter was of mostly marine origin together with some thermally mature terrestrial debris. Alternatively, the data are also consistent with predominantly authochthous inputs from a marine microbial community dominated by different kinds of bacteria.

A transition to carbonate deposition is recorded at ~10m below the top of the Lungtan Formation at Meishan-1 core at 180m and this continues throughout the Changxing Formation. These sediments were deposited under a continuously and intensely anoxic and euxinic water column as shown by the redox-sensitive proxies of low Pr/Ph ratios combined with elevated C_{35}HHI. Elevated sulfide concentrations existed in the photic zone as shown by the continuous presence of arylisoprenoids with highest concentrations recorded in Beds 11-14 of the Changhsingian stage. Importantly, the *Chlorobium* pigment derivatives are accompanied by a gradual and progressive drop in the $\delta^{15}N$ and $\delta^{13}C$ values of organic matter. A subtle negative excursion can be seen in the $\delta^{13}C_{carb}$ synchronously with the occurrence of elevated aryl isoprenoids and sea-level maximum through Beds 11-14.

The most profound biogeochemical changes become evident near to the main extinction horizon at Beds 24-25 where relative sea-level drops to a minimum and biomarkers provide evidence for intense euxinia. Strontium isotopes suggest a rapid intensification of weathering that is also marked by rapidly declining $\delta^{13}C$ values of carbonate carbon including the sharp spike at the point of maximum faunal change. It is here we also seen the first 'spike' in 2-MeHI, a minimum in $\delta^{15}N_{org}$ and many other changes in sterane and triterpane abundances. The following interval of shale deposition in the Yinkeng Formation is marked by rapid and dramatic fluctuations in most of the biomarker proxies measured. Evidently, the microbial community and composition of sedimentary organic matter were seeing extreme fluctuations with enhanced cyanobacterial primary productivity accompanied by profound anomalies triterpane stereoisomers. Peaks in the H/S ratio and the gammacerane/hopane ratio provide evidence for periods of heightened bacterial productivity and water-column stratification. Anomalous transitions in the $\beta\alpha/\beta\alpha+\alpha\beta$ ratios of $C_{29\text{-}30}$ hopanes, extended hopanes and methylhopanes point are not likely due to differences in thermal maturity, or a signal for collapse of the terrestrial ecosystem and allochthonous inputs of

soil but, rather, a reflection of significant variability in the pathways of organic matter diagenesis. Some of these changes have been recognised previously and have been reported to occur as two distinct phases (Xie *et al.*, 2007; Xie *et al.*, 2005). However, our data, including the $\delta^{13}C_{carb}$ (Fig. 3B), $\delta^{13}C_{org}$ (Fig. 3C), 2-methylhopane index (Fig. 4F) and *Chlorobium* abundance (Fig. 3E) provide support for not just two, but for multiple episodes of enhanced bacterial productivity in the Early Triassic. Seen in the light of the extended record provided by the Meishan-1 core, the faunal turnover itself was presaged by long period of euxinic conditions beginning in the Wuchiapingian and continuing through the Changhsingian stage. Conditions unfavourable for O_2-respiring organisms did not appear suddenly but persisted for several millions of years prior to the extinction. Viewed alongside the pattern of taxon loss at Meishan (Jin et al. 2000) it can be seen that the gradual and continual loss in faunal diversity in the Changxing Fm., culminating in a sudden collapse in Beds 24-25, closely follows the pattern of biogeochemical change evident from the various biomarker and isotopic proxies. These factors must be taken into account when considering the agents responsible for such a pattern of biological change.

Numerous OAE's are in evidence in the geological record of the Phanerozoic. These are best documented in the Mesozoic Eon and often marked by negative C-isotopic excursions (Kump, 1991) although some are better known for the positive direction in $\delta^{13}C$ of inorganic carbon in high TOC shales as seen at the Toarcian and Frasnian-Famennian events (Hesselbo *et al.*, 2000; Joachimski *et al.*, 2001). One of the recurring themes that has attracted attention is the co-occurrence of high abundances of *Chlorobium* biomarkers, cyanobacterial 2-methylhopanoids and abnormally light values of $\delta^{15}N_{org}$ that have been interpreted as disruption of the N-cycle induced by euxinia. OAE's are further characterized by both transient (Kuypers *et al.*, 2001) and long term (Falkowski & Knoll, 2007; Falkowski *et al.*, 2004; Knoll *et al.*, 2007b) changes in plankton communities pointing to the link between nitrogen budgets and plankton evolution and succession (Fennel *et al.*, 2005). As the data shown in Figures 2 and 4 suggest, cyanobacterial primary productivity was episodically enhanced after the faunal turnover, as evidenced by extreme fluctuations in the 2-methylhopane index and the zero to negative values in $\delta^{15}N_{org}$ data (Dumitrescu & Brassell, 2006; Kuypers *et al.*, 2004). This could, therefore, be seen as a consequence of events leading up to the extinction and not necessarily a causal phenomenon.

539 Instead, looking to events preceding the main phase of biological extinction, the evidence
540 gathered in this study suggests the inception of euxinic conditions most likely has a geological
541 underpinning in the final aggregation of Pangea with its associated volcanic, tectonic, climatic
542 and continental weathering processes (Faure *et al.*, 1995), combined with oceans predisposed to
543 sluggish circulation patterns, instigating a super-anoxic episode lasting for millions of years
544 (Isozaki, 1995; Isozaki, 2003).
545

546 **6. Acknowledgements.**

547 The authors are grateful to numerous colleagues who provided encouragement, information and
548 suggestions throughout this study. We are especially indebted to the late Professor Jin Yu-Gan
549 who inspired our study of events at the Permian-Triassic boundary and who instigated the Meishan
550 drilling project. Xiangdong Wang, Hua Zhang, Yue Wang and postgraduate students of the Late
551 Paleozoic Research Group at Nanjing joined in the three-month drilling program and in collecting
552 the cores. Kliti Grice, Emma Grosjean, Jürgen Rullkötter, Carolyn Colonero, Samuel Bowring,
553 Douglas Erwin, Charles Henderson, Andrew Knoll and Tom Algeo provided invaluable suggestions
554 and/or laboratory support. NSF USA and NSF China enabled our participation in US-China
555 Workshops in Geology and Paleontology that led to this collaboration. Research at Nanjing was
556 supported by the 973 (2006CB806400) project of the MST of China, NSFC and the CAS/SAFEA
557 International Partnership Program for Creative Research Teams. Research at MIT was supported by
558 the NASA Exobiology Program (Grant# NNG05GN62G).
559

560 **7. References**

561

562 Algeo, T.J., Ellwood, B., Nguyen, T.K.T., Rowe, H., Maynard, J.B., (2007) The Permian-
563 Triassic boundary at Nhi Tao, Vietnam: Evidence for recurrent influx of sulfidic
564 watermasses to a shallow-marine carbonate platform. *Palaeogeography,*
565 *Palaeoclimatology, Palaeoecology*, 252(1-2), 304-327.
566 Altabet, M.A., Francois, R., (1994) Sedimentary nitrogen isotopic ratio as a recorder for surface
567 ocean nitrate utilization. *Global Biogeochemical Cycles*, 8, 103–116.
568 Benton, M.J., (2003) *When Life Nearly Died: The Greatest Mass Extinction of all Time*. Thames
569 and Hudson, London.
570 Berner, R., (2006) Carbon, sulfur and O2 across the Permian-Triassic boundary. *Journal of*
571 *Geochemical Exploration*, 88(1-3), 416-418.
572 Bisseret, P., Zundel, M., Rohmer, M., (1985) Prokaryotic triterpenoids. 2. 2b-Methylhopanoids
573 from *Methylobacterium organophilum* and *Nostoc muscorum*, a new series of prokaryotic
574 triterpenoids. *European Journal of Biochemistry*, 150, 29-34.

575 Bowring, S.A., Erwin, D.H., Isozaki, Y., (1999) The tempo of mass extinction and recovery: The
576 end-Permian example. *Proceedings of the National Academy of Sciences*, 96(16), 8827-
577 8828.
578 Bowring, S.A., Erwin, D.H., Jin, Y.G., Martin, M.W., Davidek, K., Wang, W., (1998) U/Pb
579 Zircon Geochronology and Tempo of the End-Permian Mass Extinction. *Science*,
580 280(5366), 1039-1045.
581 Brassell, S.C., Eglinton, G., Maxwell, J.R., (1983) The geochemistry of terpenoids and steroids.
582 *Biochemical Society Transactions*, 11, 575-586.
583 Bravo, J.M., Perzl, M., Hartner, T., Kannenberg, E.L., Rohmer, M., (2001) Novel methylated
584 triterpenoids of the gammacerane series from the nitrogen-fixing bacterium
585 Bradyrhizobium japonicum USDA 110. *European Journal of Biochemistry*, 268(5),
586 1323-1331.
587 Brincat, D., Abbott, G.D., (2001) Some Aspects of the Molecular Biogeochemistry of Laminated
588 and Massive Rocks from the Naples Beach Section (Santa Barbara-Ventura Basin). In:
589 C.M. Isaacs, J. Rullkotter (Eds.), *The Monterey Formation: From Rocks to Molecules*
590 (Ed. by C.M. Isaacs, J. Rullkotter), pp. 140-149. Columbia University Press, New York.
591 Brocks, J.J., Love, G.D., Summons, R.E., Knoll, A.H., Logan, G.A., Bowden, S.A., (2005)
592 Biomarker evidence for green and purple sulphur bacteria in a stratified
593 Palaeoproterozoic sea. *Nature*, 437(7060), 866.
594 Brocks, J.J., Summons, R.E., (2003) Sedimentary Hydrocarbons, Biomarkers for Early Life. In:
595 D.H.a.K.K.T. Heinrich (Ed.), *Treatise on Geochemistry* (Ed. by D.H.a.K.K.T. Heinrich),
596 pp. 63-115. Pergamon, Oxford.
597 Campbell, I.H., Czamanske, G.K., Fedorenko, V.A., Hill, R.I., Stepanov, V., (1992)
598 Synchronism of the Siberian Traps and the Permian-Triassic Boundary. *Science*,
599 258(5089), 1760-1763.
600 Cao, C., Wang, W., Jin, Y.G., (2002) Carbon isotope excursions across the Permian-Triassic
601 boundary in the Meishan section, Zhejiang Province, China. *Chinese Science Bulletin*, 47,
602 1125-1129.
603 Collister, J.W., Summons, R.E., Lichtfouse, E., Hayes, J.M., (1992) An isotopic biogeochemical
604 study of the Green River oil shale. *Organic Geochemistry*, 19(1-3), 265.
605 Crowley, J.L., Bowring, S.A., Shen, S.Z., Wang, Y., Cao, C., Jin, Y.G., (2006) U-Pb zircon
606 geochronology of the end-Permian mass extinction. *Geochimica et Cosmochimica Acta*,
607 70(18, Supplement 1), A119.
608 Dumitrescu, M., Brassell, S.C., (2006) Compositional and isotopic characteristics of organic
609 matter for the early Aptian Oceanic Anoxic Event at Shatsky Rise, ODP Leg 198.
610 *Palaeogeography, Palaeoclimatology, Palaeoecology*, 235(1-3), 168-191.
611 Erwin, D.H., (1994) The Permo-Triassic extinction. *Nature*, 367, 231-236.
612 Erwin, D.H., (2006) *Extinction: how life on earth nearly ended 250 million years ago*. Princeton
613 University Press, Princeton.
614 Falkowski, P., Knoll, A.H., (2007) The Evolution of Photosynthetic Organisms in the Oceans.
615 In: *The Evolution of Photosynthetic Organisms in the Oceans* (Ed. by P. Falkwoski, A.H.
616 Knoll), pp. 133-163. Elsevier, Boston.
617 Falkowski, P.G., Katz, M.E., Knoll, A.H., Quigg, A., Raven, J.A., Schofield, O., Taylor, F.J.R.,
618 (2004) The Evolution of Modern Eukaryotic Phytoplankton. *Science*, 305(5682), 354-
619 360.

620 Farrimond, P., Talbot, H.M., Watson, D.F., Schulz, L.K., Wilhelms, A., (2004)
621 Methylhopanoids: Molecular indicators of ancient bacteria and a petroleum correlation
622 tool. *Geochimica et Cosmochimica Acta*, 68(19), 3873-3882.
623 Faure, K., de Wit, M.J., Willis, J.P., (1995) Late Permian global coal hiatus linked to 13C-
624 depleted CO2 flux into the atmosphere during the final consolidation of Pangea. *Geology*,
625 23(6), 507-510.
626 Fennel, K., Follows, M., Falkowski, P.G., (2005) The co-evolution of the nitrogen, carbon and
627 oxygen cycles in the Proterozoic ocean. *American Journal of Science*, 305(6-8), 526-545.
628 Fenton, S., Grice, K., Twitchett, R.J., Böttcher, M.E., Looy, C.V., Nabbefeld, B., (2007)
629 Changes in biomarker abundances and sulfur isotopes of pyrite across the Permian-
630 Triassic (P/Tr) Schuchert Dal section (East Greenland). *Earth and Planetary Science*
631 *Letters*, 262(1-2), 230-239.
632 Foster, C., Logan, G., Summons, R.E., Gorter, J., Edwards, D., (1997) Carbon isotopes, kerogen
633 types and the Permian-Triassic boundary in Australia: Implications for exploration.
634 *Australian Petroleum Production and Exploration Association Journal*, 37, 442-459.
635 Foster, C.B., Logan, G.A., Summons, R.E., (1998) The Permian-Triassic boundary in Australia:
636 where is it and how is it expressed? *Proceedings of The Royal Society of Victoria*, 110,
637 247-266.
638 Galfetti, T., Bucher, H., Ovtcharova, M., Schaltegger, U., Brayard, A., Brühwiler, T.,
639 Goudemand, N., Weissert, H., Hochuli, P.A., Cordey, F., Guodun, K., (2007) Timing of
640 the Early Triassic carbon cycle perturbations inferred from new U-Pb ages and
641 ammonoid biochronozones. *Earth and Planetary Science Letters*, 258(3-4), 593-604.
642 Gorter, J., Foster, C.B., Summons, R.E., (1995) Carbon isotopes and the Permian-Triassic
643 boundary in the north Perth, Bonaparte and Carnarvon Basins, Western Australia.
644 *Petroleum Exploration Society of Australia Journal*, 24, 21-38.
645 Grantham, P.J., (1986) Sterane isomerisation and moretane/hopane ratios in crude oils derived
646 from Tertiary source rocks. *Organic Geochemistry*, 9(6), 293-304.
647 Grantham, P.J., Posthuma, J., DeGroot, K., (1980) Variation and significance of the C_{27} and C_{28}
648 triterpane content of a North Sea core and various North Sea crude oils. In: A.G.
649 Douglas, J.R. Maxwell (Eds.), *Advances in Organic Geochemistry 1979* (Ed. by A.G.
650 Douglas, J.R. Maxwell), pp. 29-38. Pergamon Press, New York.
651 Grice, K., Cao, C., Love, G.D., Bottcher, M.E., Twitchett, R.J., Grosjean, E., Summons, R.E.,
652 Turgeon, S.C., Dunning, W., Jin, Y., (2005a) Photic Zone Euxinia During the Permian-
653 Triassic Superanoxic Event. *Science*, 307(5710), 706-709.
654 Grice, K., Schaeffer, P., Schwark, L., Maxwell, J.R., (1996) Molecular indicators of
655 palaeoenvironmental conditions in an immature Permian shale (Kupferschiefer, Lower
656 Rhine Basin, north-west Germany) from free and S-bound lipids. *Organic Geochemistry*,
657 25(3-4), 131-147.
658 Grice, K., Schaeffer, P., Schwark, L., Maxwell, J.R., (1997) Changes in palaeoenvrionmental
659 conditions during deposition of the Permian Kupferschiefer (Lower Rhine Basin,
660 northwest Germany) inferred from molecular and isotopic compositions of biomarker
661 components. *Organic Geochemistry*, 26(11-12), 677-690.
662 Grice, K., Summons, R.E., Grosjean, E., Twichett, R.J., Dunning, W., Wang, S.X., Boettcher,
663 M.E., (2005b) Novel depositional conditions of the Northern Onshore Perth Basin (Basal
664 Triassic). *AAPEA Journal*, 45, 263-273.

Haq, B.U., Hardenbol, J., Vail, P.R., (1988) Mesozoic and Cenozoic chronostratigraphy and cycles of sea-level change. In: C.K. Wilgus, B.S. Hastings, H. Posamentier, J.V. Wagoner, C.A. Ross, C.g.S.C. Kendall (Eds.), *Sea-Level Changes - An Integrated ApproachSEPM Special Publication 42* (Ed. by C.K. Wilgus, B.S. Hastings, H. Posamentier, J.V. Wagoner, C.A. Ross, C.g.S.C. Kendall), pp. 71-108.

Hartgers, W.A., Sinninghe Damsté, J.S., Requejo, A.G., Allan, J., Hayes, J.M., Ling, Y., Tiang-Min, X., Primack, J., de Leeuw, J.W., (1993) A molecular and carbon isotopic study towards the origin and diagenetic fate of diaromatic carotenoids. *Organic Geochemistry*, 22, 703-725.

Harvey, H.R., McManus, G.B., (1991) Marine ciliates as a widespread source of tetrahymanol and hopan-3B-ol in sediments. *Geochim. Cosmochim. Acta*, 55, 3387-3390.

Hays, L., Beatty, T., Henderson, C.M., Love, G.D., Summons, R.E., (2007) Evidence for photic zone euxinia through the end-Permian mass extinction in the Panthalassic Ocean (Peace River Basin, Western Canada). *Palaeoworld*, 16(1-3), 39-50.

Hesselbo, S.P., Grocke, D.R., Jenkyns, H.C., Bjerrum, C.J., Farrimond, P., Morgans Bell, H.S., Green, O.R., (2000) Massive dissociation of gas hydrate during a Jurassic oceanic anoxic event. *Nature*, 406(6794), 392.

Holser, W.T., (1977) Catastrophic chemical events in the history of the ocean. *Nature*, 267(5610), 403.

Holser, W.T., Schonlaub, H.-P., Attrep, M., Boeckelmann, K., Klein, P., Magaritz, M., Orth, C.J., Fenninger, A., Jenny, C., Kralik, M., Mauritsch, H., Pak, E., Schramm, J.-M., Stattegger, K., Schmoller, R., (1989) A unique geochemical record at the Permian/Triassic boundary. *Nature*, 337(6202), 39.

Imhoff, J., (2006) The phototrophic Alpha-proteobacteria. In: M. Dworkin, S. Falkow, E. Rosenberg, K.-H. Schleifer, E. Stackebrandt (Eds.), *The Prokaryotes: A Handbook on the Biology of Bacteria, 5* (Ed. by M. Dworkin, S. Falkow, E. Rosenberg, K.-H. Schleifer, E. Stackebrandt), pp. 41-64. Springer.

Isozaki, Y., (1995) Superanoxia across the Permo-Triassic boundary: record in accreted deep-sea pelagic chert in Japan. *Canadian Society of Petroleum Geologists, Memoir 17*, 805-812.

Isozaki, Y., (1997) Permo-Triassic Boundary Superanoxia and Stratified Superocean: Records from Lost Deep Sea. *Science*, 276(5310), 235-238.

Isozaki, Y., (2003) Guadalupian-Lopingian boundary event in mid-Panthalassa: Correlation of accreted deep-sea chert and mid-oceanic atoll carbonate. In: *XVth International Congress on Carboniferous and Permian Stratigraphy.* (Ed. by T.E. Wong), pp. 111-124. Royal Netherlands Academy of Arts and Sciences, Utrecht, the Netherlands.

Jin, Y., Wang, Y., Henderson, C.M., Wardlaw, B.R., Shen, S., Cao, C., Wang, W., (2006) The Global Stratotype Section and Point (GSSP) for the base-Changhsingian Stage (Upper Permian). *Episodes*, 29(3), 175-182.

Jin, Y., Wang, Y., Wang, W., Shang, Q.H., Cao, C., Erwin, D.H., (2000) Pattern of Marine Mass Extinction Near the Permian-Triassic Boundary in South China. *Science*, 289, 432-436.

Joachimski, M.M., Ostertag-Henning, C., Pancost, R.D., Strauss, H., Freeman, K.H., Littke, R., Sinninghe Damste, J.S., Racki, G., (2001) Water column anoxia, enhanced productivity and concomitant changes in [delta]13C and [delta]34S across the Frasnian-Famennian boundary (Kowala -- Holy Cross Mountains/Poland). *Chemical Geology*, 175(1-2), 109.

Junium, C.K.A., M.A., (2007) Nitrogen cycling during the Cretaceous, Cenomanian-Turonian Oceanic Anoxic Event II. *Geochemistry Geophysics Geosystems*, 8(3), ID Q03002.

711 Kamo, S.L., Czamanske, G.K., Amelin, Y., Fedorenko, V.A., Davis, D.W., Trofimov, V.R.,
712 (2003) Rapid eruption of Siberian flood-volcanic rocks and evidence for coincidence
713 with the Permian-Triassic boundary and mass extinction at 251 Ma. *Earth and Planetary*
714 *Science Letters*, 214(1-2), 75-91.
715 Kamo, S.L., Czamanske, G.K., Krogh, T.E., (1996) A minimum U---Pb age for Siberian flood-
716 basalt volcanism. *Geochimica et Cosmochimica Acta*, 60(18), 3505.
717 Kleemann, G., Poralla, K., Englert, G., Kjøsen, H., Liaaen-Jensen, S., Neunlist, S., Rohmer, M.,
718 (1990) Tetrahymanol from the phototrophic bacteriaum *Rhodopseudomonas palustris*:
719 first report of a gammacerane triterpene from a prokaryote. *J. of General Microbiology*,
720 136, 2551-2553.
721 Knoll, A.H., Bambach, R.K., Canfield, D.E., Grotzinger, J.P., (1996) Comparative Earth History
722 and Late Permian Mass Extinction. *Science*, 273, 452-457.
723 Knoll, A.H., Bambach, R.K., Payne, J.L., Pruss, S., Fischer, W.W., (2007a) Paleophysiology and
724 end-Permian mass extinction. *Earth and Planetary Science Letters*, 256(3-4), 295.
725 Knoll, A.H., Summons, R.E., Waldbauer, J.R., Zumberge, J., (2007b) The Geological Succession
726 of Primary Producers in the Oceans. In: P. Falkwoski, A.H. Knoll (Eds.), *The Evolution*
727 *of Photosynthetic Organisms in the Oceans* (Ed. by P. Falkwoski, A.H. Knoll), pp. 133-
728 163. Elsevier, Boston.
729 Kodner, R.B., Pearson, A., Summons, R.E., Knoll, A.H., (2008) Sterols in red and green algae:
730 quantification, phylogeny, and relevance for the interpretation of geologic steranes.
731 *Geobiology*, 6(4), 411-420.
732 Koopmans, M.P., Köster, J., Van Kaam-Peters, H.M.E., Kenig, F., Schouten, S., Hartgers, W.A.,
733 de Leeuw, J.W., Sinninghe Damste, J.S., (1996) Diagenetic and catagenetic products of
734 isorenieratene: Molecular indicators for photic zone anoxia. *Geochimica et*
735 *Cosmochimica Acta*, 60(22), 4467.
736 Korte, C., Jasper, T., Kozur, H.W., Veizer, J., (2006) 87Sr/86Sr record of Permian seawater.
737 *Palaeogeography, Palaeoclimatology, Palaeoecology*, 240(1-2), 89-107.
738 Korte, C., Kozur, H.W., Bruckschen, P., Veizer, J., (2003) Strontium isotope evolution of Late
739 Permian and Triassic seawater. *Geochimica et Cosmochimica Acta*, 67(1), 47-62.
740 Korte, C., Kozur, H.W., Joachimski, M.M., Strauss, H., Veizer, J., Schwark, L., (2004) Carbon,
741 sulfur, oxygen and strontium isotope records, organic geochemistry and biostratigraphy
742 across the Permian/Triassic boundary in Abadeh, Iran. *International Journal of Earth*
743 *Sciences*, 93(4), 565.
744 Köster, J., Van Kaam-Peters, H.M.E., Koopmans, M.P., De Leeuw, J.W., Sinninghe Damste,
745 J.S., (1997) Sulphurisation of homohopanoids: Effects on carbon number distribution,
746 speciation, and 22S/22R epimer ratios. *Geochimica et Cosmochimica Acta*, 61(12), 2431-
747 2452.
748 Kump, L., (1991) Interpreting carbon-isotope excursions: Strangeloveoceans. *Geology*, 19, 299-
749 302.
750 Kump, L.R., Pavlov, A., Arthur, M.A., (2005) Massive release of hydrogen sulfide to the surface
751 ocean and atmosphere during intervals of oceanic anoxia. *Geology*, 33, 397–400.
752 Kuypers, M.M.M., Blokker, P., Erbacher, J., Kinkel, H., Pancost, R.D., Schouten, S., Sinninghe
753 Damste, J.S., (2001) Massive Expansion of Marine Archaea During a Mid-Cretaceous
754 Oceanic Anoxic Event. *Science*, 293(5527), 92-95.

Kuypers, M.M.M., van Breugel, Y., Schouten, S., Erba, E., Damste, J.S.S., (2004) N2-fixing cyanobacteria supplied nutrient N for Cretaceous oceanic anoxic events. *Geology*, 32(10), 853-856.

McArthur, J.M., Howarth, R.J., Bailey, T.R., (2001) Strontium Isotope Stratigraphy: LOWESS Version 3: Best Fit to the Marine Sr-Isotope Curve for 0-509 Ma and Accompanying Look-up Table for Deriving Numerical Age. *The Journal of Geology*, 109(2), 155-170.

Meyer, K.M., Kump, L.R., Ridgwell, A., (2008) Biogeochemical controls on photic-zone euxinia during the end-Permian mass extinction. *Geology*, 36(9), 747-750.

Moldowan, J.M., Sundararaman, P., Schoell, M., (1986) Sensitivity of biomarker properties to depositional environment and/or source input in the lower Toarcian of SW-Germany. In: D. Leythaeuser, J. Rullkötter (Eds.), *Advances in Organic Geochemistry 1985, Org. Geochem., 10* (Ed. by D. Leythaeuser, J. Rullkötter), pp. 915-926, Pergamon.

Mundil, R., Ludwig, K.R., Metcalfe, I., Renne, P.R., (2004) Age and Timing of the Permian Mass Extinctions: U/Pb Dating of Closed-System Zircons. *Science*, 305(5691), 1760-1763.

Newton, R.J., Pevitt, E.L., Wignall, P.B., Bottrell, S.H., (2004) Large shifts in the isotopic composition of seawater sulphate across the Permo-Triassic boundary in northern Italy. *Earth and Planetary Science Letters*, 218(3-4), 331-345.

Ohkouchi, N., Kashiyama, Y., Kuroda, J., Ogawa, N.O., Kitazato, H., (2006) An importance of diazotrophic cyanobacteria as a primary producer during Cretaceous Oceanic Anoxic Event 2. *Biogeosciences Discussions*, 3, 575-605.

Ourisson, G., Rohmer, M., Poralla, K., (1987) Prokaryotic hopanoids and other polyterpenoid sterol surrogates. *Annual Review of Microbiology*, 41, 301-333.

Overmann, J., Cypionka, H., Pfenning, N., (1992) An extremely low-light-adapted phototrophic sulfur bacterium from the Black Sea. *Limnology and Oceanography*, 37(1), 150-155.

Palmer, M.R., Edmond, J.M., (1993) Uranium in river water. *Geochimica et Cosmochimica Acta*, 57(20), 4947-4955.

Pancost, R.D., Crawford, N., Magness, S., Turner, A., Jenkyns, H.C., Maxwell, J.R., (2004) Further evidence for the development of photic-zone euxinic conditions during Mesozoic oceanic anoxic events. *Journal of the Geological Society*, 161(3), 353-364.

Pancost, R.D., Crawford, N., Maxwell, J.R., (2002) Molecular evidence for basin-scale photic zone euxinia in the Permian Zechstein Sea. *Chemical Geology*, 188, 217-227.

Payne, J.L., Kump, L.R., (2007) Evidence for recurrent Early Triassic massive volcanism from quantitative interpretation of carbon isotope fluctuations. *Earth and Planetary Science Letters*, 256(1-2), 264-306.

Payne, J.L., Lehrmann, D.J., Wei, J., Orchard, M.J., Schrag, D.P., Knoll, A.H., (2004) Large Perturbations of the Carbon Cycle During Recovery from the End-Permian Extinction. *Science*, 305(5683), 506-509.

Peters, K.E., Moldowan, J.M., Walters, C.C., (2004) *The Biomarker Guide*. Cambridge University Press, Cambridge, UK; New York.

Prauss, M.L., (2007) Availability of reduced ntrogen chemospecies in photic-zone waters as the ultimate cause of fossil prasinophyte prosperity. *Palaios*, 22(5), 489-499.

Rashby, S.E., Sessions, A.L., Summons, R.E., Newman, D.K., (2007) Biosynthesis of 2-methylbacteriohopanepolyols by an anoxygenic phototroph. *Proceedings of the National Academy of Sciences of the United States of America*, 104 (38), 15099-15104.

800 Raup, D.M., Sepkoski, J.J.J., (1982) Mass Extinctions in the Marine Fossil Record. *Science*,
801 215(4539), 1501-1503.
802 Riccardi, A.L., Arthur, M.A., Kump, L.R., (2006) Sulfur isotopic evidence for chemocline
803 upward excursions during the end-Permian mass extinction. *Geochimica et*
804 *Cosmochimica Acta*(70), 5740-5752.
805 Rohmer, M., Bouvier-Nave, P., Ourisson, G., (1984) Distribution of Hopanoid Triterpenes in
806 Prokaryotes. *Journal of General Microbiology*, 130, 1137-1150.
807 Schoell, M., McCaffrey, M.A., Fago, F.J., Moldowan, J.M., (1992) Carbon isotopic
808 compositions of 28,30-bisnorhopanes and other biological markers in a Monterey crude
809 oil. *Geochim. Cosmochim. Acta*, 56(3), 1391-1399.
810 Seifert, W.K., Moldowan, J.M., (1978) Applications of steranes, terpanes and monoaromatics to
811 the maturation, migration and source of crude oils. *Geochim. Cosmochim. Acta*, 42, 77-
812 95.
813 Seifert, W.K., Moldowan, J.M., (1980) The effect of thermal stress on source rock quality as
814 measured by hopane stereochemistry. In: A.G. Douglas, J.R. Maxwell (Eds.), *Advances*
815 *in Organic Geochemistry 1979* (Ed. by A.G. Douglas, J.R. Maxwell), pp. 229-237.
816 Pergamon Press, Oxford.
817 Seifert, W.K., Moldowan, J.M., Smith, G.W., Whitehead, E.V., (1978) First proof of structure of
818 a C_{28}-pentacyclic triterpane in petroleum. *Nature*, 271, 436-437.
819 Sephton, M.A., Looy, C.V., Brinkhuis, H., Wignall, P.B., de Leeuw, J.W., Visscher, H., (2005)
820 Catastrophic soil erosion during the end-Permian biotic crisis. *Geology*, 33(12), 941-944.
821 Sephton, M.A., Looy, C.V., Veefkind, R.J., Brinkhuis, H., De Leeuw, J.W., Visscher, H., (2002)
822 Synchronous record of $\delta^{13}C$ shifts in the oceans and atmosphere at the end of the
823 Permian. *Geological Society of America*, Special Paper 356, 455-462.
824 Sinninghe Damsté, J.S., Kuypers, M.M.M., Pancost, R.D., Schouten, S., (2008) The carbon
825 isotopic response of algae, (cyano)bacteria, archaea and higher plants to the late
826 Cenomanian perturbation of the global carbon cycle: Insights from biomarkers in black
827 shales from the Cape Verde Basin (DSDP Site 367). *Organic Geochemistry*, 39 (12),
828 1703-1718.
829 Sinninghe Damsté, J.S., Schouten, S., van Duin, A.C.T., (2001) Isorenieratene derivatives in
830 sediments: possible controls on their distribution. *Geochimica et Cosmochimica Acta*, 65,
831 1557-1571.
832 Summons, R.E., Jahnke, L.L., Hope, J.M., Logan, G.A., (1999) 2-Methylhopanoids as
833 biomarkers for cyanobacterial oxygenic photosynthesis. *Nature*, 400, 554-557.
834 Summons, R.E., Powell, T., (1986a) Chlorobiaceae in Paleozoic Seas Revealed by Biological
835 Markers, Isotopes and Geology. *Nature*, 319(6056), 763-765.
836 Summons, R.E., Powell, T.G., (1986b) Chlorobiaceae in Paleozoic seas revealed by biological
837 markers, isotopes and geology. *Nature*, 319, 763-765.
838 Summons, R.E., Powell, T.G., (1987) Identification of aryl isoprenoids in source rocks and crude
839 oils: Biological markers for the green sulphur bacteria. *Geochimica et Cosmochimica*
840 *Acta*, 51, 557-566.
841 Talbot, H.M., Farrimond, P., (2007) Bacterial populations recorded in diverse sedimentary
842 biohopanoid distributions. *Organic Geochemistry*, 38(8), 1212-1225.
843 Talbot, H.M., Watson, D.F., Pearson, E.J., Farrimond, P., (2003) Diverse biohopanoid
844 compositions of non-marine sediments. *Organic Geochemistry*, 34(10), 1353-1371.

Ten Haven, H.L., Rohmer, M., Rullkotter, J., Bisseret, P., (1989) Tetrahymanol, the most likely precursor of gammacerane, occurs ubiquitously in marine sediments. *Geochimica et Cosmochimica Acta*, 53(11), 3073.

Tsuzuki, K., Ôhashi, A., Arai, Y., Masuda, K., Takano, A., Shiojima, K., Ageta, H., Cai, S.-Q., (2001) Triterpenoids from Adiantum caudatum. *Phytochemistry*, 58(2), 363-367.

Valentine, J.W., Jablonski, D., (1986) Mass Extinctions: Sensitivity of Marine Larval Types. *PNAS*, 83(18), 6912-6914.

van Breugel, Y., Baas, M., Schouten, S., Mattioli, E., Sinninghe Damsté, J.S., (2006) Isorenieratane record in black shales from the Paris Basin, France: Constraints on recycling of respired CO_2 as a mechanism for negative carbon isotope shifts during the Toarcian oceanic anoxic event. *Paleoceanography*, 21, PA4220.

Veizer, J., Compston, W., (1976) 87Sr/86Sr in Precambrian carbonates as an index of crustal evolution. *Geochimica et Cosmochimica Acta*, 40(8), 905-914.

Visscher, H., Looy, C.V., Collinson, M.E., Brinkhuis, H., van Konijnenburg-van Cittert, J.H.A., Kurschner, W.M., Sephton, M.A., (2004) Environmental mutagenesis during the end-Permian ecological crisis. *Proceedings of the National Academy of Sciences of the United States of America*, 101(35), 12952-12956.

Volkman, J., Barrett, S., Blackburn, S., Mansour, M., Sikes, E., Gelin, F., (1998) Microalgal biomakers: A review of recent research developments. *Org. Geochem.*, 29(5-7), 1163-1180.

Volkman, J.K., (1986) A review of sterol markers for marine and terrigenous organic matter. *Org. Geochem.*, 9(2), 83-99.

Wakeham, S.G., Amann, R., Freeman, K.H., Hopmans, E.C., Jorgensen, B.B., Putnam, I.F., Schouten, S., Sinninghe Damste, J.S., Talbot, H.M., Woebken, D., (2007) Microbial ecology of the stratified water column of the Black Sea as revealed by a comprehensive biomarker study. *Organic Geochemistry*, In Press, Corrected Proof.

Wang, C., (2007) Anomalous hopane distributions at the Permian-Triassic boundary, Meishan, China - Evidence for the end-Permian marine ecosystem collapse. *Organic Geochemistry*, 38(1), 52-66.

Wang, C., LIiu, Y., Liu, H., Zhu, L., Shi, Q., (2005) Geochemical significance of the relative enrichment of pristane and the negative excursion of δ13CPr across the Permian-Triassic Boundary at Meishan, China. *Chinese Science Bulletin*, 50(19), 2213-2225.

Wang, C., Visscher, H., (2007) Abundance anomalies of aromatic biomarkers in the Permian-Triassic boundary section at Meishan, China -- Evidence of end-Permian terrestrial ecosystem collapse. *Palaeogeography, Palaeoclimatology, Palaeoecology*, 252(1-2), 291-303.

Wang, W., Kano, A., Okumura, T., Ma, Y., Matsumoto, R., Matsuda, N., Ueno, K., Chen, X., Kakuwa, Y., Gharaie, M.H.M., Ilkhchi, M.R., (2007) Isotopic chemostratigraphy of the microbialite-bearing Permian-Triassic boundary section in the Zagros Mountains, Iran. *Chemical Geology*, 244(3-4), 708-714.

Watson, J.S., Sephton, M.A., Looy, C.V., Gilmour, I., (2005) Oxygen-containing aromatic compounds in a Late Permian sediment. *Organic Geochemistry*, 36(3), 371-384.

Weidlich, O., Kiessling, W., Flugel, E., (2003) Permian-Triassic boundary interval as a model for forcing marine ecosystem collapse by long-term atmospheric oxygen drop. *Geology*, 31(11), 961-964.

Wignall, P., Twitchett, R., (2002) Extent, duration and nature of the Permian-Triassic superanoxic event. In: C. Koeberl, K.C. MacLeod (Eds.), *Catastrophic Events and Mass Extinctions: Impacts and Beyond:* (Ed. by C. Koeberl, K.C. MacLeod), pp. 395-413. Geological Society of America Special Paper 356, Boulder, Colorado.

Wignall, P.B., Twitchett, R.J., (1996) Ocean Anoxia and the End Permian Mass Extinction. *Science*, 272(5265), 1155-1158.

Xie, S., Pancost, R.D., Huang, J., Wignall, P.B., Yu, J., Tang, X., Chen, L., Huang, X., Lai, X., (2007) Changes in the global carbon cycle occurred as two episodes during the Permian–Triassic crisis. *Geology*, 35(12), 1083-1086.

Xie, S., Pancost, R.D., Yin, H., Wang, H., Evershed, R.P., (2005) Two episodes of microbial change coupled with Permo/Triassic faunal mass extinction. *Nature*, 434, 494-497.

Xu, D.-Y., Yan, Z., (1993) Carbon isotope and iridium event markers near the Permian/Triassic boundary in the Meishan section, Zhejiang Province, China. *Palaeogeography, Palaeoclimatology, Palaeoecology*, 104(1-4), 171-176.

Yin, H., Zhang, K., Tong, J., Yang, Z., Wu, S., (2001) The Global Stratotype Section and Point (GSSP) of the Permian-Triassic Boundary. *Episodes*, 24(2), 102-114.

Zhang, K., Tong, J., Yin, H., Wu, S., (1996) Sequence stratigraphy of the Permian-Triassic boundary section of Changxing, Zhejiang. *Acta Geologica Sinica*, 70(3), 270-281.

Zundel, M., Rohmer, M., (1985a) Hopanoids of the methylotrophic bacteria Methylococcus capsulatus and Methylomonas sp. as possible presursors of C_{29} and C_{30} hopanoid chemical fossils. *FEMS Microbiology Letters*, 28, 61-64.

Zundel, M., Rohmer, M., (1985b) Prokaryotic triterpenoids. 1. 3β-Methylhopanoids from Acetobacter sp. and Methylococcus capsulatus. *European Journal of Biochemistry*, 150, 23-27.

8. Legends to Figures

Figure 1. A geological map of the Meishan locality and the site of the Meishan-1 core.

Figure 2. Stratigraphy and lithology of the Meishan-1 core plotted together with a relative sea-level curve for the Changhsingian and basal Griesbachian stages. With the exception of $\delta^{13}C_{carb}$, which is a compilation of previously reported outcrop data and the Meishan core data (Cao *et al.*, 2002), values of bulk geochemical parameters are for the samples measured in this study.

Figure 3. Values of hydrocarbon-derived geochemical parameters diagnostic for water column and sedimentary redox conditions plotted against the Meishan-1 core stratigraphy. Pristane/phytane (Pr/Ph) data were calculated from the total ion currents of full scan GC-MS data. The C_{35}HHI (%), which is the abundance of C_{35} hopane 22S + 22R isomers as a percentage of the summed $C_{31\text{-}35}$ homohopanes, and the abundance of 28,30-dinorhopane (28,30-DNH/ 28,30-DNH + C_{30} αβ-hopane *100) data were derived from GC-MS data run in MRM mode. The absolute abundances of isorenieratane and aryl isoprenoids, normailsed to total organic carbon contents, were derived from GC-MS SIM data using an internal standard and calculated response factors.

Figure 4. Values of hydrocarbon-derived geochemical parameters diagnostic for components of the plankton communities plotted against the Meishan-1 core stratigraphy. All data were derived from GC-MS data collected in MRM mode using an internal standard for quantification. However, peak areas were not corrected for the different response factors of individual hydrocarbons. A: hopane/sterane ratio was calculated from the abundances of 19 isomers of the $C_{27\text{-}35}$ hopanes and the main 24 isomers of the $C_{27\text{-}30}$ steranes. B & C: The % C* sterane were calculated from C* Sterane abundance of diasteranes 20(R+S) and aaa plus abb (R+S) from C_{27} to C_{30}. D: Gamma/C_{30}H was the ratio of gammacerane to C_{30} αβ-hopane and E and F: 3β- and 2α-methylhopane indices were calculated from the percentage abundance of the C_{31} methylhopane relative to sum of C_{31} methylhopane and C_{30} αβ-hopane.

Figure 5. Values of hydrocarbon-derived geochemical parameters diagnostic for thermal maturity and/or lithology plotted against the Meishan-1 core stratigraphy. All ratios were calculated from GC-MS data collected in the MRM mode. The individual ratios are as defined in the column headings.

Figure 6. Cross-correlations of various source and maturity parameters for the Meishan-1 core. Samples are color-coded according to age and lithology. The data display both strong and weak correlations indicative of the complex interplay between biomarker lipid sources and lithologies reflecting different styles of sedimentary diagenesis.

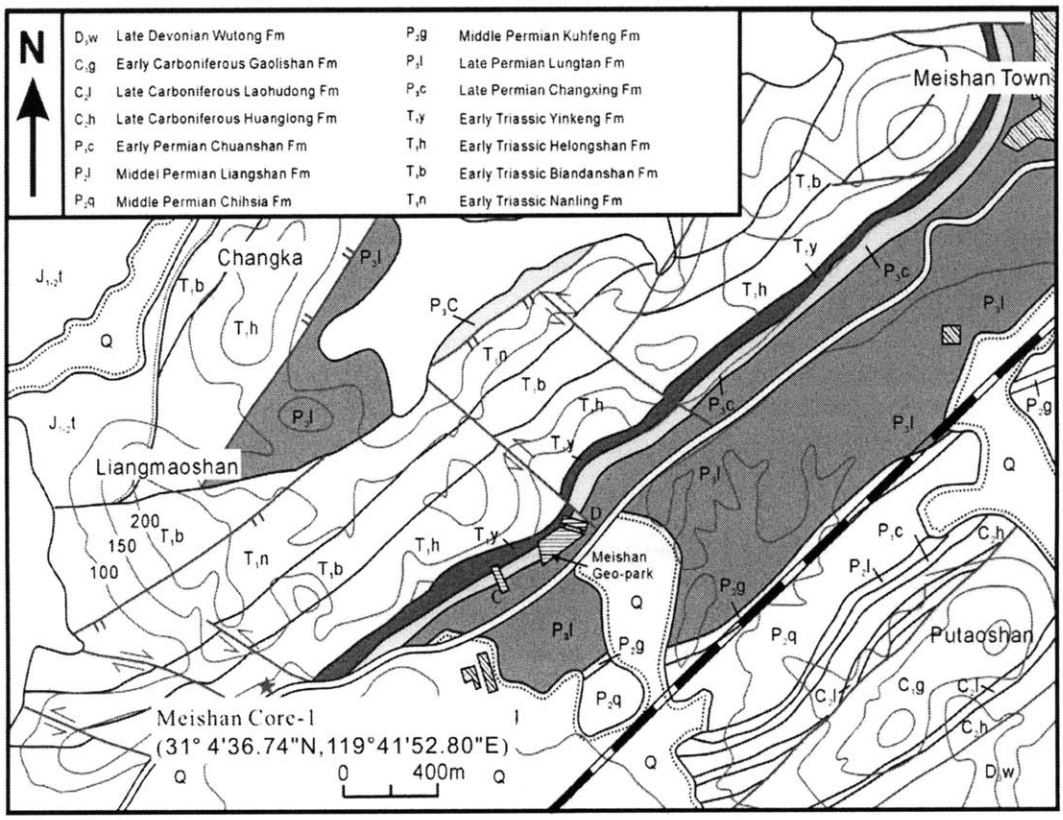

Fig. 1. A geological map of the Meishan locality and the site of the Meishan-1 core.

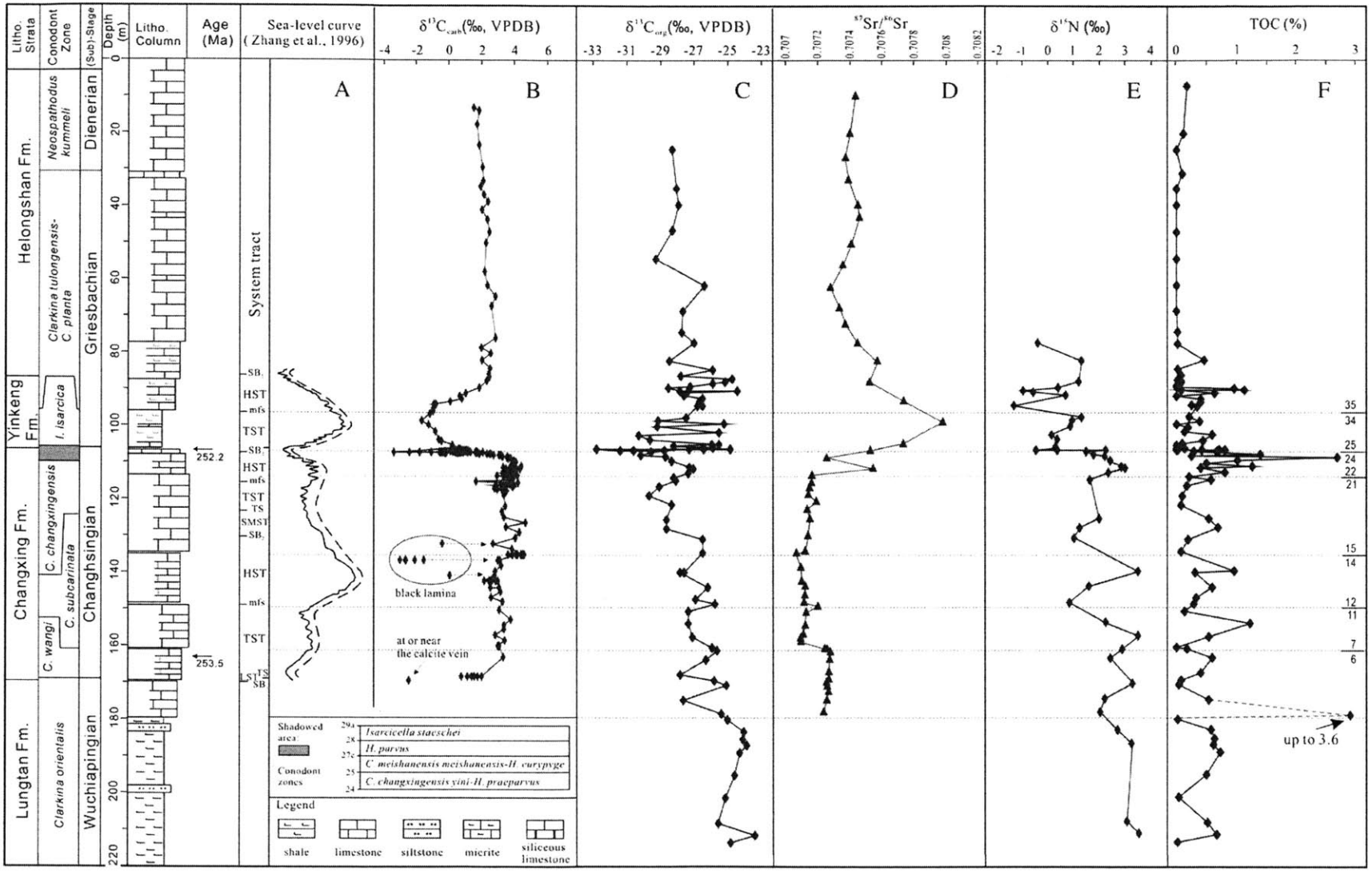

Fig. 2. Stratigraphy and lithology of the Meishan-1 core plotted together with a relative sea-level curve for the Changhsingian and basal Griesbachian stages. With the exception of $\delta^{13}C_{carb}$, which is a compilation of previously reported outcrop data and the Meishan core data (Cao et al., 2002), values of bulk geochemical parameters are for the samples measured in this study.

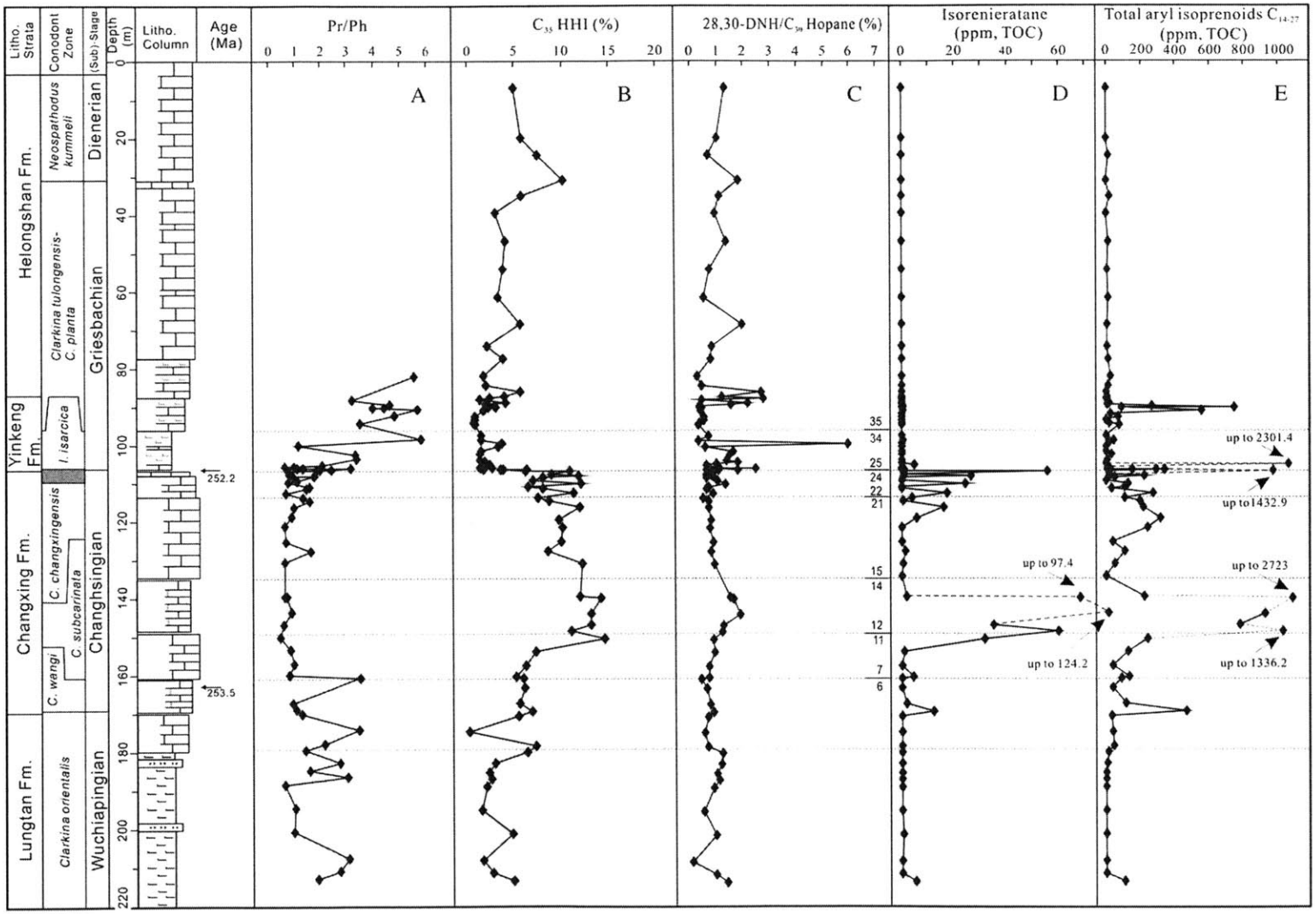

Fig. 3. Values of hydrocarbon-derived geochemical parameters diagnostic for water column and sedimentary redox conditions plotted against the Meishan-1 core stratigraphy. Pristane/phytane (Pr/Ph) data were calculated from the total ion currents of full scan GC-MS data. The C_{35}HHI (%), which is the abundance of C_{35} hopane 22S + 22R isomers as a percentage of the summed C_{31-35} homohopanes, and the abundance of 28,30-dinorhopane (28,30-DNH/ 28,30-DNH + C_{30} αβ-hopane *100) data were derived from GC-MS data run in MRM mode. The absolute abundances of isorenieratane and aryl isoprenoids, normalised to total organic carbon contents, were derived from GC-MS SIM data using an internal standard and calculated response factors.

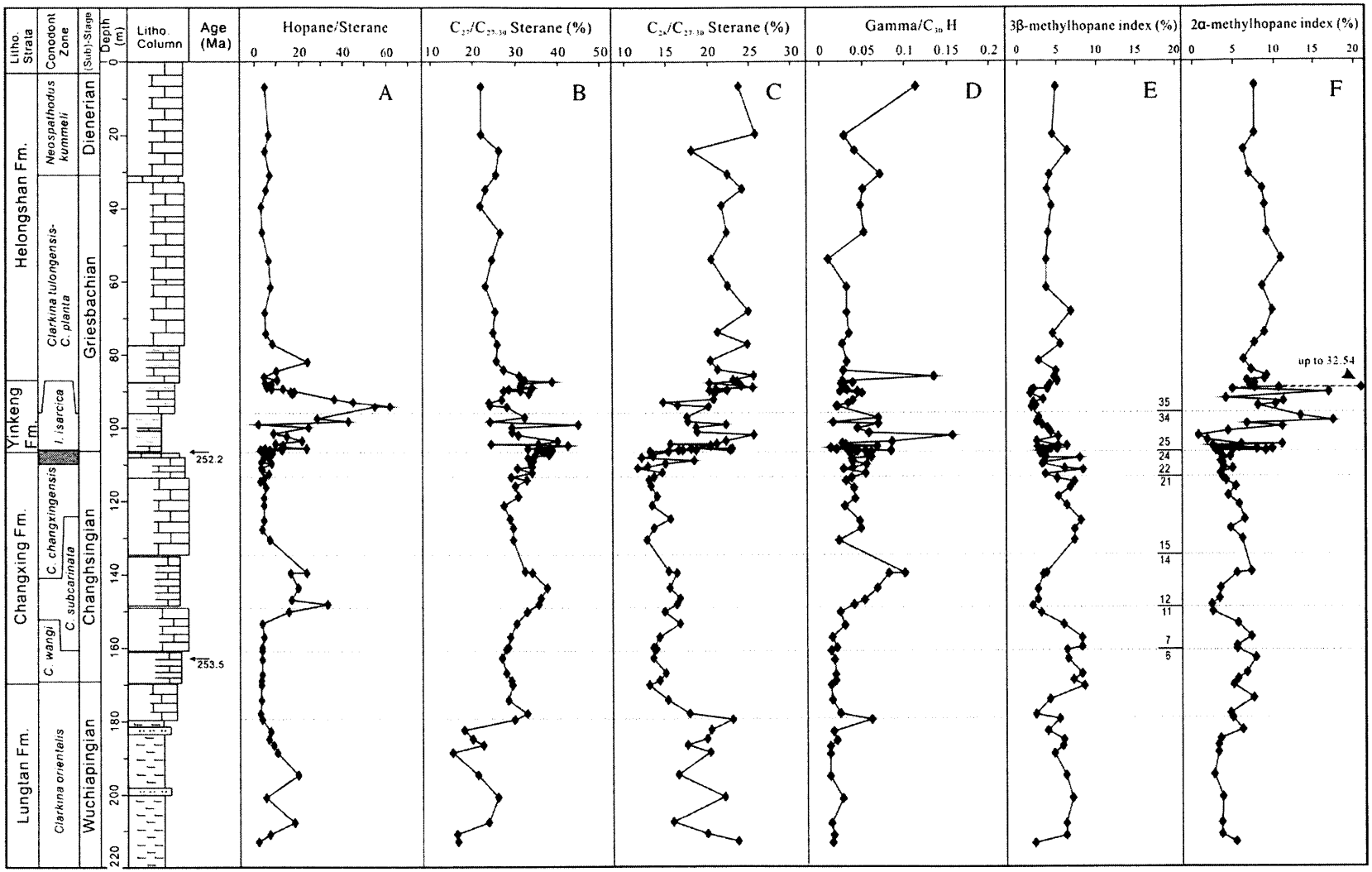

Fig. 4. Values of hydrocarbon-derived geochemical parameters diagnostic for components of the plankton communities plotted against the Meishan-1 core stratigraphy. All data were derived from GC-MS data collected in MRM mode using an internal standard for quantification. However, peak areas were not corrected for the different response factors of individual hydrocarbons. A: hopane/sterane ratio was calculated from the abundances of 19 isomers of the C_{27-35} hopanes and the main 24 isomers of the C_{27-30} steranes. B and C: The %C* sterane were calculated from C* Sterane abundance of diasteranes 20(R+S) and aaa plus abb (R + S) from C_{27} to C_{30}. D: Gamma/C_{30}H was the ratio of gammacerane to C_{30} αβ-hopane and E and F: 3β- and 2α-methylhopane indices were calculated from the percentage abundance of the C_{31} methylhopane relative to sum of C_{31} methylhopane and C_{30} αβ-hopane.

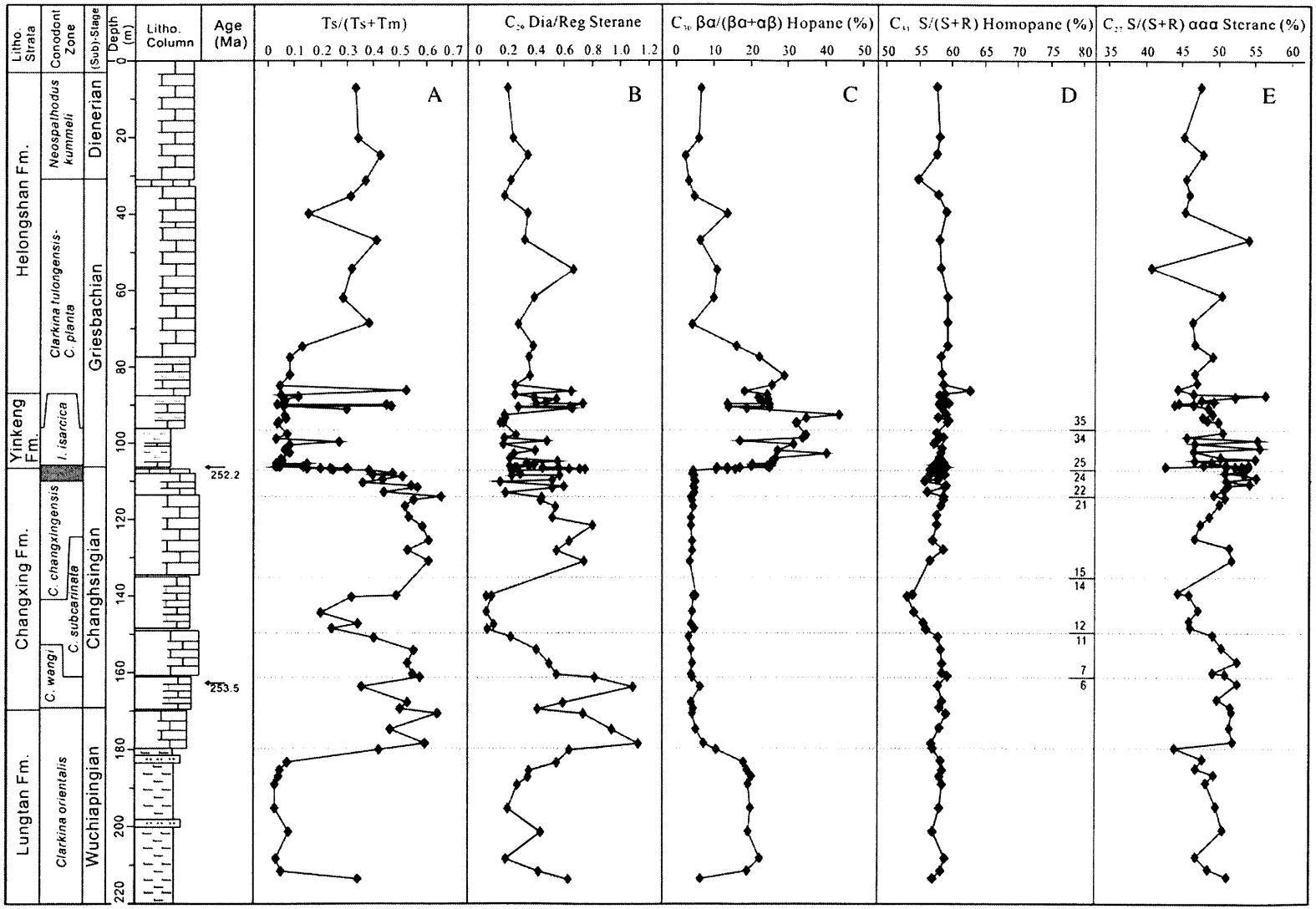

Fig. 5. Values of hydrocarbon-derived geochemical parameters diagnostic for thermal maturity and/or lithology plotted against the Meishan-1 core stratigraphy. All ratios were calculated from GC-MS data collected in the MRM mode. The individual ratios are as defined in the column headings.

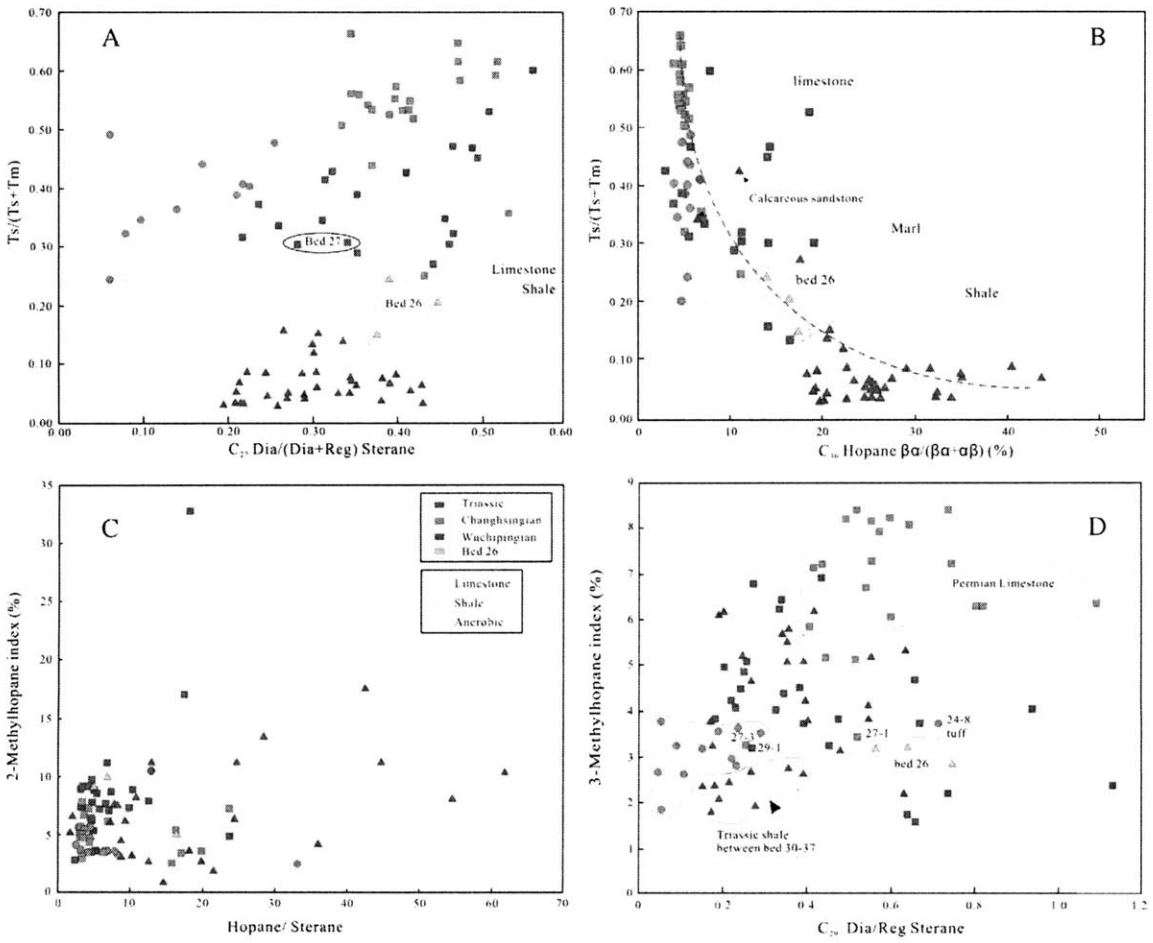

Fig. 6. Cross-correlations of various source and maturity parameters for the Meishan-1 core. Samples are color-coded according to age and lithology. The data display both strong and weak correlations indicative of the complex interplay between biomarker lipid sources and lithologies reflecting different styles of sedimentary diagenesis.